The Real Corrections To The Virtual Photon Impact Factor

Dissertation
zur Erlangung des Doktorgrades
des Fachbereichs Physik
der Universität Hamburg

vorgelegt von
Albrecht Kyrieleis
aus Göttingen

Hamburg
2003

Abstract

We investigate the interaction of two virtual photons in the high energy limit of Quantum Chromodynamics (QCD). We are motivated by two closely linked problems: the calculation of the $\gamma^*\gamma^*$ total cross section, $\sigma^{\gamma^*\gamma^*}$, in the framework of NLO BFKL and the NLO extensions to the colour dipole picture. We calculate the squared amplitude for the process $\gamma^* + q \to q\bar{q}g + q$ in arbitrary space-time dimensions for both longitudinal and transverse photon polarisation. In transverse configuration space the result is found to factorise supporting in this way the photon wave function interpretation. This is the first step in the calculation of the $q\bar{q}g$ Fock component of the γ^* wave function. The squared vertex for the transition Reggeon-$\gamma^* \to q\bar{q}g$ is extracted in order to calculate the NLO real corrections to the γ^* impact factor. Together with the virtual corrections this will allow for the calculation of $\sigma^{\gamma^*\gamma^*}$. The infrared divergences are dimensionally regularised and their cancellation against those from the virtual corrections is performed. After the introduction of Feynman parameters in each Feynman diagram, part of the $q\bar{q}g$ phase space integration is performed analytically. The various divergences emerging due to the independent treatment of the diagrams are regularised. A procedure is worked out to obtain for each diagram a finite phase space integral. In the case of longitudinal photon polarisation, this method is implemented in a computer program and the full phase space integration is carried out numerically. First numerical tests of the calculation are successfully performed.

Zusammenfassung

Wir untersuchen die Wechselwirkung zweier virtueller Photonen im Hochenergielimes der Quantenchromodynamik (QCD). Die Motivation liegt in zwei eng verwandten Problemen: Die Berechnung des totalen $\gamma^*\gamma^*$ Wirkungsquerschnitts, $\sigma^{\gamma^*\gamma^*}$, im Rahmen von NLO BFKL und die NLO Erweiterungen des Farbdipol-Modells. Wir berechnen die quadrierte Amplitude für den Prozess $\gamma^*+q \to q\bar{q}g+q$ in beliebig vielen Raum-Zeit Dimensionen für longitudinale und transversale Photonpolarisation. Im transversalen Konfigurationsraum faktorisiert das Resultat, was die Deutung im Sinne der Photon Wellenfunktion ermöglicht; das ist der erste Schritt in der Berechnung der $q\bar{q}g$-Fock-Komponente der Photon Wellenfunktion. Der quadrierte Vertex des Übergang Reggeon-$\gamma^* \to q\bar{q}g$ wird extrahiert, um die reellen NLO Korrekturen zum γ^* Impact Factor zu berechnen. Zusammen mit den virtuellen Korrekturen wird das die Berechnung von $\sigma^{\gamma^*\gamma^*}$ ermöglichen. Die Infrarotdivergenzen werden dimensional regularisiert und gegen die aus den virtuellen Korrekturen gekürzt. Nach der Einführung von Feynman Parametern in jedem Feynman Diagram wird ein Teil der $q\bar{q}g$-Phasenraumintegration analytisch durchgeführt. Die verschiedene Divergenzen, die durch die separate Behandlung der einzelnen Feynman Diagramme auftauchen, werden regularisiert. Eine Prozedur wird ausgearbeitet, wie von jedem Diagram ein endliches Phasenraumintegral abgeleitet werden kann. Für longitudinale Photonpolarisation wird diese Prozedur in einem Computerprogram implementiert und die komplette Phaseraumintegration numerisch ausgeführt. Erste numerische Tests der Rechnung werden erfolreich durchgeführt.

Contents

Chapter 1

Introduction

About 30 years after its formulation Quantum Chromodynamics (QCD) has been widely accepted as the theory of the strong interaction: the symmetries of these interactions are exactly incorporated with a SU(3) colour group, the asymptotic freedom of QCD can explain the scaling properties of measured cross sections and there are hints to progress in the approach to the confinement problem (e.g. from lattice QCD).

Asymptotic freedom means the vanishing of the strong coupling as the momentum transfer becomes large (compared to $\Lambda_{QCD} \approx 200$ MeV). A small coupling constant allows for the application of perturbative methods. In the non-perturbative regime, however, the prospects of predictions of measurable quantities from first principles are still strongly limited. The successful application of perturbative QCD therefore usually relies on the factorisation of the scattering process into a hard, calculable part, and a non-perturbative one which has to be fitted to the measurement. In many processes with leptons in the initial state (e.g. ep-DIS or e^+e^--scattering) it is a large virtuality of the photon that makes perturbative calculations possible. This is why virtual photon interactions are of crucial interest for perturbative QCD.

A subclass of processes is the $2 \to 2$ hadronic scattering at small scattering angle. This corresponds to the limit of large center-of-mass energy at fixed momentum transfer t, also called Regge limit. In the framework of Regge theory, scattering processes are associated with the exchange of Reggeons [1]. Each Reggeon correspond to a t-dependent pole $\alpha(t)$, called Regge trajectory, of the scattering amplitude in the complex angular momentum plane. In the Regge limit, the $2 \to 2$ scattering process is dominated by the exchange of a leading Reggeon and the amplitude takes a factorised (reggeized form): effective vertices incorporate the coupling of the external particles to this Reggeon; in particular, the energy dependence for fixed exchanged quantum numbers is found to be independent from the scattering particles.

Let us now consider elastic scattering. The leading Reggeon is called the Pomeron with the trajectory $\alpha_{I\!P}(t)$. Due to unitarity the imaginary part of the elastic amplitude at zero scattering angle is proportional to the total cross section. Therefore, a particle-independent high energy behaviour of total cross sections is expected. Various measurements of hadronic cross sections revealed a universal, weak growth with energy:

$$\sigma_{tot}^{hadr} \propto s^{\alpha_{I\!P}(0)-1} \quad , \qquad \alpha_{I\!P}(0) = 1.08. \tag{1.1}$$

QCD as the theory of hadronic interactions should in principle be able to describe small angle scattering. The high energy limit of elastic hadronic amplitudes (at fixed t) is of outstanding importance for QCD: due to its universality $\alpha_{I\!P}(0)$ is expected to be of fundamental meaning in the structure of QCD and it would be desirable to understand the origin of this constant from first principles.

In order to make contact between the concept of Regge trajectories and perturbative QCD, one can study them as functions of α_s. From the reggeized form of an $2 \rightarrow 2$ amplitude follows that at any fixed order of α_s this amplitude depends on the energy as $\alpha_s^n \, ln \; s^m$ (n, m being natural numbers). Let us first consider the high energy elastic scattering of elementary particles, say quarks. In order to account for the leading energy dependence, the terms of type $(\alpha_s \, ln \; s)^n$ from the amplitudes of all orders in α_s can be summed up defining in this way the leading logarithmic approximation (LLA). The result of this resummation is the famous BFKL equation (Balitsky-Fadin-Kuraev-Lipatov) derived 25 years ago [2]. Thinking of a total cross section rather than of a forward scattering amplitude the contributions have a simple structure: any n-gluon final state contributes, where the gluons are separated by large rapidity gaps, also known as multi-Regge-kinematics (MRK).

Turning now from quarks to arbitrary scattering particles it is of crucial importance that in the Reggeized form of an amplitude the energy dependent part factorises from those incorporating the properties of the external particles. The BFKL resummation therefore remains unchanged. The imaginary part of an elastic hadronic amplitude, or equivalently, the total cross section, can be written as a convolution of two impact factors (Φ) with the solution of the BFKL equation ($\mathcal{G}$). The impact factors contain all information on the coupling of the external particles to the BFKL ladder. To describe the $\gamma^*\gamma^*$ total cross section in the LO BFKL approach the impact factor for the virtual photon is needed. At not too small photon virtuality it is calculable in pQCD. Independent of the external particles, the BFKL approach provides an exponent for the s dependence of total cross sections:

$$\sigma_{tot} \propto s^{\omega_{\mathrm{BFKL}}} \quad , \qquad \omega_{\mathrm{BFKL}} = \frac{4N_c ln2}{\pi}\alpha_s \tag{1.2}$$

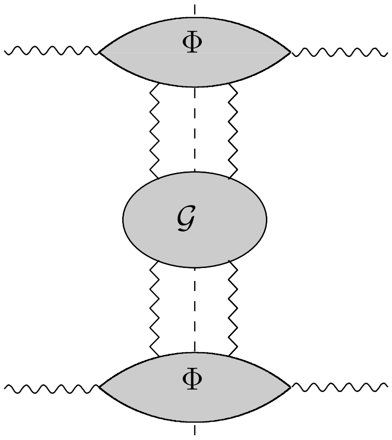

For a reasonable value of $\alpha_s = 0.2$ this leads to $\omega_{\mathrm{BFKL}} \approx 0.5$. So, BFKL predicts a substantially stronger growth of total cross sections with energy than it is observed in hadron-hadron scattering.

In order to confront the BFKL predictions with experiments various observables have been proposed. At HERA the proton structure function $F_2(Q^2, x)$ has been precisely measured, corresponding to the measurement of the total $\gamma^* p$ cross section. Since $x \approx Q^2/W^2$ for small x (W being the $\gamma^* p$ energy), the small-x behaviour of F_2 reflects the high energy behaviour of $\sigma_{tot}^{\gamma^* p}$ at fixed photon virtuality Q^2. For $Q^2 \approx 0$ a hadronic behaviour of this cross section was observed. At larger Q^2, however, $\sigma_{tot}^{\gamma^* p}$ was found to rise much stronger with energy than in the case of hadronic scattering (typically $\propto W_{\gamma^* p}^{0.3}$). Still, we cannot expect the BFKL approach to be applicable for the calculation of this observable, because the proton is a large non-perturbative object.

It has been proposed to look at the production of a forward jet in DIS originating from a parton of large transverse momentum [6, 7, 8]. The BFKL formalism is expected to apply in this case because the high transverse momentum of the jet introduces a large scale into the process. This possibility to apply BFKL has also been discussed in the case of hadron-hadron scattering [9].

The scattering of virtual photons is of particular importance: the $\gamma^*\gamma^*$ total cross section can be measured quite easily over a large range of photon virtualities; especially from the forthcoming e^+e^- collider excellent data can be expected. On the one hand, large virtualities of the photons allow for a completely perturbative calculation of this cross section. On the other hand, lowering these virtualities continuously leads into the situation of hadron-hadron scattering at very small virtualities. Virtual photon scattering provides one of the clearest transitions between hard and soft physics, both from experimental and theoretical side. The application of the BFKL approach to this process has been first proposed in [31, 32]. At LEP the $\gamma^*\gamma^*$ total cross section has been measured to rise approximately as $W^{0.3}_{\gamma^*\gamma^*}$. Assuming that $W_{\gamma\gamma}$ is large enough for the process to be dominated by the

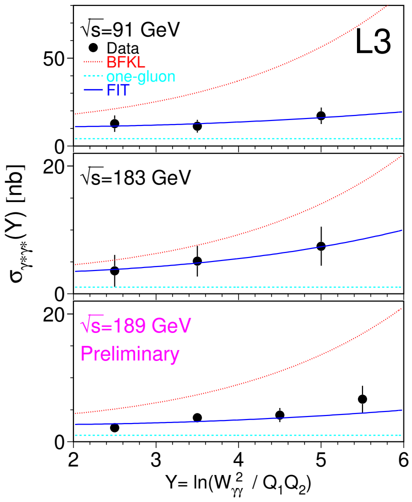

Figure 1.1: $\sigma^{\gamma^*\gamma^*}_{tot}$ measured at LEP compared to the LO BFKL result

leading Regge pole only, the growth with energy given by LO BFKL is too strong.

Thus, deviations from the hadronic high energy behaviour were seen, as predicted by BFKL, but the energy exponent $\omega_{\rm BFKL}$ appears to be too large. Besides this, there are further problems connected with LO BFKL. By changing the energy scale from s_0 to s' a contribution to the LLA can be rewritten: $\alpha_s\, ln\, \frac{s}{s_0} = \alpha_s\, ln\, \frac{s}{s'} + \alpha_s\, ln\, \frac{s'}{s_0}$. In the second term α_s multiplies a constant instead of a logarithm of the energy, it therefore belongs to the next-to-leading logarithmic approximation (NLLA) and can be neglected. This means that the scale of the energy is arbitrary in the LLA. It is therefore impossible to calculate the absolute value of a cross section in the LO BFKL approach; it can only be guessed by using a scale typical for the process. Finally, the scale of the coupling constant is unclear in LO BFKL since no UV-divergent terms contribute to the LLA and therefore, no renormalisation is done.

Due to these problems the calculation of next-to-leading corrections to BFKL is mandatory, which means collecting terms of type $\alpha_s(\alpha_s ln\ \ s)^n$. One class of the contributions stem, as in the LLA, from n-gluon states in MRK, but calculated at one-loop level. In addition, there are contributions at Born level from n-particle states, where all but two particles are separated in rapidity (leading to the loss of one large logarithm of the energy in comparison to LLA). These states consist of gluons and a 2-gluon pair or a quark-antiquark pair. The NLO corrections to the BFKL kernel have been calculated by Fadin, Lipatov, Camici and Ciafaloni. After 10 years of work the result for $t = 0$ was published in 1998 [3, 4]. It turned out that the inclusion of next-to-leading effects indeed lowers the exponent ω_{BFKL} to values around 0.3 for realistic values of α_s [36, 37, 38]. This value seems to be compatible with the measurements.

As argued above, the $\gamma^*\gamma^*$ total cross section is the ideal observable to test BFKL. The calculation of this cross section would be the first completely perturbative, consistent computation of a measurable cross section in the framework of NLO BFKL. The only piece missing is the photon impact factor at NLO. The main motivation for this work is the calculation of the NLO impact factor for virtual photons in order to perform a stringent test of NLO BFKL. Note that, in the combination of the impact factors and the BFKL Green function the dependence on the energy scale s_0 drops out. The result for the $\gamma^*\gamma^*$ total cross section is therefore independent of s_0.

The γ^* impact factor is important also from another point of view: it is well known that the LO photon impact factor can be interpreted in terms of the photon wave function and a colour dipole cross section [17, 19]. In recent years this colour dipole picture has proven to be extremely useful in the analysis of HERA data in the small-x region, in particular the low-Q^2 region of the F_2 structure function and the diffractive final states [22, 23]. The validity of the colour dipole picture (or, maybe, its generalisation to higher multi-pole terms) beyond LO therefore presents an issue which has to be investigated. At NLO, the validity of the colour dipole picture should come out of the calculation of the NLO photon impact factor.

If we consider $\sigma^{tot}_{\gamma^*\gamma^*}$ with the Q_1^2, Q_2^2 being the virtualities of the photons, the collinear limit $Q_1^2 \ll Q_2^2$ is of particular value: the cross section is known from the DGLAP (Dokshitzer-Gribov-Lipatov-Altarelli-Parisi) resummation in this limit. In order to be able to analyse the collinear structure of the impact factor and to perform this important consistency check we need to know the impact factor, as much as possible, in an analytic form. It will, therefore, be the strategy of this thesis to carry out the integration over momenta, and to arrive at Feynman parameter representation of the matrix elements.

Let us turn now to the γ^* impact factor itself. The NLO corrections are divided into virtual (a) and real (b) corrections as depicted in fig.1.2. The program for the calculation of these corrections can be roughly outlined as follows: First, the products of certain effective vertices must be computed; then, the infrared divergences in the virtual and real corrections have to be extracted and cancelled against each other. Finally, a phase space integration has to be carried out in both parts of the corrections. As for the

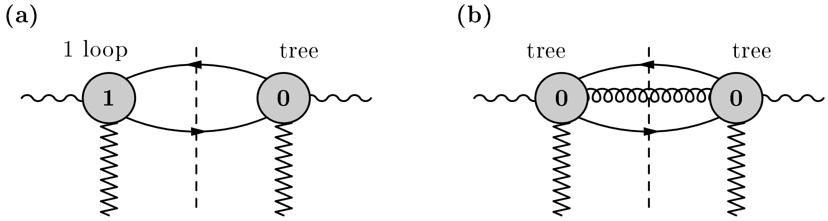

Figure 1.2: The next-to-leading corrections to the γ^* impact factor

virtual contribution, the $q\bar{q}$ production vertex at one-loop level is needed; it has been calculated by Bartels, Ciao and Gieseke [10]. The calculation of the real corrections due to the emission of an additional gluon is the main subject of this thesis. In the following the structure of this work is outlined.

The first step in the calculation of the real corrections is the computation of the squared effective vertex for $q\bar{q}g$ production. To this end, the squared LO amplitude for the process $q + \gamma^* \to q + q\bar{q}g$ in the high energy limit is calculated; both, longitudinal and transverse photon polarisation are considered. The high energy limit implies a large rapidity gap between the $q\bar{q}g$ system and the final state quark. The amplitude therefore includes the configuration where the gluon is separated in rapidity also from the $q\bar{q}$ pair. This central limit, however, belongs to the LLA and must be subtracted from the amplitude to get the correct contribution to the NLO impact factor.

Moreover, we have to deal with the infrared divergences due to a soft or collinear gluon. Working in $D = 4 - 2\epsilon$ space-time dimensions we subtract from the squared vertex its approximation in the collinear and soft limits. These limits exhibit ϵ poles after performing the phase space integration. It is shown that these poles exactly cancel the ones extracted from the virtual corrections. The outcome of this procedure, are finite expressions for the virtual and real corrections. What remains to be done is to perform the remaining phase space integration.

Besides the possibility of calculating $\sigma^{tot}_{\gamma^*\gamma^*}$, the NLO γ^* impact factor offers information that is of high theoretical interest as mentioned above. It is therefore desirable to perform as much of the phase space integration as possible analytically. To this end Feynman parameters are introduced in the expression for the real corrections. This in turn enforces the independent treatment of the different Feynman diagrams or small groups of them. In doing so, various divergences appear that cancel in the sum of all diagrams. An essential achievement of this thesis is the construction of finite expressions for each diagram using different methods for the regularisation of these additional divergences. Then, part of the phase space integration is performed analytically.

In the final part of the thesis we have performed, for the longitudinal polarisation of the photon, the remaining numerical integrations. This includes two phase space variables (longitudinal momenta of the outgoing quarks and gluon) and the Feynman parameters. To this end we have written a program in MATHEMATICA and used the Monte Carlo routine VEGAS to do the integrations. The results demonstrate, that, in fact, our expressions for the matrix elements are finite. Moreover, as far as the real corrections for the photon impact factor are concerned, we have reached the stage were systematic numerical studies of the NLO impact factor can be started. The methods presented in this thesis also allow to carry out the analogous steps for the transverse polarisation of the photon, but a few further studies have to be performed before we can present the desired numerical results.

Let us outline the organisation of this thesis. After a review of virtual photon scattering, the definition of the NLO γ^* impact factors is presented and the results for the virtual corrections are summarised. In chapter 4, the process $q + \gamma^* \to q + q\bar{q}g$ is considered; the implications for the extension of the colour dipole picture are investigated and the squared vertex for $q\bar{q}g$ production is calculated. The collinear and soft divergences are extracted and cancelled in chapter 5. The next chapter is devoted to the analytical integration in the real corrections after the introduction of Feynman parameters. The procedure is defined to provide finite expressions for each Feynman diagram. The topic of the last chapter is the numerical analysis for longitudinal photon polarisation.

Chapter 2

Virtual photon scattering

In this chapter we discuss some aspects of virtual photon interactions and thereby settle the environment for the main part of this thesis. We will always work in the limit where the center-of-mass energy is much larger than all other energies in the scattering process. This high energy limit is also referred to as the

Regge Limit : all kinematic variables $\ll$ center-of-mass energy

2.1 The photon wave function at LO

Let us consider the scattering of a virtual photon and a massless quark at tree level in the high energy limit; fig. 2.1 shows the notations. It is convenient to use Sudakov variables in this limit. We introduce the light-cone vector $q' = q + xp$ with $q'^2 = p^2 = 0$. It follows that $2pq' = s$ up to terms of order t/s where s and t are the squared cms energy and the momentum transfer, respectively. $Q^2 = -q^2$ is the photon virtuality, $x = Q^2/s$ the Bjorken scaling variable. Now, we decompose all momenta :

$$\begin{aligned} k &= \alpha q' + \beta p + k_\perp \\ r &= \alpha_r q' + x_{I\!P} p + r_\perp \end{aligned}$$

Exploiting the on-shell conditions for the external fermions the Regge limit ($Q^2, |t| \ll s$) in terms of the Sudakov variables reads

$$\alpha \sim 1 \;, \qquad \alpha_r, \beta, x_{I\!P}, \frac{\boldsymbol{k}^2}{s}, \frac{\boldsymbol{r}^2}{s} \ll 1.$$

Here, we used two-dimensional Euclidean transverse vectors, $\boldsymbol{k}^2 = -k_\perp^2$. Fig 2.1 shows the two amplitudes contributing to this process. In the high energy limit the lower quark line simplifies to give

$$\bar{u}(p')\gamma^\mu u(p) \approx 2p^\mu \delta_{\lambda_p, \lambda_{p'}}$$

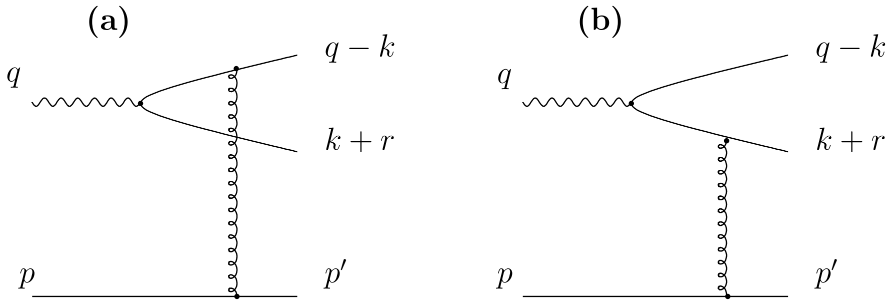

Figure 2.1: the process $\gamma^* + q \to q\bar{q} + q$ at LO

As for the gluon propagator we use the representation

$$g_{\mu\nu} = \frac{2}{s}(q'_\mu p_\nu + q'_\nu p_\mu) + g^{\perp}_{\mu\nu}.$$

The contraction with the lower quark line shows that only the first term in $g_{\mu\nu}$ gives a contribution in our approximation, the others are suppressed by powers of t/s. Thus, from the gluon propagator we retain just p_ν entering the upper part of the amplitudes. As polarisation vectors for the photon we use

$$\epsilon_L = \frac{1}{Q}(q' + xp)\,, \qquad \epsilon_T^{\pm} = \frac{1}{\sqrt{2}}(0, 1, \pm i, 0).$$

We square the sum of the amplitudes and average (sum) over initial (final) helicities and colours of the quarks. We take the sum of the two transverse photon polarisations and obtain:

$$|\mathcal{M}_{L,T}|^2 = 4\, C_F\, g^4 e^2 e_f^2\, \frac{s^2}{\boldsymbol{r}^2}\, \alpha(1-\alpha)\; |\psi_{L,T}(\alpha, \boldsymbol{k})|^2$$

with

$$|\psi_L(\alpha, \boldsymbol{k})|^2 = 4\,\alpha^2(1-\alpha)^2 Q^2 \left(\frac{1}{D(\boldsymbol{k})} - \frac{1}{D(\boldsymbol{k}+\boldsymbol{r})}\right)^2,$$
$$|\psi_T(\alpha, \boldsymbol{k})|^2 = 2\left[\alpha^2 + (1-\alpha)^2\right] \left(\frac{\boldsymbol{k}}{D(\boldsymbol{k})} - \frac{\boldsymbol{k}+\boldsymbol{r}}{D(\boldsymbol{k}+\boldsymbol{r})}\right)^2,$$

where $D(\boldsymbol{k}) = \boldsymbol{k}^2 + \alpha(1-\alpha)Q^2$. Here, g is the strong coupling constant and e is the absolute value of the elementary charge, ee_f gives the charge of the quark. We will see that the function $\psi_{L,T}$ can be interpreted as the amplitude for the transition $\gamma^* \to q\bar{q}$ and hence as a photon wave function.

2.2 The colour dipole picture

The cross section for the process in the last section can be written as

$$\sigma_{L,T}^{\gamma^* q} = \int d\alpha\, d^2\boldsymbol{k}\, d^2\boldsymbol{r} \frac{1}{\boldsymbol{r}^4} \left(\frac{\alpha_s C_F}{\pi}\right) \frac{4\pi\alpha_s}{3} \sum_f e_f^2 \frac{3\alpha_{\mathrm{em}}}{4\pi^2} \left|\psi_{L,T}(\alpha,\boldsymbol{k})\right|^2 \tag{2.1}$$

Now, we exchange the quark by a proton. As we are in the Regge limit we expect, due to Regge factorisation, that the coupling of the proton to the t-channel gluon is independent from the $\gamma^* \to q\bar{q}$ transition. At small x the proton is expected to be dominated by the gluon. The proton is therefore introduced in shape of the unintegrated gluon density $\mathcal{F}(x,\boldsymbol{r}^2)$; to obtain the $\gamma^* p$ cross section we have to exchange in (2.1):

$$\frac{\alpha_s C_F}{\pi} \to \mathcal{F}(x,\boldsymbol{r}^2)$$

$\mathcal{F}$ is connected with the usual gluon density $g(x,Q^2)$ by

$$xg(x,Q^2) = \int^{Q^2} \frac{d^2\boldsymbol{r}}{\pi\boldsymbol{r}^2}\, \mathcal{F}(x,\boldsymbol{r}^2).$$

Let us move from the space of transverse momentum to the transverse coordinate space. The Fourier transform of $\psi_{L,T}$ with respect to $\boldsymbol{k}$ reads

$$\begin{aligned}
\int \frac{d^2\boldsymbol{k}}{(2\pi)^2}\, e^{i\boldsymbol{k}\boldsymbol{\rho}}\, \psi_L(\alpha,\boldsymbol{k}) &= \sqrt{8}\alpha(1-\alpha)Q\, \left(1-e^{-i\boldsymbol{r}\boldsymbol{\rho}}\right) \int \frac{d^2\boldsymbol{k}}{(2\pi)^2} \frac{e^{i\boldsymbol{k}\boldsymbol{\rho}}}{D(\boldsymbol{k})} \qquad (2.2)\\
\int \frac{d^2\boldsymbol{k}}{(2\pi)^2}\, e^{i\boldsymbol{k}\boldsymbol{\rho}}\, \psi_T(\alpha,\boldsymbol{k}) &= 2\sqrt{\alpha^2+(1-\alpha)^2}\, \left(1-e^{-i\boldsymbol{r}\boldsymbol{\rho}}\right) \int \frac{d^2\boldsymbol{k}}{(2\pi)^2}\, e^{i\boldsymbol{k}\boldsymbol{\rho}} \frac{\boldsymbol{k}}{D(\boldsymbol{k})}
\end{aligned}$$

The phase factor $e^{-i\boldsymbol{r}\boldsymbol{\rho}}$ arises from the substitution $(\boldsymbol{k}+\boldsymbol{r}) \to \boldsymbol{k}'$ in the second part of ψ_L. Note that the $\boldsymbol{r}$ dependence appears as a factor now; we therefore define

$$\sqrt{\sum_f e_f^2 \frac{3\alpha_{\mathrm{em}}}{4\pi^2}} \int \frac{d^2\boldsymbol{k}}{(2\pi)^2}\, e^{i\boldsymbol{k}\boldsymbol{\rho}}\, \psi_{L,T}(\alpha,\boldsymbol{k}) = \left(1-e^{-i\boldsymbol{r}\boldsymbol{\rho}}\right) \varphi_{L,T}(\alpha,\boldsymbol{\rho}) \tag{2.3}$$

Now, we express $|\psi|^2$ in the $\gamma^* p$ cross section through the Fourier back transform of (2.2):

$$
\begin{aligned}
\sigma^{\gamma^* p} &= \int d\alpha\, d^2\boldsymbol{k} \frac{d^2\boldsymbol{r}}{\boldsymbol{r}^4} \frac{4\pi\alpha_s}{3} \mathcal{F}(x, \boldsymbol{r}^2) \\
&\times \int \frac{d^2\boldsymbol{\rho}}{(2\pi)^2} e^{-i\boldsymbol{k\rho}} \left(1 - e^{i\boldsymbol{r\rho}}\right) \varphi^*(\alpha, \boldsymbol{\rho}) \\
&\times \int \frac{d^2\boldsymbol{\rho}'}{(2\pi)^2} e^{-i\boldsymbol{k\rho}'} \left(1 - e^{-i\boldsymbol{r\rho}'}\right) \varphi(\alpha, \boldsymbol{\rho}') \\
&= \int d\alpha \frac{d^2\boldsymbol{r}}{\boldsymbol{r}^4} \frac{4\pi\alpha_s}{3} \mathcal{F}(x, \boldsymbol{r}^2) \int \frac{d^2\boldsymbol{\rho}}{(2\pi)^2} \int \frac{d^2\boldsymbol{\rho}'}{(2\pi)^2} (1 - e^{i\boldsymbol{r\rho}})(1 - e^{-i\boldsymbol{r\rho}'}) \\
&\times \int d^2\boldsymbol{k}\, e^{-i\boldsymbol{k}(\boldsymbol{\rho}' - \boldsymbol{\rho})} \varphi^*(\alpha, \boldsymbol{\rho}) \varphi(\alpha, \boldsymbol{\rho}')
\end{aligned}
$$

The second step is just a rearrangement of the terms in order to get the $\delta(\boldsymbol{\rho} - \boldsymbol{\rho}')$ function after performing the $\boldsymbol{k}^2$ integral. We finally cancel this delta function with the $\boldsymbol{\rho}'$ integration and arrive at

$$
\sigma^{\gamma^* p} = \int d\alpha \int d^2\boldsymbol{\rho}\ |\varphi_{L,T}(\boldsymbol{\rho}, \alpha)|^2\, \sigma_{dipole}(\boldsymbol{\rho}) \tag{2.4}
$$

where

$$
\sigma_{dipole} = \frac{4\pi\alpha_s}{3} \int \frac{d\boldsymbol{r}^2}{\boldsymbol{r}^4} \mathcal{F}(x, \boldsymbol{r}^2)(1 - e^{i\boldsymbol{r\rho}})(1 - e^{-i\boldsymbol{r\rho}}). \tag{2.5}
$$

The interpretation of the factorised form (2.4) is the key to the well known colour dipole picture of the γ^*-proton interaction. In the proton rest frame the life time of a $q\bar{q}$ pair is much longer then the time of its interaction with the proton. The function $\varphi(\boldsymbol{\rho}, \alpha)$ is therefore interpreted as the photon wave function for the transition of the virtual photon to a $q\bar{q}$ pair separated by a relative distance $\boldsymbol{\rho}$. The interaction of this colour dipole with the proton is completely incorporated in the dipole cross section σ_{dipole}, see fig. 2.2. Note that the factorisation of the splitting $\gamma^* \to q\bar{q}$ and the dipole interaction is the outcome of a pure perturbative calculation.

As for the wave function (2.3), it may be written in a quite simple form:

$$
|\varphi_L(\alpha, \boldsymbol{\rho})|^2 = \frac{3\alpha_{\rm em}}{2\pi^2} \sum_f e_f^2 4\alpha^2 (1-\alpha)^2 Q^2 K_0^2(\delta\rho) \tag{2.6}
$$

$$
|\varphi_T(\alpha, \boldsymbol{\rho})|^2 = \frac{3\alpha_{\rm em}}{2\pi^2} \sum_f e_f^2 \left[(\alpha^2 + (1-\alpha)^2) K_1^2(\delta\rho)\right] \tag{2.7}
$$

where $\delta^2 = \alpha(1-\alpha)Q^2$ and $\rho = |\boldsymbol{\rho}|$. $K_n(z)$ is a modified Bessel function. Also the function ψ is often referred to as photon wave function. We have presented here only its square, summed over helicities at zero quark mass.

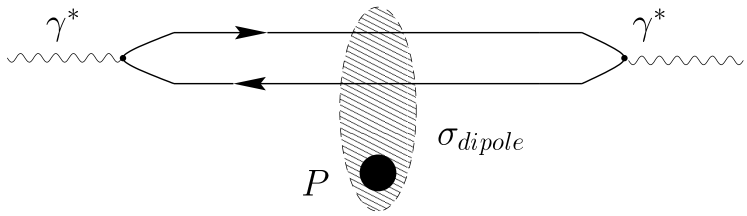

Figure 2.2: The colour dipole picture at LO

In [17, 18] the squared wave function was calculated also with non vanishing quark mass. Instead of squaring and summing over helicities one may calculate the wave function for fixed helicity states of the external fermions, see [19, 20] for massless and [21] for massive quarks.

The dipole cross section (2.5) includes all non-perturbative physics in the process. With decreasing dipole size ρ it vanishes (colour transparency). In the saturation model of Wüsthoff and Golec-Biernat [22, 23] the dipole cross section was parametrised as

$$\sigma_{dipole}(\rho) = \sigma_0(1 - e^{-\rho/R}).$$

For small $\rho \ll R$ colour transparency is realised; for large distances $\rho \gg R$ a constant value σ_0 is approached, in this way unitarity is incorporated. With this relatively simple ansatz HERA data on inclusive DIS could be fitted over a wide range of x and Q^2. With σ_{dipole} determined this way diffractive cross sections have been predicted; the cross section formula differs from the inclusive case only by a square

$$\sigma_{\text{diff}}^{\gamma^* p} = \int d\alpha \int d^2\boldsymbol{\rho} \;\; |\varphi_{L,T}(\boldsymbol{\rho}, \alpha)|^2 \, \sigma^2_{dipole}(\boldsymbol{\rho}) \tag{2.8}$$

The prediction was in very good agreement with the measurements. This can be regarded as a remarkable success of the saturation model and the colour dipole picture.

2.2.1 Extension of the colour dipole model

The main property of the colour dipole picture is the decoupling of the γ^* splitting in a $q\bar{q}$ pair from the interaction with the proton. If this feature holds also at higher orders of α_s we expect further Fock components of the photon wave function to appear

$$|\gamma^* > = |q\bar{q} > + |q\bar{q}g > + |q\bar{q}gg > + \dots$$

These states correspond to higher colour multi-poles participating in the interaction.

At next-to-leading order, in particular, we expect the $q\bar{q}g$ Fock component of the wave function and a corresponding interaction. In addition, there will be corrections to the dipole cross section. It is unclear whether colour transparency is still realised. The answer to these questions is contained in the calculation of the NLO corrections to the process $\gamma^* + q \to q\bar{q} + q'$. The main part of this thesis is the calculation of the real corrections.

2.3 High energy $\gamma^*\gamma^*$ scattering

Let us now come to the process of $\gamma^*\gamma^*$ scattering. We denote the two virtualities by Q_1^2 and Q_2^2, and the squared center of mass energy by s. We are interested in the behaviour of the total $\gamma^*\gamma^*$ cross section in the high energy limit

$$\Lambda_{QCD} \ll Q_1^2, Q_2^2 \ll s. \tag{2.9}$$

From general properties of scattering amplitudes we know that at any order of α_s the total cross section involves (large) logarithms of s. In order to calculate its leading energy dependence it is possible to collect from any order of α_s those terms of type $(\alpha_s \ln s)^n$, this is the leading logarithmic approximation (LLA). The relevant contributions are ladder type diagrams with gluon rungs. The (LO) BFKL equation incorporates the summation of these contributions from all orders in α_s. This summation decouples from the external particles and is therefore of universal nature. The coupling of the external particles, in particular the virtual photons, will be discussed in subsequent sections.

2.3.1 BFKL at LO

In the Regge limit, scattering amplitudes take a specific factorised form. This follows from the assumption of the analyticity for the unitary, Lorentz invariant S-Matrix. Let us consider the process of $2 \to 2$ scattering. $\sqrt{s}$ and t are the center-of-mass energy and the momentum transfer,respectively. The amplitude for this process in the Regge limit (with negative signature) reads

$$\mathcal{A}_8 = \frac{s}{t}\Gamma_A(t)\left[\left(\frac{s}{-t}\right)^{\omega(t)} + \left(\frac{-s}{-t}\right)^{\omega(t)}\right]\Gamma_B(t)\,. \tag{2.10}$$

The vertices $\Gamma_{A,B}$ and ω are now considered as functions of the strong coupling and expanded

$$\begin{aligned}\omega(t) &= g^2\omega^{(1)}(t) + g^2\omega^{(2)}(t)\\ \Gamma_{A,B} &= g\Gamma^{(0)}_{A,B} + g^2\Gamma^{(1)}_{A,B},\end{aligned}$$

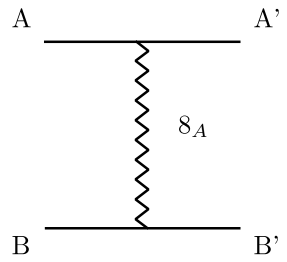

Figure 2.3: The reggeized gluon

(2.10) then becomes

$$\mathcal{A}_8 = \alpha_s \frac{s}{t} \left\{ 2\Gamma_A^{(0)}\Gamma_B^{(0)} + \alpha_s \Gamma_A^{(0)} \omega^{(1)} \left[\ln \frac{s}{-t} + \ln \frac{-s}{-t} \right] \Gamma_B^{(0)} \right.$$
$$\left. + 2\alpha_s (\Gamma_A^{(0)}\Gamma_B^{(1)} + \Gamma_A^{(1)}\Gamma_B^{(0)}) \right\} \quad (2.11)$$

The perturbative calculation of $\mathcal{A}_8$ reveals the same analytical structure as (2.11) and the vertices and $\omega^{(1)}$ can be calculated. Note that the first two terms are of type $(\alpha_s \ln s)^n$, that is, they contribute to the LLA. It is easy to see that we have to use $\Gamma_{A,B}^{(0)}$ and $\omega^{(1)}$ in (2.10) in order obtain the LLA terms in the expansion. It is assumed that at each order in α_s there will be agreement with the perturbative calculation. This is the assumption of the reggeization of the gluon. It guarantees that with the knowledge of $\Gamma_{A,B}^{(0)}$ and $\omega^{(1)}$, which are obtained from a pQCD calculation at order α_s^2, (2.10) provides us with the sum of the diagrams from all orders in α_s each of them taken in the LLA. The Regge trajectory of the gluon is

$$j(t) = 1 + \omega(t)$$

and corresponds in particular to the exchange of an antisymmetric colour octet. We symbolise the amplitude with gluon quantum numbers in the t-channel (2.10) as depicted in fig.2.3 .

In order to determine the trajectory ω we consider quarks as external particles, $q + q \to q' + q'$. The comparison of the tree level diagram with (2.11) leads to

$$\Gamma_{qq}^a = t_{ij}^a \delta_{hh'}.$$

Here, h h' denote the helicities of incoming and outgoing quark; t_{ij}^a is the colour group generator which corresponds to colour octet exchange. At the one loop level we expect a logarithm of the energy to appear. With the knowledge of Γ_{qq}^a we can extract ω according to (2.11). In $D = 4 - 2\epsilon$ space-

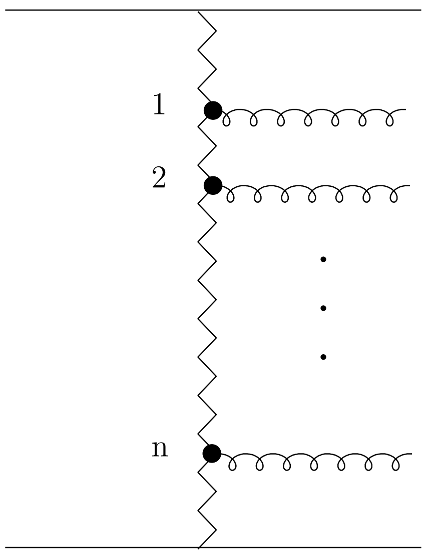

Figure 2.4: The Regge ansatz for the n-gluon production amplitude

time dimensions the gluon trajectory (minus 1) at leading order reads:

$$\omega^{(1)}(t) = \frac{2g^2 N_c}{(4\pi)^{2-\epsilon}} \frac{c_\Gamma \, (-t)^{-\epsilon}}{\epsilon} \tag{2.12}$$

with N_c being the number of colours and $c_\Gamma = 1 - \gamma_E \epsilon + \mathcal{O}(\epsilon^2)$.

Now, we come back to our original purpose of calculating the LLA contributions to the total $\gamma^*\gamma^*$ cross section, or, equivalently, the imaginary part of the elastic scattering amplitude at $t = 0$. We consider general particles A B because due to Regge factorisation we expect the t-channel exchange to be independent of the external particles. The properties of the photon will come in later. We are now faced with the exchange of a colour singlet. It is our knowledge about the colour octet exchange we will make use of to construct the contributions to the LLA in case of colour singlet exchange. Those final states in the process $A + B \to X$ that give rise to logarithms of the energy consist of gluons. The imaginary part of the elastic scattering amplitude can therefore be expressed through the sum over all these states:

$$\mathcal{I}m_s \mathcal{A}_{AB}^{A'B'} = \sum_{n=0}^{\infty} \sum_f \int \left(\mathcal{A}_{AB}^{A'B'+n} \right)^* \mathcal{A}_{AB}^{A'B'+n} d\Phi_{2+n}. \tag{2.13}$$

Here, n is the number of gluons and $d\Phi_{2+n}$ denotes the $(2+n)$-particle phase space measure. Let p_A, p_B be the initial state light cone momenta. k_i denotes the momentum of the i-th produced gluon; we introduce Sudakov variables:

$$k_i = \alpha_i p_A + \beta_i p_B + k_{i\perp}.$$

In the LLA, each gluon must provide a logarithm of the energy. This corresponds to the requirement that all gluons are separated from each other by large rapidity gaps. This is the Multi-Regge-Kinematic (MRK); in terms of the Sudakov variables it means:

$$1 \gg \alpha_1 \gg \alpha_2 \ldots \gg \alpha_{n+1} \gg -t/s \tag{2.14}$$
$$-t/s \ll \beta_1 \ll \beta_2 \ldots \ll \beta_{n+1} \ll 1 \tag{2.15}$$

and the momenta transfer in the t-channel $t_i = -\boldsymbol{q}_i^2$ must be fixed.

We make a Regge ansatz for the n-gluon production amplitude

$$\begin{aligned}\mathcal{A}_{AB}^{A'B'+n} &= 2s \\ &\times \Gamma_{AA'}^{c_1} \left[\left(\frac{s_1}{s_0} \right)^{\omega(t_1)} \frac{1}{t_1} \right] \gamma_{c_1 c_2}^{a_1} \ldots \gamma_{c_n c_{n+1}}^{a_n} \left[\left(\frac{s_{n+1}}{s_0} \right)^{\omega(t_{n+1})} \frac{1}{t_{n+1}} \right] \Gamma_{BB'}^{c_{n+1}}\end{aligned} \tag{2.16}$$

In the t-channel, there are reggeized gluons, giving rise to n+1 propagators with momentum transfer $t_1 \ldots t_{n+1}$. The energy scale s_0 is irrelevant here, but will become important in the NLLA. The final state gluons carry the colour index a_i and couple to the reggeized gluons via the Reggeon-Reggeon-gluon (RRG) vertex $\gamma_{c_i c_{i+1}}^{a_i}$. The nature of the external particles is completely contained in the vertices Γ_A, Γ_B. Fig. 2.4 visualises the Regge ansatz (2.16) for the n-gluon production amplitude.

Let us demonstrate the calculation of the RRG vertex. It can be ex-

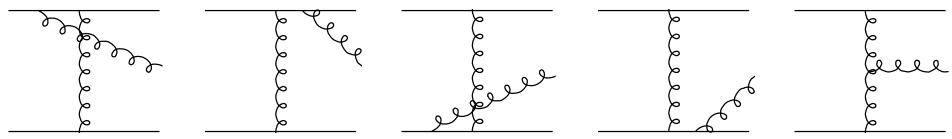

Figure 2.5: The contributions to the RRG vertex

tracted from the $qq \to qq + g$ amplitude (in the Regge limit) at tree level. The contributing diagrams are shown in fig. 2.5. The sum of these diagrams factorises into two vertices Γ_{qq}^0, two propagators of reggeized gluons at lowest order (being equal to the gluon propagators), and the RRG vertex. One identifies

$$\gamma_{c_i c_{i+1}}^{a_i} = g f_{c_i c_{i+1} a_i} e_\mu^* C\mu. \tag{2.17}$$

Here, e^*_μ is the polarisation vector of the emitted gluon, $f_{c_i c_{i+1} a_i}$ is the structure constant of SU(N) and C^μ reads

$$C^\mu(q_{i+1,q_i}) = -(q_i + q_{i+1})^\mu_\perp - \left(\alpha_i + \frac{2\boldsymbol{q}_i^2}{\beta_{i+1}s}\right) p_A^\mu - \left(\beta_{i+1} + \frac{2\boldsymbol{q}_{i+1}^2}{\alpha_i s}\right) p_B^\mu. \tag{2.18}$$

For the next steps needed to obtain $\mathcal{I}m_s \mathcal{A}_{AB}^{A'B'}$ (2.13), we consider its partial wave. Since we are interested in the elastic forward amplitude we contract the t-channel colour states with the singlet projector. The phase space integration is performed respecting the MRK kinematics. The partial wave can finally be presented in a form where a Green function $\mathcal{G}_\omega$ incorporates the sum of the gluon ladders with any number of rungs. $\mathcal{G}_\omega$ may therefore be called the Green function for the scattering of two reggeized gluons. The sum can be written as the perturbative solution of an integral equation, the famous BFKL equation [2]:

$$\omega \mathcal{G}_\omega(\boldsymbol{q}_1, \boldsymbol{q}_2) = \delta^{D-2}(\boldsymbol{q}_1 - \boldsymbol{q}_2) + \int d^{D-2}q\, \mathcal{K}(\boldsymbol{q}_1, \boldsymbol{q})\, \mathcal{G}_\omega(\boldsymbol{q}, \boldsymbol{q}_2). \tag{2.19}$$

The integral kernel reads

$$\mathcal{K}(\boldsymbol{q}_1, \boldsymbol{q}_2) = 2\omega^{(1)}(-\boldsymbol{q}_1^2)\, \delta^{D-2}(\boldsymbol{q}_1 - \boldsymbol{q}_2) + \mathcal{K}_r(\boldsymbol{q}_1, \boldsymbol{q}_2). \tag{2.20}$$

It has two contributions. While the gluon trajectory $\omega^{(1)}$ (2.12) can be thought of as the virtual part, $\mathcal{K}_r$ contains the gluon production

$$\begin{aligned}\mathcal{K}_r(\boldsymbol{q}_1, \boldsymbol{q}_2) &= \frac{1}{2(2\pi)^{D-1}(N_c - 1)\boldsymbol{q}_1^2 \boldsymbol{q}_2^2} \sum_{c_1 c_2, a} \left|\gamma^a_{c_1 c_2}(\boldsymbol{q}_1, \boldsymbol{q}_2)\right|^2 \\ &= \frac{g^2 N_c}{(2\pi)^{D-1}} \frac{2}{(\boldsymbol{q}_1 - \boldsymbol{q}_2)^2}.\end{aligned} \tag{2.21}$$

Note that the $\mathcal{K}_r$ would lead to an infrared divergent integral. However, $\omega^{(1)}$ includes an infrared pole (2.12). These divergences cancel and the BFKL equation is infrared finite.

As for the solution to (2.19) the kernel averaged over the azimuthal angle between $\boldsymbol{q}_1$ and $\boldsymbol{q}_2$ is considered. It is the averaged kernel that determined the high energy behaviour of the total cross section. The BFKL equation can be diagonalised by means of the eigenfunctions $(\boldsymbol{q}_2^2)^{\gamma-1}$ of the kernel :

$$\int d^{D-2}q\, \mathcal{K}(\boldsymbol{q}_1, \boldsymbol{q})(\boldsymbol{q}^2)^{\gamma-1} = \frac{N_c \alpha_s}{\pi} \chi^B(\gamma)(\boldsymbol{q}_1^2)^{\gamma-1} \tag{2.22}$$

with the eigenvalues

$$\chi^B(\gamma) = 2\psi(1) - \psi(\gamma) - \psi(1-\gamma), \qquad \psi(\gamma) = \Gamma'(\gamma)/\Gamma(\gamma).$$

The set of eigenfunctions with $\gamma = 1/2 + i\nu$, where the real ν ranges between $-\infty$ and ∞ is complete. The growth of the total cross section that follows from BFKL is given by the eigenvalue $\chi(\gamma = 1/2) = 4 \ln 2$. One obtains

$$\omega_{BFKL} = \frac{4N_c \ln 2}{\pi}.$$

With $\omega_{\mathrm{BFKL}} \approx 0.5$ at $\alpha_s = 0.2$ this growth is much too strong compared to the measurements.

2.3.2 BFKL at NLO

In the next-to-leading approximation all terms of type $\alpha_s(\alpha_s \ln s)^n$ are collected. The procedure to sum up the contributions to the total cross section is equal to the one in the LLA: A Regge ansatz is made for any amplitude that contributes. The result is presented in the form of the NLO BFKL equation. As in the LLA, in the t-channel of the amplitudes the gluon quantum numbers are exchanged in this approximation. Thus, the gluon reggeization plays the key rôle also here.

One class of contributions is that of n-gluon final states in the MRK. (2.13) and (2.16) are still valid. However, the next-to-leading order corrections to the gluon trajectory and to the RRG vertex have to be included now. The two-loop corrections to the gluon trajectory, $\omega^{(2)}$, have been calculated in [27]. The corrections to the gluon productions vertex were obtained in [28]. Both corrections are obtained in the same manner as demonstrated for $\omega^{(1)}$: for an appropriate processes the perturbative calculation is compared to the Regge ansatz which allows the extraction of the desired component. Note that in the MRK also next-to-leading corrections to the particle-particle-Reggeon vertices $\Gamma_{A,B}$ (see (2.16)) lead to an amplitude that contributes to the NLLA. These corrections do not affect the summation of the ladder diagrams; therefore they are included in the impact factor for the scattering particle rather than in the Green function, see below.

The other way to obtain a term of type $\alpha_s(\alpha_s \ln s)^n$ is to drop a logarithm of s in an amplitude of the LLA. This is achieved in the configuration where not all final state particles are separated in rapidity, but two of them are close to each other. This is called the Quasi-Multi-Regge-kinematics (QMRK); the Sudakov variables are strongly ordered (2.14) except for one pair of particles. Besides two gluons also a $q\bar{q}$ pair in the Reggeon-Reggeon collision leads to a loss of a logarithm and therefore contributes to the NLLA. The corresponding vertices (RRGG and RRQQ) are needed at Born level, they were calculated in [29] and [30], respectively.

The different sources of NLL effects are shown in fig.2.6. The summation of the contributions in this approximation leads to the NLO BFKL equation,

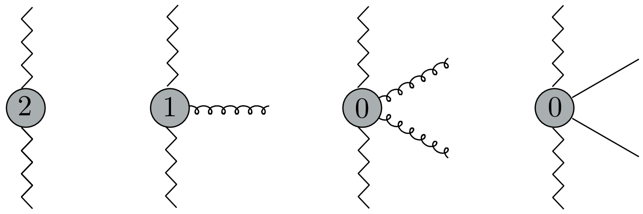

Figure 2.6: The sources of contributions to the NLLA

which has the same form as (2.19); it is the kernel that has changed [3, 4]. Also here, the infrared divergences in the kernel cancel.

The work on these next-to-leading corrections to BFKL stretched over almost ten years. The calculation of the NLO correction to the intercept ω_{BFKL} reveals a surprising result: the corrections compared to LO were large and even led to a negative intercept for moderate α_s. The reason for this turned out to originate from the two particle production in QMRK. Since no restrictions on the transverse momenta had been imposed, final states are possible where the transverse momenta of the two gluons or quarks are strongly ordered. This leads to large logarithms of transverse momenta that destabilise the expansion in $\alpha_s \ln s$.

As one solution to this problem the restriction of the produced particles in rapidity (rapidity veto effect) has been discussed, [36]. In [37] a complete DGLAP resummation of these large logarithms has been performed. Both approaches lead to a substantial change in the dependence of ω_{BFKL} on α_s; for $\alpha_s = 0.2$ the intercept turned out to range between 0.3 and 0.4. Due to this encouraging result is is promising to apply the NLO BFKL approach to various processes as, e.g., DIS, and in particular $\gamma^*\gamma^*$ scattering.

2.3.3 The application of BFKL

As already argued, virtual photons are ideal objects for perturbative QCD. In [31, 32], the calculation of the $\gamma^*\gamma^*$ total hadronic cross section has therefore been considered as a test of BFKL. At LEP, this cross section has been measured from the process $e^+ + e^- \to e^+ + e^+ X$ [34, 35]; it turned out to be much smaller than the LO BFKL prediction [33, 34]. The measurement lies well above the constant result from 2-gluon exchange.

Besides this disagreement there are some uncertainties connected with the application of BFKL at LO: In the LLA the choice of the energy scale is arbitrary; strictly speaking, the absolute value to the cross section is therefore not predictable. Secondly, α_s is not running at LO BFKL. In [33] it has been demonstrated that the variation of the cross section both with the energy scale and with α_s is considerable. However, the prediction from

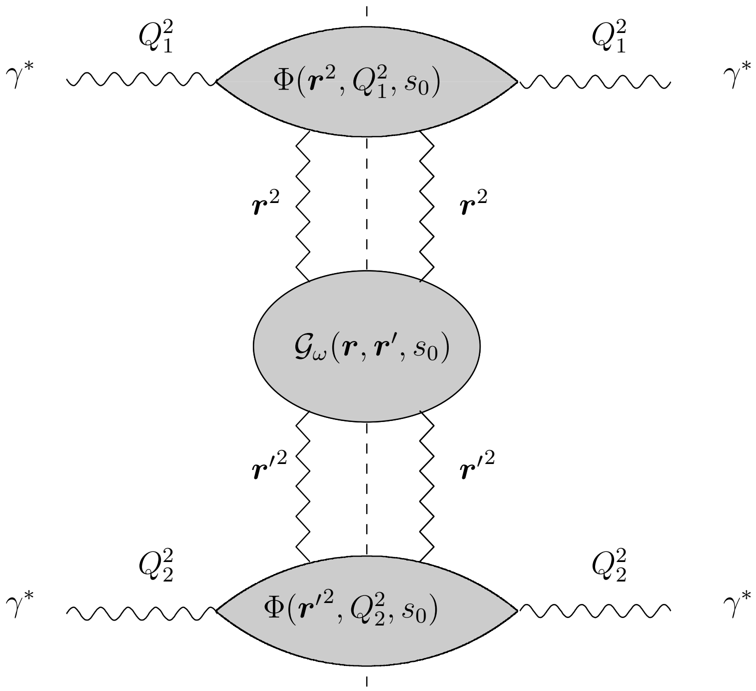

Figure 2.7: The $\gamma^*\gamma^*$ total cross section

LO BFKL still appears to be too large compared to the data from LEP. The NLO corrections seem to be clearly needed. The predicted exponent determining the growth with energy is approximately the same as measured. However, in order to perform a serious test of BFKL at NLO the photon impact factor at NLO must be known.

Let us state the total cross section as it appears in the BFKL approach. The Regge factorisation of amplitudes enabled the resummation of the contributions to the (N)LLA independently of the external particles. In the total cross section, this leads to the factorisation of the Green function $\mathcal{G}_\omega$ and impact factors $\Phi_{A,B}$.

$$\begin{aligned}\sigma_{AB}^{tot} =& \frac{1}{(2\pi)^{D-2}} \int \frac{d^{D-2}\boldsymbol{k}}{\boldsymbol{k}^2} \int \frac{d^{D-2}\boldsymbol{k}'}{\boldsymbol{k}'^2} \\ & \times \Phi_A(\boldsymbol{k}, s_0) \left[\int_{\delta-i\infty}^{\delta+i\infty} \frac{d\omega}{2\pi i} \left(\frac{s}{s_0}\right)^\omega \mathcal{G}_\omega(\boldsymbol{k}, \boldsymbol{k}', s_0) \right] \Phi_B(\boldsymbol{k}, s_0) \qquad (2.23)\end{aligned}$$

The impact factor contains all properties of the particle and is basically the squared particle-particle-Reggeon vertex integrated over the phase space; for the precise definition, see the next chapter. Fig.2.7 shows the total cross section (2.23), or equivalently the imaginary part of the elastic amplitude, in the case of $\gamma^*\gamma^*$ scattering.

It is an important difference w.r.t. the LLA that the NLO impact factors depend on the energy scale. Introducing another scale s_1 (2.23) reads

$$\begin{aligned}\sigma_{AB}^{tot} =& \frac{1}{(2\pi)^{D-2}} \int \frac{d^{D-2}\boldsymbol{k}}{\boldsymbol{k}^2} \int \frac{d^{D-2}\boldsymbol{k}'}{\boldsymbol{k}'^2} \\ & \times \left(\frac{s_1}{s_0}\right)^{\omega} \Phi_A(\boldsymbol{k}, s_0) \left[\int_{\delta-i\infty}^{\delta+i\infty} \frac{d\omega}{2\pi i} \left(\frac{s}{s_1}\right)^{\omega} \mathcal{G}_\omega(\boldsymbol{k}, \boldsymbol{k}', s_0)\right] \Phi_B(\boldsymbol{k}, s_0)\end{aligned}$$

Since s_0, s_1 are fixed i.e. do not grow with s, the additional factor leads to subleading logarithms and can be neglected in the LLA. In the NLLA, however, it has to be kept and there is freedom in its distribution among the Green function and the impact factors. As the cross section is independent of s_0, the choice of the energy scales in the Green function and in the impact factors has to be consistent.

2.3.4 The limit $Q_1^2 \ll Q_2^2$

Let us consider now the $\gamma^*\gamma^*$ total cross section in NLO BFKL (2.23) with the symmetric choice of the energy scale $s_0 = k_1 k_2$, where $k_i = |\boldsymbol{k}_i|$. In the limit $Q_1^2 \ll Q_2^2$ a more physical scale may be given by $Q_1 Q_2$. We therefore write

$$\begin{aligned}\sigma_{\gamma^*\gamma^*}^{tot} =& \frac{1}{(2\pi)^{D-2}} \int \frac{d^{D-2}\boldsymbol{k}}{\boldsymbol{k}^2} \int \frac{d^{D-2}\boldsymbol{k}'}{\boldsymbol{k}'^2} \int_{\delta-i\infty}^{\delta+i\infty} \frac{d\omega}{2\pi i} \\ & \times \Phi_{\gamma^*}(\boldsymbol{k}, Q_1) \left(\frac{Q_1}{k}\right)^{\omega} \left[\left(\frac{s}{Q_1 Q_2}\right)^{\omega} \mathcal{G}_\omega(\boldsymbol{k}, \boldsymbol{k}')\right] \Phi_{\gamma^*}(\boldsymbol{k}', Q_2) \left(\frac{Q_2}{k'}\right)^{\omega}\end{aligned} \tag{2.24}$$

Here, we suppressed the dependence of the green function on the energy scale. Now, we introduce the representation of the Green function in the Mellin space

$$\mathcal{G}_\omega(\boldsymbol{k}, \boldsymbol{k}') = \int \frac{d\gamma}{2\pi i} \left(\frac{k^2}{k'^2}\right)^{\gamma} \frac{1}{\omega - \chi(\gamma)};$$

$\chi(\gamma)$ is the eigenfunction of the kernel. Putting this into (2.24) and reshuffling the terms the total cross section can be cast into the form:

$$\sigma_{\gamma^*\gamma^*}^{tot} = \frac{1}{(2\pi)^{D-2}} \int_{\delta-i\infty}^{\delta+i\infty} \left(\frac{s}{Q_1 Q_2}\right)^{\omega} \int \frac{d\gamma}{2\pi i} \left(\frac{Q_1^2}{Q_2^2}\right)^{\gamma} \frac{\psi(\gamma - \frac{\omega}{2})\psi(-\gamma - \frac{\omega}{2})}{\omega - \chi(\gamma)}. \tag{2.25}$$

The function ψ is the Mellin transform of the impact factor:

$$\psi(\nu, Q) = \int \frac{d^2\boldsymbol{k}}{\boldsymbol{k}^2} \left(\frac{Q^2}{\boldsymbol{k}^2}\right)^{\nu} \Phi_{\gamma^*}(\boldsymbol{k}, Q) \tag{2.26}$$

In the collinear limit $Q_1^2 \ll Q_2^2$ the cross section (2.25) has to agree with the known result from the DGLAP resummation. This condition is used in [37] to restrict the choice of a physical energy scale.

The collinear limit of (2.25) corresponds to a certain structure of poles in the γ-space. With the knowledge of σ^{tot} in this limit part of the pole structure of ψ has been predicted in [39]. However, in order to compute the absolute value of the total $\gamma^*\gamma^*$ cross section, in particular for $Q_1^2 \sim Q_2^2$, the complete calculation of the NLO γ^* impact factor Φ_{γ^*} is needed. With the result for Φ_{γ^*} the collinear poles can be calculated via (2.26) and the predictions for them can be checked.

Chapter 3

The NLO γ^* impact factor

We come now to the central object of this thesis, the NLO γ^* impact factor. Fig.3.1 shows the different contributions. The virtual corrections (a) stem from the on-loop corrections to the $q\bar{q}$ production vertex which are known. The other type of corrections are due to the emission of an additional gluon (b) and represent the subject of this work.

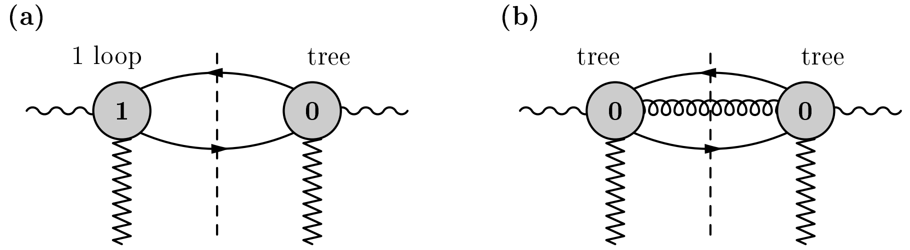

Figure 3.1: The NLO contributions to the γ^* impact factor.

In this chapter we will start with an accurate definition of impact factors. After a short discussion of the LO impact factor we summarise the results for the virtual corrections. The calculation of the real corrections is subject to the next chapter.

3.1 The definition of impact factors

Let us consider the elastic scattering of two particles A and B with momenta p_A and p_B in the Regge limit ($s \to \infty$, $t =$ fixed). In leading order in α_s we write the scattering amplitude T_{AB} in the form:

$$T^{(0)}_{AB}(s, t = q^2) = is \int \frac{d^{D-2}\boldsymbol{r}}{(2\pi)^{D-2}} \tilde{\Phi}^{(0)}_A \frac{1}{\boldsymbol{r}^2} \frac{1}{(\boldsymbol{q}-\boldsymbol{r})^2} \tilde{\Phi}^{(0)}_B \, . \tag{3.1}$$

The impact factors $\Phi_A^{(0)}$ and $\Phi_B^{(0)}$ for the external particles (quarks, gluons, or photons) are of order α_s. The exchanged gluons carry transverse momenta $\boldsymbol{r}$ and $(\boldsymbol{q}-\boldsymbol{r})$ respectively. Taking the cut amplitude we define the total cross section for the scattering of A and B via the optical theorem as

$$\sigma_{AB}^{(0)} = \frac{1}{s}\mathrm{Im}T_{AB}^{(0)}(s,t=0) = \int \frac{d^{D-2}\boldsymbol{r}}{(2\pi)^{D-2}}\Phi_A^{(0)}\frac{1}{\boldsymbol{r}^4}\Phi_B^{(0)}\,. \tag{3.2}$$

Here we have dropped the tilde symbol on the impact factors to denote the additional s-channel cut. This equation can be used as the definition of the leading order impact factors $\Phi_A^{(0)}$ and $\Phi_B^{(0)}$. Note that we have summed over the colour indices of the t-channel gluons implicitly. The total cross section can also be written as

$$\sigma_{AB}^{(0)} = \frac{1}{2s}\int |\mathcal{M}_{AB}^{(0)}|^2 d\phi\,, \tag{3.3}$$

where $1/2s$ denotes the flux factor (in the high energy limit), $\mathcal{M}_{AB}^{(0)}$ the matrix element for the scattering process $A+B \to A'+B'$ with the exchange of a gluon, and $d\phi$ stands for the phase space of the final state $A'+B'$. For our case of interest, $\gamma^* q$ (or $\gamma^*\gamma^*$) scattering, A' denotes a $q\bar{q}$ pair, B' a quark (or a $q\bar{q}$ pair).

In the Regge limit, the scattering amplitude $\mathcal{M}_{AB}$ for the scattering $A+B \to A'+B'$ (with the invariant masses of the particles or systems A' and B' being finite (Fig. 3.2) is described by the exchange of a reggeized gluon and can be written in the following form:

$$\mathcal{M}_{AB} = \frac{s}{t}\Gamma^a_{A\to A'}\left[\left(\frac{s}{-t}\right)^{\omega(t)} + \left(\frac{-s}{-t}\right)^{\omega(t)}\right]\Gamma^a_{B\to B'}\,. \tag{3.4}$$

The index a denotes the colour of the exchanged reggeized gluon. In leading order, we put $\omega(t)$ in (3.4) equal to zero and obtain

$$\mathcal{M}_{AB}^{(0)} = \Gamma^{(0),a}_{A\to A'}\frac{2s}{t}\Gamma^{(0),a}_{B\to B'}\,. \tag{3.5}$$

Inserting this expression into (3.3), we arrive at (3.2).

In the next order, α_s^3, eq.(3.2) receives several corrections. In order to illustrate the general pattern it is instructive to start from (3.3). There are three new contributions on the right-hand-side of (3.3). The first one comes from the same intermediate state A', B' as in the leading order case, but there are higher order corrections inside the vertex functions $\Gamma_{A\to A'}$ or $\Gamma_{B\to B'}$ of the scattering amplitude $A+B \to A'+B'$ (or its complex conjugate). A second correction is due to the reggeization of the exchanged gluon: from (3.4) it follows that in next-to-leading order reggeization provides an

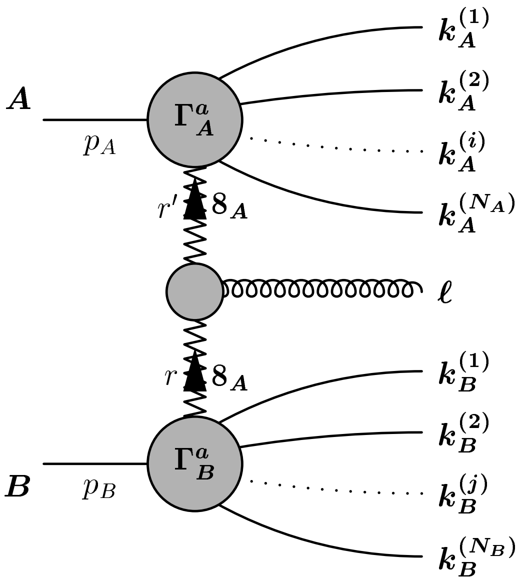

Figure 3.2: Kinematics for $A{+}B \to A'{+}B'$ with initial state momenta p_A, p_B and final state momenta k^i_A, k^j_B. An $\mathbf{8}_A$-Reggeon is exchanged, emitting a real gluon with momentum ℓ which is supposed to be separated from the other final state particles by large rapidity gaps.

extra term in $\mathcal{M}_{AB}$ proportional to $\Gamma^{(0),a}_{A\to A'}\omega(t)\ln(s/-t)\Gamma^{(0),a}_{B\to B'}$. The third correction comes from the production of an extra gluon in the intermediate state : $A + B \to A' + g + B'$. In the high energy limit, we divide this intermediate state into configurations with one or two large rapidity gaps: in the former case, the extra gluon belongs to the fragmentation region of A or B and the corresponding Regge ansatz of the amplitude involves the the vertex $\Gamma^{(0),a}_{X\to X'g}$ (X being A, B); in the latter case the gluon belongs to the central region, the Regge ansatz now includes the Reggeon-Reggeon-gluon vertex (see sec.4.3).

Correspondingly, we separate the integral over the phase space $d\phi$. We begin with the configuration with one single rapidity gap. If $N_{A'}$ ($N_{B'}$) particles in the final state belong to the system A' (B') and carry momenta $k^i_{A'}$ ($k^j_{B'}$), we may write the phase-space in D dimensions explicitly as

$$d\phi = d\tilde{\phi}_{A'}d\tilde{\phi}_{B'}(2\pi)^D\delta^{(D)}(p_A + p_B - \textstyle\sum_i k^i_{A'} - \sum_j k^j_{B'}) \qquad (3.6)$$

with

$$d\tilde{\phi}_{A'} = \prod_{i=1}^{N_A} \frac{d^D k^i_{A'}}{(2\pi)^{D-1}}\delta^+({k^i_{A'}}^2 - {m^i_A}^2) \qquad (3.7)$$

and

$$d\tilde{\phi}_{B'} = \prod_{j=1}^{N_B} \frac{d^D k_{B'}^j}{(2\pi)^{D-1}} \delta^+ ({k_{B'}^j}^2 - {m_B^j}^2) \,. \tag{3.8}$$

Introducing the explicit integration over the Reggeon momentum r with a Sudakov decomposition $r = \alpha_r q' + \beta_r p + r_\perp$ via one extra delta function and

$$\frac{d^D r}{(2\pi)^D} = \frac{s}{2} \frac{d\alpha_r}{2\pi} \frac{d\beta_r}{2\pi} \frac{d^{D-2}\boldsymbol{r}}{(2\pi)^{D-2}} \tag{3.9}$$

we may write

$$d\phi = d\phi_{A'} \frac{s d\beta_r}{2\pi} d\phi_{B'} \frac{s d\alpha_r}{2\pi} \frac{1}{2s} \frac{d^{D-2}\boldsymbol{r}}{(2\pi)^{D-2}} \,, \tag{3.10}$$

where $d\phi_{A'} = d\tilde{\phi}_{A'} (2\pi)^D \delta^{(D)}(p_A + r - \sum_i k_{A'}^i)$ and $d\phi_{B'} = (2\pi)^D d\tilde{\phi}_{B'} \delta^{(D)}(p_B - r - \sum_j k_{B'}^j)$ are the usual phase space measures for the final state particles belonging to the systems A' and B' respectively. For an intermediate state with two rapidity gaps (gluon in the central region) we have two t-channel Reggeon momenta, r and r'. Denoting the momentum of the produced gluon by $\ell \equiv r - r' = \alpha_\ell q' + \beta_\ell p + \ell_\perp$ eq. (3.10) will be generalised to:

$$d\phi = (\frac{1}{2s})^2 \;\; d\phi_{A'} \frac{s d\beta_r}{2\pi} \;\; \frac{s d\alpha_r}{2\pi} d\phi_g \frac{s d\beta_{r'}}{2\pi} \;\; \frac{s d\alpha_{r'}}{2\pi} d\phi_{B'} \;\; \frac{d^{D-2}\boldsymbol{r}}{(2\pi)^{D-2}} \frac{d^{D-2}\boldsymbol{r}'}{(2\pi)^{D-2}} \tag{3.11}$$

where

$$d\phi_g = \frac{d^D \ell}{(2\pi)^{D-1}} \delta^+(\ell^2) (2\pi)^D \delta^{(D)}(r - r' + \ell) \tag{3.12}$$

is the phase space measure for the gluon in the central region.

Returning to the impact factor representation (3.2), the NLO corrections due to the extra gluon in the s-channel can be grouped into two parts. The gluon in the fragmentation region of A or B leads to corrections of the impact factor Φ_A or Φ_B, respectively, whereas the gluon in the central region represents the first rung of the BFKL ladder (in the leading-logarithmic approximation) [2]. Together with the other NLO corrections mentioned before, the entire sum of NLO corrections to the total cross section can be cast into the following form:

$$\begin{aligned}
\sigma_{AB}^{(1)} &= \frac{1}{s} \mathrm{Im}\, T_{AB}^{(1)}(s, t=0) \\
&= \int \frac{d^{D-2}\boldsymbol{r}}{(2\pi)^{D-2}} \Phi_A^{(1)} \frac{1}{\boldsymbol{r}^4} \Phi_B^{(0)} + \int \frac{d^{D-2}\boldsymbol{r}}{(2\pi)^{D-2}} \Phi_A^{(0)} \frac{1}{\boldsymbol{r}^4} \Phi_B^{(1)} \\
&\quad + \int \frac{d^{D-2}\boldsymbol{r}}{(2\pi)^{D-2}} \Phi_A^{(0)} \ln(s/\boldsymbol{r}^2) 2\omega^{(1)}(\boldsymbol{r}^2) \frac{1}{\boldsymbol{r}^4} \Phi_B^{(0)} \\
&\quad + \ln(s/s_0) \int \frac{d^{D-2}\boldsymbol{r}}{(2\pi)^{D-2}} \frac{d^{D-2}\boldsymbol{r}'}{(2\pi)^{D-2}} \Phi_A^{(0)} \frac{1}{\boldsymbol{r}^4} \mathcal{K}_{\mathrm{real}}(\boldsymbol{r}, \boldsymbol{r}') \frac{1}{\boldsymbol{r}'^4} \Phi_B^{(0)} \,.
\end{aligned} \tag{3.13}$$

Here $\mathcal{K}_{real}(\boldsymbol{r}, \boldsymbol{r}')$ denotes the square of the gluon production vertex, the BFKL kernel. Later on it will be convenient to rewrite the reggeization of the gluon (third term on the right-hand-side): putting $\ln(s/\boldsymbol{r}^2) = \ln(s/s_0) + \ln(s_0/\boldsymbol{r}^2)$ the $\ln(s/s_0)$ piece will cancel the infrared singularity of the BFKL Kernel in the limit $\boldsymbol{r} - \boldsymbol{r}' \to 0$.

Note that the property of factorisation of amplitudes in the Regge limit (3.4) has led to the factorisation of the impact factors in the expression for the total cross section at lowest order (3.2) and also at next order in α_s (3.13). This feature is a general consequence of Regge theory and is expected to hold in arbitrary order perturbation theory. For the impact factor we state the general definition:

$$\Phi_A = \frac{\delta^{ab}}{\sqrt{N_c^2 - 1}} \sum_{A'} \int \left\langle \Gamma^a_{A \to A'} \Gamma^{b\,*}_{A \to A'} \right\rangle d\phi_{A'} \frac{s d\beta_r}{2\pi} \tag{3.14}$$

The average symbol $\langle\rangle$ stands for the sum over colour and helicity in the intermediate state A'. In the following we will use the short hand notation

$$\Phi_A = \sum_{A'} \int |\Gamma_{A \to A'}|^2 d\phi_{A'} \frac{s d\beta_r}{2\pi}, \tag{3.15}$$

In particular, in the square of the matrix elements we have included the colour projector $\delta^{ab}/\sqrt{N_c^2 - 1}$.

3.2 The γ^* impact factor at LO

For future reference, and in order to define the notation the Born level impact factor shall be briefly discussed. The amplitude $T_{\gamma^* q}$ for the scattering $\gamma^* + q' \to q\bar{q} + q'$ (Fig. 3.3) has been calculated in [10] to next-to-leading order in α_s. We write $T_{\gamma^* q}$ as an expansion in the strong coupling g

$$T_{\gamma^* q} = g^2 T^{(0)}_{\gamma^* q} + g^4 T^{(1)}_{\gamma^* q} . \tag{3.16}$$

The momenta are labelled as in Fig. 3.3. The kinematical variables we use are the centre-of-mass energy s of the incoming virtual photon and the incoming quark, the virtuality of the photon, Q^2, the Bjorken variable $x = Q^2/2p \cdot q$, the momentum transfers $t = r^2$, $t_a = k^2$, $t_b = (q - k - r)^2$, and the invariant mass M^2 of the outgoing $q\bar{q}$-system. In addition we use a Sudakov decomposition of the momentum k with respect to the light cone momenta $q' = q - xp$ and p with $2p \cdot q' = s$, $k = \alpha q' + \beta p + k_\perp$. Two dimensional transverse momenta are denoted as $\boldsymbol{k}^2 = -k_\perp^2$.

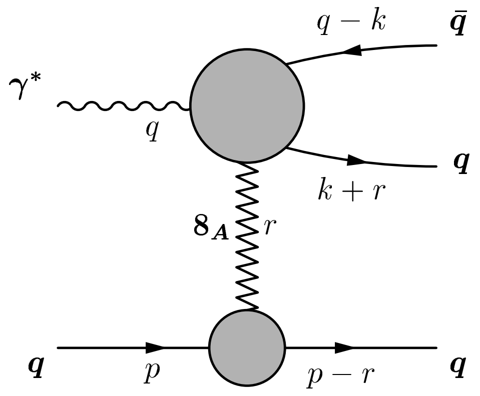

Figure 3.3: Kinematics of the process $\gamma^* + q' \to q\bar{q} + q'$.

The Born impact factor is obtained from $T^{(0)}_{\gamma^* q}$. To leading order we may write

$$T^{(0)}_{\gamma^* q} = \Gamma^{(0),a}_{\gamma^* \to q\bar{q}} \, \frac{2s}{t} \, \Gamma^{(0),a}_{qq} \tag{3.17}$$

with the Born level vertices

$$\Gamma^{(0),a}_{qq} = \frac{1}{s} \bar{u}(p-r,\, \lambda_{q'}) \, \not{q}' \lambda^a u(p,\, \lambda_q)\,, \tag{3.18}$$

$$\Gamma^{(0),a}_{\gamma^* \to q\bar{q}} = -iee_f \left(\frac{H^a_T}{st_a} - \frac{\bar{H}^a_T}{st_b} \right)\,, \tag{3.19}$$

where

$$H^a_T = \bar{u}(k+r,\lambda) \, \not{p} \, \not{k} \, \not{\epsilon} \, \lambda^a v(q-k,\lambda')\,, \tag{3.20}$$

$$\bar{H}^a_T = \bar{u}(k+r,\lambda) \, \not{\epsilon} \, (\not{q} - \not{k} - \not{r}) \, \not{p} \, \lambda^a v(q-k,\lambda') \tag{3.21}$$

and λ^a are the generators of the colour group $SU(N_c)$. Squaring the Born level vertices (3.18) and averaging (summing) over incoming (outgoing) colours and helicities we obtain for the coupling to the reggeized gluons with colours (a, b) , contracted with the colour singlet projector (cf. (3.14) and (3.15)):

$$|\Gamma^{(0)}_{qq}|^2 = \frac{\sqrt{N_c^2 - 1}}{2N_c}\,. \tag{3.22}$$

The $\gamma^* \to q\bar{q}$-vertex $|\Gamma^{(0)}_{\gamma^* \to q\bar{q}}|^2 = |\Gamma^{(0)}_{\gamma^* \to q\bar{q}}(\boldsymbol{k}, \alpha)|^2$ for a longitudinally polarised γ^* coupling to a quark flavour f reads

$$|\Gamma^{(0)}_{\gamma^* \to q\bar{q}}|^2_L = 4\sqrt{N_c^2 - 1} e^2 e_f^2 \alpha^3 (1-\alpha)^3 Q^2 \left(\frac{1}{D(\boldsymbol{k})} - \frac{1}{D(\boldsymbol{k}+\boldsymbol{r})} \right)^2\,, \tag{3.23}$$

where $D(\boldsymbol{k}) = \boldsymbol{k}^2 + \alpha(1-\alpha)Q^2$. Here the exchanged reggeized gluons must be in the colour singlet. For the sum over the two transverse photon polarisations we have

$$|\Gamma^{(0)}_{\gamma^*\to q\bar{q}}|^2_T = 2\sqrt{N_c^2-1}\,e^2 e_f^2 \alpha(1-\alpha)\left[\alpha^2+(1-\alpha)^2\right]\left(\frac{\boldsymbol{k}}{D(\boldsymbol{k})}-\frac{\boldsymbol{k}+\boldsymbol{r}}{D(\boldsymbol{k}+\boldsymbol{r})}\right)^2 . \tag{3.24}$$

The LO impact factor follows from the definition in eq. (3.15), from the two-particle phase space measure

$$d\phi_{q\bar{q}}\frac{s d\beta_r}{2\pi} = \frac{d\alpha}{2\alpha(1-\alpha)}\frac{d^{D-2}\boldsymbol{k}}{(2\pi)^{D-1}} \tag{3.25}$$

and from the Born level vertices (3.23, 3.24). Expanding Φ_{γ^*} in the strong coupling,

$$\Phi_{\gamma^*} = g^2\Phi^{(0)}_{\gamma^*} + g^4\Phi^{(1)}_{\gamma^*}, \tag{3.26}$$

we write the Born level impact factor as

$$\Phi^{(0)}_{\gamma^*;T,L} = \int \frac{d^{D-2}\boldsymbol{k}}{(2\pi)^{D-1}}\frac{d\alpha}{2\alpha(1-\alpha)}|\Gamma^{(0)}_{\gamma^*\to q\bar{q}}|^2_{T,L} \equiv \int d^{D-2}\boldsymbol{k}\,d\alpha\,\mathcal{I}_{2;T,L}(\alpha,\boldsymbol{k};\boldsymbol{r},Q)\,. \tag{3.27}$$

The last equation defines the integrand of the LO impact factor:

$$\mathcal{I}_{2;L}(\alpha,\boldsymbol{k};\boldsymbol{r},Q) = \frac{2e^2e_f^2\sqrt{N_c^2-1}}{(2\pi)^{D-1}}\alpha^2(1-\alpha)^2Q^2\left(\frac{1}{D(\boldsymbol{k})}-\frac{1}{D(\boldsymbol{k}+\boldsymbol{r})}\right)^2 \tag{3.28}$$

$$\mathcal{I}_{2;T}(\alpha,\boldsymbol{k};\boldsymbol{r},Q) = \frac{e^2e_f^2\sqrt{N_c^2-1}}{(2\pi)^{D-1}}\left[\alpha^2+(1-\alpha)^2\right]\left(\frac{\boldsymbol{k}}{D(\boldsymbol{k})}-\frac{\boldsymbol{k}+\boldsymbol{r}}{D(\boldsymbol{k}+\boldsymbol{r})}\right)^2 \tag{3.29}$$

Because of the symmetry of the squared matrix element under the exchange $q \leftrightarrow \bar{q}$, namely $\alpha \leftrightarrow 1-\alpha$, $\boldsymbol{k} \leftrightarrow -\boldsymbol{r}-\boldsymbol{k}$, we have the relation $\mathcal{I}_2(\alpha,\boldsymbol{k};\boldsymbol{r},Q) = \mathcal{I}_2(1-\alpha,-\boldsymbol{r}-\boldsymbol{k};\boldsymbol{r},Q)$.

3.3 The virtual corrections

The virtual corrections to the photon impact factor have been calculated except for the phase-space integration in [10]. We therefore only quickly summarise the result here. According to (3.15) the virtual corrections stem from the (γ^* + Reggeon $\to q\bar{q}$)-vertex at next-to-leading order in α_s. This vertex, $\Gamma^{(1),a}_{\gamma^*\to q\bar{q}}$, can be extracted from the comparison of the amplitude $T_{\gamma^* q}$ at one-loop level with its Reggeized form. In the following we use dimensional regularisation; divergences appear as poles when the space-time dimension $D = 4-2\epsilon$ approaches $D = 4$. The Regge ansatz of the amplitude $\gamma^* + q' \to q\bar{q} + q'$ reads:

$$T_{\gamma^* q} = \frac{s}{t}\Gamma^a_{\gamma^*\to q\bar{q}} \left[\left(\frac{s}{-t}\right)^{\omega(t)} + \left(\frac{-s}{-t}\right)^{\omega(t)} \right] \Gamma^a_{qq} \,. \tag{3.30}$$

Expanding all elements in terms of the strong coupling g

$$\omega = g^2\omega^{(1)} + g^2\omega^{(2)} \tag{3.31}$$

$$\Gamma^a_{\gamma^*\to q\bar{q}} = g\Gamma^{(0),a}_{\gamma^*\to q\bar{q}} + g^2\Gamma^{(1),a}_{\gamma^*\to q\bar{q}} \tag{3.32}$$

$$\Gamma^a_{qq} = g\Gamma^{(0),a}_{qq} + g^2\Gamma^{(1),a}_{qq} \tag{3.33}$$

and recalling the expansion of $T_{\gamma^* q}$ (3.16) one obtains at the order g^2:

$$\begin{aligned} T^{(1)}_{\gamma^* q} &= \Gamma^{(1),a}_{\gamma^*\to q\bar{q}} \frac{2s}{t} \Gamma^{(0),a}_{qq} + \Gamma^{(0),a}_{\gamma^*\to q\bar{q}} \frac{2s}{t} \Gamma^{(1),a}_{qq} \\ &+ \Gamma^{(0),a}_{\gamma^*\to q\bar{q}} \frac{s}{t} \omega^{(1)} \left[\ln\frac{s}{-t} + \ln\frac{-s}{-t} \right] \Gamma^{(0),a}_{qq} \end{aligned} \tag{3.34}$$

The Born level vertices have already been mentioned (3.18, 3.19). The next-to-leading corrections the quark-quark-Reggeon vertex $\Gamma^{(1),a}_{qq}$ have been calculated in 1994 [11]. The one-loop correction to the gluon trajectory reads:

$$\omega^{(1)}(t) = \frac{2N_c}{(4\pi)^{2-\epsilon}} \frac{c_\Gamma}{\epsilon}(-t)^{-\epsilon} \quad , \qquad c_\Gamma \equiv \frac{\Gamma(1+\epsilon)\Gamma^2(1-\epsilon)}{\Gamma(1-2\epsilon)} \tag{3.35}$$

Thus, all parts of (3.34) are known except for the vertex $\Gamma^{(1),a}_{\gamma^*\to q\bar{q}}$. Since the amplitude $T^{(1)}_{\gamma^* q}$ has been calculated in [10], this vertex can be extracted.

Let us now focus on the divergences of the virtual corrections. In $T^{(1)}_{\gamma^* q}$ the divergent contribution from the self-energy insertions on all four external quark are included leading to explicitly labelled UV poles. The amplitude is split into a finite part F and divergent part D as

$$T^{(1)}_{\gamma^* q} = F_{\gamma^* q} + \frac{c_\Gamma}{(4\pi)^{2-\epsilon}} T^{(0)}_{\gamma^* q} D \,. \tag{3.36}$$

The divergent part can then be written as the sum of three terms

$$D = D_{\gamma^*\to q\bar{q}} + D_\omega + D_{qq} \,, \tag{3.37}$$

following the expansion of the Regge ansatz in powers of α_s (3.34). The three terms denote the divergent parts of the vertex $\Gamma^{(1)}_{\gamma^*\to q\bar{q}}$, of the Regge trajectory of the gluon, $\omega^{(1)}(t)$, which is accompanied by the large leading logarithms in s, and of the vertex $\Gamma^{(1)}_{qq}$, respectively. They have the form ([10]):

$$D_{\gamma^*\to q\bar{q}} = -\frac{2C_F}{\epsilon^2} - \frac{3C_F}{\epsilon} + \frac{\beta_0}{\epsilon_{\rm UV}} + \frac{2C_F}{\epsilon}\ln\left(-M^2\right) + \frac{C_A}{\epsilon}\left(\ln\frac{\alpha(1-\alpha)\,t}{M^2} + \ln\frac{s_0}{-t}\right), \tag{3.38}$$

$$D_\omega = \frac{C_A}{\epsilon}\left[\ln\frac{s}{s_0} + \ln\frac{-s}{s_0}\right] \tag{3.39}$$

and

$$D_{qq} = -\frac{2C_F}{\epsilon^2} - \frac{3C_F}{\epsilon} + \frac{\beta_0}{\epsilon_{\rm UV}} + \frac{2C_F}{\epsilon}\ln(-t) + \frac{C_A}{\epsilon}\ln\frac{s_0}{-t}\,. \tag{3.40}$$

As already mentioned in sec.3.1, in the general expression for the NLO cross section, (3.13), we would like $\omega^{(1)}$ to cancel the IR-divergence from the gluon emission in the central region. In (3.39), we have therefore introduced the energy scale s_0: instead of $\ln s/(-t)$ we write $\ln s/(-t) = \ln s/s_0 + \ln s_0/(-t)$ and absorb the second term into $D_{\gamma^*\to q\bar{q}}$ and D_{qq} in (3.38, 3.40). This second term is split into equal parts, because the real corrections will be calculated using a symmetric splitting of the gluon phase space.

Turning to the ultraviolet divergent pieces in $D_{\gamma^*\to q\bar{q}}$ and D_q, they are are proportional to $\beta_0 = (11N_c - 2n_f)/6$, and in [10] it has been shown that they are removed by the renormalisation of the strong coupling.

To conclude, the virtual corrections to the photon impact factor are given as:

$$\Phi^{(1,virtual)}_{\gamma^*} = \frac{\delta_{ab}}{\sqrt{N_c^2-1}}\int\frac{d^{D-2}\boldsymbol{k}}{(2\pi)^{D-1}}\frac{d\alpha}{2\alpha(1-\alpha)}\Gamma^{(1),a}_{\gamma^*\to q\bar{q}}\Gamma^{(0),b\,*}_{\gamma^*\to q\bar{q}} + \text{c.c.}\,. \tag{3.41}$$

Making use of (3.36) and (3.38) — the latter one without the UV pole which we will discuss later — we can immediately deduce the IR divergent part of the virtual correction to the impact factor:

$$\begin{aligned}\Phi^{(1,virtual)}_{\gamma^*}\Big|^{IRdivergent} &= \frac{c_\Gamma}{(4\pi)^{2-\epsilon}}\Phi^{(0)}_{\gamma^*}\,\left[D^{IR}_{\gamma^*\to q\bar{q}} + \text{c.c.}\right]\\ = \int d\boldsymbol{k}\int_0^1 d\alpha\,\mathcal{I}_2(\alpha,\boldsymbol{k};\boldsymbol{r},Q)&\frac{c_\Gamma}{(4\pi)^{2-\epsilon}}\\ \times\left\{\frac{C_A}{\epsilon}\left[2\log s_0 + 2\log\alpha(1-\alpha) - 2\log M^2\right] + \frac{C_F}{\epsilon}\left[-\frac{4}{\epsilon} + 4\log M^2 - 6\right]\right\}.\end{aligned} \tag{3.42}$$

Below we will see that these divergent terms cancel against those from the real corrections.

Chapter 4

The process $\gamma^* + q \rightarrow (q\bar{q}g) + q$ (the real corrections)

The real corrections to the photon impact factor stem from the emission of a gluon in the fragmentation region of the photon. According to our definition of the NLO impact factor (3.14) there is a phase space integral over the squared vertex $\Gamma^{(0)}_{\gamma^* \to q\bar{q}g}$. The integration region is constrained by the requirement that the gluon is emitted in the fragmentation region of the photon.

In this chapter we will study the the process $\gamma^* + q \to (q\bar{q}g) + q$ at tree level with a large rapidity gap between outgoing quark and the $q\bar{q}g$ system and calculate from this the vertex $\Gamma^{(0)}_{\gamma^* \to q\bar{q}g}$ [12, 15]. To ensure that the gluon and the $q\bar{q}$ pair are close in rapidity we subtract the configuration where they are separated by a large rapidity gap. In the subtraction term $\Gamma^{(0)}_{\gamma^* \to q\bar{q}g}$ can be approximated. In this way we will arrive at the real corrections to the γ^* impact factor in sec. 4.3.

As indicated in sec. 2.2.1, the NLO corrections to the photon impact factor contain the information on how the colour dipole picture changes at next-to-leading order. The real corrections are expected to provide (at least to the main part) the structure of a $q\bar{q}g$ Fock component of the photon wave function. In sec. 4.5 we will see that, indeed, already from the matrix element for $\gamma^* + q \to (q\bar{q}g) + q$ the existence of such a $q\bar{q}g$ Fock component can be derived.

A study of the process $\gamma^* + q \to (q\bar{q}g) + q$ includes the subprocess $\gamma^* + g \to q\bar{q}g$ with an off-shell incoming gluon. Together with the NLO corrections to the production process $\gamma^* + g \to q\bar{q}$ which has been calculated in [10], it provides the complete NLO corrections to the photon-gluon fusion process with off-shell incoming bosons. With a suitable jet-definition, it will be possible to calculate 2-jet (in nLO) and 3-jet (LO) production in DIS using the k_T factorisation.

4.1 Kinematics and calculational techniques

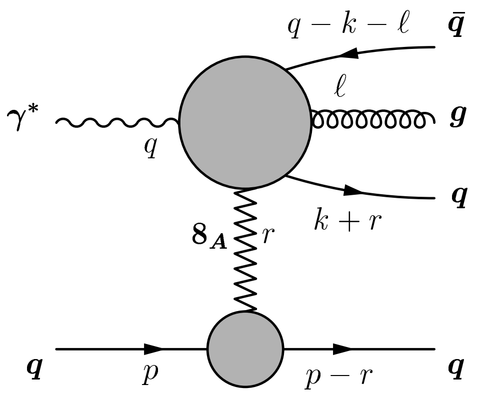

Figure 4.1: Kinematics of the process $\gamma^* + q' \to q\bar{q}g + q'$.

The notations of the scattering process are depicted in Fig 4.1. As in the last chapter, Q^2 and s are the photon virtuality and the $\gamma^* q$ center-of-mass energy respectively. The momentum transfer is denoted by r (with $r^2 = t$), the outgoing gluon carries momentum ℓ and the momenta of the quark and antiquark are $k + r$ and $q - k - \ell$, respectively. We express these momenta in terms of their Sudakov variables,

$$k = \alpha q' + \beta p + k_\perp \; , \tag{4.1}$$

$$\ell = \alpha_\ell q' + \beta_\ell p + \ell_\perp \; , \tag{4.2}$$

$$r = \alpha_r q' + \beta_r p + r_\perp \; , \tag{4.3}$$

We are interested in the limit of large energy s:

$$Q^2, \boldsymbol{k}^2, \boldsymbol{\ell}^2 \ll s \quad , \quad \alpha, \alpha_\ell \sim \mathcal{O}(1) \tag{4.4}$$

From the on-shell conditions of the outgoing quarks and gluons we obtain $\alpha_r = t/s$ and

$$\beta_\ell s = \frac{\boldsymbol{\ell}^2}{\alpha_\ell} \; , \tag{4.5}$$

$$\beta s = -\frac{(\boldsymbol{k}+\boldsymbol{\ell})^2}{1-\alpha-\alpha_\ell} - \frac{\boldsymbol{\ell}^2}{\alpha_\ell} - Q^2 \; , \tag{4.6}$$

$$\beta_r s = \frac{(\boldsymbol{k}+\boldsymbol{r})^2}{\alpha} + \frac{(\boldsymbol{k}+\boldsymbol{\ell})^2}{1-\alpha-\alpha_\ell} + \frac{\boldsymbol{\ell}^2}{\alpha_\ell} + Q^2. \tag{4.7}$$

Before we continue let us establish the connection between Sudakov variables and the language of rapidity gaps. The rapidity y of a particle with respect to the z-axis is defined as:

$$y \equiv \frac{1}{2} \ln \left(\frac{E + p_z}{E - p_z} \right) . \tag{4.8}$$

Thinking of the particular choice for the Sudakov basis $q' = \frac{\sqrt{s}}{2}(1,0,0,1)$, $p = \frac{\sqrt{s}}{2}(1,0,0,-1)$ we immediately see that

$$y = \frac{1}{2} \ln \left(\frac{\alpha}{\beta} \right) . \tag{4.9}$$

In our case the particles of the $q\bar{q}g$ system have all a rapidity of the order $\ln(s/t)$ which is very large compared to the proton's rapidity $(-\infty)$; we have one rapidity gap. The gluon in the middle of the central region corresponds to $y_\ell = 0$, in other words: $\alpha_\ell \sim \beta_\ell \sim \sqrt{s/t} \ll \alpha,\, 1-\alpha$. Thus, by doing this calculation in the kinematics (4.4) we include the case $\alpha_\ell \ll \alpha$ and therefore the central region.

The Feynman diagrams for our process are listed in Fig. 4.2. The graphs in the second line (denoted by $B_1, \ldots, B_5$) are obtained from the diagrams of the first line $(A_1, \ldots, A_5)$ by interchanging the quark and antiquark, i.e. by transforming $k + r \to q - k - \ell$. In terms of the Sudakov components

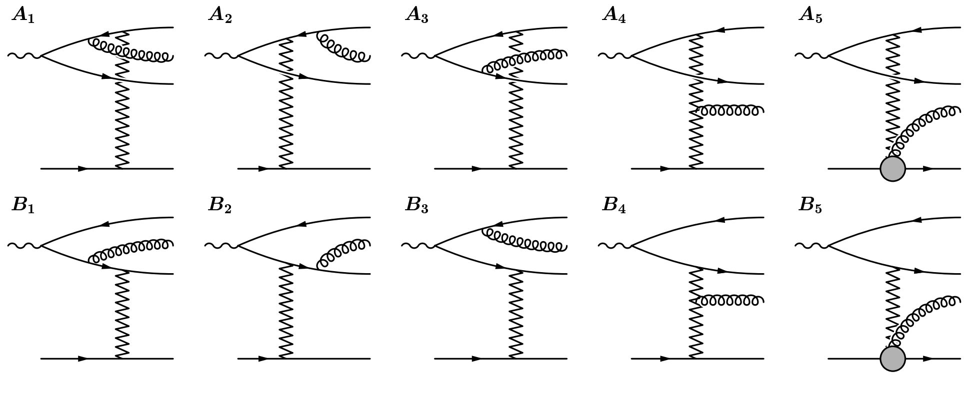

Figure 4.2: Feynman diagrams for the process $\gamma^* + q \to q\bar{q}g + q$.

this transformation reads:

$$\alpha \to 1 - \alpha - \alpha_\ell \tag{4.10}$$
$$\boldsymbol{k} \to -(\boldsymbol{k} + \boldsymbol{r} + \boldsymbol{\ell}). \tag{4.11}$$

In correspondence with this transformation we introduce the shorthand notation:

$$\alpha_1 \equiv \alpha \ , \tag{4.12}$$
$$\bar{\alpha}_1 \equiv (1 - \alpha - \alpha_\ell) \ , \tag{4.13}$$
$$\alpha_2 \equiv (1 - \alpha) \ , \tag{4.14}$$
$$\bar{\alpha}_2 \equiv (\alpha + \alpha_\ell). \tag{4.15}$$

where the bars stand for the transformation (4.10), (4.11).

The denominators, that will occur during the calculation, have the form:

$$\begin{aligned} D_1 &= (k + \ell + r - q)^2 \\ &= -\bar{\alpha}_1 Q^2 - (\boldsymbol{k} + \boldsymbol{\ell} + \boldsymbol{r})^2 - \frac{\bar{\alpha}_1}{\alpha_1} (\boldsymbol{k} + \boldsymbol{r})^2 - \frac{\bar{\alpha}_1}{\alpha_\ell} \boldsymbol{\ell}^2 \end{aligned} \tag{4.16}$$

$$\begin{aligned} D_2 &= (k + r - q)^2 \\ &= -\alpha_2 Q^2 - \frac{1}{\alpha_1} (\boldsymbol{k} + \boldsymbol{r})^2 \end{aligned} \tag{4.17}$$

$$\begin{aligned} D_3 &= (k + \ell + r)^2 \\ &= -(\boldsymbol{k} + \boldsymbol{\ell} + \boldsymbol{r})^2 + \frac{\bar{\alpha}_2}{\alpha_1} (\boldsymbol{k} + \boldsymbol{r})^2 + \frac{\bar{\alpha}_2}{\alpha_\ell} \boldsymbol{\ell}^2 \\ &= \frac{1}{\alpha_\ell \, \alpha_1} (-\alpha_\ell (\boldsymbol{k} + \boldsymbol{r}) + \alpha_1 \boldsymbol{\ell})^2 \end{aligned} \tag{4.18}$$

$$\begin{aligned} D_4 &= (k - q)^2 \\ &= -\boldsymbol{k}^2 + \frac{\alpha_2}{\bar{\alpha}_1} (\boldsymbol{k} + \boldsymbol{\ell})^2 + \frac{\alpha_2}{\alpha_\ell} \boldsymbol{\ell}^2 \\ &= \frac{1}{\alpha_\ell \, \bar{\alpha}_1} (\alpha_\ell (\boldsymbol{k} + \boldsymbol{\ell}) + \bar{\alpha}_1 \boldsymbol{\ell})^2 \end{aligned} \tag{4.19}$$

$$\begin{aligned} D_5 &= (\ell - r)^2 \\ &= -\alpha_\ell Q^2 - \frac{\alpha_\ell}{\alpha_1} (\boldsymbol{k} + \boldsymbol{r})^2 - \frac{\alpha_\ell}{\bar{\alpha}_1} (\boldsymbol{k} + \boldsymbol{\ell})^2 - (\boldsymbol{\ell} - \boldsymbol{r})^2 \end{aligned} \tag{4.20}$$

$$\begin{aligned} D_6 &= k^2 \\ &= -\alpha_1 Q^2 - \boldsymbol{k}^2 - \frac{\alpha_1}{\bar{\alpha}_1} (\boldsymbol{k} + \boldsymbol{\ell})^2 - \frac{\alpha_1}{\alpha_\ell} \boldsymbol{\ell}^2 \end{aligned} \tag{4.21}$$

$$\begin{aligned} D_7 &= (k + \ell)^2 \\ &= -\bar{\alpha}_2 Q^2 - \frac{1}{\bar{\alpha}_1} (\boldsymbol{k} + \boldsymbol{\ell})^2 \ . \end{aligned} \tag{4.22}$$

Under the transformation (4.10)–(4.11) the denominators D_1 to D_7 obey the following relations:

$$D_1 = \bar{D}_6 \ , \tag{4.23}$$
$$D_2 = \bar{D}_7 \ , \tag{4.24}$$
$$D_3 = \bar{D}_4 \ , \tag{4.25}$$
$$D_5 = \bar{D}_5 \ . \tag{4.26}$$

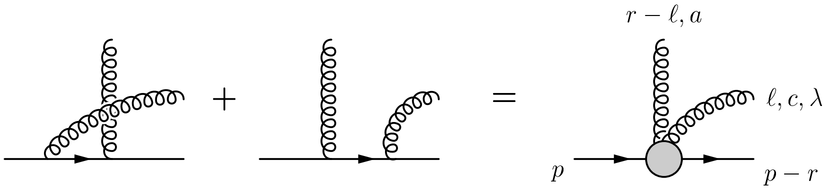

Figure 4.3: Emission of a gluon from the lower quark line.

The polarisation vectors of the photon are

$$\varepsilon_L = \frac{1}{Q}(q' + xp) \; , \tag{4.27}$$

$$\varepsilon_T^1 = (0,1,0,0) \; , \quad \varepsilon_T^2 = (0,0,1,0). \tag{4.28}$$

When it comes to the summation over transverse polarisations we will make use of the identity $\sum_{i=j=1,2} (\epsilon_T^i \, k_\perp)(\epsilon_T^j \, \ell_\perp) = \boldsymbol{k\ell}$. In the longitudinal case one may write $\varepsilon_L = q/Q + 2xp/Q$. Gauge invariance allows to simply put $\varepsilon_L = 2xp/Q$ in our calculation.

The calculation is performed in the Feynman gauge. As to the internal (t-channel) gluon numerators, we use the decomposition

$$g_{\mu\nu} = \frac{2}{s}\left(p_\mu q'_\nu + p_\nu q'_\mu\right) + g^\perp_{\mu\nu}. \tag{4.29}$$

In the high energy limit we retain only the first term, since the contributions of the other terms will be suppressed by powers of t/s. For the diagrams where the produced gluon couples to the lower fermion line, this may not be immediately obvious, since some of the light cone components of the t channel gluon are not small; we have checked the approximation against a calculation involving the full numerator, and we have obtained the same answer. In the diagrams A_5 and B_5 we have combined two Feynman graphs (Fig. 4.3) into one effective diagram. Since the produced gluon is far from the lower quark in rapidity, we can simplify the emission vertex:

$$\bar{u}(p-r,h')\left[\frac{\not{q}'(\not{p}-\not{\ell})\gamma^\lambda}{(p-\ell)^2}t^a t^c + \frac{\gamma^\lambda(\not{p}+\not{\ell}-\not{r})\not{q}'}{(p+\ell-r)^2}t^c t^a\right]u(p,h) \approx \frac{2p^\lambda}{\alpha_\ell}[t^c, t^a]\delta_{hh'} \; . \tag{4.30}$$

Here we have used that ℓ has large components only in the q' direction; h and h' denote the helicities of the lower incoming and outgoing quarks, respectively, and the Lorentz index λ is to be contracted with the polarisation vector of the outgoing gluon with colour index c. t^a and t^c are the colour group generators in the fundamental representation, and a denotes the colour index carried by the t-channel gluon.

The calculation is done in $D = 4 - 2\epsilon$ space-time dimensions in order to dimensionally regularise the divergences later on. The phase space over the final state (including the δ-functions from the on-shell conditions) is given by:

$$d\Phi_4 = \frac{d\alpha\, d\alpha_\ell\, d^{D-2}\boldsymbol{k}\, d^{D-2}\boldsymbol{\ell}\, d^{D-2}\boldsymbol{r}}{8s(2\pi)^{3D-4}\alpha_1\bar{\alpha}_1\alpha_\ell}\,. \tag{4.31}$$

4.2 The matrix elements

Let us denote $|\mathcal{M}_{q\bar{q}g}|^2_{L,T}$ the squared matrix element, averaged (summed) over the helicities and colours of the incoming (outgoing) quarks and summed over equal photon polarisations. It can be written in this factorised form:

$$|\mathcal{M}_{q\bar{q}g}|^2_{L,T} = \frac{1}{N_c^2 - 1}\, g^6\, \delta^{ab}\, |\Gamma^{(0)}_{\gamma^*\to q\bar{q}g}|^2_{L,T} \left(\frac{2\,s}{t}\right)^2 \delta^{ab}\, |\Gamma^{(0)}_{qq}|^2_{L,T}, \tag{4.32}$$

and by using (3.22) we extract the squared vertex $|\Gamma^{(0)}_{\gamma^*\to q\bar{q}g}|^2$ (summed over helicities and colours of the $q\bar{q}g$ state). With the strong coupling g and ee_f being the charge of the quark flavour f the result has the following form :

$$|\Gamma^{(0)}_{\gamma^*\to q\bar{q}g}|^2_L = 4\,e^2 e_f^2\, \sqrt{N_c^2 - 1}\; Q^2 \sum_{i,j=1}^{5} \left(\mathcal{AA}^L_{ij} + \mathcal{AB}^L_{ij} + \mathcal{BA}^L_{ij} + \mathcal{BB}^L_{ij}\right), \tag{4.33}$$

$$|\Gamma^{(0)}_{\gamma^*\to q\bar{q}g}|^2_T = e^2 e_f^2\, \sqrt{N_c^2 - 1} \sum_{i,j=1}^{5} \left(\mathcal{AA}^T_{ij} + \mathcal{AB}^T_{ij} + \mathcal{BA}^T_{ij} + \mathcal{BB}^T_{ij}\right); \tag{4.34}$$

A basic feature of the LO colour picture is the factorisation into the transition of the γ^* into a colour dipole (and back) and the interaction with the target. This property is expected to hold also in NLO. In our result we have therefore tried to factorise as much as possible.

According to the labelling of fig. 4.2 we denote the product of graph A_i with graph A_j by $\mathcal{AA}_{ij}$ etc. For future convenience we use $C_A = N_c$ and $C_F = (N_c^2 - 1)/(2N_c)$ instead of N_c and $1/N_c$. Note the relation $1/N_c = (C_A - 2C_F)$.

4.2.1 Longitudinal polarisation

The result for longitudinal photon polarisation reads:

$$\mathcal{A}\mathcal{A}^L_{11} = C_F\,\frac{2}{D_1^2\,D_2^2}\,(1-\epsilon)\,\alpha_1\,\bar{\alpha}_1\,\boldsymbol{A}_1^2 \tag{4.35}$$

$$\mathcal{A}\mathcal{A}^L_{12} = -\,(C_A - 2C_F)\,\frac{1}{D_1\,D_2^2\,D_4}\,\big((1-\epsilon)\,\alpha_1\,\alpha_2\,\boldsymbol{A}_1\,\boldsymbol{A}_2 - \alpha_1\,\alpha_2^2\,\bar{\alpha}_1\,\boldsymbol{r}^2\big) \tag{4.36}$$

$$\mathcal{A}\mathcal{A}^L_{13} = C_F\,\frac{2}{D_1^2\,D_2\,D_3}\,\big((1-\epsilon)\,\bar{\alpha}_1^2\,\boldsymbol{A}_1\,\boldsymbol{A}_3\,+\bar{\alpha}_1^2\,(\boldsymbol{k}+\boldsymbol{r})\,(\boldsymbol{k}+\boldsymbol{\ell}+\boldsymbol{r})\big) \tag{4.37}$$

$$\mathcal{A}\mathcal{A}^L_{14} = -\,C_A\,\frac{1}{D_1\,D_2^2\,D_5}\Bigg(\frac{1}{2\,\alpha_\ell}\,\alpha_1\,\big(\alpha_2\,\bar{\alpha}_1 + 2\,(1-\epsilon)\,\alpha_\ell^2\big)\,\boldsymbol{A}_1\,\boldsymbol{A}_4 \\ +\,\frac{1}{2}\alpha_1\,\alpha_2\,\bar{\alpha}_1^2\,D_2 + \frac{1}{2\,\alpha_\ell}\,\alpha_1\,\alpha_2^2\,\bar{\alpha}_1\,\boldsymbol{A}_1\boldsymbol{r} - \alpha_1\,\alpha_2^2\,\bar{\alpha}_1\,\boldsymbol{r}^2\Bigg) \tag{4.38}$$

$$\mathcal{A}\mathcal{A}^L_{15} = C_A\,\frac{1}{\alpha_\ell\,D_1\,D_2^2\,D_5}\,\alpha_1\,\alpha_2^2\,\bar{\alpha}_1^2\,\boldsymbol{r}^2 \tag{4.39}$$

$$\mathcal{A}\mathcal{A}^L_{22} = C_F\,\frac{2}{\bar{\alpha}_1\,D_2^2\,D_4^2}\,(1-\epsilon)\,\alpha_1\,\alpha_2^2\,\boldsymbol{A}_2^2 \tag{4.40}$$

$$\mathcal{A}\mathcal{A}^L_{23} = -\,(C_A - 2C_F)\,\frac{1}{D_1\,D_2\,D_3\,D_4}\,((1-\epsilon)\,\alpha_2\,\bar{\alpha}_1\,\boldsymbol{A}_2\,\boldsymbol{A}_3 \tag{4.41}$$

$$+\,\alpha_2\,\bar{\alpha}_1\,(\boldsymbol{k}+\boldsymbol{r}-\alpha_1\,\boldsymbol{r})\,(\boldsymbol{k}+\boldsymbol{\ell}+\bar{\alpha}_1\,\boldsymbol{r})) \tag{4.42}$$

$$\mathcal{A}\mathcal{A}^L_{24} = C_A\,\frac{1}{D_2^2\,D_4\,D_5}\Bigg(\frac{1}{2\,\alpha_\ell\,\bar{\alpha}_1}\,\alpha_1\,\alpha_2\,\big(\alpha_2\,\bar{\alpha}_1 + 2\,(1-\epsilon)\,\alpha_\ell^2\big)\,\boldsymbol{A}_2\,\boldsymbol{A}_4 \\ +\,\frac{1}{2}\alpha_1\,\alpha_2^2\,\bar{\alpha}_1\,D_2 + \frac{1}{2\,\alpha_\ell}\,\alpha_1\,\alpha_2^2\,\bar{\alpha}_1\,\boldsymbol{A}_2\boldsymbol{r} + \alpha_1\,\alpha_2^2\,\bar{\alpha}_1\,\boldsymbol{r}^2\Bigg) \tag{4.43}$$

$$\mathcal{A}\mathcal{A}^L_{25} = -\,C_A\,\frac{1}{\alpha_\ell\,D_2^2\,D_4\,D_5}\,\alpha_1\,\alpha_2^3\,\bar{\alpha}_1\,\boldsymbol{r}^2 \tag{4.44}$$

$$\mathcal{A}\mathcal{A}^L_{33} = C_F\,\frac{2}{\alpha_1\,D_1^2\,D_3^2}\,(1-\epsilon)\,\bar{\alpha}_1^3\,\boldsymbol{A}_3^2 \tag{4.45}$$

$$\mathcal{A}\mathcal{A}^L_{34} = C_A\,\frac{1}{D_1\,D_2\,D_3\,D_5}\Bigg(\frac{1}{2\,\alpha_\ell}\bar{\alpha}_1\,\big(\alpha_1\,\bar{\alpha}_1 - \alpha_\ell - 2\,(1-\epsilon)\,\alpha_\ell^2\big)\,\boldsymbol{A}_3\,\boldsymbol{A}_4 \\ -\,\frac{1}{2}\,\alpha_1\,\bar{\alpha}_1^2\,\bar{\alpha}_2\,D_2 + \alpha_1\,\alpha_2\,\bar{\alpha}_1^2\,D_7 + \frac{1}{2\,\alpha_\ell}\,\alpha_1\,\alpha_2\,\bar{\alpha}_1^2\,\boldsymbol{A}_3\boldsymbol{r} \\ +\,\alpha_1\,\alpha_2\,\bar{\alpha}_1^2\,\boldsymbol{r}^2 + \frac{3}{2}\,\alpha_2\,\bar{\alpha}_1\,\boldsymbol{A}_3\,(\boldsymbol{k}+\boldsymbol{\ell})\Bigg) \tag{4.46}$$

$$\mathcal{A}\mathcal{A}^L_{35} = -\,C_A\,\frac{1}{\alpha_\ell\,D_1\,D_2\,D_3\,D_5}\,\alpha_1\,\alpha_2\,\bar{\alpha}_1^2\,\bar{\alpha}_2\,\boldsymbol{r}^2 \tag{4.47}$$

$$\mathcal{AA}^L_{44} = C_A\, \frac{1}{D_2^2\, D_5^2}\, \left(\frac{2}{\bar{\alpha}_1}\, \boldsymbol{A}_4^2\, \alpha_1\, \big((1-\epsilon)\, \alpha_\ell^2 + \alpha_2\, \bar{\alpha}_1 \big) + \alpha_1\, \alpha_2\, \alpha_\ell\, \bar{\alpha}_1\, D_2 \right) \tag{4.48}$$

$$\mathcal{AA}^L_{45} = 0 \tag{4.49}$$

$$\widetilde{\mathcal{AA}}^L_{44} = C_A\, \frac{1}{D_2^2\, D_5^2}\, \left(\frac{2}{\bar{\alpha}_1}\, \boldsymbol{A}_4^2\, \alpha_1\, \big((1-\epsilon)\, \alpha_\ell^2 + \alpha_2\, \bar{\alpha}_1 \big) \right. \\ \left. + \alpha_1\, \alpha_2\, \alpha_\ell\, \bar{\alpha}_1\, D_2 + 2\, \alpha_1\, \alpha_2^2\, \bar{\alpha}_1\, \boldsymbol{r}^2 \right) \tag{4.50}$$

$$\widetilde{\mathcal{AA}}^L_{45} = -\, C_A\, \frac{1}{D_2^2\, D_5^2} \alpha_1\, \alpha_2^2\, \bar{\alpha}_1\, \boldsymbol{r}^2 \tag{4.51}$$

$$\mathcal{AA}^L_{55} = 0 \tag{4.52}$$

$$\mathcal{AB}^L_{11} = (C_A - 2C_F)\, \frac{1}{D_1\, D_2\, D_6\, D_7}\, ((1-\epsilon)\, \alpha_1\, \bar{\alpha}_1\, \boldsymbol{A}_1\, \boldsymbol{B}_1 \\ + \alpha_1\, \bar{\alpha}_1\, (\boldsymbol{k} + \alpha_1\, \boldsymbol{r})\, (\boldsymbol{k} + \boldsymbol{\ell} + \bar{\alpha}_2\, \boldsymbol{r})) \tag{4.53}$$

$$\mathcal{AB}^L_{12} = -\, C_F\, \frac{2}{D_1\, D_2\, D_3\, D_7}\, (\, (1-\epsilon)\, \bar{\alpha}_1\, \bar{\alpha}_2\, \boldsymbol{A}_1\, \boldsymbol{B}_2 \\ + \bar{\alpha}_1\, \bar{\alpha}_2\, (\boldsymbol{k} + \boldsymbol{r})\, (\boldsymbol{k} + \boldsymbol{\ell} + \boldsymbol{r})) \tag{4.54}$$

$$\mathcal{AB}^L_{13} = (C_A - 2C_F)\, \frac{1}{D_1\, D_2\, D_4\, D_6}\, \big((1-\epsilon)\, \alpha_1^2\, \boldsymbol{A}_1\, \boldsymbol{B}_3 - \alpha_1^2\, \alpha_2\, \bar{\alpha}_1\, \boldsymbol{r}^2 \big) \tag{4.55}$$

$$\mathcal{AB}^L_{14} = C_A\, \frac{1}{D_1\, D_2\, D_5\, D_7} \left(\frac{1}{2\, \alpha_\ell}\, \bar{\alpha}_1\, \big(\alpha_1\, \bar{\alpha}_1 - \alpha_\ell - (1-\epsilon)\, 2\, \alpha_\ell^2 \big)\, \boldsymbol{A}_1\, \boldsymbol{B}_4 \right. \\ + \alpha_1\, \bar{\alpha}_1^2\, \bar{\alpha}_2\, D_2 - \frac{1}{2} \alpha_1\, \alpha_2\, \bar{\alpha}_1^2\, D_7 + \frac{1}{2\, \alpha_\ell}\, \alpha_1\, \alpha_2\, \bar{\alpha}_1\, \bar{\alpha}_2\, \boldsymbol{A}_1 \boldsymbol{r} \\ \left. - \alpha_1\, \alpha_2\, \bar{\alpha}_1\, \bar{\alpha}_2\, \boldsymbol{r}^2 - \frac{3}{2}\, \bar{\alpha}_1\, \bar{\alpha}_2\, \boldsymbol{A}_1\, (\boldsymbol{k} + \boldsymbol{r}) \right) \tag{4.56}$$

$$\mathcal{AB}^L_{15} = -\, C_A\, \frac{1}{\alpha_\ell\, D_1\, D_2\, D_5\, D_7} \alpha_1\, \alpha_2\, \bar{\alpha}_1^2\, \bar{\alpha}_2\, \boldsymbol{r}^2 \tag{4.57}$$

$$\mathcal{AB}^L_{22} = (C_A - 2C_F)\, \frac{1}{D_2\, D_3\, D_4\, D_7}\, ((1-\epsilon)\, \alpha_2\, \bar{\alpha}_2\, \boldsymbol{A}_2\, \boldsymbol{B}_2 \\ + \alpha_2\, \bar{\alpha}_2\, (\boldsymbol{k} + \boldsymbol{r} - \alpha_1\, \boldsymbol{r})\, (\boldsymbol{k} + \boldsymbol{\ell} + \bar{\alpha}_1\, \boldsymbol{r})) \tag{4.58}$$

$$\mathcal{AB}^L_{23} = -\, C_F\, \frac{2}{\bar{\alpha}_1\, D_2\, D_4^2\, D_6}\, (1-\epsilon)\, \alpha_1^2\, \alpha_2\, \boldsymbol{A}_2 \boldsymbol{B}_3 \tag{4.59}$$

$$\mathcal{AB}^L_{24} = -\, C_A\, \frac{1}{D_2\, D_4\, D_5\, D_7} \left(\frac{1}{2\, \alpha_\ell}\, \alpha_2\, \big(\alpha_1\, \bar{\alpha}_1 - \alpha_\ell - 2\, (1-\epsilon)\, \alpha_\ell^2 \big)\, \boldsymbol{A}_2\, \boldsymbol{B}_4 \right. \\ + \alpha_1\, \alpha_2\, \bar{\alpha}_1\, \bar{\alpha}_2\, D_2 - \frac{1}{2} \alpha_1\, \alpha_2^2\, \bar{\alpha}_1\, D_7 + \frac{1}{2\, \alpha_\ell}\, \alpha_1\, \alpha_2\, \bar{\alpha}_1\, \bar{\alpha}_2\, \boldsymbol{A}_2 \boldsymbol{r} \\ \left. + \alpha_1\, \alpha_2\, \bar{\alpha}_1\, \bar{\alpha}_2\, \boldsymbol{r}^2 - \frac{3}{2}\, \alpha_2\, \bar{\alpha}_2\, \boldsymbol{A}_2\, (\boldsymbol{k} + \boldsymbol{r}) \right) \tag{4.60}$$

$$\mathcal{AB}^L_{25} = C_A\, \frac{1}{\alpha_\ell\, D_2\, D_4\, D_5\, D_7} \alpha_1\, \alpha_2^2\, \bar{\alpha}_1\, \bar{\alpha}_2\, \boldsymbol{r}^2 \tag{4.61}$$

$$\mathcal{AB}^L_{33} = (C_A - 2C_F)\,\frac{1}{D_1\,D_3\,D_4\,D_6}\,((1-\epsilon)\,\alpha_1\,\bar\alpha_1\,\boldsymbol{A}_3\,\boldsymbol{B}_3$$
$$+\alpha_1\,\bar\alpha_1\,(\boldsymbol{k}+\boldsymbol{r}-\alpha_1\,\boldsymbol{r})\,(\boldsymbol{k}+\boldsymbol{\ell}+\bar\alpha_1\,\boldsymbol{r})) \tag{4.62}$$

$$\mathcal{AB}^L_{34} = -\,C_A\,\frac{1}{D_1\,D_3\,D_5\,D_7}\left(\frac{1}{2\,\alpha_1\,\alpha_\ell}\bar\alpha_1^2\,\left(\alpha_1\,\bar\alpha_2 + 2\,(1-\epsilon)\,\alpha_\ell^2\right)\,\boldsymbol{A}_3\,\boldsymbol{B}_4\right.$$
$$\left.+\,\frac{1}{2}\alpha_1\,\bar\alpha_1^2\,\bar\alpha_2\,D_7 + \frac{1}{2\,\alpha_\ell}\alpha_1\,\bar\alpha_1^2\,\bar\alpha_2\,\boldsymbol{A}_3\boldsymbol{r} + \alpha_1\,\bar\alpha_1^2\,\bar\alpha_2\,\boldsymbol{r}^2\right) \tag{4.63}$$

$$\mathcal{AB}^L_{35} = C_A\,\frac{1}{\alpha_\ell\,D_1\,D_3\,D_5\,D_7}\alpha_1\,\bar\alpha_1^2\,\bar\alpha_2^2\,\boldsymbol{r}^2 \tag{4.64}$$

$$\mathcal{AB}^L_{44} = -\,C_A\,\frac{1}{D_2\,D_5^2\,D_7}\left(\left(2\,\alpha_1\,\bar\alpha_1 + \alpha_\ell - 2\,(1-\epsilon)\,\alpha_\ell^2\right)\boldsymbol{A}_4\,\boldsymbol{B}_4\right. \tag{4.65}$$
$$\left.+\,\frac{1}{2}\alpha_1\,\alpha_\ell\,\bar\alpha_1\,\bar\alpha_2\,D_2 + \frac{1}{2}\alpha_1\,\alpha_2\,\alpha_\ell\,\bar\alpha_1\,D_7 - \alpha_\ell^2\,(\boldsymbol{k}+\boldsymbol{\ell})\,(\boldsymbol{k}+\boldsymbol{r})\right)$$

$$\mathcal{AB}^L_{45} = 0 \tag{4.66}$$

$$\widetilde{\mathcal{AB}}^L_{44} = -\,C_A\,\frac{1}{D_2\,D_5^2\,D_7}\left(\left(2\,\alpha_1\,\bar\alpha_1 + \alpha_\ell - 2\,(1-\epsilon)\,\alpha_\ell^2\right)\boldsymbol{A}_4\,\boldsymbol{B}_4\right.$$
$$+\,\frac{1}{2}\alpha_1\,\alpha_\ell\,\bar\alpha_1\,\bar\alpha_2\,D_2 + \frac{1}{2}\alpha_1\,\alpha_2\,\alpha_\ell\,\bar\alpha_1\,D_7 - \alpha_\ell^2\,(\boldsymbol{k}+\boldsymbol{\ell})\,(\boldsymbol{k}+\boldsymbol{r})$$
$$\left.+\,2\,\alpha_1\,\alpha_2\,\bar\alpha_1\,\bar\alpha_2\,\boldsymbol{r}^2\right) \tag{4.67}$$

$$\widetilde{\mathcal{AB}}^L_{45} = C_A\,\frac{1}{D_2\,D_5^2\,D_7}\alpha_1\,\alpha_2\,\bar\alpha_1\,\bar\alpha_2\,\boldsymbol{r}^2 \tag{4.68}$$

$$\mathcal{AB}^L_{55} = 0\,. \tag{4.69}$$

We have used the following abbreviations:

$$\boldsymbol{A}_1 = \alpha_2\,\boldsymbol{\ell} + \alpha_\ell\,(\boldsymbol{k}+\boldsymbol{r}) \tag{4.70}$$
$$\boldsymbol{A}_2 = \bar\alpha_1\,\boldsymbol{\ell} + \alpha_\ell\,(\boldsymbol{k}+\boldsymbol{\ell}) \tag{4.71}$$
$$\boldsymbol{A}_3 = \alpha_1\,\boldsymbol{\ell} - \alpha_\ell\,(\boldsymbol{k}+\boldsymbol{r}) \tag{4.72}$$
$$\boldsymbol{A}_4 = \alpha_2\,(\boldsymbol{\ell}-\boldsymbol{r}) + \alpha_\ell\,(\boldsymbol{k}+\boldsymbol{r}) \tag{4.73}$$
$$\boldsymbol{B}_1 = \bar\alpha_2\,\boldsymbol{\ell} - \alpha_\ell\,(\boldsymbol{k}+\boldsymbol{\ell}) \tag{4.74}$$
$$\boldsymbol{B}_2 = \alpha_1\,\boldsymbol{\ell} - \alpha_\ell\,(\boldsymbol{k}+\boldsymbol{r}) \tag{4.75}$$
$$\boldsymbol{B}_3 = \bar\alpha_1\,\boldsymbol{\ell} + \alpha_\ell\,(\boldsymbol{k}+\boldsymbol{\ell}) \tag{4.76}$$
$$\boldsymbol{B}_4 = \bar\alpha_2\,(\boldsymbol{\ell}-\boldsymbol{r}) - \alpha_\ell\,(\boldsymbol{k}+\boldsymbol{\ell})\,. \tag{4.77}$$

For future convenience we have already combined diagrams. The expressions with the $\widetilde{\ }$ correspond to the original diagrams. Note that $-2\widetilde{\mathcal{AA}}^L_{45}$ is present in $\widetilde{\mathcal{AA}}^L_{44}$ as one term (and correspondingly in the $\mathcal{AB}$ diagrams and for transverse polarisation). Since $\mathcal{AA}^L_{45} = \mathcal{AA}^L_{54}$ we have set :

$$\begin{aligned} \mathcal{AA}^L_{44} &= \widetilde{\mathcal{AA}^L_{44}} + \widetilde{\mathcal{AA}^L_{45}} + \widetilde{\mathcal{AA}^L_{54}}\,, \\ \mathcal{AA}^L_{45} &= \mathcal{AA}^L_{54} = \ 0 \end{aligned} \tag{4.78}$$

and

$$\begin{aligned} \mathcal{AB}^L_{44} &= \widetilde{\mathcal{AB}^L_{44}} + \widetilde{\mathcal{AB}^L_{45}} + \widetilde{\mathcal{BA}^L_{54}}\,, \\ \mathcal{AB}^L_{45} &= \mathcal{BA}^L_{54} = \ 0 \end{aligned} \tag{4.79}$$

From now on we will only use the combined expressions.

In the above definitions, the vectors $\boldsymbol{B}_i$ are obtained from the $\boldsymbol{A}_i$ by the transformations (4.10), (4.11). Note also the additional relations

$$\boldsymbol{A}_2 = \boldsymbol{B}_3\,, \qquad \boldsymbol{A}_3 = \boldsymbol{B}_2\,. \tag{4.80}$$

The remaining terms $\mathcal{AA}_{ij}$ (with $i > j$) and $\mathcal{BA}_{ij}$ (with $i > j$) follow from the symmetry properties $\mathcal{AA}_{ij} = \mathcal{AA}_{ji}$ and $\mathcal{AB}_{ij} = \mathcal{BA}_{ji}$. In order to find $\mathcal{BA}_{ij}$ and $\mathcal{AB}_{ji}$ (with $i < j$), and all the $\mathcal{BB}_{ij}$'s we use the substitutions (4.10), (4.11).

We also note that in the sum of the four $(ij) = (44)$ matrix elements: $\mathcal{AA}_{44} + \mathcal{AB}_{44} + \mathcal{BA}_{44} + \mathcal{BB}_{44}$, the term proportional to D_2 in $\mathcal{AA}_{44}$, the terms proportional to D_2 and D_7 in $\mathcal{AB}_{44}$, and the analogous terms in $\mathcal{BA}_{44}$ and $\mathcal{BB}_{44}$ cancel against each other.

Finally, the factorisation of part of the whole sum of diagrams shell be stated here. In most of the diagrams the term proportional to a product of two of the vectors $\boldsymbol{A}_i, \boldsymbol{B}_i$ is accompanied by $(1-\epsilon)$. The sum of the $(1-\epsilon)$ parts from all diagrams factorises:

$$\begin{aligned} &\sum_{i,j=1}^{5} \left(\mathcal{AA}^L_{ij} + \mathcal{AB}^L_{ij} + \mathcal{BA}^L_{ij} + \mathcal{BB}^L_{ij}\right) \\ &\qquad = \ 2(1-\epsilon)\left(C_F\,(\boldsymbol{v} - \bar{\boldsymbol{v}})^2 + C_A\,\boldsymbol{v}\bar{\boldsymbol{v}}\right) + \text{reminder} \end{aligned} \tag{4.81}$$

with:

$$\begin{aligned} \boldsymbol{v} = &\sqrt{\frac{\bar{\alpha}_1}{\alpha_1}}\left(\frac{\boldsymbol{B}_2}{D_3 D_7}\,\bar{\alpha}_2 + \frac{\boldsymbol{B}_4}{D_5 D_7}\,\alpha_\ell\right) \\ &+ \sqrt{\frac{\alpha_1}{\bar{\alpha}_1}}\left(\frac{\boldsymbol{A}_4}{D_2 D_5}\,\alpha_\ell - \frac{\boldsymbol{A}_1}{D_1 D_2}\,\bar{\alpha}_1 - \frac{\boldsymbol{A}_3}{D_1 D_3}\,\frac{\bar{\alpha}_1^2}{\alpha_1}\right) \end{aligned} \tag{4.82}$$

The vector $\bar{\boldsymbol{v}}$ is again related to $\boldsymbol{v}$ by the transformation (4.10, 4.11).

4.2.2 Transverse polarisation

The result for transverse photon polarisation can be simplified by expressing certain parts in terms of the results for the longitudinal polarisation.

$$\begin{aligned}
\mathcal{A}\mathcal{A}^T_{11} = C_F\, &\frac{4}{{D_1}^2\,{D_2}^2}\alpha_1\,\bar\alpha_1\,(1-\epsilon)\Big((\boldsymbol{k}+\boldsymbol{\ell}+\boldsymbol{r})^2\,(\boldsymbol{k}+\boldsymbol{r})^2 \\
&+\frac{1}{\alpha_1^2}\bar\alpha_1\Big((\boldsymbol{k}+\boldsymbol{r})^2+\alpha_1\,Q^2\Big)\Big(2\,\alpha_1\,(\boldsymbol{k}+\boldsymbol{r})(\boldsymbol{k}+\boldsymbol{\ell}+\boldsymbol{r}) \\
&+\bar\alpha_1\,((\boldsymbol{k}+\boldsymbol{r})^2+\alpha_1\,Q^2)\Big)\Big)+\frac{2\,(\boldsymbol{k}+\boldsymbol{r})^2}{{\alpha_1}^2}\,\mathcal{A}\mathcal{A}^L_{11}
\end{aligned}\tag{4.83}$$

$$\begin{aligned}
\mathcal{A}\mathcal{A}^T_{12} = &-(C_A-2C_F)\,\frac{2}{D_1\,{D_2}^2\,D_4}\Big[\bar\alpha_1\,(\boldsymbol{k}+\boldsymbol{r})^2\,(\boldsymbol{k}\boldsymbol{r}+\alpha_2\boldsymbol{r}^2) \\
&+\alpha_1\,\alpha_2\,\bar\alpha_1\,\boldsymbol{r}(\boldsymbol{k}+\boldsymbol{r})\,Q^2 \\
&+(1-\epsilon)\Big(\Big(-\alpha_1\,\bar\alpha_1\,\boldsymbol{k}(\boldsymbol{k}+\boldsymbol{\ell}+\boldsymbol{r})-\bar\alpha_1^2\,\boldsymbol{k}(\boldsymbol{k}+\boldsymbol{r}) \\
&+\alpha_1\,\alpha_2\,(\boldsymbol{k}+\boldsymbol{\ell})(\boldsymbol{k}+\boldsymbol{\ell}+\boldsymbol{r})+\alpha_2\,\bar\alpha_1\,(\boldsymbol{k}+\boldsymbol{\ell})(\boldsymbol{k}+\boldsymbol{r})\Big)\,(\boldsymbol{k}+\boldsymbol{r})^2 \\
&-\alpha_1\,\bar\alpha_1\,(\bar\alpha_1\,\boldsymbol{k}(\boldsymbol{k}+\boldsymbol{r})-\alpha_2\,(\boldsymbol{k}+\boldsymbol{\ell})(\boldsymbol{k}+\boldsymbol{r}))\,Q^2\Big)\Big] \\
&+\frac{2\,(\boldsymbol{k}+\boldsymbol{r})^2}{{\alpha_1}^2}\,\mathcal{A}\mathcal{A}^L_{12}
\end{aligned}\tag{4.84}$$

$$\begin{aligned}
\mathcal{A}\mathcal{A}^T_{13} = C_F\, &\frac{4}{{\alpha_1}^2\,\alpha_\ell\,{D_1}^2\,D_2\,D_3}\,\bar\alpha_1\Big[-{\alpha_1}^3\,(\bar\alpha_2\,\alpha_\ell\,(\boldsymbol{k}+\boldsymbol{\ell}+\boldsymbol{r})^2-\bar\alpha_1^2\,\boldsymbol{\ell}^2)\,Q^2 \\
&+{\alpha_1}^2\,(\boldsymbol{k}+\boldsymbol{r})(\boldsymbol{k}+\boldsymbol{\ell}+\boldsymbol{r})\Big(\alpha_\ell\,(\boldsymbol{k}+\boldsymbol{\ell}+\boldsymbol{r})^2+\bar\alpha_1\,\boldsymbol{\ell}^2-\bar\alpha_1\,\alpha_\ell\,Q^2\Big) \\
&+\alpha_\ell\,(\boldsymbol{k}+\boldsymbol{r})^2\Big(-\alpha_1\,\bar\alpha_2\,(\boldsymbol{k}+\boldsymbol{\ell}+\boldsymbol{r})^2\;+\bar\alpha_1^2\,(\boldsymbol{k}+\boldsymbol{r})^2 \\
&+\alpha_1\,\bar\alpha_1\,(\boldsymbol{k}+\boldsymbol{r})(\boldsymbol{k}+\boldsymbol{\ell}+\boldsymbol{r})-\alpha_1\,\bar\alpha_1^2\,(-\frac{\boldsymbol{\ell}^2}{\alpha_\ell}-\alpha_1\,Q^2)\Big) \\
&+\alpha_1\,(1-\epsilon)\Big(-{\alpha_1}^2\,\bar\alpha_1^2\,\boldsymbol{\ell}^2\,Q^2-\alpha_1\,\alpha_\ell\,(\boldsymbol{k}+\boldsymbol{r})(\boldsymbol{k}+\boldsymbol{\ell}+\boldsymbol{r}) \\
&\cdot\Big(\alpha_2\,(\boldsymbol{k}+\boldsymbol{\ell}+\boldsymbol{r})^2-4\,\bar\alpha_1\,(\boldsymbol{k}+\boldsymbol{r})(\boldsymbol{k}+\boldsymbol{\ell}+\boldsymbol{r})+\frac{\alpha_1\,\bar\alpha_1\,\boldsymbol{\ell}^2}{\alpha_\ell}-\bar\alpha_1^2\,Q^2\Big) \\
&+\alpha_\ell\,(\boldsymbol{k}+\boldsymbol{r})^2\Big((-2\,\alpha_1\,\bar\alpha_1+\alpha_2\,\bar\alpha_2)\,(\boldsymbol{k}+\boldsymbol{\ell}+\boldsymbol{r})^2-\bar\alpha_1^2\,(\boldsymbol{k}+\boldsymbol{r})^2 \\
&\quad+\bar\alpha_1\,(-\alpha_1+\bar\alpha_1-\bar\alpha_2)\,(\boldsymbol{k}+\boldsymbol{r})(\boldsymbol{k}+\boldsymbol{\ell}+\boldsymbol{r})+\alpha_1\,\bar\alpha_1^2\,(-\frac{\boldsymbol{\ell}^2}{\alpha_\ell}-Q^2)\Big)\Big)\Big]
\end{aligned}\tag{4.85}$$

$$
\begin{aligned}
\mathcal{A}\mathcal{A}^T_{14} = &- C_A\, \frac{1}{D_1\, {D_2}^2\, D_5} \Big[\bar{\alpha}_1^2\, (\boldsymbol{k}+\boldsymbol{r})^2\, (-(\boldsymbol{k}+\boldsymbol{r})^2 + \frac{\alpha_1\, \boldsymbol{\ell}^2}{\alpha_\ell} - \alpha_1\, Q^2) \\
&+ \frac{2\,\alpha_\ell}{\alpha_1}\,(1-\epsilon) \Big(\alpha_1\, \bar{\alpha}_1 \Big((\boldsymbol{k}+\boldsymbol{r})^2 + \alpha_1\, Q^2 \Big) \,(\, 2(\boldsymbol{k}+\boldsymbol{\ell})(\boldsymbol{k}+\boldsymbol{r}) \\
&\quad + \boldsymbol{r}(\boldsymbol{k}+\boldsymbol{r}) + \bar{\alpha}_1\, Q^2) \\
&\quad + (\boldsymbol{k}+\boldsymbol{r})^2 \Big({\alpha_1}^2\, (\boldsymbol{k}+\boldsymbol{\ell})(\boldsymbol{k}+\boldsymbol{\ell}+\boldsymbol{r}) + \bar{\alpha}_1^2\, (\boldsymbol{k}+\boldsymbol{r})^2 + \alpha_1\, \bar{\alpha}_1^2\, Q^2 \Big) \Big) \\
&+ \alpha_1\, \bar{\alpha}_1\, (\boldsymbol{k}+\boldsymbol{r})^2 \Big(- \boldsymbol{k}(\boldsymbol{k}+\boldsymbol{\ell}) + (\boldsymbol{\ell}-\boldsymbol{r})\,(\boldsymbol{k}+\boldsymbol{\ell}+\boldsymbol{r}) - \boldsymbol{r}^2 \Big) \\
&+ \bar{\alpha}_1\, (-(\boldsymbol{k}+\boldsymbol{r})^2 - \alpha_1\, Q^2) \Big(\alpha_\ell\, (\, 2(\boldsymbol{k}+\boldsymbol{\ell})(\boldsymbol{k}+\boldsymbol{r}) + \boldsymbol{r}(\boldsymbol{k}+\boldsymbol{r})) \\
&\quad + \bar{\alpha}_1\, (2\,\boldsymbol{\ell} - \boldsymbol{r})(\boldsymbol{k}+\boldsymbol{r}) \Big) \Big] \\
&+ \frac{2\,(\boldsymbol{k}+\boldsymbol{r})^2}{{\alpha_1}^2}\, \mathcal{A}\mathcal{A}^L_{14}
\end{aligned} \tag{4.86}
$$

$$
\mathcal{A}\mathcal{A}^T_{15} = C_A\, \frac{2}{\alpha_1\, \alpha_\ell\, D_1\, {D_2}^2\, D_5}\, ({\alpha_1}^2 + {\alpha_2}^2)\, \bar{\alpha}_1^2\, (\boldsymbol{k}+\boldsymbol{r})^2\, \boldsymbol{r}^2 \tag{4.87}
$$

$$
\mathcal{A}\mathcal{A}^T_{22} = \frac{2\,({\alpha_1}^2 + {\alpha_2}^2\,)\,(\boldsymbol{k}+\boldsymbol{r})^2}{{\alpha_1}^2\, {\alpha_2}^2}\, \mathcal{A}\mathcal{A}^L_{22} \tag{4.88}
$$

$$
\begin{aligned}
\mathcal{A}\mathcal{A}^T_{23} = &- (C_A - 2C_F)\, \frac{2}{D_1\, D_2\, D_3\, D_4} \Big[(-\alpha_1 + \bar{\alpha}_1) \\
&\cdot \Big(- \boldsymbol{k}(\boldsymbol{k}+\boldsymbol{r})\,(\boldsymbol{k}+\boldsymbol{\ell})(\boldsymbol{k}+\boldsymbol{\ell}+\boldsymbol{r}) + \boldsymbol{k}(\boldsymbol{k}+\boldsymbol{\ell})\,(\boldsymbol{k}+\boldsymbol{r})(\boldsymbol{k}+\boldsymbol{\ell}+\boldsymbol{r}) \Big) \\
&+ \Big(\alpha_1\, (\boldsymbol{k}+\boldsymbol{\ell})(\boldsymbol{k}+\boldsymbol{r}) + \bar{\alpha}_1\, (\boldsymbol{k}+\boldsymbol{r})^2 \Big) \Big(\frac{(-\alpha_1 + \bar{\alpha}_1)}{\alpha_1}\, \boldsymbol{k}(\boldsymbol{k}+\boldsymbol{\ell}+\boldsymbol{r}) \\
&\quad - \alpha_2\, (\boldsymbol{k}+\boldsymbol{\ell}+\boldsymbol{r})^2 + \frac{{\alpha_2}^2\, \bar{\alpha}_1}{\alpha_1} (\frac{(\boldsymbol{k}+\boldsymbol{r})^2}{\alpha_1} + \frac{\boldsymbol{\ell}^2}{\alpha_\ell}) \Big) \\
&+ \epsilon \Big(\Big(- \bar{\alpha}_1\, \boldsymbol{k}(\boldsymbol{k}+\boldsymbol{\ell}+\boldsymbol{r}) + \alpha_2\, (\boldsymbol{k}+\boldsymbol{\ell})(\boldsymbol{k}+\boldsymbol{\ell}+\boldsymbol{r}) \Big) \\
&\quad \cdot \Big(\frac{(\alpha_1 - \bar{\alpha}_2)}{\alpha_1} (\boldsymbol{k}+\boldsymbol{r})^2 + 2\,(\boldsymbol{k}+\boldsymbol{r})(\boldsymbol{k}+\boldsymbol{\ell}+\boldsymbol{r}) \Big) \\
&+ \Big(- \bar{\alpha}_1\, \boldsymbol{k}(\boldsymbol{k}+\boldsymbol{r}) + \alpha_2\, (\boldsymbol{k}+\boldsymbol{\ell})(\boldsymbol{k}+\boldsymbol{r}) \Big) \Big(- \alpha_2\, (\boldsymbol{k}+\boldsymbol{\ell}+\boldsymbol{r})^2 \\
&\quad - 2\,(\boldsymbol{k}+\boldsymbol{r})(\boldsymbol{k}+\boldsymbol{\ell}+\boldsymbol{r}) + \alpha_1\, \bar{\alpha}_1\, (\frac{(\boldsymbol{k}+\boldsymbol{r})^2}{\alpha_1} + \frac{\boldsymbol{\ell}^2}{\alpha_\ell}) \Big) \Big) \Big] \\
&+ \frac{4\,(\boldsymbol{k}+\boldsymbol{r})(\boldsymbol{k}+\boldsymbol{\ell}+\boldsymbol{r})}{\alpha_2\, \bar{\alpha}_1}\, \mathcal{A}\mathcal{A}^L_{23}
\end{aligned} \tag{4.89}
$$

$$\mathcal{A}\mathcal{A}^T_{24} = C_A\,\frac{1}{{D_2}^2\,D_4\,D_5}\left[\frac{2\,\alpha_\ell\,(1-\epsilon)}{\bar\alpha_1}\Bigg(\right. \tag{4.90}$$
$$\alpha_1\,\Big(-\bar\alpha_1\,\boldsymbol{k}(\boldsymbol{k}+\boldsymbol{\ell})+\alpha_2\,(\boldsymbol{k}+\boldsymbol{\ell})^2\Big)\,(\boldsymbol{k}+\boldsymbol{r})^2$$
$$+\,\bar\alpha_1\,\Big(-\bar\alpha_1\,\boldsymbol{k}(\boldsymbol{k}+\boldsymbol{r})+\alpha_2\,(\boldsymbol{k}+\boldsymbol{\ell})(\boldsymbol{k}+\boldsymbol{r})\Big)\,\Big((\boldsymbol{k}+\boldsymbol{r})^2+\alpha_1\,Q^2\,\Big)\Bigg)$$
$$+\,\alpha_1\,(\boldsymbol{k}+\boldsymbol{r})^2\,\Big(\alpha_\ell\,\boldsymbol{k}(\boldsymbol{k}+\boldsymbol{\ell})-\alpha_2\,(\boldsymbol{k}+\boldsymbol{\ell})^2+\bar\alpha_1\,\boldsymbol{k}(\boldsymbol{\ell}-2\,\boldsymbol{r})$$
$$+\,\frac{\alpha_2\,\bar\alpha_1\,\boldsymbol{\ell}^2}{\alpha_\ell}+\alpha_2\,(2\,\boldsymbol{\ell}-\boldsymbol{r})\,(\boldsymbol{k}+\boldsymbol{\ell})\Big)$$
$$-\,\alpha_2\,\Big((\boldsymbol{k}+\boldsymbol{r})^2+\alpha_1\,Q^2\Big)\,\Big(\alpha_\ell\,(\boldsymbol{k}+\boldsymbol{\ell})(\boldsymbol{k}+\boldsymbol{r})+\bar\alpha_1\,(\boldsymbol{k}+\boldsymbol{r})^2$$
$$\left.+\,\bar\alpha_1\,(\boldsymbol{\ell}+\boldsymbol{r})\,(\boldsymbol{k}+\boldsymbol{r})\Big)\right]+\frac{2\,(\boldsymbol{k}+\boldsymbol{r})^2}{{\alpha_1}^2}\,\mathcal{A}\mathcal{A}^L_{24}$$

$$\mathcal{A}\mathcal{A}^T_{25} = -\,C_A\,\frac{2}{\alpha_1\,\alpha_\ell\,{D_2}^2\,D_4\,D_5}\alpha_2\,({\alpha_1}^2+{\alpha_2}^2)\,\bar\alpha_1\,(\boldsymbol{k}+\boldsymbol{r})^2\,\boldsymbol{r}^2 \tag{4.91}$$

$$\mathcal{A}\mathcal{A}^T_{33} = 2\,\left[\frac{(\boldsymbol{k}+\boldsymbol{\ell}+\boldsymbol{r})^2}{\bar\alpha_1^2}+\frac{\boldsymbol{\ell}^2}{{\alpha_\ell}^2}\right]\,\mathcal{A}\mathcal{A}^L_{33} \tag{4.92}$$

$$\mathcal{A}\mathcal{A}^T_{34} = -\,C_A\,\frac{1}{D_1\,D_2\,D_3\,D_5}\left[2\,\epsilon\,\Bigg(\frac{-2}{\alpha_2}\bar\alpha_1\,\alpha_\ell\,((\boldsymbol{k}+\boldsymbol{r})(\boldsymbol{k}+\boldsymbol{\ell}+\boldsymbol{r}))^2\right. \tag{4.93}$$
$$+\,(\boldsymbol{k}+\boldsymbol{\ell})(\boldsymbol{k}+\boldsymbol{r})$$
$$\cdot\Big(-\alpha_2\,\alpha_\ell\,(\boldsymbol{k}+\boldsymbol{\ell}+\boldsymbol{r})^2+\bar\alpha_1\,\alpha_\ell\,(\boldsymbol{k}+\boldsymbol{r})^2+\alpha_1\,\bar\alpha_1\,\boldsymbol{\ell}^2\Big)$$
$$+\,\alpha_1\,\bar\alpha_1^2\,\boldsymbol{\ell}^2\,Q^2+\frac{\alpha_\ell}{\alpha_1\,\alpha_2}\,(\boldsymbol{k}+\boldsymbol{r})(\boldsymbol{k}+\boldsymbol{\ell}+\boldsymbol{r})\,\Big(\bar\alpha_1\,(2\,\alpha_1\,\bar\alpha_2$$
$$+\,\alpha_2\,(-\bar\alpha_1+\bar\alpha_2))\,(\boldsymbol{k}+\boldsymbol{r})^2+2\,\alpha_1\,\alpha_2\,\boldsymbol{\ell}(\boldsymbol{k}+\boldsymbol{\ell})-\alpha_1\,\alpha_2\,\bar\alpha_1^2\,Q^2\Big)$$
$$+\,\bar\alpha_1\,(\boldsymbol{k}+\boldsymbol{r})^2\,\Bigg(\frac{(\alpha_1-\bar\alpha_2)\,\alpha_\ell\,(\boldsymbol{k}+\boldsymbol{\ell})(\boldsymbol{k}+\boldsymbol{\ell}+\boldsymbol{r})}{\alpha_1\,\bar\alpha_1}+\alpha_\ell\,(\boldsymbol{k}+\boldsymbol{\ell}+\boldsymbol{r})^2$$
$$+\,\frac{\bar\alpha_1\,\alpha_\ell\,(\boldsymbol{k}+\boldsymbol{r})^2}{\alpha_1}+\bar\alpha_1\,\boldsymbol{\ell}^2+\bar\alpha_1\,\alpha_\ell\,Q^2\Bigg)\Bigg)$$
$$+\,\frac{3\,(\alpha_1-\bar\alpha_1)\,\bar\alpha_1\,(\boldsymbol{k}+\boldsymbol{r})^2\,\boldsymbol{r}(\boldsymbol{k}+\boldsymbol{\ell}+\boldsymbol{r})}{\alpha_1}\;+(\boldsymbol{\ell}+\boldsymbol{r})\,(\boldsymbol{k}+\boldsymbol{\ell}+\boldsymbol{r})$$
$$\cdot\Big((\alpha_1-\bar\alpha_1)\,(\boldsymbol{k}+\boldsymbol{\ell})(\boldsymbol{k}+\boldsymbol{r})+\frac{\bar\alpha_1^2\,(\boldsymbol{k}+\boldsymbol{r})^2}{\alpha_1}+\alpha_1\,\bar\alpha_1\,\bar\alpha_2\,Q^2\Big)$$
$$-\,\frac{1}{{\alpha_1}^2\,\alpha_\ell}\Big({\alpha_1}^2\,\alpha_\ell\,(\boldsymbol{k}+\boldsymbol{\ell}+\boldsymbol{r})^2-\alpha_2\,\bar\alpha_1\,\alpha_\ell\,(\boldsymbol{k}+\boldsymbol{r})^2-\alpha_1\,\alpha_2\,\bar\alpha_1\,\boldsymbol{\ell}^2\Big)$$
$$\cdot\Big(2\,\alpha_1\,\alpha_\ell\,(\boldsymbol{k}+\boldsymbol{\ell})(\boldsymbol{k}+\boldsymbol{r})+\bar\alpha_1\,\alpha_\ell\,(\boldsymbol{k}+\boldsymbol{r})^2+\alpha_1\,\bar\alpha_1\,(\boldsymbol{\ell}-2\boldsymbol{r})\,(\boldsymbol{k}+\boldsymbol{r})\Big)$$

$$
\begin{aligned}
&- (\boldsymbol{k}+\boldsymbol{\ell})(\boldsymbol{k}+\boldsymbol{\ell}+\boldsymbol{r}) \\
&\cdot \Big(\alpha_\ell\,(\boldsymbol{k}+\boldsymbol{r})^2 + \alpha_1\,\bar{\alpha}_2\,\alpha_\ell\,Q^2 + (\alpha_1 - \bar{\alpha}_1)\,(\boldsymbol{\ell}+\boldsymbol{r})\,(\boldsymbol{k}+\boldsymbol{r})\Big) \\
&+ (\boldsymbol{k}+\boldsymbol{r})(\boldsymbol{k}+\boldsymbol{\ell}+\boldsymbol{r})\,\Big(\frac{\bar{\alpha}_1}{\alpha_1\,\alpha_2}({\alpha_2}^2\,\bar{\alpha}_1 - \alpha_1\,\alpha_2\,\bar{\alpha}_2 \\
&\quad + 2\,\alpha_2\,(\bar{\alpha}_1 - \bar{\alpha}_2)\,\alpha_\ell - 4\,\alpha_1\,\bar{\alpha}_2\,\alpha_\ell)\,(\boldsymbol{k}+\boldsymbol{r})^2 - 2\,\bar{\alpha}_1\,\bar{\alpha}_2\,\alpha_\ell\,Q^2 \\
&\quad - \frac{(-\alpha_1 + \bar{\alpha}_1)}{\alpha_\ell}(-\alpha_\ell\,(\boldsymbol{k}+\boldsymbol{\ell})^2 + \bar{\alpha}_1\,\boldsymbol{\ell}^2 - \bar{\alpha}_1\,\alpha_\ell\,Q^2) \\
&\quad + \frac{(-\alpha_1 + \bar{\alpha}_1\ )}{\alpha_2}(2\,\alpha_\ell\,(\boldsymbol{k}+\boldsymbol{\ell})(\boldsymbol{k}+\boldsymbol{r}) - \alpha_2\,(\boldsymbol{\ell}+\boldsymbol{r})\,(\boldsymbol{k}+\boldsymbol{\ell}) \\
&\quad - 2\,\bar{\alpha}_1\,(\boldsymbol{\ell}+\boldsymbol{r})\,(\boldsymbol{k}+\boldsymbol{r}))\Big)\Big] + \frac{4\,(\boldsymbol{k}+\boldsymbol{r})(\boldsymbol{k}+\boldsymbol{\ell}+\boldsymbol{r})}{\alpha_2\,\bar{\alpha}_1}\,\mathcal{A}\mathcal{A}^L_{34}
\end{aligned} \tag{4.94}
$$

$$
\mathcal{A}\mathcal{A}^T_{35} = \, -\ C_A\,\frac{2}{\alpha_\ell\,D_1\,D_2\,D_3\,D_5}\,\bar{\alpha}_1\,(\alpha_2\,\bar{\alpha}_1 + \alpha_1\,\bar{\alpha}_2)\,(\boldsymbol{k}+\boldsymbol{r})(\boldsymbol{k}+\boldsymbol{\ell}+\boldsymbol{r})\,\boldsymbol{r}^2 \tag{4.95}
$$

$$
\begin{aligned}
\mathcal{A}\mathcal{A}^T_{44} = C_A\,&\frac{2}{{D_2}^2\,{D_5}^2}\Big[\frac{2\,{\alpha_\ell}^2}{\alpha_1\,\bar{\alpha}_1}(1-\epsilon)\,\Big({\alpha_1}^2\,(\boldsymbol{k}+\boldsymbol{\ell})^2\,(\boldsymbol{k}+\boldsymbol{r})^2 \\
&\quad + \bar{\alpha}_1^2\,(\boldsymbol{k}+\boldsymbol{r})^4 + {\alpha_1}^2\,\bar{\alpha}_1\,(\boldsymbol{k}+\boldsymbol{\ell})(\boldsymbol{k}+\boldsymbol{r})\,Q^2 \\
&\quad + \alpha_1\,\bar{\alpha}_1\,(2\,(\boldsymbol{k}+\boldsymbol{r})^2 + \alpha_1\,Q^2\ )\,((\boldsymbol{k}+\boldsymbol{\ell})(\boldsymbol{k}+\boldsymbol{r}) + \bar{\alpha}_1\,Q^2)\Big) \\
&+ \alpha_1\,\Big(-\alpha_\ell\,(\boldsymbol{k}+\boldsymbol{\ell})^2\,(\boldsymbol{k}+\boldsymbol{r})^2 + 2\,\bar{\alpha}_1\,(\boldsymbol{k}+\boldsymbol{r})^2\,(\boldsymbol{\ell}-\boldsymbol{r})^2 \\
&\quad + \alpha_\ell\,(\boldsymbol{k}+\boldsymbol{r})^2\,\Big(-\frac{\bar{\alpha}_1\,(\boldsymbol{k}+\boldsymbol{r})^2}{\alpha_1} - \bar{\alpha}_1\,Q^2 + 3\,(\boldsymbol{\ell}-\boldsymbol{r})\,(\boldsymbol{k}+\boldsymbol{\ell})\Big)\ \Big) \\
&- 3\,\alpha_\ell\,\Big((\boldsymbol{k}+\boldsymbol{r})^2 + \alpha_1\,Q^2\Big) \\
&\cdot \Big(\alpha_\ell\,(\boldsymbol{k}+\boldsymbol{\ell})(\boldsymbol{k}+\boldsymbol{r}) + \bar{\alpha}_1\,(\boldsymbol{\ell}-\boldsymbol{r})\,(\boldsymbol{k}+\boldsymbol{r})\Big)\Big] + \frac{2\,(\boldsymbol{k}+\boldsymbol{r})^2}{{\alpha_1}^2}\,\mathcal{A}\mathcal{A}^L_{44}
\end{aligned} \tag{4.96}
$$

$$
\mathcal{A}\mathcal{A}^T_{45} = 0 \tag{4.97}
$$

$$
\begin{aligned}
\widetilde{\mathcal{A}\mathcal{A}}^{T}_{44} = C_A\, \frac{2}{{D_2}^2\, {D_5}^2} \Bigg[& \frac{2\,{\alpha_\ell}^2}{\alpha_1\,\bar\alpha_1}(1-\epsilon) \Bigg({\alpha_1}^2\,(\boldsymbol{k}+\boldsymbol{\ell})^2\,(\boldsymbol{k}+\boldsymbol{r})^2 \\
& \quad + \bar\alpha_1^2\,(\boldsymbol{k}+\boldsymbol{r})^4 + {\alpha_1}^2\,\bar\alpha_1\,(\boldsymbol{k}+\boldsymbol{\ell})(\boldsymbol{k}+\boldsymbol{r})\,Q^2 \\
& \quad + \alpha_1\,\bar\alpha_1\,(2\,(\boldsymbol{k}+\boldsymbol{r})^2 + \alpha_1\,Q^2\ )\,((\boldsymbol{k}+\boldsymbol{\ell})(\boldsymbol{k}+\boldsymbol{r}) + \bar\alpha_1\,Q^2) \Bigg) \\
& + \alpha_1 \Big(-\alpha_\ell\,(\boldsymbol{k}+\boldsymbol{\ell})^2\,(\boldsymbol{k}+\boldsymbol{r})^2 + 2\,\bar\alpha_1\,(\boldsymbol{k}+\boldsymbol{r})^2 \Big((\boldsymbol{\ell}-\boldsymbol{r})^2 + \boldsymbol{r}^2 \Big) \\
& \quad + \alpha_\ell\,(\boldsymbol{k}+\boldsymbol{r})^2 \Big(-\frac{\bar\alpha_1\,(\boldsymbol{k}+\boldsymbol{r})^2}{\alpha_1} - \bar\alpha_1\,Q^2 + 3\,(\boldsymbol{\ell}-\boldsymbol{r})\,(\boldsymbol{k}+\boldsymbol{\ell}) \Big) \Big) \\
& - 3\,\alpha_\ell \Big((\boldsymbol{k}+\boldsymbol{r})^2 + \alpha_1\,Q^2 \Big) \\
& \cdot \Big(\alpha_\ell\,(\boldsymbol{k}+\boldsymbol{\ell})(\boldsymbol{k}+\boldsymbol{r}) + \bar\alpha_1\,(\boldsymbol{\ell}-\boldsymbol{r})\,(\boldsymbol{k}+\boldsymbol{r}) \Big) \Bigg] + \frac{2\,(\boldsymbol{k}+\boldsymbol{r})^2}{{\alpha_1}^2}\,\widetilde{\mathcal{A}\mathcal{A}}^{L}_{44}
\end{aligned}
\tag{4.98}
$$

$$
\widetilde{\mathcal{A}\mathcal{A}}^{T}_{45} = \ -C_A\, \frac{2}{\alpha_1\,{D_2}^2\,{D_5}^2}({\alpha_1}^2 + {\alpha_2}^2)\,\bar\alpha_1\,(\boldsymbol{k}+\boldsymbol{r})^2\,\boldsymbol{r}^2
\tag{4.99}
$$

$$
\mathcal{A}\mathcal{A}^{T}_{55} = 0
\tag{4.100}
$$

$$
\begin{aligned}
\mathcal{A}\mathcal{B}^{T}_{11} = \ -(C_A - 2C_F)\, \frac{2}{D_1\,D_2\,D_6\,D_7} \Bigg[& \\
& \Big(\bar\alpha_1\,\boldsymbol{k}(\boldsymbol{k}+\boldsymbol{r}) + \alpha_1\,(\boldsymbol{k}+\boldsymbol{r})(\boldsymbol{k}+\boldsymbol{\ell}+\boldsymbol{r}) \Big) \\
& \quad \cdot \Big((\boldsymbol{k}+\boldsymbol{\ell})^2 - 2\,\bar\alpha_1\,(\boldsymbol{k}+\boldsymbol{\ell})(\boldsymbol{k}+\boldsymbol{r}) + \alpha_2\,\bar\alpha_1\,Q^2 \Big) \\
& + \Big(\bar\alpha_1\,\boldsymbol{k}(\boldsymbol{k}+\boldsymbol{\ell}) + \alpha_1\,(\boldsymbol{k}+\boldsymbol{\ell})(\boldsymbol{k}+\boldsymbol{\ell}+\boldsymbol{r}) \Big) \Big(-2\,\alpha_1\,(\boldsymbol{k}+\boldsymbol{\ell})(\boldsymbol{k}+\boldsymbol{r}) \\
& \quad + (\boldsymbol{k}+\boldsymbol{r})^2 + \alpha_1\,\bar\alpha_2\,Q^2 \Big) \\
& + \epsilon \Bigg((\boldsymbol{k}+\boldsymbol{\ell})(\boldsymbol{k}+\boldsymbol{r}) \Big((\alpha_1\,\bar\alpha_1 + \alpha_2\,\bar\alpha_2)\,\boldsymbol{k}(\boldsymbol{k}+\boldsymbol{\ell}+\boldsymbol{r}) \\
& \quad - 2\,\bar\alpha_1\,\bar\alpha_2\,\boldsymbol{k}(\boldsymbol{k}+\boldsymbol{r}) - 2\,\alpha_1\,\alpha_2\,(\boldsymbol{k}+\boldsymbol{\ell})(\boldsymbol{k}+\boldsymbol{\ell}+\boldsymbol{r}) \\
& \quad + 2\,\alpha_1\,\bar\alpha_1\,(\boldsymbol{k}+\boldsymbol{\ell})(\boldsymbol{k}+\boldsymbol{r}) \Big) \\
& + (-\alpha_1\,\bar\alpha_1 + \alpha_2\,\bar\alpha_2) \Big(\boldsymbol{k}(\boldsymbol{k}+\boldsymbol{r})\,(\boldsymbol{k}+\boldsymbol{\ell})(\boldsymbol{k}+\boldsymbol{\ell}+\boldsymbol{r}) \\
& \quad - \boldsymbol{k}(\boldsymbol{k}+\boldsymbol{\ell})\,(\boldsymbol{k}+\boldsymbol{r})(\boldsymbol{k}+\boldsymbol{\ell}+\boldsymbol{r}) \Big) \\
& + \bar\alpha_1\,(\boldsymbol{k}+\boldsymbol{r})^2 \Big(\boldsymbol{k}(\boldsymbol{k}+\boldsymbol{\ell}) + \alpha_1\,\bar\alpha_1\,Q^2 \Big) \\
& + \alpha_1\,(\boldsymbol{k}+\boldsymbol{\ell})^2 \Big((\boldsymbol{k}+\boldsymbol{r})(\boldsymbol{k}+\boldsymbol{\ell}+\boldsymbol{r}) + \alpha_1\,\bar\alpha_1\,Q^2 \Big) \\
& + \alpha_1\,\bar\alpha_1\,Q^2 \Big(\bar\alpha_1\,\boldsymbol{k}(\boldsymbol{k}+\boldsymbol{\ell}) + \alpha_1\,(\boldsymbol{k}+\boldsymbol{r})(\boldsymbol{k}+\boldsymbol{\ell}+\boldsymbol{r}) + \alpha_1\,\bar\alpha_1\,Q^2 \Big) \Bigg) \Bigg]
\end{aligned}
\tag{4.101}
$$

$$
\begin{aligned}
\mathcal{A}\mathcal{B}_{12}^{T} = &- C_F\, \frac{4}{D_1\, D_2\, D_3\, D_7} \bigg[\frac{1}{\alpha_1} (\alpha_2\, \bar{\alpha}_1^2 - 2\, \alpha_1\, \bar{\alpha}_1\, \bar{\alpha}_2 - \alpha_1\, \bar{\alpha}_2^2) \\
&\cdot (\boldsymbol{k}+\boldsymbol{\ell})(\boldsymbol{k}+\boldsymbol{\ell}+\boldsymbol{r})\, (\boldsymbol{k}+\boldsymbol{r})^2 - \alpha_1\, \bar{\alpha}_2^2\, (\boldsymbol{k}+\boldsymbol{\ell})(\boldsymbol{k}+\boldsymbol{\ell}+\boldsymbol{r})\, Q^2 \\
&+ \frac{1}{\alpha_1} (\boldsymbol{k}+\boldsymbol{\ell})(\boldsymbol{k}+\boldsymbol{r}) \Big(\alpha_1\, (\alpha_2\, \bar{\alpha}_1 + \alpha_1\, \bar{\alpha}_2)\, (\boldsymbol{k}+\boldsymbol{\ell}+\boldsymbol{r})^2 \\
&\quad + \bar{\alpha}_1\, (\bar{\alpha}_1 - \bar{\alpha}_2\ )\, \bar{\alpha}_2\, (\boldsymbol{k}+\boldsymbol{r})^2 \\
&\quad + \alpha_1\, \bar{\alpha}_1\, \bar{\alpha}_2\, (4\, (\boldsymbol{k}+\boldsymbol{r})(\boldsymbol{k}+\boldsymbol{\ell}+\boldsymbol{r}) - \bar{\alpha}_2\, Q^2\ ) \Big) \\
&+ \epsilon \bigg(\frac{(\alpha_1\, \bar{\alpha}_1^2 + 2\, \alpha_1\, \bar{\alpha}_1\, \bar{\alpha}_2 - \alpha_2\, \bar{\alpha}_2^2)}{\alpha_1}\, (\boldsymbol{k}+\boldsymbol{\ell})(\boldsymbol{k}+\boldsymbol{\ell}+\boldsymbol{r})\, (\boldsymbol{k}+\boldsymbol{r})^2 \\
&+ \alpha_1\, \bar{\alpha}_1^2\, (\boldsymbol{k}+\boldsymbol{\ell})(\boldsymbol{k}+\boldsymbol{\ell}+\boldsymbol{r})\, Q^2 \\
&+ \frac{1}{\alpha_1} (\boldsymbol{k}+\boldsymbol{\ell})(\boldsymbol{k}+\boldsymbol{r}) \Big(\alpha_1\, (\alpha_1\, \bar{\alpha}_1 + \alpha_2\, \bar{\alpha}_2)\, (\boldsymbol{k}+\boldsymbol{\ell}+\boldsymbol{r})^2 \\
&\quad - \bar{\alpha}_1\, (\bar{\alpha}_1 - \bar{\alpha}_2\ )\, \bar{\alpha}_2\, (\boldsymbol{k}+\boldsymbol{r})^2 \\
&\quad + \alpha_1\, \bar{\alpha}_1\, \bar{\alpha}_2\, (-4\, (\boldsymbol{k}+\boldsymbol{r})(\boldsymbol{k}+\boldsymbol{\ell}+\boldsymbol{r}) - \bar{\alpha}_1\, Q^2) \Big) \bigg) \bigg]
\end{aligned} \tag{4.102}
$$

$$
\begin{aligned}
\mathcal{A}\mathcal{B}_{13}^{T} = &(C_A - 2C_F)\, \frac{2}{D_1\, D_2\, D_4\, D_6} \bigg[\Big(\bar{\alpha}_1\, \boldsymbol{k}^2 - \alpha_2\, \boldsymbol{k}(\boldsymbol{k}+\boldsymbol{\ell}+\boldsymbol{r}) \Big) \\
&\cdot \Big(\alpha_2\, (\boldsymbol{k}+\boldsymbol{\ell})(\boldsymbol{k}+\boldsymbol{r}) - \bar{\alpha}_1\, (\boldsymbol{k}+\boldsymbol{r})^2 \Big) \\
&+ ({\alpha_1}^2 - {\alpha_2}^2) \Big(\boldsymbol{k}(\boldsymbol{k}+\boldsymbol{r})\, (\boldsymbol{k}+\boldsymbol{\ell})(\boldsymbol{k}+\boldsymbol{\ell}+\boldsymbol{r}) \\
&\quad - \boldsymbol{k}(\boldsymbol{k}+\boldsymbol{\ell})\, (\boldsymbol{k}+\boldsymbol{r})(\boldsymbol{k}+\boldsymbol{\ell}+\boldsymbol{r}) \Big) \\
&- \alpha_1 \Big(- \boldsymbol{k}(\boldsymbol{k}+\boldsymbol{\ell}+\boldsymbol{r}) + (\boldsymbol{k}+\boldsymbol{\ell})^2 + \frac{\bar{\alpha}_1}{\alpha_\ell}\, \boldsymbol{\ell}^2 \Big) \\
&\quad \cdot \Big(\alpha_1\, (\boldsymbol{k}+\boldsymbol{\ell})(\boldsymbol{k}+\boldsymbol{r}) + \bar{\alpha}_1\, (\boldsymbol{k}+\boldsymbol{r})^2 + \alpha_1\, \bar{\alpha}_1\, Q^2 \Big) \\
&+ \epsilon \bigg(- \bar{\alpha}_1 \Big(- \bar{\alpha}_1\, \boldsymbol{k}^2 + \alpha_2\, \boldsymbol{k}(\boldsymbol{k}+\boldsymbol{\ell}) \Big)\, (\boldsymbol{k}+\boldsymbol{r})^2 \\
&\quad + ({\alpha_1}^2 - {\alpha_2}^2\ ) \Big(- \boldsymbol{k}(\boldsymbol{k}+\boldsymbol{r})\, (\boldsymbol{k}+\boldsymbol{\ell})(\boldsymbol{k}+\boldsymbol{\ell}+\boldsymbol{r}) \\
&\qquad + \boldsymbol{k}(\boldsymbol{k}+\boldsymbol{\ell}+\boldsymbol{r})\, (\boldsymbol{k}+\boldsymbol{\ell})(\boldsymbol{k}+\boldsymbol{r}) \\
&\quad - \boldsymbol{k}(\boldsymbol{k}+\boldsymbol{\ell})\, (\boldsymbol{k}+\boldsymbol{r})(\boldsymbol{k}+\boldsymbol{\ell}+\boldsymbol{r}) \Big) \\
&\quad + (\boldsymbol{k}+\boldsymbol{r})(\boldsymbol{k}+\boldsymbol{\ell}+\boldsymbol{r}) \Big(- \alpha_2\, \bar{\alpha}_1\, \boldsymbol{k}^2 + {\alpha_1}^2\, (\boldsymbol{k}+\boldsymbol{\ell})^2 + \frac{{\alpha_1}^2\, \bar{\alpha}_1}{\alpha_\ell}\, \boldsymbol{\ell}^2 \Big) \\
&\quad + \frac{\alpha_1\, \bar{\alpha}_1}{\alpha_\ell} \Big(\bar{\alpha}_1\, \boldsymbol{\ell}^2 + \alpha_\ell\, \boldsymbol{\ell}(\boldsymbol{k}+\boldsymbol{\ell}) \Big) \Big((\boldsymbol{k}+\boldsymbol{r})^2 + \alpha_1\, Q^2 \Big) \bigg) \bigg] \\
&+ \frac{4\, \boldsymbol{k}(\boldsymbol{k}+\boldsymbol{r})}{{\alpha_1}^2}\, \mathcal{A}\mathcal{B}_{13}^{L}
\end{aligned} \tag{4.103}
$$

$$
\begin{aligned}
\mathcal{AB}^T_{14} = C_A \, \frac{1}{D_1\, D_2\, D_5\, D_7} \Big[& - 2\,\epsilon \,\Big(\frac{-2}{\alpha_2} \bar\alpha_1\, \alpha_\ell \, [(\boldsymbol{k}+\boldsymbol{\ell})(\boldsymbol{k}+\boldsymbol{r})]^2 \\
& + \frac{(\alpha_1\,\bar\alpha_1 - \alpha_2\,\bar\alpha_2)\,\alpha_\ell}{\alpha_1} (\boldsymbol{k}+\boldsymbol{\ell})(\boldsymbol{k}+\boldsymbol{\ell}+\boldsymbol{r})\,(\boldsymbol{k}+\boldsymbol{r})^2 \\
& - \alpha_\ell\,(\boldsymbol{k}+\boldsymbol{r})(\boldsymbol{k}+\boldsymbol{\ell}+\boldsymbol{r})\,\Big((\boldsymbol{k}+\boldsymbol{\ell})^2 + \alpha_1\,\bar\alpha_1\,Q^2\Big) \\
& - \bar\alpha_1\,\alpha_\ell\,Q^2\,\Big(\alpha_1\,(\boldsymbol{k}+\boldsymbol{\ell})^2 + \bar\alpha_1\,(\boldsymbol{k}+\boldsymbol{r})^2 + \alpha_1\,\bar\alpha_1\,Q^2\Big) \\
& + \alpha_\ell\,(\boldsymbol{k}+\boldsymbol{\ell})(\boldsymbol{k}+\boldsymbol{r})\,\Big(2\,(\boldsymbol{\ell}-\boldsymbol{r})\,(\boldsymbol{k}+\boldsymbol{\ell}+\boldsymbol{r}) \\
& \quad + (\frac{2\,\bar\alpha_1\,\bar\alpha_2}{\alpha_2} + \frac{\bar\alpha_1\,(-\bar\alpha_1+\bar\alpha_2)}{\alpha_1})\,(\boldsymbol{k}+\boldsymbol{r})^2 - \bar\alpha_1^2\,Q^2\,\Big)\Big) \\
& - ((\boldsymbol{k}+\boldsymbol{r})^2 + \alpha_1\,\bar\alpha_2\,Q^2) \\
& \cdot \Big(- \alpha_\ell\,(\boldsymbol{k}+\boldsymbol{\ell})(\boldsymbol{k}+\boldsymbol{\ell}+\boldsymbol{r}) + \bar\alpha_1\,(\boldsymbol{\ell}-2\boldsymbol{r})\,(\boldsymbol{k}+\boldsymbol{\ell})\Big) \\
& - \frac{1}{\alpha_1}(\boldsymbol{k}+\boldsymbol{r})^2\,\Big(- \bar\alpha_1\,\alpha_\ell\,(\boldsymbol{k}+\boldsymbol{\ell})^2 - \alpha_2\,\bar\alpha_1^2\,\alpha_\ell\,Q^2 \\
& \quad + \bar\alpha_1\,(-\alpha_1+\bar\alpha_1\,)\,(\boldsymbol{\ell}+\boldsymbol{r})\,(\boldsymbol{k}+\boldsymbol{\ell})\,\Big) \\
& + (\boldsymbol{k}+\boldsymbol{\ell})(\boldsymbol{k}+\boldsymbol{r})\,\Big[- \frac{\bar\alpha_1\,(-\alpha_1+\bar\alpha_1)\,(\alpha_2+2\,\alpha_\ell)}{\alpha_1\,\alpha_2}(\boldsymbol{k}+\boldsymbol{r})^2 \\
& \quad + \frac{2\,\bar\alpha_1\,\bar\alpha_2\,\alpha_\ell}{\alpha_2}(\frac{1}{\alpha_1}(\boldsymbol{k}+\boldsymbol{r})^2 + \alpha_2\,Q^2) \\
& \quad + \frac{(-\alpha_1+\bar\alpha_1)}{\alpha_2\,\alpha_\ell}\Big(\,\alpha_2\,(-\alpha_\ell\,(\boldsymbol{k}+\boldsymbol{\ell})^2 + \bar\alpha_1\,\boldsymbol{\ell}^2 - \bar\alpha_1\,\alpha_\ell\,Q^2 \\
& \qquad + \alpha_\ell\,(\boldsymbol{\ell}-2\boldsymbol{r})\,(\boldsymbol{k}+\boldsymbol{\ell}+\boldsymbol{r})) - 2\,\alpha_\ell\,(\alpha_\ell\,(\boldsymbol{k}+\boldsymbol{r})(\boldsymbol{k}+\boldsymbol{\ell}+\boldsymbol{r}) \\
& \qquad - \bar\alpha_1\,(\boldsymbol{\ell}-2\boldsymbol{r})\,(\boldsymbol{k}+\boldsymbol{r}))\Big)\Big] \\
& + (-\alpha_1+\bar\alpha_1)\,\Big((\boldsymbol{k}+\boldsymbol{r})(\boldsymbol{k}+\boldsymbol{\ell}+\boldsymbol{r})\,(\boldsymbol{\ell}-2\boldsymbol{r})\,(\boldsymbol{k}+\boldsymbol{\ell}) \\
& \quad - (\boldsymbol{k}+\boldsymbol{\ell})(\boldsymbol{k}+\boldsymbol{\ell}+\boldsymbol{r})\,(\boldsymbol{\ell}-2\boldsymbol{r})\,(\boldsymbol{k}+\boldsymbol{r})\Big) \\
& + ((\boldsymbol{k}+\boldsymbol{\ell})^2 + \alpha_2\,\bar\alpha_1\,Q^2)\,\Big(2\,\alpha_\ell\,(\boldsymbol{k}+\boldsymbol{r})(\boldsymbol{k}+\boldsymbol{\ell}+\boldsymbol{r}) \\
& \quad + \bar\alpha_1\,(\boldsymbol{\ell}+\boldsymbol{r})\,(\boldsymbol{k}+\boldsymbol{r})\Big)\Big] + \frac{4\,(\boldsymbol{k}+\boldsymbol{\ell})(\boldsymbol{k}+\boldsymbol{r})}{\alpha_2\,\bar\alpha_1}\,\mathcal{AB}^L_{14}
\end{aligned}
\tag{4.104}
$$

$$
\mathcal{AB}^T_{15} = \, - C_A \, \frac{2}{\alpha_\ell\, D_1\, D_2\, D_5\, D_7}\, \bar\alpha_1\,(\alpha_2\,\bar\alpha_1 + \alpha_1\,\bar\alpha_2)\,(\boldsymbol{k}+\boldsymbol{\ell})(\boldsymbol{k}+\boldsymbol{r})\,\boldsymbol{r}^2
\tag{4.105}
$$

$$
\begin{aligned}
\mathcal{AB}_{22}^T = & -(C_A - 2C_F)\,\frac{2}{D_2\,D_3\,D_4\,D_7}\Bigg[\frac{(\alpha_1 - \bar{\alpha}_1\,)}{\alpha_1}\,(\boldsymbol{k}+\boldsymbol{r})^2 \\
& \cdot\Big(\bar{\alpha}_2\,\boldsymbol{k}(\boldsymbol{k}+\boldsymbol{\ell}) + \alpha_2\,(\boldsymbol{k}+\boldsymbol{\ell})(\boldsymbol{k}+\boldsymbol{\ell}+\boldsymbol{r})\Big) \\
& - \frac{(-\alpha_2\,\bar{\alpha}_1 + \alpha_1\,\bar{\alpha}_2\,)}{\bar{\alpha}_1}\,(\boldsymbol{k}+\boldsymbol{\ell})^2\,\Big(\bar{\alpha}_2\,\boldsymbol{k}(\boldsymbol{k}+\boldsymbol{r}) + \alpha_2\,(\boldsymbol{k}+\boldsymbol{r})(\boldsymbol{k}+\boldsymbol{\ell}+\boldsymbol{r})\Big) \\
& - 2\,(\boldsymbol{k}+\boldsymbol{\ell})(\boldsymbol{k}+\boldsymbol{r})\,\Big(\bar{\alpha}_2^2\,\boldsymbol{k}(\boldsymbol{k}+\boldsymbol{r}) + {\alpha_2}^2\,(\boldsymbol{k}+\boldsymbol{\ell})(\boldsymbol{k}+\boldsymbol{\ell}+\boldsymbol{r}) \\
& \quad + \alpha_2\,\bar{\alpha}_2\,(\boldsymbol{k}(\boldsymbol{k}+\boldsymbol{\ell}) + (\boldsymbol{k}+\boldsymbol{r})(\boldsymbol{k}+\boldsymbol{\ell}+\boldsymbol{r}))\Big) \\
& + \epsilon\,\Bigg((\boldsymbol{k}+\boldsymbol{\ell})(\boldsymbol{k}+\boldsymbol{r})\,\Big((\alpha_1\,\bar{\alpha}_1 + \alpha_2\,\bar{\alpha}_2)\,\boldsymbol{k}(\boldsymbol{k}+\boldsymbol{\ell}+\boldsymbol{r}) - 2\,\bar{\alpha}_1\,\bar{\alpha}_2\,\boldsymbol{k}(\boldsymbol{k}+\boldsymbol{r}) \\
& \quad - 2\,\alpha_1\,\alpha_2\,(\boldsymbol{k}+\boldsymbol{\ell})(\boldsymbol{k}+\boldsymbol{\ell}+\boldsymbol{r})\Big) + 2\,\alpha_2\,\bar{\alpha}_2\,[(\boldsymbol{k}+\boldsymbol{\ell})(\boldsymbol{k}+\boldsymbol{r})]^2 \\
& + (\alpha_1\,\bar{\alpha}_1 - \alpha_2\,\bar{\alpha}_2) \\
& \cdot\Big(\boldsymbol{k}(\boldsymbol{k}+\boldsymbol{r})\,(\boldsymbol{k}+\boldsymbol{\ell})(\boldsymbol{k}+\boldsymbol{\ell}+\boldsymbol{r}) - \boldsymbol{k}(\boldsymbol{k}+\boldsymbol{\ell})\,(\boldsymbol{k}+\boldsymbol{r})(\boldsymbol{k}+\boldsymbol{\ell}+\boldsymbol{r})\Big) \\
& + (\alpha_1\,\bar{\alpha}_1 - \alpha_2\,\bar{\alpha}_2)\,\Big(\frac{\bar{\alpha}_2}{\alpha_1}\,\boldsymbol{k}(\boldsymbol{k}+\boldsymbol{\ell})\,(\boldsymbol{k}+\boldsymbol{r})^2 - \frac{\alpha_2\,\bar{\alpha}_2}{\alpha_1\,\bar{\alpha}_1}\,(\boldsymbol{k}+\boldsymbol{\ell})^2\,(\boldsymbol{k}+\boldsymbol{r})^2 \\
& \quad + \frac{\alpha_2}{\bar{\alpha}_1}\,(\boldsymbol{k}+\boldsymbol{\ell})^2\,(\boldsymbol{k}+\boldsymbol{r})(\boldsymbol{k}+\boldsymbol{\ell}+\boldsymbol{r})\Big)\Bigg)\Bigg]
\end{aligned}
\tag{4.106}
$$

$$
\begin{aligned}
\mathcal{AB}_{23}^T = & -C_F\,\frac{4}{\bar{\alpha}_1\,D_2\,{D_4}^2\,D_6}\,{\alpha_1}^2\,(1-\epsilon) \\
& \cdot\Big(\bar{\alpha}_1\,\boldsymbol{k}^2 - \alpha_2\,(\boldsymbol{k}+\boldsymbol{\ell})^2 - \frac{\alpha_2\,\bar{\alpha}_1\,\boldsymbol{\ell}^2}{\alpha_\ell}\Big)\,\boldsymbol{\ell}(\boldsymbol{k}+\boldsymbol{r}) \\
& + \frac{2\,\boldsymbol{k}(\boldsymbol{k}+\boldsymbol{r})}{{\alpha_1}^2}\,\mathcal{AB}_{23}^L
\end{aligned}
\tag{4.107}
$$

$$
\begin{aligned}
\mathcal{A}\mathcal{B}_{24}^{T} = & -C_A\,\frac{1}{D_2\,D_4\,D_5\,D_7}\Bigg[\qquad (4.108)\\
& 2\,\epsilon\left[\frac{\alpha_2\,(-\alpha_1\,\bar{\alpha}_1+\alpha_2\,\bar{\alpha}_2)\,\alpha_\ell}{\alpha_1\,\bar{\alpha}_1}(\boldsymbol{k}+\boldsymbol{\ell})^2\,(\boldsymbol{k}+\boldsymbol{r})^2\right.\\
& +\alpha_\ell\,\boldsymbol{k}(\boldsymbol{k}+\boldsymbol{\ell})\left(2\,(\boldsymbol{k}+\boldsymbol{\ell})(\boldsymbol{k}+\boldsymbol{r})+\frac{(\alpha_1\,\bar{\alpha}_1-\alpha_2\,\bar{\alpha}_2)}{\alpha_1}\,(\boldsymbol{k}+\boldsymbol{r})^2\right)\\
& -\alpha_\ell\,\boldsymbol{k}(\boldsymbol{k}+\boldsymbol{r})\left((\boldsymbol{k}+\boldsymbol{\ell})^2+2\,(\boldsymbol{k}+\boldsymbol{\ell})(\boldsymbol{k}+\boldsymbol{r})+\alpha_1\,\bar{\alpha}_1\,Q^2\right)\\
& \left.-\frac{\alpha_2\,\alpha_\ell}{\bar{\alpha}_1}\,(\boldsymbol{k}+\boldsymbol{\ell})(\boldsymbol{k}+\boldsymbol{r})\left((\boldsymbol{k}+\boldsymbol{\ell})^2-2\,(\boldsymbol{k}+\boldsymbol{\ell})(\boldsymbol{k}+\boldsymbol{r})-\alpha_1\,\bar{\alpha}_1\,Q^2\right)\right]\\
& +(\boldsymbol{k}+\boldsymbol{\ell})(\boldsymbol{k}+\boldsymbol{r})\left(\frac{2\,\alpha_2\,\alpha_\ell\,((\boldsymbol{k}+\boldsymbol{\ell})^2+\alpha_2\,\bar{\alpha}_1\,Q^2)}{\bar{\alpha}_1}\right.\\
& \quad +(\bar{\alpha}_1-\alpha_1\ )\left(\alpha_2\,(-\frac{(\boldsymbol{k}+\boldsymbol{\ell})^2}{\bar{\alpha}_1}-\frac{(\boldsymbol{k}+\boldsymbol{r})^2}{\alpha_1}+\frac{\boldsymbol{\ell}^2}{\alpha_\ell}-Q^2\ )\right.\\
& \quad \left.\left.+\frac{1}{\bar{\alpha}_1}(-2\,\alpha_\ell\,\boldsymbol{k}(\boldsymbol{k}+\boldsymbol{\ell})+\bar{\alpha}_1\,\boldsymbol{k}\,(\boldsymbol{\ell}-2\boldsymbol{r})+2\,\alpha_2\,(\boldsymbol{\ell}-2\boldsymbol{r})\,(\boldsymbol{k}+\boldsymbol{\ell}))\right)\right)\\
& +(\bar{\alpha}_1\ -\alpha_1)\Bigg(-\boldsymbol{k}(\boldsymbol{k}+\boldsymbol{r})\,(\boldsymbol{\ell}-2\boldsymbol{r})\,(\boldsymbol{k}+\boldsymbol{\ell})\\
& \quad +\boldsymbol{k}(\boldsymbol{k}+\boldsymbol{\ell})\,(\boldsymbol{\ell}-2\boldsymbol{r})\,(\boldsymbol{k}+\boldsymbol{r})\\
& \quad -\frac{1}{\alpha_1}(\boldsymbol{k}+\boldsymbol{r})^2\left(2\,\alpha_\ell\,\boldsymbol{k}(\boldsymbol{k}+\boldsymbol{\ell})+\alpha_2\,(\boldsymbol{\ell}+\boldsymbol{r})\,(\boldsymbol{k}+\boldsymbol{\ell})\ \right)\\
& \quad \left.+\frac{1}{\bar{\alpha}_1}(\boldsymbol{k}+\boldsymbol{\ell})^2\left(\alpha_\ell\,\boldsymbol{k}(\boldsymbol{k}+\boldsymbol{r})-\alpha_2\,(\boldsymbol{\ell}-2\boldsymbol{r})(\boldsymbol{k}+\boldsymbol{r})\right)\right)\\
& +\frac{\alpha_2}{\alpha_1}\left((\boldsymbol{k}+\boldsymbol{\ell})^2+\alpha_2\,\bar{\alpha}_1\,Q^2\right)\left(\alpha_\ell\,(\boldsymbol{k}+\boldsymbol{r})^2+\alpha_1\,(\boldsymbol{\ell}+\boldsymbol{r})\,(\boldsymbol{k}+\boldsymbol{r})\right)\Bigg]\\
& +\frac{4\,(\boldsymbol{k}+\boldsymbol{\ell})(\boldsymbol{k}+\boldsymbol{r})}{\alpha_2\,\bar{\alpha}_1}\,\mathcal{A}\mathcal{B}_{24}^{L}
\end{aligned}
$$

$$
\mathcal{A}\mathcal{B}_{25}^{T} = C_A\,\frac{2}{\alpha_\ell\,D_2\,D_4\,D_5\,D_7}\,\alpha_2\,(\alpha_2\,\bar{\alpha}_1+\alpha_1\,\bar{\alpha}_2)\,(\boldsymbol{k}+\boldsymbol{\ell})(\boldsymbol{k}+\boldsymbol{r})\,\boldsymbol{r}^2 \qquad (4.109)
$$

$$
\begin{aligned}
\mathcal{AB}^T_{33} = & -(C_A - 2C_F)\,\frac{2}{D_1\,D_3\,D_4\,D_6}\Bigg[\qquad (4.110)\\
& -\Big(\alpha_1\,(\boldsymbol{k}+\boldsymbol{\ell})(\boldsymbol{k}+\boldsymbol{\ell}+\boldsymbol{r}) + \bar{\alpha}_1\,(\boldsymbol{k}+\boldsymbol{r})(\boldsymbol{k}+\boldsymbol{\ell}+\boldsymbol{r})\Big)\\
& \quad \cdot\Big(-\bar{\alpha}_1\,\boldsymbol{k}^2 + 2\,\alpha_1\,\boldsymbol{k}(\boldsymbol{k}+\boldsymbol{\ell}+\boldsymbol{r}) + \alpha_1\,\bar{\alpha}_2\,(\frac{(\boldsymbol{k}+\boldsymbol{\ell})^2}{\bar{\alpha}_1} + \frac{\boldsymbol{\ell}^2}{\alpha_\ell})\Big)\\
& -\Big(\alpha_1\,\boldsymbol{k}(\boldsymbol{k}+\boldsymbol{\ell}) + \bar{\alpha}_1\,\boldsymbol{k}(\boldsymbol{k}+\boldsymbol{r})\Big)\Big(2\,\bar{\alpha}_1\,\boldsymbol{k}(\boldsymbol{k}+\boldsymbol{\ell}+\boldsymbol{r})\\
& \quad -\alpha_1\,(\boldsymbol{k}+\boldsymbol{\ell}+\boldsymbol{r})^2 + \alpha_2\,\bar{\alpha}_1\,(\frac{(\boldsymbol{k}+\boldsymbol{r})^2}{\alpha_1} + \frac{\boldsymbol{\ell}^2}{\alpha_\ell})\Big)\\
& +\epsilon\Bigg((\alpha_1\,\bar{\alpha}_1 + \alpha_2\,\bar{\alpha}_2)\,\boldsymbol{k}(\boldsymbol{k}+\boldsymbol{\ell}+\boldsymbol{r})\,(\boldsymbol{k}+\boldsymbol{\ell})(\boldsymbol{k}+\boldsymbol{r})\\
& \quad +\bar{\alpha}_2\,\bar{\alpha}_1\,\Big(-2\,\boldsymbol{k}(\boldsymbol{k}+\boldsymbol{\ell}+\boldsymbol{r})\,\boldsymbol{k}(\boldsymbol{k}+\boldsymbol{r}) + \boldsymbol{k}^2\,(\boldsymbol{k}+\boldsymbol{r})(\boldsymbol{k}+\boldsymbol{\ell}+\boldsymbol{r})\Big)\\
& \quad +\bar{\alpha}_2\,\alpha_2\,\Big(\boldsymbol{k}(\boldsymbol{k}+\boldsymbol{r})\,(\boldsymbol{k}+\boldsymbol{\ell})(\boldsymbol{k}+\boldsymbol{\ell}+\boldsymbol{r})\\
& \qquad -\boldsymbol{k}(\boldsymbol{k}+\boldsymbol{\ell})\,(\boldsymbol{k}+\boldsymbol{r})(\boldsymbol{k}+\boldsymbol{\ell}+\boldsymbol{r})\Big)\\
& \quad +\alpha_1\,\alpha_2\,\Big(-2\,\boldsymbol{k}(\boldsymbol{k}+\boldsymbol{\ell}+\boldsymbol{r})\,(\boldsymbol{k}+\boldsymbol{\ell})(\boldsymbol{k}+\boldsymbol{\ell}+\boldsymbol{r})\\
& \qquad +\boldsymbol{k}(\boldsymbol{k}+\boldsymbol{\ell})\,(\boldsymbol{k}+\boldsymbol{\ell}+\boldsymbol{r})^2\Big)\\
& \quad -\alpha_1\,\bar{\alpha}_1\,\Big(\boldsymbol{k}(\boldsymbol{k}+\boldsymbol{r})\,(\boldsymbol{k}+\boldsymbol{\ell})(\boldsymbol{k}+\boldsymbol{\ell}+\boldsymbol{r})\\
& \qquad -\boldsymbol{k}(\boldsymbol{k}+\boldsymbol{\ell})\,(\boldsymbol{k}+\boldsymbol{r})(\boldsymbol{k}+\boldsymbol{\ell}+\boldsymbol{r})\Big)\\
& \quad +\frac{\alpha_1\,\bar{\alpha}_1^2}{\alpha_\ell}\Big(-\alpha_\ell\,(\boldsymbol{k}+\boldsymbol{r})(\boldsymbol{k}+\boldsymbol{\ell}+\boldsymbol{r}) + \alpha_1\,\boldsymbol{\ell}^2\Big)\Big(\frac{(\boldsymbol{k}+\boldsymbol{\ell})^2}{\bar{\alpha}_1} + \frac{\boldsymbol{\ell}^2}{\alpha_\ell}\Big)\\
& \quad +\frac{{\alpha_1}^2\,\bar{\alpha}_1}{\alpha_\ell}\Big(-\alpha_\ell\,\boldsymbol{k}(\boldsymbol{k}+\boldsymbol{\ell}) + \bar{\alpha}_1\,\boldsymbol{\ell}^2\Big)\Big(\frac{(\boldsymbol{k}+\boldsymbol{r})^2}{\alpha_1} + \frac{\boldsymbol{\ell}^2}{\alpha_\ell}\Big)\\
& \quad -\alpha_1\,\bar{\alpha}_1\,\Big(-2\,(\boldsymbol{k}(\boldsymbol{k}+\boldsymbol{\ell}+\boldsymbol{r}))^2 + \boldsymbol{k}^2\,(\boldsymbol{k}+\boldsymbol{\ell}+\boldsymbol{r})^2\\
& \qquad -(\boldsymbol{k}+\boldsymbol{\ell})^2\,(\boldsymbol{k}+\boldsymbol{r})^2 + \frac{\alpha_1\,\bar{\alpha}_1\,\boldsymbol{\ell}^4}{{\alpha_\ell}^2}\Big)\Bigg)\Bigg]
\end{aligned}
$$

$$\mathcal{AB}_{34}^T = -C_A \frac{1}{D_1 D_3 D_5 D_7} \Bigg[\tag{4.111}$$

$$2\epsilon \Bigg(\alpha_\ell \Big(\alpha_1 (\boldsymbol{k}+\boldsymbol{\ell})^2 - \bar{\alpha}_2 (\boldsymbol{k}+\boldsymbol{\ell})(\boldsymbol{k}+\boldsymbol{r}) \Big) (\boldsymbol{k}+\boldsymbol{\ell}+\boldsymbol{r})^2$$

$$- \frac{(\bar{\alpha}_1 - \bar{\alpha}_2)\,\alpha_\ell}{\alpha_1} (\boldsymbol{k}+\boldsymbol{\ell})(\boldsymbol{k}+\boldsymbol{\ell}+\boldsymbol{r})\,(\boldsymbol{k}+\boldsymbol{r})^2$$

$$- \alpha_\ell (\boldsymbol{k}+\boldsymbol{r})(\boldsymbol{k}+\boldsymbol{\ell}+\boldsymbol{r}) \Big((\boldsymbol{k}+\boldsymbol{\ell})^2 + \bar{\alpha}_1^2 Q^2 \Big)$$

$$+ \bar{\alpha}_1 \alpha_\ell \Big(\frac{(\boldsymbol{k}+\boldsymbol{r})^2}{\alpha_1} + \frac{\boldsymbol{\ell}^2}{\alpha_\ell} \Big)$$

$$\cdot \Big(\bar{\alpha}_1 (\boldsymbol{k}+\boldsymbol{\ell})(\boldsymbol{k}+\boldsymbol{r}) + \alpha_1 ((\boldsymbol{k}+\boldsymbol{\ell})^2 + \bar{\alpha}_1 Q^2) \Big) \Bigg)$$

$$- \bar{\alpha}_1 \Big(\frac{(\boldsymbol{k}+\boldsymbol{r})^2}{\alpha_1} + \frac{\boldsymbol{\ell}^2}{\alpha_\ell} \Big) \Big(\bar{\alpha}_1 \alpha_\ell (\boldsymbol{k}+\boldsymbol{\ell})(\boldsymbol{k}+\boldsymbol{r})$$

$$+ 2\alpha_1 \alpha_\ell \Big((\boldsymbol{k}+\boldsymbol{\ell})^2 + \bar{\alpha}_1 Q^2 \Big) + \alpha_1 \bar{\alpha}_1 (\boldsymbol{\ell} - 2\boldsymbol{r})\,(\boldsymbol{k}+\boldsymbol{\ell}) \Big)$$

$$+ (\boldsymbol{k}+\boldsymbol{\ell}+\boldsymbol{r})^2 \Big(-2\alpha_1 \alpha_\ell (\boldsymbol{k}+\boldsymbol{\ell})^2 + \bar{\alpha}_2 \alpha_\ell (\boldsymbol{k}+\boldsymbol{\ell})(\boldsymbol{k}+\boldsymbol{r})$$

$$+ \alpha_1 \bar{\alpha}_2 ((\boldsymbol{\ell} - 2\boldsymbol{r})\,(\boldsymbol{k}+\boldsymbol{\ell})) \Big)$$

$$+ 3(\bar{\alpha}_1 - \bar{\alpha}_2) \Big(-(\boldsymbol{k}+\boldsymbol{r})(\boldsymbol{k}+\boldsymbol{\ell}+\boldsymbol{r})\,\boldsymbol{r}(\boldsymbol{k}+\boldsymbol{\ell})$$

$$+ (\boldsymbol{k}+\boldsymbol{\ell})(\boldsymbol{k}+\boldsymbol{r})\,\boldsymbol{r}(\boldsymbol{k}+\boldsymbol{\ell}+\boldsymbol{r}) \Big)$$

$$+ ((\boldsymbol{k}+\boldsymbol{\ell})^2 + \bar{\alpha}_1^2 Q^2)$$

$$\cdot \Big(\alpha_\ell (\boldsymbol{k}+\boldsymbol{r})(\boldsymbol{k}+\boldsymbol{\ell}+\boldsymbol{r}) + \alpha_1 (\boldsymbol{\ell}+\boldsymbol{r})\,(\boldsymbol{k}+\boldsymbol{\ell}+\boldsymbol{r}) \Big)$$

$$+ \frac{(\bar{\alpha}_1 - \bar{\alpha}_2)}{\alpha_1 \bar{\alpha}_1 \alpha_\ell} (\boldsymbol{k}+\boldsymbol{\ell})(\boldsymbol{k}+\boldsymbol{\ell}+\boldsymbol{r}) \Big(2\bar{\alpha}_1 {\alpha_\ell}^2 (\boldsymbol{k}+\boldsymbol{r})^2 + {\alpha_1}^2 \bar{\alpha}_1 \boldsymbol{\ell}^2$$

$$- {\alpha_1}^2 \alpha_\ell \Big((\boldsymbol{k}+\boldsymbol{\ell})^2 + \bar{\alpha}_1 Q^2 \Big)$$

$$- \alpha_1 \bar{\alpha}_1 \alpha_\ell \Big((\boldsymbol{k}+\boldsymbol{\ell})(\boldsymbol{k}+\boldsymbol{r}) + \boldsymbol{\ell}(\boldsymbol{k}+\boldsymbol{r}) \Big) \Big) \Bigg]$$

$$+ \frac{4(\boldsymbol{k}+\boldsymbol{\ell})(\boldsymbol{k}+\boldsymbol{\ell}+\boldsymbol{r})}{\bar{\alpha}_1^2} \mathcal{AB}_{34}^L$$

$$\mathcal{AB}_{35}^T = C_A \frac{2}{\alpha_\ell D_1 D_3 D_5 D_7} \alpha_1 (\bar{\alpha}_1^2 + \bar{\alpha}_2^2)\,(\boldsymbol{k}+\boldsymbol{\ell})(\boldsymbol{k}+\boldsymbol{\ell}+\boldsymbol{r})\,\boldsymbol{r}^2 \tag{4.112}$$

$$
\begin{aligned}
\mathcal{AB}^T_{44} = &-C_A\,\frac{1}{D_2\,{D_5}^2\,D_7}\Bigg[-4\,{\alpha_\ell}^2\,((\boldsymbol{k}+\boldsymbol{\ell})(\boldsymbol{k}+\boldsymbol{r}))^2 \\
&+\frac{(\alpha_1+\bar{\alpha}_1)\,{\alpha_\ell}^2}{\alpha_1\,\bar{\alpha}_1}\,(\boldsymbol{k}+\boldsymbol{\ell})^2\,(\boldsymbol{k}+\boldsymbol{r})^2 \\
&+4\,\epsilon\,\Bigg(4\,{\alpha_\ell}^2\,((\boldsymbol{k}+\boldsymbol{\ell})(\boldsymbol{k}+\boldsymbol{r}))^2-\frac{(\alpha_1-\bar{\alpha}_2)\,{\alpha_\ell}^2}{\alpha_1\,\bar{\alpha}_1}\,(\boldsymbol{k}+\boldsymbol{\ell})^2\,(\boldsymbol{k}+\boldsymbol{r})^2 \\
&\quad+{\alpha_\ell}^2\,Q^2\,\Big(\alpha_1\,(\boldsymbol{k}+\boldsymbol{\ell})^2+\bar{\alpha}_1\,(\boldsymbol{k}+\boldsymbol{r})^2+\alpha_1\,\bar{\alpha}_1\,Q^2\Big) \\
&\quad-\frac{{\alpha_\ell}^2}{\alpha_1\,\bar{\alpha}_1}\,(\boldsymbol{k}+\boldsymbol{\ell})(\boldsymbol{k}+\boldsymbol{r})\,\Big(\alpha_1\,(-\alpha_1+\alpha_2)\,(\boldsymbol{k}+\boldsymbol{\ell})^2 \\
&\qquad+\bar{\alpha}_1\,(-\bar{\alpha}_1+\bar{\alpha}_2\ )\,(\boldsymbol{k}+\boldsymbol{r})^2-\alpha_1\,\bar{\alpha}_1\,(\alpha_1+\bar{\alpha}_1)\,Q^2\Big)\Bigg) \\
&+\frac{\bar{\alpha}_1\,\alpha_\ell}{\alpha_1}\,(\boldsymbol{k}+\boldsymbol{r})^2\,\Big(\alpha_2\,\alpha_\ell\,Q^2\ \ -3\,(\boldsymbol{\ell}-\boldsymbol{r})\,(\boldsymbol{k}+\boldsymbol{\ell})\Big) \\
&+\frac{\alpha_1\,\alpha_\ell}{\bar{\alpha}_1}\,(\boldsymbol{k}+\boldsymbol{\ell})^2\,\Big(\bar{\alpha}_2\,\alpha_\ell\,Q^2\ \ +3\,(\boldsymbol{\ell}-\boldsymbol{r})\,(\boldsymbol{k}+\boldsymbol{r})\ \Big) \\
&+(\boldsymbol{k}+\boldsymbol{\ell})(\boldsymbol{k}+\boldsymbol{r})\,\Bigg(\frac{-2\,\alpha_\ell\,(\alpha_2\,\bar{\alpha}_1+\alpha_1\,\bar{\alpha}_2+2\,(\alpha_1-\alpha_2)\,\alpha_\ell)}{\bar{\alpha}_1}\,(\boldsymbol{k}+\boldsymbol{\ell})^2 \\
&\quad-\frac{2\,\alpha_\ell\,(\alpha_2\,\bar{\alpha}_1+\alpha_1\,\bar{\alpha}_2+2\,(\bar{\alpha}_1-\bar{\alpha}_2)\,\alpha_\ell)}{\alpha_1}\,(\boldsymbol{k}+\boldsymbol{r})^2 \\
&\quad+4\,(\alpha_2+\bar{\alpha}_2)\,{\alpha_\ell}^2\,Q^2 \\
&\quad+2\,(\alpha_2\,\bar{\alpha}_1+\alpha_1\,\bar{\alpha}_2)\,\Big(-\alpha_\ell\,Q^2+2\,(\boldsymbol{\ell}-\boldsymbol{r})^2\Big) \\
&\quad-6\,(\alpha_1-\alpha_2)\,\alpha_\ell\,(\boldsymbol{\ell}-\boldsymbol{r})\,(\boldsymbol{k}+\boldsymbol{\ell}) \\
&\quad+6\,(\bar{\alpha}_1-\bar{\alpha}_2)\,\alpha_\ell\,(\boldsymbol{\ell}-\boldsymbol{r})\,(\boldsymbol{k}+\boldsymbol{r})\ \Bigg) \\
&+3\,\alpha_2\,\bar{\alpha}_1\,\alpha_\ell\,Q^2\,(\boldsymbol{\ell}-\boldsymbol{r})\,(\boldsymbol{k}+\boldsymbol{r})-3\,\alpha_1\,\bar{\alpha}_2\,\alpha_\ell\,Q^2\,(\boldsymbol{\ell}-\boldsymbol{r})\,(\boldsymbol{k}+\boldsymbol{\ell})\Bigg]
\end{aligned}
\tag{4.113}
$$

$$
\mathcal{AB}^T_{45} = 0 \tag{4.114}
$$

$$\begin{aligned}
\widetilde{\mathcal{AB}}^T_{44} = &- C_A \, \frac{1}{D_2\, {D_5}^2\, D_7} \Bigg[- 4\, {\alpha_\ell}^2 \, ((\boldsymbol{k}+\boldsymbol{\ell})(\boldsymbol{k}+\boldsymbol{r}))^2 \\
&+ \frac{(\alpha_1 + \bar\alpha_1)\, {\alpha_\ell}^2}{\alpha_1\, \bar\alpha_1}\, (\boldsymbol{k}+\boldsymbol{\ell})^2\, (\boldsymbol{k}+\boldsymbol{r})^2 \\
&+ 4\,\epsilon \Bigg(4\, {\alpha_\ell}^2\, ((\boldsymbol{k}+\boldsymbol{\ell})(\boldsymbol{k}+\boldsymbol{r}))^2 - \frac{(\alpha_1 - \bar\alpha_2)\, {\alpha_\ell}^2}{\alpha_1\, \bar\alpha_1}\, (\boldsymbol{k}+\boldsymbol{\ell})^2\, (\boldsymbol{k}+\boldsymbol{r})^2 \\
&\quad + {\alpha_\ell}^2\, Q^2 \Big(\alpha_1\, (\boldsymbol{k}+\boldsymbol{\ell})^2 + \bar\alpha_1\, (\boldsymbol{k}+\boldsymbol{r})^2 + \alpha_1\, \bar\alpha_1\, Q^2 \Big) \\
&\quad - \frac{{\alpha_\ell}^2}{\alpha_1\, \bar\alpha_1}\, (\boldsymbol{k}+\boldsymbol{\ell})(\boldsymbol{k}+\boldsymbol{r}) \Big(\alpha_1\, (-\alpha_1 + \alpha_2)\, (\boldsymbol{k}+\boldsymbol{\ell})^2 \\
&\qquad + \bar\alpha_1\, (-\bar\alpha_1 + \bar\alpha_2\ )\, (\boldsymbol{k}+\boldsymbol{r})^2 - \alpha_1\, \bar\alpha_1\, (\alpha_1 + \bar\alpha_1)\, Q^2 \Big) \Bigg) \\
&+ \frac{\bar\alpha_1\, \alpha_\ell}{\alpha_1}\, (\boldsymbol{k}+\boldsymbol{r})^2 \Big(\alpha_2\, \alpha_\ell\, Q^2\ - 3\, (\boldsymbol{\ell}-\boldsymbol{r})\, (\boldsymbol{k}+\boldsymbol{\ell}) \Big) \\
&+ \frac{\alpha_1\, \alpha_\ell}{\bar\alpha_1}\, (\boldsymbol{k}+\boldsymbol{\ell})^2 \Big(\bar\alpha_2\, \alpha_\ell\, Q^2\ + 3\, (\boldsymbol{\ell}-\boldsymbol{r})\, (\boldsymbol{k}+\boldsymbol{r})\ \Big) \\
&+ (\boldsymbol{k}+\boldsymbol{\ell})(\boldsymbol{k}+\boldsymbol{r}) \Bigg(\frac{-2\, \alpha_\ell\, (\alpha_2\, \bar\alpha_1 + \alpha_1\, \bar\alpha_2 + 2\, (\alpha_1 - \alpha_2)\, \alpha_\ell)}{\bar\alpha_1}\, (\boldsymbol{k}+\boldsymbol{\ell})^2 \\
&\quad - \frac{2\, \alpha_\ell\, (\alpha_2\, \bar\alpha_1 + \alpha_1\, \bar\alpha_2 + 2\, (\bar\alpha_1 - \bar\alpha_2)\, \alpha_\ell)}{\alpha_1}\, (\boldsymbol{k}+\boldsymbol{r})^2 \\
&\quad + 4\, (\alpha_2 + \bar\alpha_2)\, {\alpha_\ell}^2\, Q^2 \\
&\quad + 2\, (\alpha_2\, \bar\alpha_1 + \alpha_1\, \bar\alpha_2) \Big(- \alpha_\ell\, Q^2 + 2\, \boldsymbol{r}^2 + 2\, (\boldsymbol{\ell}-\boldsymbol{r})^2 \Big) \\
&\quad - 6\, (\alpha_1 - \alpha_2)\, \alpha_\ell\, (\boldsymbol{\ell}-\boldsymbol{r})\, (\boldsymbol{k}+\boldsymbol{\ell}) \\
&\quad + 6\, (\bar\alpha_1 - \bar\alpha_2)\, \alpha_\ell\, (\boldsymbol{\ell}-\boldsymbol{r})\, (\boldsymbol{k}+\boldsymbol{r})\ \Bigg) \\
&+ 3\, \alpha_2\, \bar\alpha_1\, \alpha_\ell\, Q^2\, (\boldsymbol{\ell}-\boldsymbol{r})\, (\boldsymbol{k}+\boldsymbol{r}) - 3\, \alpha_1\, \bar\alpha_2\, \alpha_\ell\, Q^2\, (\boldsymbol{\ell}-\boldsymbol{r})\, (\boldsymbol{k}+\boldsymbol{\ell}) \Bigg]
\end{aligned} \tag{4.115}$$

$$\widetilde{\mathcal{AB}}^T_{45} = C_A \, \frac{2}{D_2\, {D_5}^2\, D_7}\, (\alpha_2\, \bar\alpha_1 + \alpha_1\, \bar\alpha_2)\, (\boldsymbol{k}+\boldsymbol{\ell})(\boldsymbol{k}+\boldsymbol{r})\, \boldsymbol{r}^2 \tag{4.116}$$

$$\mathcal{AB}^T_{55} = 0 \tag{4.117}$$

Also here, the original expressions $\widetilde{\mathcal{AA}}^T_{45}$ and $\widetilde{\mathcal{AA}}^T_{54}$ are contained in $\widetilde{\mathcal{AA}}^T_{44}$ and we get simpler expressions by introducing

$$\begin{aligned}
\mathcal{AA}^T_{44} &= \widetilde{\mathcal{AA}^T_{44}} + \widetilde{\mathcal{AA}^T_{45}} + \widetilde{\mathcal{AA}^T_{54}}\,, \\
\mathcal{AA}^T_{45} &= \mathcal{AA}^T_{54} =\ 0
\end{aligned}$$

and correspondingly for the $\mathcal{AB}$ diagrams.

The remaining expressions, e.g. $\mathcal{BA}_{ij}$ $(i < j)$, are derived from the listed ones exactly as in the longitudinal case by exploiting the symmetries.

4.3 The central limit

As indicated in sec. 4.1 the configuration where the gluon is separated from both the lower quark and the $q\bar{q}$ pair by a large rapidity gap corresponds to the limit of $\alpha_\ell \ll \alpha, 1-\alpha$. Let us study in some detail what happens in approaching this limit.

At small α_ℓ the denominators $D_1, \ldots, D_7$ ((4.16)–(4.22)) are expressed in terms of the two denominators D_2 and D_7; they in turn are closely related to the denominators $D(\boldsymbol{k}+\boldsymbol{r}) = \alpha(1-\alpha)Q^2 + (\boldsymbol{k}+\boldsymbol{r})^2$ and $D(\boldsymbol{k}+\boldsymbol{\ell}) = \alpha(1-\alpha)Q^2 + (\boldsymbol{k}+\boldsymbol{\ell})^2$, that are well known from the Born approximation:

$$
\begin{aligned}
D_1 &\to -\frac{1-\alpha}{\alpha_\ell}\boldsymbol{\ell}^2 , \\
D_2 &\to -\frac{1}{\alpha}D(\boldsymbol{k}+\boldsymbol{r}) , \\
D_3 &\to \frac{\alpha}{\alpha_\ell}\boldsymbol{\ell}^2 , \\
D_4 &\to \frac{1-\alpha}{\alpha_\ell}\boldsymbol{\ell}^2 , \\
D_5 &\to -(\boldsymbol{\ell}-\boldsymbol{r})^2 , \\
D_6 &\to -\frac{\alpha}{\alpha_\ell}\boldsymbol{\ell}^2 , \\
D_7 &\to -\frac{1}{1-\alpha}D(\boldsymbol{k}+\boldsymbol{\ell}) .
\end{aligned}
\tag{4.118}
$$

In the numerators on the rhs of (4.35)–(4.69) we expand in powers of α_ℓ and keep only the leading term. The contributions from the diagrams containing A_3 or B_3 drop out completely, since they involve an extra fermion propagator that gives a suppression by a power of α_ℓ. Similarly the diagrams with $\mathcal{A}_1$, $\mathcal{A}_2$ (or $\mathcal{B}_1$, $\mathcal{B}_2$) on both sides. Nonzero contributions come from diagrams involving $\mathcal{A}_4$ or $\mathcal{B}_4$, but they cancel in the sum. We are finally left with the contributions coming from $\mathcal{A}_5$ and $\mathcal{B}_5$. As to the $\mathcal{A}\mathcal{A}_{ij}$-terms, all non vanishing terms have the common factor $\frac{1}{(D_2)^2}$; all non vanishing $\mathcal{A}\mathcal{B}_{ij}$ terms contain $\frac{1}{D_2 D_7}$. For both photon polarisations we find the simplified form :

$$
|\Gamma^{(0)}_{\gamma^*\to q\bar{q}g}|^2\Big|_{\alpha_\ell\to 0} = |\Gamma^{(0)}_{\gamma^*\to q\bar{q}}|^2\Big|_{\substack{\boldsymbol{r}\to\boldsymbol{r}-\boldsymbol{\ell}\\ \boldsymbol{k}\to\boldsymbol{k}+\boldsymbol{\ell}}} \frac{C_A}{(\boldsymbol{\ell}-\boldsymbol{r})^2}\sum_{i,j=1}^{5}\mathcal{D}_{ij} \tag{4.119}
$$

The squared $q\bar{q}$ production vertex $\Gamma^{(0)}_{\gamma^*\to q\bar{q}}$ was given in (3.23, 3.24); it is proportional to the LO photon wave function. The matrix $\mathcal{D}_{ij}$ does not discriminate between the coupling of the t-channel gluon to the upper quark or antiquark lines, i.e. the difference between $\mathcal{A}_i$ and $\mathcal{B}_i$ is contained entirely inside the the squared vertex. The matrix itself has the rather simple form

$$\begin{pmatrix} 0 & 0 & 0 & -\frac{1}{2} & \frac{\boldsymbol{r}^2}{\boldsymbol{\ell}^2} \\ 0 & 0 & 0 & -\frac{1}{2} & \frac{\boldsymbol{r}^2}{\boldsymbol{\ell}^2} \\ 0 & 0 & 0 & 0 & 0 \\ -\frac{1}{2} & -\frac{1}{2} & 0 & 2 & 0 \\ \frac{\boldsymbol{r}^2}{\boldsymbol{\ell}^2} & \frac{\boldsymbol{r}^2}{\boldsymbol{\ell}^2} & 0 & 0 & 0 \end{pmatrix}. \tag{4.120}$$

Here, our combination of Feynman diagrams mentioned in the previous section shows its effects. Using the expressions from the single diagrams we would have additional entries in the matrix for 45, 54 and 44. They cancel of course in the sum. However, this simple form of the matrix will substantially simplify the integration of single diagrams discussed later.

The sum of all diagrams is given by

$$|\Gamma^{(0)}_{\gamma^*\to q\bar{q}g}|^2\Big|_{\alpha_\ell\to 0} = |\Gamma^{(0)}_{\gamma^*\to q\bar{q}}|^2\Big|_{\substack{\boldsymbol{r}\to\boldsymbol{r}-\boldsymbol{\ell}\\ \boldsymbol{k}\to\boldsymbol{k}+\boldsymbol{\ell}}} \frac{1}{(\boldsymbol{\ell}-\boldsymbol{r})^4}\frac{4C_A\boldsymbol{r}^2\,(\boldsymbol{\ell}-\boldsymbol{r})^2}{\boldsymbol{\ell}^2}. \tag{4.121}$$

This is exactly what we expect thinking of the Regge form of a squared amplitude with two rapidity gaps: the squared Born level vertex has shifted momenta to account for the different notation of the momenta compared to the $q\bar{q}$ production process; $(\boldsymbol{\ell}-\boldsymbol{r})^4$ is the squared propagator of the t-channel gluon and $4N_c\boldsymbol{r}^2(\boldsymbol{r}-\boldsymbol{\ell})^2/\boldsymbol{\ell}^2$ is the square of the Lipatov vertex [2]. The lower quark vertex and gluon propagator have already been removed in our Regge ansatz (4.32) for the amplitude. Thus, the gluon emission in the central region is correctly reproduced by our calculation.

It may be interesting to note that the squared matrix element may also be written in the factorised form:

$$\begin{aligned} |\mathcal{M}_{q\bar{q}g}|^2_L =& 2s^2\frac{2(2\pi)^3}{3}g^4\delta^{ab}\,\alpha(1-\alpha)\,|\Psi_L(\boldsymbol{k}+\boldsymbol{\ell},\alpha)|^2 \\ &\times 4N_c\left[\frac{\boldsymbol{r}-\boldsymbol{\ell}}{(\boldsymbol{r}-\boldsymbol{\ell})^2}+\frac{\boldsymbol{\ell}}{\boldsymbol{\ell}^2}\right]\cdot\left[\frac{\boldsymbol{r}-\boldsymbol{\ell}}{(\boldsymbol{r}-\boldsymbol{\ell})^2}+\frac{\boldsymbol{\ell}}{\boldsymbol{\ell}^2}\right]\frac{1}{\boldsymbol{r}^4}\frac{g^2\delta^{ab}}{2N_c}. \end{aligned} \tag{4.122}$$

Here,

$$|\Psi_L(\boldsymbol{k}+\boldsymbol{\ell},\alpha)|^2 = \frac{6\alpha_{\mathrm{em}}e_f^2}{\pi^2}\alpha^2(1-\alpha)^2Q^2\left(\frac{1}{D(\boldsymbol{k}+\boldsymbol{r})}-\frac{1}{D(\boldsymbol{k}+\boldsymbol{\ell})}\right)^2 \tag{4.123}$$

is the LO wave function of (longitudinal) photons. In this way it has the same structure as (4.35)–(4.69): a product of two terms, one belonging to the incoming photon, one to the outgoing. As we will see later this property is of crucial importance for the interpretation in the framework of the colour dipole picture

4.4 The subtraction of the central limit

We now turn to the formulation of the real corrections. As we have discussed in sec.3.1, contributions to the total cross section are divided according to the number of large rapidity gaps. We have presented the results for the process $\gamma^* + q \to (q\bar{q}g) + q$, imposing the constraint of a large rapidity gap between the $(q\bar{q}g)$ system and the quark. These results therefore contain, as a special case, still the configuration where the $q\bar{q}g$ system contains a second rapidity gap between the $q\bar{q}$ pair and the gluon: this piece has to be removed since it counts as a configuration with two gaps and, in order α_s^3 of the total cross section, it entirely belongs to the leading-ln s approximation (3.13).

In order to make the separation more explicit, we first divide the phase space of the produced gluon into 'upper' and 'lower' halves. Introducing

$$\alpha_\ell^{cut} = \frac{|\boldsymbol{\ell}|}{\sqrt{s}}, \tag{4.124}$$

the 'upper' region $\alpha_\ell^{cut} < \alpha_\ell < 1-\alpha$ consists of the 'upper' half of the central region plus the fragmentation region of the incoming photon, whereas the 'lower' region $\alpha_\ell < \alpha_\ell^{cut}$ contains the lower half of the central region plus the fragmentation region of the quark. In the upper region we write:

$$\begin{aligned}
&\int |\Gamma^{(0)}_{\gamma^*\to q\bar{q}g}|^2 d\phi_{q\bar{q}g} \frac{s d\beta_r}{2\pi} \Theta(\alpha_\ell - \alpha_\ell^{cut}) \\
&= \int d\boldsymbol{k}\, d\boldsymbol{\ell} \int_0^1 d\alpha \int_0^{1-\alpha} d\alpha_\ell\, \mathcal{I}_3(\alpha_\ell, \boldsymbol{\ell}; \alpha, \boldsymbol{k}; \boldsymbol{r}, Q) \Theta(\alpha_\ell - \alpha_\ell^{cut})
\end{aligned} \tag{4.125}$$

Here $\mathcal{I}_3$ denotes the full integrand involving the sum of the matrix elements of the three-particle final state.

The division into central region and fragmentation region is closely related to the choice of the energy scale s_0. In (3.13) we have introduced the energy scale s_0: since a change in s_0 can be absorbed into the NLO impact factors $\Phi_A^{(1)}$ and $\Phi_B^{(1)}$, one might expect that there exists some freedom in choosing this scale. We adopt the simplest choice, namely a constant value which is independent of kinematic variables inside the impact factors. Examples for s_0 include the (negative) virtuality of the t-channel gluon, $\boldsymbol{r}^2$, or the (negative) mass of the photon, Q^2.

In order to define the $q\bar{q}g$ contribution to the photon impact factor, $\Phi_{\gamma^*}^{(1,\mathrm{real})}$, we have to subtract, starting from (4.125), the leading-ln s piece with the energy scale s_0. This can be achieved by considering the central region limit (5.13) of the matrix element which implies

$$\mathcal{I}_3(\alpha_\ell, \boldsymbol{\ell}; \alpha, \boldsymbol{k}; \boldsymbol{r}, Q)|_{\mathrm{LL}} = \mathcal{I}_2(\alpha, \boldsymbol{k}+\boldsymbol{\ell}; \boldsymbol{r}-\boldsymbol{l}, Q) \frac{1}{(2\pi)^{2-2\epsilon}(\boldsymbol{\ell}-\boldsymbol{r})^4} \mathcal{K}_{\mathrm{real}}(\boldsymbol{r}-\boldsymbol{\ell}, \boldsymbol{r}) \frac{1}{\alpha_\ell}\,. \tag{4.126}$$

We recognise the integrand $\mathcal{I}_2$ occurring in the LO impact factor (3.27) with the value of the Reggeon momentum being shifted to $\boldsymbol{r} \to \boldsymbol{r} - \boldsymbol{\ell}$ (since the momentum $\boldsymbol{\ell}$ is carried by the outgoing gluon), the propagators associated to the t-channel (reggeized) gluons, the measure factor $1/(2\pi)^{2-2\epsilon}$ required by the definition (3.2), the real part of the BFKL kernel, and, finally, a factor $1/\alpha_\ell$. It is this factor $1/\alpha_\ell$ which, when the integration over α_ℓ is done, provides the logarithm of the energy. Our aim of finding the LL piece with energy scale s_0 leads to the following α_ℓ integral:

$$\int_0^{\alpha_\ell^{max}} \frac{d\alpha_\ell}{\alpha_\ell} \Theta(\alpha_\ell - \alpha_\ell^{cut}) = \frac{1}{2} \log \frac{(\alpha_\ell^{max})^2 s}{\boldsymbol{\ell}^2} . \tag{4.127}$$

with $\alpha_\ell^{max} \equiv |\boldsymbol{\ell}|/\sqrt{s_0}$. Therefore, we define as genuine real emission contribution to the photon impact factor the expression

$$\begin{aligned} \Phi_{\gamma^*}^{(1,real)} &= \int d\boldsymbol{k}\, d\boldsymbol{\ell} \int_0^1 d\alpha \int_{\alpha_\ell^{cut}}^\infty d\alpha_\ell \Big[\mathcal{I}_3(\alpha_\ell, \boldsymbol{\ell}; \alpha, \boldsymbol{k}; \boldsymbol{r}, Q) \Theta(1 - \alpha - \alpha_\ell) \\ &- \mathcal{I}_2(\alpha, \boldsymbol{k} + \boldsymbol{\ell}; \boldsymbol{r} - \boldsymbol{l}, Q) \frac{1}{(2\pi)^{2-2\epsilon} (\boldsymbol{\ell} - \boldsymbol{r})^4} \mathcal{K}_{real}(\boldsymbol{r} - \boldsymbol{\ell}, \boldsymbol{r}) \frac{1}{\alpha_\ell} \Theta(\frac{|\boldsymbol{\ell}|}{\sqrt{s_0}} - \alpha_\ell) \Big] . \end{aligned} \tag{4.128}$$

In this definition of our impact factor, the following remark is in place. With our choice of a constant energy scale, which has led to the subtraction, we are adding (in the LL term) and subtracting (in $\Phi_{\gamma^*}^{(1,real)}$) a region of the phase space which is kinematically forbidden. In fact, the LL subtraction (last line of Eq. (4.128)) includes the region of phase space where $\alpha_\ell > 1 - \alpha$. It is important to make sure that this "forbidden" region $|\boldsymbol{\ell}| > (1 - \alpha)\sqrt{s_0}$, $1 - \alpha < \alpha_\ell < |\boldsymbol{\ell}|/\sqrt{s_0}$ contributes a finite term and does not introduce new divergences. The finiteness results from the "good" UV behaviour of the LO impact factor, namely $\Phi_{\gamma^*}^{(0)}(\boldsymbol{r} - \boldsymbol{\ell}) \to$ const for $\boldsymbol{\ell} \to \infty$ (up to logarithms). After multiplication with the propagator $\sim 1/\boldsymbol{\ell}^4$ and with the factor $\log[|\boldsymbol{\ell}|/(1 - \alpha)\sqrt{s_0}]$ (which is due to the α_ℓ integral), the resulting $\boldsymbol{\ell}$ integral is finite. This situation is quite different from the case of partonic impact factors [16, 26, 25], where $\Phi_{q,g}^{(0)}(\boldsymbol{r} - \boldsymbol{\ell}) \sim \boldsymbol{\ell}^2$, and the $\boldsymbol{\ell}$ integral, after including the gluon propagators and the logarithmic factor, leads to a double pole in $1/\epsilon$.

4.5 The $q\bar{q}g$-component of the γ^* wave function

Let us next address the question how our results fit into the picture of the photon wave function and the colour dipole cross section. At NLO we expect, if this picture remains valid, a new Fock component of the photon, the $q\bar{q}g$ component.

As a first step, we consider our results (4.35)–(4.69), and ignore both the infrared singularities and the subtraction of the central region discussed in the previous section. We will Fourier transform into transverse configuration space and show that our results can be expressed in terms of two function $\psi(Q^2;\boldsymbol{\rho}_1,\boldsymbol{\rho}_2,\alpha,\alpha_\ell)$ and $\sigma(\alpha,\alpha_\ell,\boldsymbol{\rho}_1,\boldsymbol{\rho}_2)$ in a factorised form.

We begin with the terms proportional to $\boldsymbol{A}_i\boldsymbol{A}_j$, which are present in all $\mathcal{A}\mathcal{A}_{ij}$ (except for the elements with $j=5$). As an illustration, consider the contribution $\mathcal{A}\mathcal{A}_{11}$ to 4.33. Obviously we can write

$$\mathcal{A}\mathcal{A}_{11} = \frac{(\boldsymbol{A}_1)_m}{D_1D_2}\left(2\delta_{mn}C_F\alpha_1\bar{\alpha}_1\right)\frac{(\boldsymbol{A}_1)_n}{D_1D_2}. \tag{4.129}$$

(where the sum over m and n is included). Defining the Fourier transform of the last factor:

$$\iint\frac{d^2\boldsymbol{k}d^2\boldsymbol{\ell}}{(2\pi)^2}e^{i\boldsymbol{\rho}_1\boldsymbol{k}}e^{i\boldsymbol{\rho}_2\boldsymbol{l}}\frac{(\boldsymbol{A}_1)_n}{D_1D_2}\,, \tag{4.130}$$

and using (4.16), (4.17), and (4.35), we note that the dependence of the integrand $\frac{(\boldsymbol{A}_1)_n}{D_1D_2}$ upon $\boldsymbol{r}$ is only through the combination $\boldsymbol{k}+\boldsymbol{r}$. We therefore change the integration variable $\boldsymbol{k}$ into $\boldsymbol{k}'=\boldsymbol{k}+\boldsymbol{r}$ and obtain

$$\sqrt{\frac{Q^2}{\alpha_2\bar{\alpha}_1}}\iint\frac{d^2\boldsymbol{k}d^2\boldsymbol{\ell}}{(2\pi)^2}e^{i\boldsymbol{\rho}_1\boldsymbol{k}}e^{i\boldsymbol{\rho}_2\boldsymbol{l}}\frac{(\boldsymbol{A}_1)_n}{D_1D_2} = e^{-i\boldsymbol{\rho}_1\boldsymbol{r}}\psi_n^{(1)}(Q^2;\boldsymbol{\rho}_1,\boldsymbol{\rho}_2,\alpha,\alpha_\ell), \tag{4.131}$$

where

$$\psi_n^{(1)}(Q^2;\boldsymbol{\rho}_1,\boldsymbol{\rho}_2,\alpha,\alpha_\ell) = \sqrt{\frac{Q^2}{\alpha_2\bar{\alpha}_1}}\iint\frac{d^2\boldsymbol{k}'d^2\boldsymbol{\ell}}{(2\pi)^2}e^{i\boldsymbol{\rho}_1\boldsymbol{k}'}e^{i\boldsymbol{\rho}_2\boldsymbol{\ell}}\frac{(\boldsymbol{A}_1)_n}{D_1D_2} \tag{4.132}$$

has no dependence upon $\boldsymbol{r}$. With a similar result for the first term in (4.129), $\mathcal{A}\mathcal{A}_{11}$ takes the form:

$$\begin{aligned}\frac{Q^2}{\alpha_2\bar{\alpha}_1}\mathcal{A}\mathcal{A}_{11} = &\int\frac{d^2\boldsymbol{\rho}_1'd^2\boldsymbol{\rho}_2'}{(2\pi^2)}e^{i\boldsymbol{\rho}_1'\boldsymbol{k}}e^{i\boldsymbol{\rho}_2'\boldsymbol{l}}e^{i\boldsymbol{\rho}_1'\boldsymbol{r}}\psi_n^{(1)}(Q^2;\boldsymbol{\rho}_1',\boldsymbol{\rho}_2',\alpha,\alpha_\ell)^*\\ &\times\left(2\delta_{mn}C_F\alpha_1\bar{\alpha}_1\right)\\ &\times\int\frac{d^2\boldsymbol{\rho}_1d^2\boldsymbol{\rho}_2}{(2\pi^2)}e^{-i\boldsymbol{\rho}_1\boldsymbol{k}}e^{-i\boldsymbol{\rho}_2\boldsymbol{l}}e^{-i\boldsymbol{\rho}_1\boldsymbol{r}}\psi_n^{(1)}(Q^2;\boldsymbol{\rho}_1,\boldsymbol{\rho}_2,\alpha,\alpha_\ell).\end{aligned} \tag{4.133}$$

Integrating over the transverse momenta of the $q\bar{q}g$ system, we obtain δ-functions in the $\boldsymbol{\rho}$-vectors which allow to do the $\boldsymbol{\rho}_1'$, $\boldsymbol{\rho}_2'$ integrals:

$$\begin{aligned}&Q^2\int\frac{d\alpha\,d\alpha_\ell\,d^2\boldsymbol{k}\,d^2\boldsymbol{\ell}\,d^2\boldsymbol{r}}{\alpha_1\bar{\alpha}_1\alpha_\ell}\mathcal{A}\mathcal{A}_{11} =\\ &\qquad= \int d\alpha\,d\alpha_\ell\int d^2\boldsymbol{\rho}_1\,d^2\boldsymbol{\rho}_2\left(\psi_m^{(1)}\right)^*\sigma_{mn}^{(11)}\psi_n^{(1)}\,,\end{aligned} \tag{4.134}$$

where

$$\sigma^{(11)}_{mn}(\alpha,\alpha_l,\boldsymbol{\rho}_1,\boldsymbol{\rho}_2)=\frac{1}{\alpha_\ell}\int d^2\boldsymbol{r}e^{i\boldsymbol{\rho}_1\boldsymbol{r}}\left(2\delta_{mn}\frac{C_F\alpha_1\bar{\alpha}_1}{\boldsymbol{r}^4}\right)e^{-i\boldsymbol{\rho}_1\boldsymbol{r}}\,. \tag{4.135}$$

It is easy to see that a similar analysis applies to the terms proportional to $\boldsymbol{A}_i\boldsymbol{A}_j$ in all other $\mathcal{AA}_{ij}$. In summary, we transform the transverse momenta in the following way:

$$\frac{\boldsymbol{A}_1}{D_1D_2}: \qquad \boldsymbol{k}'=\boldsymbol{k}+\boldsymbol{r} \qquad \boldsymbol{\ell}'=\boldsymbol{\ell} \tag{4.136}$$

$$\frac{\boldsymbol{A}_2}{D_2D_4}: \qquad \boldsymbol{k}'=\boldsymbol{k}+\boldsymbol{r} \qquad \boldsymbol{\ell}'=\boldsymbol{\ell}-\frac{\alpha_\ell}{1-\alpha}\boldsymbol{r} \tag{4.137}$$

$$\frac{\boldsymbol{A}_3}{D_1D_3}: \qquad \boldsymbol{k}'=\boldsymbol{k}+\boldsymbol{r} \qquad \boldsymbol{\ell}'=\boldsymbol{\ell} \tag{4.138}$$

$$\frac{\boldsymbol{A}_4}{D_2D_5}: \qquad \boldsymbol{k}'=\boldsymbol{k}+\boldsymbol{r} \qquad \boldsymbol{\ell}'=\boldsymbol{\ell}-\boldsymbol{r}\,. \tag{4.139}$$

In this way we eliminate the dependence upon $\boldsymbol{r}$ from the Fourier transforms. The $\boldsymbol{r}$ dependence is entirely carried by σ^{ij}. We perform the transformation of the elements $\boldsymbol{B}_i$ in a similar fashion. The shifts in the $\boldsymbol{k}$ and $\boldsymbol{\ell}$ integrations are just transformed according to (4.10), (4.11).

As the next class of terms, consider the terms proportional to $\boldsymbol{r}^2$. Starting with $\mathcal{AA}_{12}$, we proceed as before, but the Fourier transformation is done only for $\frac{1}{D_1D_2}$ and $\frac{1}{D_2D_4}$, respectively: using the same shift of momenta as before, we again find the dependence upon $\boldsymbol{r}$ concentrated in phase factors, and the remaining integrals define (scalar) functions $\psi^{(1)}_{q\bar{q}g}$ and $\psi^{(2)}_{q\bar{q}g}$ which do not depend upon $\boldsymbol{r}$. The factor $\boldsymbol{r}^2$ goes into the cross section $\sigma^{(12)}_{q\bar{q}g}$.

Next those contributions to $\mathcal{AA}_{ij}$ which contain D_2 or D_7 in the numerator: the first appearance is in $\mathcal{AA}_{14}$, and a quick survey shows that these terms show up only if $i=4$ or $j=4$. Therefore, these pieces have to be part of the function $\psi^{(4)}$: e.g. $\frac{D_2}{D_2D_5}$ or $\frac{D_7}{D_2D_5}$. Again, the dependence upon $\boldsymbol{r}$ can be factored out and leads to a phase factor which is absorbed into the function σ.

Finally, we have contributions proportional to $\boldsymbol{A}_i\boldsymbol{r}$ which appear only for $j=4$: following again the same steps as before, we take the vector $\boldsymbol{A}_i$ as a part of the function $\psi^{(i)}$, and we absorb $\boldsymbol{r}$ into $\sigma^{(i4)}$. The contributions proportional to scalar products such as $(\boldsymbol{k}+\boldsymbol{r})(\boldsymbol{k}+\boldsymbol{\ell})$ are treated in a similar way: one of the two vectors belongs to the function $(\psi^{(i)})^*$,the other to $\psi^{(j)}$ (there is some freedom of how this division is done). In any case, the dependence upon $\boldsymbol{r}$ can entirely be absorbed into σ.

As result, all terms appearing on the rhs of $\mathcal{AA}_{ij}$, $\mathcal{AB}_{ij}$ etc. can be cast either into the form (4.134), or

$$\int d\alpha d\alpha_\ell\int d^2\boldsymbol{\rho}_1d^2\boldsymbol{\rho}_2\left(\psi^{(i)}_m\right)^*\sigma^{(ij)}_m\psi^{(j)} \tag{4.140}$$

or

$$\int d\alpha d\alpha_\ell \int d^2\boldsymbol{\rho}_1 d^2\boldsymbol{\rho}_2 \left(\psi^{(i)}\right) \sigma^{(ij)} \psi^{(j)} \ . \tag{4.141}$$

Thus, we have written each squared amplitude in the configuration space as a product of two either scalar or vector-like functions ψ and the function σ that contains the whole $\boldsymbol{r}$ dependence. The relationship to the $q\bar{q}g$ Fock component of the γ^* wave function and the interaction cross section, respectively, has to be investigated in more detail.

The matrix $\sigma^{(ij)}$ (here the indices i and j have to be extended in order to include $\mathcal{AA}$, $\mathcal{AB}$, $\mathcal{BA}$, and $\mathcal{BB}$, i.e. they run from 1 to 10) is not diagonal: so far our choice of the basis of ψ had been dictated by the Feynman diagrams from which we have started our calculations. If $\sigma^{(ij)}$ would indeed represent a kind of interaction matrix it would be desirable find a more physical basis in which the interactions are diagonal. As $\sigma^{(ij)}$ is symmetric, this is always possible. In this basis, our cross section can be written as a sum of squares, each of which supports the wave function interpretation. The factorised form of part of the squared matrix element (4.81) stated in the last section might serve as a starting point for the search of such a basis.

As for transverse photon polarisation, it is easy to show that the factorisation properties in the configuration space discussed up to now also hold. Thus, the results from this section exactly apply also for transverse photons.

Chapter 5

Combination of real and virtual corrections

5.1 Singular Limits of the Real Corrections

In order to formulate finite expressions for the $q\bar{q}g$ contribution to the photon impact factor we examine the divergent limits of the squared matrix element $|\mathcal{M}_{q\bar{q}g}|^2$ for the process $\gamma^* + q \to q\bar{q}g + q$. For the phase space of the $q\bar{q}g$-final state we have from (3.11), (3.12):

$$d\phi_{q\bar{q}g}\frac{s d\beta_r}{2\pi} = \frac{d\alpha}{2\alpha(1-\alpha-\alpha_\ell)}\frac{d^{D-2}\boldsymbol{k}}{(2\pi)^{D-1}}\frac{d\alpha_\ell}{2\alpha_\ell}\frac{d^{D-2}\boldsymbol{\ell}}{(2\pi)^{D-1}} \tag{5.1}$$

In the following we suppress the superscript $(D-2)$ in the integration measure of the transverse momenta. The contribution of the $q\bar{q}g$ state to the impact factor reads:

$$\int \frac{d\alpha}{2\alpha(1-\alpha-\alpha_\ell)} \int \frac{d\boldsymbol{k}}{(2\pi)^{D-1}} \int \frac{d\alpha_\ell}{2\alpha_\ell} \int \frac{d\boldsymbol{\ell}}{(2\pi)^{D-1}} \quad |\Gamma^{(0)}_{\gamma^*\to q\bar{q}g}|^2, \tag{5.2}$$

where the square of the vertex function, $|\Gamma^{(0)}_{\gamma^*\to q\bar{q}g}|^2$, follows from (4.33) and (4.34).

We begin by examining the limit in which the gluon is either collinear to the quark or to the antiquark of the $q\bar{q}g$-system. In the latter case, the gluon momentum ℓ is collinear with the momentum $q-k-\ell$ of the antiquark, resulting in $D_4 = 0$ or

$$\boldsymbol{\ell}' = \boldsymbol{\ell} + \frac{\alpha_\ell}{1-\alpha}\boldsymbol{k} = 0\ . \tag{5.3}$$

We approximate our results for $|\Gamma^{(0),a}_{\gamma^*\to q\bar{q}g}|^2$ in the region around the singularity, i.e. we calculate the residue of the pole at $D_4 = 0$. The collinear limit of QCD matrix elements is well known and can be taken from the literature

[13]. As an additional check, we have calculated the divergent limits directly from our matrix elements. For both polarisations of the photon, the $g \parallel \bar{q}$ collinear limit of (5.2) can be written as

$$|\Gamma^{(0)}_{\gamma^*\to q\bar{q}g}|^2 d\phi_{q\bar{q}g}\frac{sd\beta_r}{2\pi}\Bigg|^{coll,\bar{q}} = |\Gamma^{(0)}_{\gamma^*\to q\bar{q}}|^2 \frac{d\alpha}{2\alpha(1-\alpha)}\frac{d\boldsymbol{k}}{(2\pi)^{3-2\epsilon}}$$
$$\times\, C_F P_{gq}\left(\frac{\alpha_\ell}{1-\alpha},\epsilon\right)\frac{d\alpha_\ell}{(1-\alpha)}\frac{d\boldsymbol{\ell}}{(2\pi)^{3-2\epsilon}\boldsymbol{\ell}'^2} \tag{5.4}$$
$$= \mathcal{I}_2(\alpha,\boldsymbol{k})d\alpha\, d\boldsymbol{k}\, C_F P_{gq}\left(\frac{\alpha_\ell}{1-\alpha},\epsilon\right)\frac{d\alpha_\ell}{(1-\alpha)}\frac{d\boldsymbol{\ell}}{(2\pi)^{3-2\epsilon}\boldsymbol{\ell}'^2} \tag{5.5}$$

where $\mathcal{I}_2(\alpha,\boldsymbol{k}) \equiv \mathcal{I}_2(\alpha,\boldsymbol{k};\boldsymbol{r},Q)$ was defined in (3.27), (3.28), (3.29), and $C_F P_{gq}(z,\epsilon)$ denotes the $q \to g$ Altarelli-Parisi splitting function in $D = 4-2\epsilon$ dimensions:

$$P_{gq}(z,\epsilon) = \frac{1+(1-z)^2}{z} - \epsilon z\,. \tag{5.6}$$

The colour coefficient C_F indicates that, for the examination of singular limits it is convenient to use, as we did in the las chapter, the colour basis C_F and C_A rather than the colour factors N_c, C_F, and $1/N_c$. In this basis, the C_A part is free from collinear singularities.

In the case where the gluon is collinear to the quark, the infrared limit is obtained from (5.5) by substituting[1] α by $\bar{\alpha} = 1-\alpha-\alpha_\ell$ and $\boldsymbol{k}$ by $\bar{\boldsymbol{k}} = -\boldsymbol{k}-\boldsymbol{r}-\boldsymbol{\ell}$. The "soft-collinear" limit of (5.5) that is needed later is obtained by retaining from the splitting function only the pole $2/z$:

$$|\Gamma^{(0)}_{\gamma^*\to q\bar{q}g}|^2 d\phi_{q\bar{q}g}\frac{sd\beta_r}{2\pi}\Bigg|^{soft,coll,\bar{q}} = \mathcal{I}_2(\alpha,\boldsymbol{k})d\alpha\, d\boldsymbol{k}\, 2C_F\,\frac{d\alpha_\ell}{\alpha_\ell}\frac{d\boldsymbol{\ell}}{(2\pi)^{3-2\epsilon}\boldsymbol{\ell}'^2}\,. \tag{5.7}$$

Next, we examine the 'soft limit' where the gluon momentum $\alpha_\ell \to 0$ and $\boldsymbol{\ell} \to 0$. Formally we substitute $\ell \to \rho\ell$ or $\boldsymbol{\ell} \to \rho\boldsymbol{\ell}, \alpha_\ell \to \rho\alpha_\ell$, expand around $\rho = 0$ and keep only the leading term. As in the collinear case, the result is proportional to the Born approximation, for both polarisations of the photon. We separate the result according to different colour structures:

$$|\Gamma^{(0)}_{\gamma^*\to q\bar{q}g}|^2\Big|^{\text{soft}} = C_A\, |\Gamma^{(0)}_{\gamma^*\to q\bar{q}g}|^2\Big|^{\text{soft}}_{C_A} + C_F\, |\Gamma^{(0)}_{\gamma^*\to q\bar{q}g}|^2\Big|^{\text{soft}}_{C_F} \tag{5.8}$$

with

$$|\Gamma^{(0)}_{\gamma^*\to q\bar{q}g}|^2\Big|^{\text{soft}}_{C_A} = |\Gamma^{(0)}_{\gamma^*\to q\bar{q}}|^2\frac{4\,(\boldsymbol{\ell}-\alpha_\ell\boldsymbol{a})\cdot(\boldsymbol{\ell}+\alpha_\ell\boldsymbol{b})}{(\boldsymbol{\ell}-\alpha_\ell\boldsymbol{a})^2\,(\boldsymbol{\ell}+\alpha_\ell\boldsymbol{b})^2} \tag{5.9}$$

and

$$|\Gamma^{(0)}_{\gamma^*\to q\bar{q}g}|^2\Big|^{\text{soft}}_{C_F} = |\Gamma^{(0)}_{\gamma^*\to q\bar{q}}|^2\frac{4\,\alpha_\ell^2(\boldsymbol{a}+\boldsymbol{b})^2}{(\boldsymbol{\ell}-\alpha_\ell\boldsymbol{a})^2\,(\boldsymbol{\ell}+\alpha_\ell\boldsymbol{b})^2}\,, \tag{5.10}$$

[1]This is nothing but the $q \leftrightarrow \bar{q}$ variables exchange at fixed gluon momentum.

where, for convenience, we have defined

$$\boldsymbol{a} = \frac{\boldsymbol{k}+\boldsymbol{r}}{\alpha}, \qquad \boldsymbol{b} = \frac{\boldsymbol{k}}{1-\alpha}. \tag{5.11}$$

In the soft limit, the phase space measure (5.1) factorises in the product of the $q\bar{q}$ measure (3.25) and differentials of the gluon variables

$$d\phi_{q\bar{q}g}\frac{sd\beta_r}{2\pi} \to \left(d\phi_{q\bar{q}}\frac{sd\beta_r}{2\pi}\right)\left(\frac{d\alpha_\ell}{2\alpha_\ell}\frac{d\boldsymbol{\ell}}{(2\pi)^{D-1}}\right). \tag{5.12}$$

Our result for the soft limit agrees with [14]. We also note that, in the limit $\boldsymbol{\ell}' = \boldsymbol{\ell} + \alpha_\ell \boldsymbol{b} \to 0$, we reproduce from (5.10) and (5.12) the "soft-collinear" limit (5.7).

Finally, let us repeat here the expression in the central limit (4.121). For both photon polarisations the sum of our matrix elements splits into a product of the Born approximation and of the BFKL kernel:

$$|\Gamma^{(0)}_{\gamma^*\to q\bar{q}g}|^2\Big|_{\rm LL} = |\Gamma^{(0)}_{\gamma^*\to q\bar{q}}|^2\Big|_{\substack{\boldsymbol{r}\to\boldsymbol{r}-\boldsymbol{\ell}\\ \boldsymbol{k}\to\boldsymbol{k}+\boldsymbol{\ell}}} \frac{1}{(\boldsymbol{\ell}-\boldsymbol{r})^4}\frac{4C_A\boldsymbol{r}^2(\boldsymbol{\ell}-\boldsymbol{r})^2}{\boldsymbol{\ell}^2}. \tag{5.13}$$

The last factor is the BFKL kernel (without the gluon trajectory function)

$$\mathcal{K}_{real}(\boldsymbol{r}-\boldsymbol{\ell},\boldsymbol{r}) = \frac{C_A}{\pi}\frac{\boldsymbol{r}^2(\boldsymbol{\ell}-\boldsymbol{r})^2}{\boldsymbol{\ell}^2}, \tag{5.14}$$

The colour factor C_A signals that the C_F part of our matrix elements does not contribute to our subtraction of the central region. In the limit where the centrally emitted gluon is soft ($\boldsymbol{\ell} \ll \boldsymbol{r}$), we obtain

$$|\Gamma^{(0)}_{\gamma^*\to q\bar{q}g}|^2\Big|^{soft}_{\rm LL} = |\Gamma^{(0)}_{\gamma^*\to q\bar{q}}(\alpha,\boldsymbol{k})|^2\frac{4C_A}{\boldsymbol{\ell}^2}. \tag{5.15}$$

The same result is obtained from the soft limit (5.9), if we go into the central region limit $\alpha_\ell \ll 1$.

5.2 Finite Combinations

In this section we show explicitly the cancellation of all the IR singularities, and we present expressions consisting of well defined finite terms.

Given that all the singular terms of the virtual corrections are proportional to the LO impact factor (3.27), as one can see from (3.36), it is convenient to study the singular regions of the phase space integrals of the real corrections by integrating first only over the gluon variables. In fact, the gluon integration generates singular terms which are in turn proportional to the LO impact factor. They will be combined with the singular virtual corrections after a proper identification of the remaining integration variables.

It is also convenient to separate the different colour structure contributions into a C_A term and a C_F term

$$\mathcal{I}_3 \equiv C_A \mathcal{I}_3^{C_A} + C_F \mathcal{I}_3^{C_F} , \tag{5.16}$$

because the LL subtraction is contained only in the former term, whilst the collinear singularities are present only in the latter. Soft singularities are found in both terms.

5.2.1 The C_A term

Let us consider the C_A contribution to the real emission impact factor corrections, as specified from (4.128). We want to compute first the $\boldsymbol{\ell}$ and α_ℓ integrals at fixed $\boldsymbol{k}$ and α:

$$\begin{aligned} \left.\frac{d\Phi_{\gamma^*}^{(1)}}{d\alpha\, d\boldsymbol{k}}\right|_{C_A} = \int d\boldsymbol{\ell} \int_{\alpha_\ell^{cut}}^{\infty} d\alpha_\ell \, \Big[&\mathcal{I}_3^{C_A}(\alpha_\ell, \boldsymbol{\ell}; \alpha, \boldsymbol{k}; \boldsymbol{r}, Q)\Theta(1-\alpha-\alpha_\ell) \\ &- \mathcal{I}_2(\alpha, \boldsymbol{k}+\boldsymbol{\ell}; \boldsymbol{r}-\boldsymbol{l}, Q)\frac{2}{(2\pi)^{3-2\epsilon}} \frac{\boldsymbol{r}^2}{(\boldsymbol{r}-\boldsymbol{\ell})^2 \boldsymbol{\ell}^2} \frac{1}{\alpha_\ell} \Theta(\frac{|\boldsymbol{\ell}|}{\sqrt{s_0}} - \alpha_\ell)\Big] . \end{aligned} \tag{5.17}$$

This integral is divergent in the soft region $\alpha_\ell \to 0, \boldsymbol{\ell} \to 0$ when $\epsilon = 0$. We evaluate it in dimensional regularisation by means of the subtraction method: we subtract from the integrand its soft approximation, in such a way that the resulting integral be ϵ-finite, and re-add separately what we have subtracted in an analytically integrated form. Of course, the soft limit is not uniquely defined outside the soft region. We choose the soft approximation according to (5.9, 5.15, 5.12); we extend the soft subtraction up to the kinematic limit of the gluon longitudinal momentum, i.e., $\alpha_\ell < 1 - \alpha$:

$$\begin{aligned} \left.\frac{d\Phi_{\gamma^*}^{(1)}}{d\alpha\, d\boldsymbol{k}}\right|_{C_A}^{soft} &= \mathcal{I}_2(\alpha, \boldsymbol{k}; \boldsymbol{r}, Q)\frac{2}{(2\pi)^{3-2\epsilon}} \\ &\times \int d\boldsymbol{\ell} \int_{\alpha_\ell^{cut}}^{\infty} \frac{d\alpha_\ell}{\alpha_\ell} \left[\frac{(\boldsymbol{\ell}-\alpha_\ell \boldsymbol{a})\cdot(\boldsymbol{\ell}+\alpha_\ell \boldsymbol{b})}{(\boldsymbol{\ell}-\alpha_\ell \boldsymbol{a})^2 (\boldsymbol{\ell}+\alpha_\ell \boldsymbol{b})^2} - \frac{1}{\boldsymbol{\ell}^2}\Theta(\frac{|\boldsymbol{\ell}|}{\sqrt{s_0}} - \alpha_\ell) \right] \\ &\times \Theta(1-\alpha-\alpha_\ell) , \end{aligned} \tag{5.18}$$

and define accordingly the finite C_A part of the real corrections to the impact factor as

$$\Phi^{(1,real)}_{\gamma^*}\Big|^{finite}_{C_A} \equiv \int d\boldsymbol{k}\, d\boldsymbol{\ell} \int_0^1 d\alpha \int_0^\infty d\alpha_\ell \Big\{ \mathcal{I}_3^{C_A}(\alpha_\ell, \boldsymbol{\ell}; \alpha, \boldsymbol{k}; \boldsymbol{r}, Q)\Theta(1-\alpha-\alpha_\ell)$$

$$- \mathcal{I}_2(\alpha, \boldsymbol{k}+\boldsymbol{\ell}; \boldsymbol{r}-\boldsymbol{l}, Q)\frac{2}{(2\pi)^{3-2\epsilon}}\frac{\boldsymbol{r}^2}{(\boldsymbol{r}-\boldsymbol{\ell})^2\boldsymbol{\ell}^2}\frac{1}{\alpha_\ell}\Theta(\frac{|\boldsymbol{\ell}|}{\sqrt{s_0}}-\alpha_\ell)] \tag{5.19}$$

$$- \mathcal{I}_2(\alpha, \boldsymbol{k}; \boldsymbol{r}, Q)\frac{2}{(2\pi)^{3-2\epsilon}}\frac{1}{\alpha_\ell}\left[\frac{(\boldsymbol{\ell}-\alpha_\ell\boldsymbol{a})\cdot(\boldsymbol{\ell}+\alpha_\ell\boldsymbol{b})}{(\boldsymbol{\ell}-\alpha_\ell\boldsymbol{a})^2\,(\boldsymbol{\ell}+\alpha_\ell\boldsymbol{b})^2} - \frac{1}{\boldsymbol{\ell}^2}\Theta(\frac{|\boldsymbol{\ell}|}{\sqrt{s_0}}-\alpha_\ell)\right]$$

$$\times\,\Theta(1-\alpha-\alpha_\ell)\Big\}. \tag{5.20}$$

Note that we have shifted to zero the lower limit of integration of α_ℓ because, thanks to the LL subtraction, there is no contribution to the integral coming from the central region.

Note also that the singularities of the integrand due to the denominators $\boldsymbol{\ell}-\alpha_\ell\boldsymbol{a}$ and $\boldsymbol{\ell}+\alpha_\ell\boldsymbol{b}$ are nevertheless integrable, because of the scalar product in the numerator. This reflects the fact that the C_A part is free of collinear singularities.

The expression written in (5.18) can be computed analytically. Since the lower limit of integration in α_ℓ depends on the energy s, one gets an s dependent result. However, because of the LL-soft subtraction to the soft term, the central region contribution is suppressed, and we expect a finite expression in the $s \to \infty$ limit. We can compute the integrals of the two terms in (5.18) in this limit ($\alpha_\ell^{cut} \to 0$) separately because dimensional regularisation promotes the divergent $\log s$ contributions in UV ϵ-poles, which cancel in the difference. We have:

$$J_1 \equiv \int d\boldsymbol{\ell}\int_0^{1-\alpha}\frac{d\alpha_\ell}{\alpha_\ell}\frac{(\boldsymbol{\ell}-\alpha_\ell\boldsymbol{a})\cdot(\boldsymbol{\ell}+\alpha_\ell\boldsymbol{b})}{(\boldsymbol{\ell}-\alpha_\ell\boldsymbol{a})^2\,(\boldsymbol{\ell}+\alpha_\ell\boldsymbol{b})^2} = -c_\Gamma\pi^{1-\epsilon}\frac{(1-\alpha)^{-2\epsilon}}{2\epsilon^2}\left((\boldsymbol{a}+\boldsymbol{b})^2\right)^{-\epsilon} \tag{5.21}$$

and

$$J_2 \equiv \int d\boldsymbol{\ell}\int_0^{1-\alpha}\frac{d\alpha_\ell}{\alpha_\ell}\frac{1}{\boldsymbol{\ell}^2}\Theta(\frac{|\boldsymbol{\ell}|}{\sqrt{s_0}}-\alpha_\ell) = -\frac{\pi^{1-\epsilon}}{\Gamma(1-\epsilon)}\frac{(1-\alpha)^{-2\epsilon}}{2\epsilon^2}s_0^{-\epsilon}. \tag{5.22}$$

These two integrals have to be multiplied by $\mathcal{I}_2$ and integrated over α and $\boldsymbol{k}$. We have noticed after (3.27) that $\mathcal{I}_2$ is symmetric under the change of variables $\alpha \leftrightarrow 1-\alpha$, $\boldsymbol{k} \leftrightarrow -\boldsymbol{\ell}-\boldsymbol{k}$ corresponding to the $q \leftrightarrow \bar{q}$ exchange; $(\boldsymbol{a}+\boldsymbol{b})^2 = M^2/\alpha(1-\alpha)$ is also invariant. Therefore, we can replace $(1-\alpha)^{-2\epsilon} \to \frac{1}{2}\alpha^{-2\epsilon}+\frac{1}{2}(1-\alpha)^{-2\epsilon}$ in the right-hand-side of (5.21, 5.22) so to cast them in an explicitly symmetric form w.r.t. $\alpha \leftrightarrow 1-\alpha$. This manipulation will be useful when combining real and virtual corrections.

In conclusion, the divergent C_A part of the real corrections to the impact factor is

$$\Phi_{\gamma^*}^{(1,real)}\Big|_{C_A}^{divergent} \equiv \int d\boldsymbol{k} \int_0^1 d\alpha\, \mathcal{I}_2(\alpha, \boldsymbol{k}; \boldsymbol{r}, Q) \frac{2}{(2\pi)^{3-2\epsilon}} (J_1 - J_2)$$
$$= \int d\boldsymbol{k} \int_0^1 d\alpha\, \mathcal{I}_2(\alpha, \boldsymbol{k}; \boldsymbol{r}, Q) \frac{c_\Gamma}{(4\pi)^{2-\epsilon}} \left\{ \frac{2}{\epsilon} \left[\log M^2 - \log s_0 - \log \alpha(1-\alpha)\right] \right.$$
$$\left. + \left[(\log s_0 + \log \alpha(1-\alpha))^2 - \log^2 M^2 \right] + \mathcal{O}(\epsilon) \right\} . \qquad (5.23)$$

For consistency, the variables α and $\boldsymbol{k}$ of the above equation have to be identified with the analogous variables of (3.42).

5.2.2 The C_F term

Let us now consider the C_F contribution to the real emission impact factor corrections. The first thing to note is that, since the BFKL kernel is proportional to C_A, the LL subtraction of (4.128) does not affect the C_F part. Therefore, the whole C_F part of $\mathcal{I}_3$ contributes to the impact factor. In addition, we can shift the lower limit α_ℓ^{cut} for the α_ℓ integral to zero, just because the central region does not contribute in this case.

The C_F term contains both soft and collinear divergences. We separate the singular contributions by means of the subtraction method. In what follows, the last two parameters of $\mathcal{I}_2$ are always $\boldsymbol{r}, Q$. Therefore we simplify the notation by indicating $\mathcal{I}_2(\alpha, \boldsymbol{k}) \equiv \mathcal{I}_2(\alpha, \boldsymbol{k}; \boldsymbol{r}, Q)$.

We start by identifying the soft singular term. This is done by adding and subtracting to $\mathcal{I}_3^{C_F}$ its soft limit. We remark again that the limiting function is not unique beyond the soft region. In practice, by using expression (5.10), we adopt an asymmetric function with respect to the $q \leftrightarrow \bar{q}$ exchange at fixed non-vanishing gluon momentum:

$$\left.\frac{d\Phi_{\gamma^*}^{(1)}}{d\alpha\, d\boldsymbol{k}}\right|_{C_F}^{soft} = \mathcal{I}_2(\alpha, \boldsymbol{k}) \frac{2(\boldsymbol{a}+\boldsymbol{b})^2}{(2\pi)^{3-2\epsilon}} \int d\boldsymbol{\ell} \int_0^{1-\alpha} d\alpha_\ell\, \frac{\alpha_\ell}{(\boldsymbol{\ell} - \alpha_\ell \boldsymbol{a})^2 (\boldsymbol{\ell} + \alpha_\ell \boldsymbol{b})^2}$$
$$= \mathcal{I}_2(\alpha, \boldsymbol{k}) \frac{c_\Gamma}{(4\pi)^{2-\epsilon}} \frac{2}{\epsilon^2} \left[\alpha^{-2\epsilon} + (1-\alpha)^{-2\epsilon}\right] \left[\frac{M^2}{\alpha(1-\alpha)}\right]^{-\epsilon} , \qquad (5.24)$$

where in the last equality a symmetrization in α, as indicated after (5.22), has been performed.

Both the full C_F term $\propto \mathcal{I}_3^{C_F}$ and its soft limit (5.24) have a divergent behaviour when the gluon is either collinear to the outgoing quark or antiquark. Also for the evaluation of the collinear divergences we adopt the subtraction method. For the case of gluon collinear to the antiquark ($g \parallel \bar{q}$), we derive the limiting expression of the original integrand (i.e., without soft subtraction yet) from (5.5), which yields ($\boldsymbol{\ell}' = \boldsymbol{\ell} + \alpha_\ell \boldsymbol{b}$)

$$\begin{aligned}\left.\frac{d\Phi_{\gamma^*}^{(1)}}{d\alpha\, d\boldsymbol{k}}\right|_{C_F}^{coll,\bar{q}} &= \mathcal{I}_2(\alpha,\boldsymbol{k}) \int \frac{d\boldsymbol{\ell}}{(2\pi)^{3-2\epsilon}} \int_0^{1-\alpha} \frac{d\alpha_\ell}{(1-\alpha)} P_{gq}\left(\frac{\alpha_\ell}{1-\alpha},\epsilon\right) \frac{\Theta(\alpha_\ell\Lambda - |\boldsymbol{\ell}'|)}{\boldsymbol{\ell}'^2} \\ &= \mathcal{I}_2(\alpha,\boldsymbol{k}) \frac{\alpha^{-2\epsilon} + (1-\alpha)^{-2\epsilon}}{(4\pi)^{2-\epsilon}\Gamma(1-\epsilon)} \frac{\Lambda^{-2\epsilon}}{\epsilon} \left[\frac{1}{\epsilon} + \frac{2}{1-2\epsilon} - \frac{1}{2}\right], \qquad (5.25)\end{aligned}$$

where we have decided to perform the collinear subtraction only in a cone — specified by the Θ function — whose axis coincides with the gluon momentum being parallel to the antiquark one, and the vertex sits on the soft point. The "opening angle" of the cone is parametrized by a cutoff Λ: the bigger Λ, the wider the domain of the collinear subtraction.

In order to end up with a finite integral, we have to subtract also the collinear singularities of the soft subtraction term (5.24). For the $g \parallel \bar{q}$ we have (see (5.7)):

$$\begin{aligned}\left.\frac{d\Phi_{\gamma^*}^{(1)}}{d\alpha\, d\boldsymbol{k}}\right|_{C_F}^{soft,coll,\bar{q}} &= \mathcal{I}_2(\alpha,\boldsymbol{k}) \frac{2}{(2\pi)^{3-2\epsilon}} \int_0^{1-\alpha} \frac{d\alpha_\ell}{\alpha_\ell} \int d\boldsymbol{\ell}\, \frac{\Theta(\alpha_\ell\Lambda - |\boldsymbol{\ell}'|)}{\boldsymbol{\ell}'^2} \\ &= \mathcal{I}_2(\alpha,\boldsymbol{k}) \frac{1}{(4\pi)^{2-\epsilon}\Gamma(1-\epsilon)} \left[\alpha^{-2\epsilon} + (1-\alpha)^{-2\epsilon}\right] \frac{\Lambda^{-2\epsilon}}{\epsilon^2}\,. \qquad (5.26)\end{aligned}$$

The soft-collinear subtraction acts on the same cone defined for the collinear one. It is important that (5.26) can be obtained both as collinear limit of (5.24) and as soft limit of (5.25). This guarantees not only that the collinear singularities introduced by the soft subtraction are subtracted, but also that the soft singularities introduced by the collinear subtraction are properly subtracted.

Note that the collinear term (5.25) is proportional to $\mathcal{I}_2(\alpha,\boldsymbol{k})$. This is a consequence of the convenient choice of variable employed to parametrize the outgoing particles. In fact, when the gluon is collinear to the antiquark, the $g\bar{q}$ system has to be treated as a single entity carrying the sum of quantum numbers and momenta of the constituting particles. In this case, the $g\bar{q}$ longitudinal momentum fraction and transverse momentum are $1-\alpha$ and $-\boldsymbol{k}$ respectively. The integration over the gluon variables can therefore be independently performed leaving the LO integrand $\mathcal{I}_2$ factored out.

The treatment of the $g \parallel q$ collinear singularity can be performed in the same way as for the $g \parallel \bar{q}$ collinear case. There are only two slight differences: first of all, the collinear limit of the integrand $\mathcal{I}_3$ is proportional to $\mathcal{I}_2(\alpha+\alpha_\ell, \boldsymbol{k}+\boldsymbol{\ell})$, which involves explicitly the gluon variables α_ℓ and $\boldsymbol{\ell}$. This is due to our set of variables that does not describe the qg system and the single gluon independently. A more suitable set of variable in this case is simply obtained by changing the $q \leftrightarrow \bar{q}$ labels:

$$\bar{\alpha} \equiv 1 - \alpha - \alpha_\ell \tag{5.27a}$$
$$\bar{\boldsymbol{k}} \equiv -\boldsymbol{r} - \boldsymbol{k} - \boldsymbol{\ell} \tag{5.27b}$$
$$\boldsymbol{\ell}'' \equiv \boldsymbol{\ell} - \alpha_\ell \boldsymbol{a} \,. \tag{5.27c}$$

From Eq. (5.25) one gets

$$\begin{aligned} \left.\frac{d\Phi^{(1)}_{\gamma^*}}{d\bar{\alpha}\, d\bar{\boldsymbol{k}}}\right|^{coll,q}_{C_F} &= \mathcal{I}_2(\bar{\alpha}, \bar{\boldsymbol{k}}) \int \frac{d\boldsymbol{\ell}}{(2\pi)^{3-2\epsilon}} \int_0^{1-\bar{\alpha}} \frac{d\alpha_\ell}{(1-\bar{\alpha})} P_{gq}\left(\frac{\alpha_\ell}{1-\bar{\alpha}}, \epsilon\right) \\ &\times \left(\frac{1-\bar{\alpha}}{1-\bar{\alpha}-\alpha_\ell}\right)^2 \frac{\Theta(\alpha_\ell \Lambda - \frac{1-\bar{\alpha}-\alpha_\ell}{1-\bar{\alpha}}|\boldsymbol{\ell}''|)}{\boldsymbol{\ell}''^2} \\ &= \mathcal{I}_2(1-\bar{\alpha}, -\boldsymbol{r}-\bar{\boldsymbol{k}}) \frac{\bar{\alpha}^{-2\epsilon} + (1-\bar{\alpha})^{-2\epsilon}}{(4\pi)^{2-\epsilon}\Gamma(1-\epsilon)} \frac{\Lambda^{-2\epsilon}}{\epsilon} \left[\frac{1}{\epsilon} + \frac{2}{1-2\epsilon} - \frac{1}{2}\right] . \end{aligned} \tag{5.28}$$

The additional factors in Eq. (5.28) compared to Eq. (5.25) are due to the fact that

$$\left.\boldsymbol{\ell} + \alpha_\ell \boldsymbol{b}\right|_{\substack{\alpha \to \bar{\alpha} \\ \boldsymbol{k} \to \bar{\boldsymbol{k}}}} = \frac{1-\bar{\alpha}-\alpha_\ell}{1-\bar{\alpha}} (\boldsymbol{\ell} - \alpha_\ell \boldsymbol{a}) \,. \tag{5.29}$$

The second difference is that we cannot use as soft-collinear subtraction the soft limit of (5.28) at fixed $\bar{\alpha}$ and $\bar{\boldsymbol{k}}$, because this does not correspond to the collinear limit of the soft approximation (5.24). The right way of subtracting the soft singularity of (5.28) and at the same time the $g \parallel q$ collinear singularity of (5.24) is to take the collinear limit of the latter:

$$\begin{aligned} \left.\frac{d\Phi^{(1)}_{\gamma^*}}{d\alpha\, d\boldsymbol{k}}\right|^{soft,coll,q}_{C_F} &= \mathcal{I}_2(\alpha, \boldsymbol{k}) \frac{2}{(2\pi)^{3-2\epsilon}} \int_0^{1-\alpha} \frac{d\alpha_\ell}{\alpha_\ell} \int d\boldsymbol{\ell}\, \frac{\Theta(\alpha_\ell \Lambda - |\boldsymbol{\ell}''|)}{\boldsymbol{\ell}''^2} \,. \\ &= \mathcal{I}_2(\alpha, \boldsymbol{k}) \frac{1}{(4\pi)^{2-\epsilon}\Gamma(1-\epsilon)} \left[\alpha^{-2\epsilon} + (1-\alpha)^{-2\epsilon}\right] \frac{\Lambda^{-2\epsilon}}{\epsilon^2} \,. \end{aligned} \tag{5.30}$$

In conclusion, we write the finite part of the C_F term of the impact factor by subtracting the unintegrated expressions of (5.24, 5.25, 5.26, 5.28, 5.30) from $\mathcal{I}_3^{C_F}$

$$\Phi_{\gamma^*}^{(1,\mathrm{real})}\Big|_{C_F}^{\mathrm{finite}} \equiv \int d\boldsymbol{k}\, d\boldsymbol{\ell} \int_0^1 d\alpha \int_0^{1-\alpha} d\alpha_\ell \Bigg\{ \mathcal{I}_3^{C_F}(\alpha_\ell, \boldsymbol{\ell}; \alpha, \boldsymbol{k}; \boldsymbol{r}, Q)$$
$$- \mathcal{I}_2(\alpha, \boldsymbol{k}) \frac{2(\boldsymbol{a}+\boldsymbol{b})^2}{(2\pi)^{3-2\epsilon}} \frac{\alpha_\ell}{(\boldsymbol{\ell}-\alpha_\ell \boldsymbol{a})^2\,(\boldsymbol{\ell}+\alpha_\ell \boldsymbol{b})^2}$$
$$- \mathcal{I}_2(\alpha, \boldsymbol{k}) \frac{1}{(2\pi)^{3-2\epsilon}} \left[\frac{1}{1-\alpha} P_{gq}\left(\frac{\alpha_\ell}{1-\alpha}, \epsilon \right) - \frac{2}{\alpha_\ell} \right] \frac{\Theta(\alpha_\ell \Lambda - |\boldsymbol{\ell}+\alpha_\ell \boldsymbol{b}|)}{(\boldsymbol{\ell}+\alpha_\ell \boldsymbol{b})^2}$$
$$- \Bigg[\mathcal{I}_2(\alpha+\alpha_\ell, \boldsymbol{k}+\boldsymbol{\ell}) \frac{\alpha+\alpha_\ell}{\alpha^2} P_{gq}\left(\frac{\alpha_\ell}{\alpha+\alpha_\ell}, \epsilon \right) \Theta(\alpha_\ell \Lambda - \frac{\alpha}{\alpha+\alpha_\ell} |\boldsymbol{\ell}-\alpha_\ell \boldsymbol{a}|)$$
$$- \mathcal{I}_2(\alpha, \boldsymbol{k}) \frac{2}{\alpha_\ell} \Theta(\alpha_\ell \Lambda - |\boldsymbol{\ell}-\alpha_\ell \boldsymbol{a}|) \Bigg] \frac{1}{(2\pi)^{3-2\epsilon} (\boldsymbol{\ell}-\alpha_\ell \boldsymbol{a})^2} \Bigg\}. \tag{5.31}$$

The divergent part of the C_F term is obtained by re-adding the subtracted pieces in their integrated form. In doing this, we identify the $1-\bar{\alpha}$ and $-\boldsymbol{r}-\bar{\boldsymbol{k}}$ variables of Eq. (5.28) with the variables α and $\boldsymbol{k}$ of Eqs. (5.25, 5.26, 5.30) (and later with α and $\boldsymbol{k}$ of Eq. (3.42)), so that

$$\Phi_{\gamma^*}^{(1,\mathrm{real})}\Big|_{C_F}^{divergent} = \int d\boldsymbol{k} \int_0^1 d\alpha\, \mathcal{I}_2(\alpha, \boldsymbol{k}) \frac{c_\Gamma}{(4\pi)^{2-\epsilon}} \Bigg\{ \frac{4}{\epsilon^2} + \frac{1}{\epsilon}\left[6 - 4\log M^2\right]$$
$$+ 2\left[8 + \log^2 M^2 - 3\log \Lambda^2 - 3\log \alpha(1-\alpha) + \log^2 \frac{\alpha}{1-\alpha} \right] + \mathcal{O}(\epsilon) \Bigg\}. \tag{5.32}$$

The final expression for the one-loop correction to the photon impact factor can be obtained by summing the real contributions given in eqs.(5.19, 5.23, 5.31, 5.32) to the virtual corrections $\Phi_{\gamma^*}^{(1,virtual)}$ of [10]. One can check the cancellation of soft and collinear singularities by combining the singular piece of the virtual corrections (3.42) with the ϵ-poles of Eqs. (5.23) and (5.32). The cancellation of double and single poles is straightforward.

In conclusion, the final expression of the impact factor at NLO can be obtained by summing the finite part of the virtual corrections, the extra terms stemming from the renormalisation (see [10]), the finite terms of (5.23) and (5.32), and the integrals in (5.19) and (5.31) (evaluated at $\epsilon = 0$):

$$
\begin{aligned}
\Phi^{(1)}_{\gamma^*} = \Phi^{(1,virtual)}_{\gamma^*}\Big|^{finite} &- \frac{2\Phi^{(0)}_{\gamma^*}}{(4\pi)^2}\left\{\beta_0 \ln\frac{\boldsymbol{r}^2}{\mu^2} + C_F \ln(\boldsymbol{r}^2)\right\} \\
&+ \int_0^1 d\alpha \int \frac{d\boldsymbol{k}}{(4\pi)^2}\,\mathcal{I}_2(\alpha,\boldsymbol{k})\left\{C_A\left[\ln^2\alpha(1-\alpha)s_0 - \ln^2 M^2\right]\right. \\
&\qquad\left. + 2C_F\left[8 - 3\ln\alpha(1-\alpha)\Lambda^2 + \ln^2 M^2 + \ln^2\frac{\alpha}{1-\alpha}\right]\right\} \\
&+ C_A\,\Phi^{(1,real)}_{\gamma^*}\Big|^{finite}_{C_A} + C_F\,\Phi^{(1,real)}_{\gamma^*}\Big|^{finite}_{C_F}\ .
\end{aligned}
\tag{5.33}
$$

Chapter 6

Integrating the real corrections

For the further analysis of the photon impact factor the phase space integrals have to be performed. In this chapter the integration of the real corrections will be approached. According to the definition of the finite part of the real corrections (5.19, 5.31) we will have to integrate over two transverse momenta ($\boldsymbol{k}$, $\boldsymbol{\ell}$) and two energy variables (α, α_ℓ). The denominators of the Feynman diagrams are products of propagators and the integration can be performed after the introduction of Feynman parameters. However, the integration of the sum of all diagrams would require the introduction of a common denominator giving rise to a tremendous numerator. We therefore consider the Feynman diagrams separately. This introduces divergences that cancel in the sum of all diagrams but represent the main difficulty in the integration.

In the first section the various kinds of divergences that occur are discussed. We then introduce Feynman parameters and carry out the integration over $\boldsymbol{k}$ and $\boldsymbol{\ell}$ in $D = 2 - 2\epsilon$ space-time dimensions. The divergences discussed in momentum space then appear in the Feynman parameter space as poles in ϵ. For each diagram we define appropriate subtractions (in the Feynman parameter space) in order to arrive at finite integrals over α, α_ℓ and the Feynman parameters

As the starting point, let us rewrite the result for the finite part of the real corrections (5.19, 5.31) in terms of the contributions from the diagrams; we introduce the label $\mathcal{A}\!\!\!\mathcal{B}$ to denote one generic squared amplitude ($\mathcal{A}\mathcal{A}$, $\mathcal{A}\mathcal{B}$, $\mathcal{B}\mathcal{A}$ or $\mathcal{B}\mathcal{B}$, longitudinal or transverse polarisation)

$$\mathcal{A}\!\!\!\mathcal{B} = \mathcal{A}\mathcal{A}_{11} \text{ or } \mathcal{A}\mathcal{A}_{12} \text{ or } \mathcal{A}\mathcal{A}_{21} \ldots \text{ or } \mathcal{A}\mathcal{B}_{11}, \ldots \qquad \text{(L or T)}. \tag{6.1}$$

Using (4.33, 4.34) we arrive at:

$$\Phi_{\gamma^*}^{(1,real)}\Big|_{C_A}^{finite} = \lambda_{\mathrm{L,\,T}} \int d^{D-2}\boldsymbol{k}\, d^{D-2}\boldsymbol{\ell} \int_0^1 d\alpha \int_0^\infty d\alpha_\ell \, \frac{1}{4\alpha_1\alpha_2\alpha_\ell(2\pi)^{2D-2}}$$
$$\times \sum_{\text{all diags.}} \Bigg\{ \frac{\alpha_2}{\bar{\alpha}_1} \mathcal{B}\, \Theta(1-\alpha-\alpha_\ell) - \mathcal{B}_{\mathrm{cen}}\, \Theta(|\boldsymbol{\ell}| - \alpha_\ell\sqrt{s_0})$$
$$- [\mathcal{B}_{\mathrm{soft}} - \mathcal{B}_{\mathrm{cen,\,soft}}\, \Theta(|\boldsymbol{\ell}| - \alpha_\ell\sqrt{s_0})]\; \Theta(1-\alpha-\alpha_\ell) \Bigg\}. \quad (6.2)$$

$$\Phi_{\gamma^*}^{(1,real)}\Big|_{C_F}^{finite} = \lambda_{\mathrm{L,\,T}} \int d^{D-2}\boldsymbol{k}\, d^{D-2}\boldsymbol{\ell} \int_0^1 d\alpha \int_0^{1-\alpha} d\alpha_\ell \, \frac{1}{4\alpha_1\alpha_2\alpha_\ell(2\pi)^{2D-2}}$$
$$\times \sum_{\text{all diags.}} \Bigg\{ \frac{\alpha_2}{\bar{\alpha}_1} \left[\mathcal{B} - \mathcal{B}_{\bar{\mathrm{q}}}\, \Theta(\alpha_\ell\Lambda - |\boldsymbol{\ell}'|) - \mathcal{B}_{\mathrm{q}}\, \Theta(\alpha_\ell\Lambda - |\boldsymbol{\ell}''|) \right]$$
$$- \mathcal{B}_{\mathrm{soft}} + \mathcal{B}_{\bar{\mathrm{q}},\,soft}\, \Theta(\alpha_\ell\Lambda - |\boldsymbol{\ell}'|) + \mathcal{B}_{\mathrm{q},\,soft}\, \Theta(\alpha_\ell\Lambda - |\boldsymbol{\ell}''|) \Bigg\} \quad (6.3)$$

with

$$\lambda_{\mathrm{L}} = 4\, e^2 e_f^2 \sqrt{N_c^2 - 1}\; Q^2 \quad , \quad \lambda_{\mathrm{T}} = e^2 e_f^2 \sqrt{N_c^2-1} \quad (6.4)$$

and the two collinear vectors (see sec. 5.1):

$$\boldsymbol{\ell}' = \boldsymbol{\ell} + \frac{\alpha_\ell}{1-\alpha}\boldsymbol{k} \quad , \quad \boldsymbol{\ell}'' = \boldsymbol{\ell} - \frac{\alpha_\ell}{\alpha}(\boldsymbol{k}+\boldsymbol{r}) \quad (6.5)$$

We use the subscript on $\mathcal{B}$ to denote the different limits whose definitions we recall here:

$$\begin{aligned} \mathrm{soft} &:= \;\alpha_\ell \sim |\boldsymbol{\ell}| \to 0 \\ \bar{\mathrm{q}} &:= \;|\boldsymbol{\ell}'| \to 0 \\ \mathrm{q} &:= \;|\boldsymbol{\ell}''| \to 0 \\ \mathrm{cen} &:= \;\alpha_\ell \to 0 \end{aligned} \quad (6.6)$$

The limits are taken 'from left to right', that is the soft limit at the end:

$$\mathcal{B}_{\mathrm{x,\,soft}} \equiv [\mathcal{B}_{\mathrm{x}}]_{\mathrm{soft}} \quad (6.7)$$

When a diagram does not contribute to a certain limit, the corresponding expression is zero. The calculation of the soft, cen, and $\bar{q}$ limits is exactly as in the previous chapter for the sum of diagrams.

One remark shall be made concerning the collinear limits. In order to ensure collinear finite expressions from each diagram we treat these limits equally here; that is, in both cases we pick the residue as the corresponding propagator (D_4 or D_4) vanishes. In sec. 5.2.2 we calculated the limit $g||q$ differently: we changed the variables in the expression for this limit in order to express the result through the photon wave function being independent of the gluon momentum. However, it is easy to show that this procedure is equivalent to the one adopted here.

The integrals in (5.19, 5.31) are finite by construction, we may set $D = 2$. However, as we want to pull the sum apart for the integration we expect divergences that are then regularised dimensionally. So, we keep $D \neq 2$ for the moment.

6.1 The divergences

Let us investigate in this section what divergences occur in the $\mathcal{AB}$ ((4.35-4.69) for longitudinal and (4.83-4.117) for transverse photon polarisation). We first note that all divergences are logarithmic ones, that is, they stem from the 1-dimensional integration dx/x. Fig.6.1,6.2 show which diagram contributes to which limit (that is, diverges in this limit). The block of columns in the middle contains the limits that are needed in the definition of the real corrections (6.2, 6.3). The $\mathcal{AA}$ and $\mathcal{AB}$ diagrams differ only in the colour factors and in the collinear and soft limit. The central limit has

$\mathcal{AA}$			cen	cen/soft	soft	coll	uv (γ_T^* only)	l-uv	is	lr
11	C_F						×	×		
12	C_F,	C_A				$\bar{q}$	×	×		
22	C_F					$\bar{q}$	×	×		
13	C_F					q	×			
23	C_F,	C_A			×	q, $\bar{q}$	×			
33	C_F					q	×			
34		C_A				q	×			
15		C_A	×	×					×	×
25		C_A	×	×	×	$\bar{q}$				×
35		C_A			×	q			×	
14		C_A	×				×	×		×
24		C_A	×			$\bar{q}$	×	×		×
44		C_A	×				×	×		×

Figure 6.1: The divergences of the diagrams $\mathcal{AA}_{ij}$

contributions from (15, 25) and from the lower three diagrams. As discussed in sec. 4.3 the sum of these diagrams (14, 24, 44) in the central limit vanishes for $\mathcal{AA}$ and $\mathcal{AB}$ separately.

The second block of columns shows the divergences that occur in single diagrams but cancel in the sum of all. Let us now discuss these divergences in greater detail.

$\mathcal{AB}$			cen	cen/soft	soft	coll	uv (γ_T^* only)	l-uv	is	lr
11	C_F,	C_A					$\times$			
12	C_F					q	$\times$			
22	C_F,	C_A			$\times$	q, $\bar{q}$	$\times$			
13	C_F,	C_A				$\bar{q}$	$\times$			
23	C_F					$\bar{q}$	$\times$			
33	C_F,	C_A			$\times$	q, $\bar{q}$	$\times$			
34		C_A				q	$\times$			
15		C_A	$\times$	$\times$					$\times$	$\times$
25		C_A	$\times$	$\times$	$\times$	$\bar{q}$				$\times$
35		C_A			$\times$	q			$\times$	
14		C_A	$\times$				$\times$			$\times$
24		C_A	$\times$			$\bar{q}$	$\times$			$\times$
44		C_A	$\times$				$\times$			$\times$

Figure 6.2: The divergences of the diagrams $\mathcal{AB}_{ij}$

6.1.1 The UV divergences

The virtual corrections to the photon impact factor are UV divergent; the renormalisation has been addressed in [10]. The sum of all diagrams $\boldsymbol{\mathcal{AB}}$ making up the real corrections is finite in the UV limit, $\boldsymbol{\ell} \sim \boldsymbol{k} \to \infty$. However, we want to split this sum up and treat diagrams separately. One observes that single diagrams diverge in the UV limit.

All D_i (4.16-4.22) depend on $\boldsymbol{k}$ or $\boldsymbol{\ell}$. Denoting by n the powers of $\boldsymbol{k}^2$ and $\boldsymbol{\ell}^2$ the denominator of each diagram provides $n = 4$ in the limit $\boldsymbol{\ell} \sim \boldsymbol{k} \to \infty$. In case of longitudinal polarisation the numerator of an $\boldsymbol{\mathcal{AB}}$ has at maximum a $\boldsymbol{k}^2$ or $\boldsymbol{\ell}^2$ ($n = 1$), so all diagrams are UV finite. However, the transverse $\boldsymbol{\mathcal{AB}}$ always have one squared transverse momentum or Q^2 more in the numerator. Most diagrams therefore are UV divergent. The only exception are those involving a '5' (that is ij=5x,x5); these are UV finite. The UV divergences cancel in the sum of all diagrams.

There is another UV divergence. Looking back to the definition of the denominators D_i (4.16-4.22) one recognises that all but D_2 depend on $\boldsymbol{\ell}$. Diagrams for longitudinal polarisation that involve a D_2^2 may, in the limit $\boldsymbol{\ell} \to \infty$, provide a $\boldsymbol{\ell}^2$ in the numerator and will have a $\boldsymbol{\ell}^4$ in the denominator.

This leads to a UV divergent $\boldsymbol{\ell}$ integration; lets call these diagrams $\boldsymbol{\ell}-$uv divergent. The cancellation is easy to prove:

$$\begin{aligned}
\sum_{i,j} \mathcal{A}\mathcal{A}_{ij}^{C_F}\Big|_{\boldsymbol{\ell}\text{–uv}} &= [\mathcal{A}\mathcal{A}_{11} + \mathcal{A}\mathcal{A}_{12} + \mathcal{A}\mathcal{A}_{21} + \mathcal{A}\mathcal{A}_{22}\,]_{\boldsymbol{\ell}\to\infty}^{C_F} = 0\,, \\
\sum_{i,j} \mathcal{A}\mathcal{A}_{ij}^{C_A}\Big|_{\boldsymbol{\ell}\text{–uv}} &= [\mathcal{A}\mathcal{A}_{44} + (\mathcal{A}\mathcal{A}_{12} + \mathcal{A}\mathcal{A}_{14} + \mathcal{A}\mathcal{A}_{24} + i \leftrightarrow j)\,]_{\boldsymbol{\ell}\to\infty}^{C_A} = 0.
\end{aligned} \tag{6.8}$$

Since in this limit the divergent diagrams are proportional to $1/\boldsymbol{\ell}^2$ the $\boldsymbol{\ell}$ integration of a diagram in the $\boldsymbol{\ell}$–uv approximation will also be IR divergent. In order to provide finite expressions we will therefore subtract from an $\boldsymbol{\ell}$–uv divergent diagram not exactly its $\boldsymbol{\ell}$–uv approximation but a slightly modified expression which is free of the IR divergence.

Thinking now of diagrams for transverse polarisation with a D_2^2 in the denominator; they are UV divergent and, since the D_i keep their $\boldsymbol{\ell}$ dependence in this limit, these diagrams are also $\boldsymbol{\ell}-$uv divergent.

Both UV divergences will be treated using dimensional regularisation. Performing the calculation in $D = 2 - 2\epsilon$ space-time dimensions the divergences appear as poles in ϵ whose coefficients have to cancel in the sum of all diagrams.

6.1.2 The intersoft (is) divergence

This type of divergence is to be treated only in the case of $\mathcal{A}\mathcal{A}_{15}$ and $\mathcal{A}\mathcal{A}_{35}$ (and $\mathcal{A}\mathcal{B}$). Let us start with $\mathcal{A}\mathcal{A}_{15}^L$ and its divergences:

$$\mathcal{A}\mathcal{A}_{15}^L = \; C_A \, \frac{1}{D_1'\, D_2'^2\, D_5'} \, \alpha_1\, \alpha_2^2\, \bar{\alpha}_1^2\, \boldsymbol{r}^2; \tag{6.9}$$

here we used the abbreviations (4.12) for the α's and slightly modified D_i's:

$$\begin{aligned}
D_1' &= \alpha_\ell \left(\alpha_1 \bar{\alpha}_1 Q^2 + \alpha_1 (\boldsymbol{k} + \boldsymbol{\ell} + \boldsymbol{r})^2 + \bar{\alpha}_1 (\boldsymbol{k} + \boldsymbol{r})^2\right) + \alpha_1 \bar{\alpha}_1 \boldsymbol{\ell}^2 = -\alpha_1 \alpha_\ell D_1\,, \\
D_2' &= \alpha_1 \alpha_2 Q^2 + (\boldsymbol{k} + \boldsymbol{r})^2 = -\alpha_1 D_2\,, \\
D_5' &= \alpha_\ell \left(\alpha_1 \bar{\alpha}_1 Q^2 + \alpha_1 (\boldsymbol{k} + \boldsymbol{\ell})^2 + \bar{\alpha}_1 (\boldsymbol{k} + \boldsymbol{r})^2\right) + \alpha_1 \bar{\alpha}_1 (\boldsymbol{\ell} - \boldsymbol{r})^2 = -\alpha_1 \bar{\alpha}_1 D_5.
\end{aligned} \tag{6.10}$$

This diagram contributes to the central limit; as it does not vanish as $\alpha_\ell \to 0$, the α_ℓ integral including the $1/\alpha_\ell$ from the phase space (see 6.2, 6.3) diverges. Note that all diagrams contributing to this limit do not depend on α_ℓ anymore in this limit. $\mathcal{A}\mathcal{A}_{15}^L$ also contributes to the central/soft limit which is just the $|\boldsymbol{\ell}| \to 0$ limit of $\mathcal{A}\mathcal{A}_{15}^L\big|_{\text{cen}}$. In order to demonstrate this let us think of polar coordinates in the $[\alpha_\ell, \boldsymbol{\ell}_1, \boldsymbol{\ell}_2]$- space $\alpha_\ell = \tau f_\phi$, $\boldsymbol{\ell} = \tau \boldsymbol{g}_\phi$; the angular dependence is given by the functions $f_\phi, \boldsymbol{g}_\phi$. The soft limit corresponds to the region around the origin. Including the $1/\alpha_\ell$ from the phase space we find as the central/soft limit:

$$\text{soft } (\alpha_\ell \sim |\boldsymbol{\ell}| \sim \tau \to 0) \ : \\ \left[\frac{d\alpha_\ell d\boldsymbol{\ell}}{\alpha_\ell}\frac{1}{D_1'\,D_2'^2\,D_5'}\right]_{\text{cen}} \longrightarrow \frac{d\alpha_\ell d\boldsymbol{\ell}}{\alpha_\ell}\frac{1}{(\alpha_1\alpha_2\boldsymbol{\ell}^2)\,D_2'^2\,(\alpha_1\alpha_2\boldsymbol{r}^2)} \sim \frac{\tau^2 d\tau d^2\phi}{\tau}\frac{1}{\tau^2}; \tag{6.11}$$

the τ-integral diverges logarithmically. Note, that D_1' provides a τ^2 since its α_ℓ term is absent in the central limit; D_1', D_5' are constant. In the soft limit D_1' gives a τ. Since the other D's both are constant, the τ integral is finite, $\mathcal{AA}_{15}$ does not contribute to the soft limit.

Now, lets consider for the same diagram non-spheric polar coordinates: $\alpha_\ell = \tau^2 f_\phi$, $\boldsymbol{\ell} = \tau \boldsymbol{g}_\phi$, the measure reads $\tau^3 d\alpha_\ell d^2\phi$. We get again τ from $d\boldsymbol{\ell} d\alpha_\ell/\alpha_\ell$, τ^2 from D_1' and therefore a divergent τ-integral. However, we pick a different part of D_1'. In normal polar coordinates the coordinates used here correspond to a curve which lies, roughly speaking, between the curves corresponding to the soft and the central limit. The former is approached on a straight line; the latter corresponds to a curve in the plane $\alpha_\ell = 0$. We therefore refer to the limit $\sqrt{\alpha_\ell} \sim |\boldsymbol{\ell}| \sim \tau \to 0$ as intersoft or $'is'$.

$$\text{intersoft (is) } (\sqrt{\alpha_\ell} \sim |\boldsymbol{\ell}| \sim \tau \to 0) \ : \\ \frac{d\alpha_\ell d\boldsymbol{\ell}}{\alpha_\ell}\frac{1}{D_1'\,D_2'^2\,D_5'} \\ \longrightarrow \frac{d\alpha_\ell d\boldsymbol{\ell}}{\alpha_\ell}\frac{1}{[\alpha_\ell(\alpha_1\alpha_2 Q^2 + (\boldsymbol{k}+\boldsymbol{r})^2) + \alpha_1\alpha_2\boldsymbol{\ell}^2]\,D_2'^2\,(\alpha_1\alpha_2\boldsymbol{r}^2)} \sim \frac{\tau^3 d\tau d^2\phi}{\tau^2}\frac{1}{\tau^2} \tag{6.12}$$

Note, that in (6.12) both the integrations with respect to α_ℓ and $\boldsymbol{\ell}$ are divergent separately. However, the comparison to (6.11) shows that both integrands get equal when either $\alpha_\ell \to 0$ or $\boldsymbol{\ell} \to \infty$. Thus, the combination $(\mathcal{AA}_{15}|_{\text{cen/soft}} - \mathcal{AA}_{15}|_{\text{intersoft}})$ will be finite in both the $\boldsymbol{\ell}$–uv and the $\alpha_\ell \to 0$ limit.

Going back to our expression of the real corrections and thinking of the theta functions as integration bounds, we need for the C_A part of a diagram the combination:

$$C_A \ : \quad \frac{\alpha_2}{\bar{\alpha}_1}\mathcal{AB} - \mathcal{AB}_{\text{soft}} - (\mathcal{AB}_{\text{cen}} - \mathcal{AB}_{\text{cen,soft}}) \tag{6.13}$$

In case of $\mathcal{AA}_{15}$ (L and T) we just subtract $\mathcal{AA}_{15}|_{\text{is}}$

$$\frac{\alpha_2}{\bar{\alpha}_1}X - \Big(X|_{\text{cen}} - X|_{\text{cen/soft}}\Big) - X|_{\text{is}} \quad \text{with :} \ \ X = \mathcal{AA}_{15} \tag{6.14}$$

This combination is finite as $\alpha_\ell \to 0$, because the first and the last two terms get equal; it is $\boldsymbol{\ell}-$uv-finite because $\mathcal{A}\mathcal{A}_{15}$ is not $\boldsymbol{\ell}-$uv-divergent and the last two terms get equal. Finally, the intersoft limit is finite, because also the terms in the brackets get equal in this limit. Thus, the subtraction of the $\mathcal{A}\mathcal{A}_{15}|_{\mathrm{is}}$ simultaneously cures different divergences of $\mathcal{A}\mathcal{A}_{15}$ and $\mathcal{A}\mathcal{A}_{15}|_{\mathrm{cen/soft}}$.

Let us now switch to $\mathcal{A}\mathcal{A}_{35}$. According to fig.6.1 it contributes to the central, soft and intersoft limit. With the same kind of argumentation as above one can show that in addition to the is-limit of the original expression also the is-limit of the soft approximation has to be subtracted to arrive at a finite combination :

$$\frac{\alpha_2}{\bar{\alpha}_1} X - X|_{\mathrm{cen}} - X|_{\mathrm{soft}} - \Big(X|_{\mathrm{is}} - X|_{\mathrm{soft,is}} \Big) \quad \text{with :} \quad X = \mathcal{A}\mathcal{A}_{35} \tag{6.15}$$

Finally, we remark that in case of $\mathcal{A}\mathcal{A}_{25}$ there are both soft and central/soft divergences, but in the is-limit they get equal. According to (6.13) the soft and cen/soft limit appear as difference; the combination for $\mathcal{A}\mathcal{A}_{25}$ is therefore intersoft finite and there is no need to subtract any intersoft limit.

What remains is to prove that the is-limits we have subtracted (6.14, 6.15) cancel as we re-add them. Indeed, it is easy to show that

$$\text{L,T} : \quad \mathcal{A}\mathcal{A}_{15}|_{\mathrm{is}} + (\mathcal{A}\mathcal{A}_{35}|_{\mathrm{is}} - \mathcal{A}\mathcal{A}_{35}|_{\mathrm{soft}}) = 0 \qquad \text{and also for } \mathcal{A}\mathcal{B} \tag{6.16}$$

6.1.3 The lr-divergence

In the limit $\alpha_\ell \to 0$ our expressions can be written as:

$$\begin{aligned}
\mathcal{A}\mathcal{A}^L_{ij}\big|_{\mathrm{cen}} &= \frac{\alpha_1^3\,\alpha_2^3\,C_A}{(\boldsymbol{\ell}-\boldsymbol{r})^2}\,\frac{1}{D^2(\boldsymbol{k}+\boldsymbol{r})}\,D_{ij} \\
\mathcal{A}\mathcal{B}^L_{ij}\big|_{\mathrm{cen}} &= \frac{-\alpha_1^3\,\alpha_2^3\,C_A}{(\boldsymbol{\ell}-\boldsymbol{r})^2}\,\frac{1}{D(\boldsymbol{k}+\boldsymbol{r})D(\boldsymbol{k}+\boldsymbol{\ell})}\,D_{ij}
\end{aligned} \tag{6.17}$$

and for transverse polarisation:

$$\begin{aligned}
\mathcal{A}\mathcal{A}^T_{ij}\big|_{\mathrm{cen}} &= \frac{2\,\alpha_1\,\alpha_2\,(1-2\alpha_1\alpha_2)\,C_A}{(\boldsymbol{\ell}-\boldsymbol{r})^2}\,\frac{(\boldsymbol{k}+\boldsymbol{r})^2}{D^2(\boldsymbol{k}+\boldsymbol{r})}\,D_{ij} \\
\mathcal{A}\mathcal{B}^T_{ij}\big|_{\mathrm{cen}} &= \frac{-2\,\alpha_1\,\alpha_2\,(1-2\alpha_1\alpha_2)\,C_A}{(\boldsymbol{\ell}-\boldsymbol{r})^2}\,\frac{(\boldsymbol{k}+\boldsymbol{r})(\boldsymbol{k}+\boldsymbol{\ell})}{D(\boldsymbol{k}+\boldsymbol{r})D(\boldsymbol{k}+\boldsymbol{\ell})}\,D_{ij}
\end{aligned} \tag{6.18}$$

where $D(\boldsymbol{k}) = \alpha_1\alpha_2 Q^2 + \boldsymbol{k}^2$. The matrix D_{ij} reads :

$$\begin{pmatrix}
0 & 0 & 0 & -\frac{1}{2} & \frac{\boldsymbol{r}^2}{\boldsymbol{\ell}^2} \\
0 & 0 & 0 & -\frac{1}{2} & \frac{\boldsymbol{r}^2}{\boldsymbol{\ell}^2} \\
0 & 0 & 0 & 0 & 0 \\
-\frac{1}{2} & -\frac{1}{2} & 0 & 2 & 0 \\
\frac{\boldsymbol{r}^2}{\boldsymbol{\ell}^2} & \frac{\boldsymbol{r}^2}{\boldsymbol{\ell}^2} & 0 & 0 & 0
\end{pmatrix} .$$

This form of the expressions becomes clearer when one considers the sum $\mathcal{AA}+\mathcal{AB}+\mathcal{BA}+\mathcal{BB}$. The denominators then combine to the typical structure of the photon wave function (cf. (4.121)).

By the way, from the matrix D_{ij} one can be immediately read that only the diagrams 15, 25 (51, 52) diverge as $|\boldsymbol{\ell}| \to 0$ and therefore contribute to the cen/soft limit. However, the $\boldsymbol{\ell}$ integral is not uv-divergent due to the upper bound on the $\boldsymbol{\ell}$ integration in (6.2, 6.3), namely $\alpha_\ell s_0$.

Note, that when $\boldsymbol{\ell} \to \boldsymbol{r}$ the expressions (6.17, 6.18) lead to a logarithmic divergence, we call this the lr-divergence. However, $\mathcal{AA}_{ij}|_{\mathrm{cen}}$ and $\mathcal{AB}_{ij}|_{\mathrm{cen}}$ get equal up to the sign in this limit. Our strategy for the treatment of the lr-divergence is therefore to integrate the couple $(\mathcal{AA}_{ij}|_{\mathrm{cen}} + \mathcal{AB}_{ij}|_{\mathrm{cen}})$ instead of the diagrams separately (and also $\mathcal{BB}_{\mathrm{cen}} + \mathcal{BA}_{\mathrm{cen}}$). In the Feynman parameter space this translates into the requirement of equal Feynman parameters for both diagrams as we will see later.

6.2 Introduction of Feynman parameters

All squared amplitudes $\mathcal{A\!B}$ have the general structure:

$$\mathcal{A\!B} = \frac{Nu}{D'_i D'_j D'_k D'_l} \quad , \qquad D' = D'(\boldsymbol{k}, \boldsymbol{\ell}, Q^2, \boldsymbol{r}) \tag{6.19}$$

For longitudinal photon polarisation the Numerator Nu is a polynomial in the transverse momenta and Q^2 with $\boldsymbol{k}, \boldsymbol{\ell}$ to the power of 2 at maximum:

$$\mathrm{L} \ : \ Nu = \lambda_1\, \boldsymbol{k}^2 + \lambda_2\, \boldsymbol{\ell}^2 + \lambda_3\, \boldsymbol{kr} + \ldots + \lambda_4\, Q^2 + \lambda_5\, \boldsymbol{r}^2 \tag{6.20}$$

In the transverse case the maximum exponent is 4:

$$\mathrm{T} \ : \ Nu = \lambda_1 \boldsymbol{k}^4 + \lambda_2\, \boldsymbol{\ell}^4 + \ldots + \lambda_4\, \boldsymbol{k}^2(\boldsymbol{kr}) + \ldots + \lambda_5\, Q^2 \boldsymbol{k}^2 + \ldots + \lambda_6 Q^4 \ldots \tag{6.21}$$

The λ_i are functions of α, α_ℓ.

$\bar{D}$ stands for one of the 7 propagators, we use here the slightly modified expressions (6.22-6.28). In some cases two $\bar{D}$ are equal, but it is always '$\bar{D}^4$'.

$$\begin{aligned}
\bar{D}_1 =& -\alpha_1\alpha_\ell D_1 \\
=& \;\alpha_\ell\left[\alpha_1\bar{\alpha}_1 Q^2 + \alpha_1(\boldsymbol{k}+\boldsymbol{\ell}+\boldsymbol{r})^2 + \bar{\alpha}_1(\boldsymbol{k}+\boldsymbol{r})^2\right] + \alpha_1\bar{\alpha}_1\boldsymbol{\ell}^2 \qquad (6.22)\\
\bar{D}_2 =& -\alpha_1 D_2 \\
=& \;\alpha_1\alpha_2 Q^2 + (\boldsymbol{k}+\boldsymbol{r})^2 \qquad (6.23)\\
\bar{D}_3 =& \alpha_\ell\alpha_1 D_3 \\
=& (\alpha_1\,\boldsymbol{\ell} - \alpha_\ell\,(\boldsymbol{k}+\boldsymbol{r}))^2 \qquad (6.24)\\
\bar{D}_4 =& \alpha_\ell\bar{\alpha}_1 \\
=& (\bar{\alpha}_1\,\boldsymbol{\ell} + \alpha_\ell\,(\boldsymbol{k}+\boldsymbol{\ell}))^2 \qquad (6.25)\\
\bar{D}_5 =& -\alpha_1\bar{\alpha}_1 D_5 \\
=& \;\alpha_\ell\left(\alpha_1\bar{\alpha}_1 Q^2 + \alpha_1(\boldsymbol{k}+\boldsymbol{\ell})^2 + \bar{\alpha}_1(\boldsymbol{k}+\boldsymbol{r})^2\right) + \alpha_1\bar{\alpha}_1(\boldsymbol{\ell}-\boldsymbol{r})^2 \qquad (6.26)\\
\bar{D}_6 =& -\alpha_\ell\bar{\alpha}_1 D_6 \\
=& \alpha_\ell\left[\alpha_1\bar{\alpha}_1\, Q^2 + \bar{\alpha}_1\boldsymbol{k}^2 + \alpha_1\,(\boldsymbol{k}+\boldsymbol{\ell})^2\right] + \alpha_1\bar{\alpha}_1\,\boldsymbol{\ell}^2 \qquad (6.27)\\
\bar{D}_7 =& -\bar{\alpha}_1 D_7 \\
=& \bar{\alpha}_1\bar{\alpha}_2\, Q^2 + (\boldsymbol{k}+\boldsymbol{\ell})^2\;. \qquad (6.28)
\end{aligned}$$

To approach the integration we introduce Feynman parameters

$$\frac{1}{\bar{D}_1\,\bar{D}_2\,\bar{D}_3\,\bar{D}_4} = 6\int_0^1 d\beta_1\,d\beta_2\,d\beta_3\,d\beta_4\;\frac{\delta(1-\sum\beta_i)}{\left[\beta_1\bar{D}_1+\beta_2\bar{D}_2+\beta_3\bar{D}_3+\beta_4\bar{D}_4\right]^4} \qquad (6.29)$$

The indices on the $\bar{D}'s$ just label 4 different propagators. A squared $\bar{D}_i$ leads to an additional β_i in the numerator

$$\frac{1}{\bar{D}_1^2\,\bar{D}_2\,\bar{D}_3} = 6\int_0^1 d\beta_1\,d\beta_2\,d\beta_3\;\frac{\beta_1\,\delta(1-\sum\beta_i)}{\left[\beta_1\bar{D}_1+\beta_2\bar{D}_2+\beta_3\bar{D}_3\right]^4} \qquad (6.30)$$

and correspondingly for two squared $\bar{D}'s$. The general formula is given in the appendix.

Thus, any squared amplitude $\mathcal{AB}$ in the combined $\{\alpha_\ell, \boldsymbol{\ell}, \beta_i\}$ space has the following form; let us call this the mixed representation of $\mathcal{AB}$.

$$\mathcal{AB} = 6\int_0^1 \prod_i d\beta_i\;\delta(1-\sum\beta_i)\;\frac{f_\beta\,Nu}{\left[\sum\beta_i\bar{D}_i\right]^4} \qquad (6.31)$$

here, f_β denotes the β_i stemming from one or two squared $\bar{D}_i$ (see (6.30)). The sum of propagators in the denominator can be written as:

$$\sum_i \beta_i\,\bar{D}_i = \alpha\,\boldsymbol{k}^2 + \beta\,\boldsymbol{\ell}^2 + 2\,\gamma\,\boldsymbol{k\ell} + 2\eta\,\boldsymbol{kr} + 2\mu\,\boldsymbol{\ell r} + \bar{D}_r \qquad (6.32)$$

The parameters we introduced are functions of the Sudakov variables α_1, α_ℓ and the Feynman parameters β_i; $\bar{D}_r$ additionally depends on Q^2 and $\boldsymbol{r}^2$.

Let us investigate in the following how the various limits discussed above show up in the mixed representation. First, we note that with the terms $\boldsymbol{k}^4, \boldsymbol{\ell}^4$ or $\boldsymbol{\ell}^2\boldsymbol{k}^2$ in the numerator (6.21) the expression (6.31) is divergent in the limit $\boldsymbol{\ell} \sim \boldsymbol{k} \to \infty$; in $D = 2 - 2\epsilon$ transverse dimensions the UV-divergence occurring in case of transverse polarisation will appear as pole in ϵ. For all UV finite $\mathcal{AB}$ the $\boldsymbol{k}, \boldsymbol{\ell}$ integration will be convergent in $D = 2$. The divergences of $\mathcal{AB}$ will appear as divergences of the β_i integrals, as we will see.

6.2.1 The soft, collinear and central limits

The soft limit of $\mathcal{AB}$ in momentum space is reached essentially by putting $\boldsymbol{\ell} \to \rho\boldsymbol{\ell}, \alpha_\ell \to \rho\alpha_\ell$ and expanding around $\rho = 0$, retaining only the leading term. This can be thought of as a change of the variables $\{\alpha_\ell, \boldsymbol{\ell}\}$ to 3 dimensional polar coordinates and the expansion around the origin. From $d\boldsymbol{\ell}\, d\alpha_\ell/\alpha_\ell$ we receive a ρ. In the mixed representation (6.31) of $\mathcal{AB}$ we expect the soft limit in some corner of the combined $\{\alpha_\ell, \boldsymbol{\ell}, \beta_i\}$ space. To get $\mathcal{AB}_{\text{soft}}$ we have to take each $\bar{D}_i$ in the denominator of (6.31) (and Nu) in the soft limit. According to (6.22-6.28) the $\bar{D}$ have different soft behaviour:

$$\bar{D}_i\big|_{\text{soft}} = \bar{D}_i\big|_{\substack{\boldsymbol{\ell} \to \rho\boldsymbol{\ell} \\ \alpha_\ell \to \rho\alpha_\ell}} \sim \rho^{x_i} \quad (\text{as } \rho \to 0)$$
$$x_1 = 1,\ x_2 = 0, x_3 = 2,\ x_4 = 2,\ x_5 = 0,\ x_6 = 1,\ x_7 = 0 \tag{6.33}$$

This dictates how the β_i have to be weighted with ρ to approach the soft limit. As an example let us consider

$$\mathcal{A}\mathcal{A}^L_{35} = \frac{\alpha_\ell\, \alpha_1^5\, \bar{\alpha}_1^3\, \alpha_2\, \bar{\alpha}_2\, \boldsymbol{r}^2}{\bar{D}_1\, \bar{D}_2\, \bar{D}_3\, \bar{D}_5} = 6 \int d\beta_1\, d\beta_2\, d\beta_3\, d\beta_5\, \delta(\textstyle\sum \beta_i - 1)\, A_{35}$$
$$A_{35} = \frac{\alpha_\ell\, \alpha_1^5\, \bar{\alpha}_1^3\, \alpha_2\, \bar{\alpha}_2\, \boldsymbol{r}^2}{\left[\beta_1\bar{D}_1 + \beta_2\bar{D}_2 + \beta_3\bar{D}_3 + \beta_5\bar{D}_5\right]^4}; \tag{6.34}$$

Having (6.33) in mind we put in A_{35}

$$\begin{aligned} &\boldsymbol{\ell} \to \rho\boldsymbol{\ell},\ \alpha_\ell \to \rho\alpha_\ell \\ &\beta_1 \to \rho\beta_1, \\ &\beta_2 \to \rho^2\beta_2, \\ &\beta_5 \to \rho^2\beta_5 \end{aligned} \tag{6.35}$$

Expanding the denominator in (6.34) around $\rho = 0$ we see that all $\beta_i\bar{D}_i$ are of order ρ^2 and we pick from every $\bar{D}_i$ the soft limit. The curve given by (6.35) is therefore the path in the $\{\alpha_\ell, \boldsymbol{\ell}, \beta_i\}$ space on which one reaches the soft approximation of $\mathcal{A}_{35}$. Let us put this slightly different: we cancel the delta function by the β_3 integration; the integration region is then given by the condition $\beta_1 + \beta_2 + \beta_5 \leq 1$. In the vicinity of the origin of the $\{\alpha_\ell, \boldsymbol{\ell}, \beta_1, \beta_2, \beta_5\}$ space we think of 6 dimensional non spherical polar coordinates with the distance to the origin being ρ. The transform shall be such that the old variables transform to expressions that depend on ρ as in (6.35). The integration measure (including $1/\alpha_\ell$) leads

$$\frac{1}{\alpha_\ell} d\alpha_\ell d\boldsymbol{\ell} d\beta_1 d\beta_2 d\beta_5 \to \frac{1}{\rho}\rho^7 d\rho \; d^5\phi. \tag{6.36}$$

From (6.34) it follows that the numerator is of order ρ. Since the denominator gives a ρ^8 we are left with a logarithmic divergent ρ integral - the soft divergence of $\mathcal{A}\mathcal{A}_{35}$ in the mixed representation.

The generalisation to any $\mathcal{AB}$ is straightforward. According to (6.33) each $\bar{D}_i$ is associated with a maximum exponent x_i in the soft limit, $\bar{D}_i\big|_{\text{soft}} \sim \rho^{x_i}$. Given a certain $\mathcal{AB}$ with a set of propagators we call the maximum x_i occurring $x_{\max}$. The 'weights' of the β_i are now derived from the requirement that $\beta_i \, \bar{D}_i\big|_{\text{soft}} \sim \rho^{x_{\max}}$ for each i:

$$\begin{aligned} \underline{\text{soft}} \;: \qquad & \boldsymbol{\ell} \to \rho\boldsymbol{\ell}, \; \alpha_\ell \to \rho\alpha_\ell \\ & \beta_i \to \rho^{(x_{\max}-x_i)} \, \beta_i \end{aligned} \tag{6.37}$$

It is understood that one then has to expand around $\rho = 0$ keeping only the leading term in order to actually reach the soft limit; we will continue to suppress this in the following. Note that the numerator of (6.31) which has to be taken also in the limit (6.37) may contain β_i through f_β.

In the same spirit the other infrared limits discussed in momentum space can be reformulated in the mixed representation. The corner of the β_i subspace associated with a particular limit is always determined by the behaviour of the $\bar{D}_i$ in that limit. The collinear limit $g||\bar{q}$ was defined as $\boldsymbol{\ell}' = \boldsymbol{\ell} + \alpha_\ell/\alpha_2 \, \boldsymbol{k} \to 0$. In $\mathcal{AB}$ we therefore first express $\boldsymbol{\ell}$ through $\boldsymbol{\ell}'$ and then let $\boldsymbol{\ell}' \to \rho\boldsymbol{\ell}'$. The collinear limit, $\rho \to 0$, of all propagators except for $\bar{D}_4$ is reached just by setting $\boldsymbol{\ell} = -\alpha_\ell/\alpha_2 \, \boldsymbol{k}$, that is $\boldsymbol{\ell}' = 0$; $\bar{D}_4$ is proportional to $\boldsymbol{\ell}'^2$ and remains unchanged. Therefore:

$$\begin{aligned} & \bar{D}_i\big|_{\bar{\text{q}}} = \bar{D}_i\Big|_{\;\boldsymbol{\ell}' \to \rho\boldsymbol{\ell}'} \sim \rho^{q_i} \\ & q_{i\neq 4} = 0\,, \; q_4 = 2 \end{aligned} \tag{6.38}$$

Thus, the $\bar{q}$-collinear limit reads:

$$\begin{aligned} \bar{q} \;: \qquad & \boldsymbol{\ell}' \to \rho\boldsymbol{\ell}' \\ & \beta_4 \to \beta_4 \\ & \beta_{i\neq 4} \to \rho^2 \beta_i. \end{aligned} \tag{6.39}$$

Recall that after cancellation of the delta function in (6.31) the integration region is bounded by $\sum \beta_i = 1$. The limit (6.39) therefore corresponds to that corner of the $\{\boldsymbol{\ell}', \beta_i\}$ space where $\beta_4 \approx 1$ while $|\boldsymbol{\ell}'|$ and all other β_i are close to zero.

Let us now ask how to approach the soft limit of the collinear approximation just calculated. First, note that in the soft limit ($\boldsymbol{\ell} \sim \alpha_\ell \to 0$) $\boldsymbol{\ell}'$ remains unchanged. The soft limit of a function of α_ℓ and $\boldsymbol{\ell}'$ in momentum space is therefore the limit of $\boldsymbol{\ell}' \sim \alpha_\ell \to 0$. As mentioned, in the collinear limit all $\bar{D}$ except for $\bar{D}_4$ don't depend on $\boldsymbol{\ell}'$; the soft limit of these expressions is just the limit $\alpha_\ell \to 0$. One finds that the $\bar{D}_i\big|_{\mathrm{coll}}$ have the same 'behaviour' in the soft limit as the $\bar{D}_i$ in the soft limit (see (6.33)) :

$$
\begin{aligned}
\bar{D}_i\big|_{\mathrm{soft}} &= \bar{D}_i\Big|_{\substack{\boldsymbol{\ell}\to\rho\boldsymbol{\ell} \\ \alpha_\ell \to \rho\alpha_\ell}} \sim \rho^{x_i} \\
\bar{D}_i\big|_{\bar{\mathrm{q}},\mathrm{soft}} &= \bar{D}_i\big|_{\bar{\mathrm{q}}}\Big|_{\substack{\boldsymbol{\ell}'\to\rho\boldsymbol{\ell}' \\ \alpha_\ell \to \rho\alpha_\ell}} \sim \rho^{x'_i} \\
\text{where: } & x_i = x'_i
\end{aligned}
\tag{6.40}
$$

With this we can state as the collinear/soft limit:

$$
\begin{aligned}
\bar{q},\mathrm{soft}\ :\qquad & \text{first } \bar{q}\,,\text{then}\quad \boldsymbol{\ell}' \to \rho\boldsymbol{\ell}',\ \alpha_\ell \to \rho\alpha_\ell \\
& \qquad\qquad\qquad \beta_i \to \rho^{(x_{\max}-x_i)}\beta_i \\
& \text{with } x_i \text{ from (6.33)}
\end{aligned}
\tag{6.41}
$$

Recall that $\bar{q}$ in (6.41) means the introduction of ρ's according to (6.39) and expanding around $\rho = 0$ setting $\rho = 1$ afterwards.

All what was said up to here about the limit $g||\bar{q}$ exactly applies to the other collinear limit, $g||q$, with the only modification that $\bar{D}_4, \beta_4$ and $\boldsymbol{\ell}'$ have to be exchanged by $\bar{D}_3, \beta_3$ and $\boldsymbol{\ell}''$.

Finally, let us consider the central limit. The introduction of Feynman parameters has not changed so much; in (6.31) we just expand around $\alpha_\ell = 0$ under the β_i integral. In the soft limit of the central approximation, however, the propagators $\bar{D}_i$ behave differently compared to the soft limit of the full expressions. From (6.22-6.28) taken at $\alpha_\ell = 0$ we derive:

$$
\begin{aligned}
\bar{D}_i\big|_{\mathrm{cen,soft}} &= \bar{D}_i\big|_{\alpha_\ell\to 0}\Big|_{\substack{\boldsymbol{\ell}\to\rho\boldsymbol{\ell} \\ \alpha_\ell \to \rho\alpha_\ell}} \sim \rho^{c_i} \\
c_1 = 2,\ c_2 = 0, c_3 = 2,&\ c_4 = 2,\ c_5 = 0,\ c_6 = 2,\ c_7 = 0
\end{aligned}
\tag{6.42}
$$

Only c_1, c_6 differ from the corresponding x_i. Let us denote by $c_{\max}$ the maximum c_i that occurs in the actual $\mathcal{AB}$. The central/soft approximation is then reached via:

$$\begin{aligned} \text{cen,soft}\ : \qquad & \text{first cen, then} \quad \boldsymbol{\ell}' \to \rho\boldsymbol{\ell},\ \alpha_\ell \to \rho\alpha_\ell \\ & \qquad\qquad\qquad \beta_i \to \rho^{(c_{\max}-c_i)}\beta_i \\ & \text{with } c_i \text{ from (6.42)} \end{aligned} \tag{6.43}$$

6.2.2 The limits $\boldsymbol{\ell}-$uv, is, lr

The $\boldsymbol{\ell}$ integration of some squared amplitudes $\mathcal{AB}$ involving a $\bar{D}^2$ is UV-divergent; we called the limit $\boldsymbol{\ell} \to \infty$ the $\boldsymbol{\ell}-$uv limit. The divergence arose because all $\bar{D}_i$ except for $\bar{D}_2$ depend on $\boldsymbol{\ell}$. Let us parametrise the approach to this limit as $\boldsymbol{\ell} \to 1/\rho\,\boldsymbol{\ell}$

$$\begin{aligned} & \bar{D}_i\big|_{\boldsymbol{\ell}\text{–uv}} = \bar{D}_i\big|_{\ \boldsymbol{\ell} \to 1/\rho\,\boldsymbol{\ell}} \sim \rho^{u_i} \quad (\text{as } \rho \to 0) \\ & u_{i\neq 2} = -2\,,\ u_2 = 0 \end{aligned} \tag{6.44}$$

The maximum exponent $u_{\max}$ in any $\boldsymbol{\ell}-$uv divergent $\mathcal{AB}$ is zero. The requirement $\beta_i\ \bar{D}_i\big|_{\boldsymbol{\ell}\text{–uv}} \sim \rho^{u_{\max}} = 1$ leads to

$$\begin{aligned} \underline{\boldsymbol{\ell}-\text{uv}}\ : \qquad & \boldsymbol{\ell} \to 1/\rho\,\boldsymbol{\ell} \\ & \beta_2 \to \beta_2 \\ & \beta_{i\neq 2} \to \rho^2\beta_i. \end{aligned} \tag{6.45}$$

Thus, after cancellation of the delta function in the mixed representation (6.31) the $\boldsymbol{\ell}-$uv limit corresponds to that corner of the $\{\beta_i\}$ subspace where $\beta_2 \approx 1$ and all other $\beta_i \approx 0$.

We next address the intersoft limit $\alpha_\ell \to \rho\alpha_\ell, \boldsymbol{\ell} \to \sqrt{\rho}\,\boldsymbol{\ell}$. In complete analogy to the limits already discussed we find:

$$\begin{aligned} & \bar{D}_i\big|_{\text{is}} = \bar{D}_i\big|_{\substack{\boldsymbol{\ell} \to \sqrt{\rho}\,\boldsymbol{\ell} \\ \alpha_\ell \to \rho\,\alpha_\ell}} \sim \rho^{\,y_i} \\ & y_1 = 1,\ y_2 = 0, y_3 = 1,\ y_4 = 1,\ y_5 = 0,\ y_6 = 1,\ y_7 = 0 \end{aligned} \tag{6.46}$$

The comparison to (6.33) shows that except for $\bar{D}_3$ and $\bar{D}_4$ we get the same exponents as in the soft limit. The intersoft limit reads:

$$\begin{aligned} \underline{\text{is}}\ : \qquad & \boldsymbol{\ell} \to \sqrt{\rho}\ \boldsymbol{\ell} \\ & \alpha_\ell \to \rho\,\alpha_\ell \\ & \beta_i \to \rho^{(y_{\max}-y_i)}\beta_i. \end{aligned} \tag{6.47}$$

Finally, let us consider the lr-limit: the diagrams that contribute to the central limit diverge as $\boldsymbol{\ell} \to \boldsymbol{r}$. Let us look at the propagator structure of those diagrams with the lr problem:

ij	$\mathcal{AA}_{ij}$	$\mathcal{AB}_{ij}$
15,14	$\bar D_1 \bar D_5\, \bar D_2^2$	$\bar D_1 \bar D_5\, \bar D_2 \bar D_7$
25,24	$\bar D_4 \bar D_5\, \bar D_2^2$	$\bar D_4 \bar D_5\, \bar D_2 \bar D_7$
44	$\bar D_5^2\, \bar D_2^2$	$\bar D_5^2\, \bar D_2 \bar D_7$

For each ij there is disagreement between $\mathcal{AA}$ and $\mathcal{AB}$ in one $\bar D$: $\bar D_2$ in $\mathcal{AA}$ and $\bar D_7$ in $\mathcal{AB}$. As shown above, the combination $\mathcal{AA}_{ij} + \mathcal{AB}_{ij}$ is lr-finite. This is because

$$\text{as } \boldsymbol{\ell} \to \boldsymbol{r} \;:\quad \bar D_7\big|_{\alpha_\ell=0} \to \bar D_2\big|_{\alpha_\ell=0}\,. \tag{6.48}$$

To ensure that the sum of $\mathcal{AA}$ and $\mathcal{AB}$ is lr-finite also in the mixed representation under the β_i integral they must depend on the same set of β_i . In case of $\mathcal{AA}_{15}$ for instance, we will therefore parametrise:

$$\begin{aligned}
\mathcal{AA}_{15} \sim \frac{1}{\bar D_1 \bar D_5 \bar D_2^2} &= \int \{d\beta_i\} \frac{\delta(1-\sum \beta_i)}{[\beta_1 \bar D_1 + \beta_5 \bar D_5 + (\beta_2+\beta_7)\bar D_2]^4} \\
\mathcal{AB}_{15} \sim \frac{1}{\bar D_1 \bar D_5 \bar D_2 \bar D_7} &= \int \{d\beta_i\} \frac{\delta(1-\sum \beta_i)}{[\beta_1 \bar D_1 + \beta_5 \bar D_5 + \beta_2 \bar D_2 + \beta_7 \bar D_7]^4}
\end{aligned}$$

The other $\mathcal{AB}$ contributing to the lr-limit are parametrised correspondingly.

6.3 The integration

Let us have a look back to our initial expression for the real corrections (6.2, 6.3). For each diagram we want to carry out the integration over $\boldsymbol{k}$ and $\boldsymbol{\ell}$ at fixed $Q^2, \boldsymbol{r}, \alpha, \alpha_\ell$. This requires the subtraction of further approximations which will be discussed in the next chapter. For a given diagram $\mathcal{AB}$ we introduced Feynman parameters and saw how the various divergences appear in the combined $\{\boldsymbol{\ell}, \alpha_\ell, \beta_i\}$ space. Now, we bring the transformation from momentum to $\{\beta_i\}$ space to an end and perform the $\boldsymbol{k}$ and $\boldsymbol{\ell}$ integration; We will see that in the $\{\beta_i\}$ space the divergences sit in the same corners as before in the $\{\beta_i\}$ subspace of $\{\boldsymbol{\ell}, \alpha_\ell, \beta_i\}$.

The $\boldsymbol{\ell}$ integration of the different limits of $\mathcal{AB}$ has different bounds as indicated by the θ-functions. According to these bounds we are confronted with three kinds of integrals.

6.3.1 $\int \mathcal{AB}$

Let us first consider now the integration of the full $\mathcal{AB}$; the $\boldsymbol{\ell}$-integration stretches over full space. After introduction of Feynman parameters we write (see 6.31):

$$\mathcal{AB} = \int_0^1 \prod_i d\beta_i \; \delta(1 - \sum \beta_i) \, \frac{Nu}{\left[\sum_i \beta_i \, \bar{D}_i\right]^4} \tag{6.49}$$

here, we absorbed the factor $6f_\beta$ into Nu. Let us repeat its structure (see (6.20, 6.21)):

$$\begin{aligned} &\mathrm{L} \;\; : \; Nu = \lambda_1 \, \boldsymbol{k}^2 + \lambda_2 \, \boldsymbol{\ell}^2 + \lambda_3 \, \boldsymbol{kr} + \ldots + \lambda_4 \, Q^2 + \lambda_5 \, \boldsymbol{r}^2 \\ &\mathrm{T} \;\; : \; Nu = \lambda_1 \boldsymbol{k}^4 + \lambda_2 \, \boldsymbol{\ell}^4 + \ldots + \lambda_4 \, \boldsymbol{k}^2(\boldsymbol{kr}) + \ldots + \lambda_5 \, Q^2 \boldsymbol{k}^2 + \ldots + \lambda_6 Q^2 \ldots \end{aligned} \tag{6.50}$$

We decompose the denominator:

$$De = \sum_i \beta_i \, \bar{D}_i = \alpha \, \boldsymbol{k}^2 + \beta \, \boldsymbol{\ell}^2 + 2 \, \gamma \, \boldsymbol{k\ell} + 2\eta \, \boldsymbol{kr} + 2\mu \, \boldsymbol{\ell r} + \bar{D}_r ; \tag{6.51}$$

the dependence on Q^2 and $\boldsymbol{r}^2$ is contained in $\bar{D}_r$. Thus, we are led to the integral

$$I_1 = \int_{\mathbb{R}^D} d^D \boldsymbol{k} \int_{\mathbb{R}^D} d^D \boldsymbol{\ell} \, \frac{Nu}{De^{\,4}} . \tag{6.52}$$

The angular part of the integration gets very easy as soon as we get rid of the mixed scalar products in (6.51). The derivation of the substitution is straightforward, here we state the result. With the transform

$$\begin{aligned} \boldsymbol{k} &= \boldsymbol{k}' - \frac{\gamma}{\alpha} \boldsymbol{\ell}' - \frac{1}{\det\Omega} (\beta\eta - \gamma\mu) \boldsymbol{r} \\ \boldsymbol{\ell} &= \boldsymbol{\ell}' - \frac{1}{\det\Omega} (\alpha\mu - \gamma\eta) \boldsymbol{r} \end{aligned} \tag{6.53}$$

one finds from (6.51) :

$$De = \alpha \boldsymbol{k}'^{2} + \omega \, \boldsymbol{\ell}'^{2} \, + R \, ; \tag{6.54}$$

here, we defined

$$\omega = \frac{1}{\alpha} \det\Omega \, , \quad R = D_r - \frac{1}{\det\Omega} (\eta^2 \beta + \alpha\mu^2 - \eta\mu\gamma) \boldsymbol{r}^2 \, , \quad \Omega = \begin{pmatrix} \alpha & \gamma \\ \gamma & \beta \end{pmatrix} \tag{6.55}$$

We apply the substitution (6.53) also to the Numerator Nu of (6.52) and are left with $(D = 2 - 2\epsilon)$:

$$I_1 = \int d^{2-2\epsilon} \boldsymbol{k} \, d^{2-2\epsilon} \boldsymbol{\ell} \, \frac{Nu'}{[\alpha \boldsymbol{k}^2 + \omega \boldsymbol{\ell}^2 + R]^4} \tag{6.56}$$

Due to the angular symmetry many terms in the numerator give zero, the only non-vanishing are

$$
\begin{aligned}
Nu' = &A\,\boldsymbol{k}^4 + B\,\boldsymbol{\ell}^4 + C\,\boldsymbol{k}^2\boldsymbol{\ell}^2 + D\,\boldsymbol{k}^2 + E\,\boldsymbol{\ell}^2 + F \\
&+ P\,(\boldsymbol{k\ell})^2 + I\,(\boldsymbol{\ell r})^2 + N\,(\boldsymbol{kr})^2
\end{aligned}
\tag{6.57}
$$

The integral is given by:

$$
\begin{aligned}
I_1 = \frac{\pi^{2-2\epsilon}}{6\,(\alpha\omega)^{1-\epsilon}R^{2\epsilon}} \Bigg\{ &\Gamma(2\epsilon)\Bigg[(2-\epsilon)(1-\epsilon)\left(\frac{A}{\alpha^2} + \frac{B}{\omega^2}\right) \\
&+ (1-\epsilon)^2\,\frac{C+\frac{1}{2}P}{\alpha\omega}\Bigg] + \\
&+ (1-\epsilon)\Gamma(1-2\epsilon)\,\frac{1}{R}\left(\frac{D+\frac{\boldsymbol{r}^2}{2}N}{\alpha} + \frac{E+\frac{\boldsymbol{r}^2}{2}I}{\omega}\right) + \Gamma(2+2\epsilon)\frac{F}{R^2}\Bigg\}
\end{aligned}
\tag{6.58}
$$

All parameters in (6.58) generally depend on the Sudakov variables α_1, α_ℓ, on $Q^2, \boldsymbol{r}^2$ and on the Feynman parameters β_i. While α, ω and R (don't confuse α with a Sudakov variable!) are determined by the propagator structure of $\mathcal{AB}$, the Numerator is encoded in $A - N$.

Note the factor $\Gamma(2\epsilon)$. Since $\Gamma(2\epsilon) = \frac{1}{2\epsilon} + \mathcal{O}(1)$, this is the only diverging part of the formula (6.58) in the limit $\epsilon \to 0$. The $\Gamma(2\epsilon)$ incorporates the regularised UV divergence of I_1 stemming from the $\boldsymbol{k}^4, \boldsymbol{\ell}^4, \boldsymbol{k}^2\boldsymbol{\ell}^2$ and $(\boldsymbol{k\ell})^2$ parts of the numerator (6.57) which only occur in case of transverse photon polarisation.

In the mixed representation of $\mathcal{AB}$ (6.49) the integrand $\frac{Nu}{De^4}$ divergences in various limits in $\{\boldsymbol{\ell}, \alpha_\ell, \beta_i\}$. After integration we get I_1. Let us see what happens to the divergences. We specified any limit x in the mixed representation by a substitution rule for $\alpha_\ell, \boldsymbol{\ell}, \beta_i$ that introduces a parameter ρ. In order to reach the limit one has to expand around $\rho = 0$ keeping the leading term and set $\rho = 1$ in it. According to (6.49) we write

$$
\begin{aligned}
\mathcal{AB}_x &= \int \{d\beta_i\}\, f_x(\boldsymbol{\ell}, \beta_i)\, \delta(\textstyle\sum \beta_i - 1) \\
&\text{with :} \quad f_x(\boldsymbol{\ell}, \beta_i) = \left[\left.\frac{Nu}{De^4}\right|_{\substack{\boldsymbol{\ell} \to \rho\boldsymbol{\ell} \\ \beta_i \to \rho^{p_i}\beta_i}} \right]_{\rho \to 0}
\end{aligned}
$$

For the sake of brevity we suppressed here the α_ℓ limit. Now we look at the corresponding integral I_1 in that limit.We interchange the $\boldsymbol{\ell}$ integration and the approach of the limit.

$$I_1|_x = \int d^D\boldsymbol{k} d^D\boldsymbol{\ell}\, f_x(\boldsymbol{\ell},\beta_i) = \left(\left[\int d^D\boldsymbol{k} d^D\boldsymbol{\ell}\ \frac{Nu}{De^4}\bigg|_{\boldsymbol{\ell}\,\to\,\rho\boldsymbol{\ell}}\right]_{\beta_i\,\to\,\rho^{p_i}\beta_i}\right)_{\rho\,\to\,0} \tag{6.59}$$

Let us concentrate on the inner brackets and see what happens to ρ after integration; we compute

$$\tilde{I}_1 = \int d^D\boldsymbol{k} d^D\boldsymbol{\ell}\ \frac{Nu}{De^4}\bigg|_{\Xi} \ ; \qquad \Xi\ :\quad |\boldsymbol{\ell}| \to \rho|\boldsymbol{\ell}| \tag{6.60}$$

In the denominator of

$$\frac{Nu}{De^4} = \frac{Nu}{[\alpha\,\boldsymbol{k}^2 + \beta\,\boldsymbol{\ell}^2 + 2\,\gamma\,\boldsymbol{k}\boldsymbol{\ell} + 2\eta\,\boldsymbol{k}\boldsymbol{r} + 2\mu\,\boldsymbol{\ell}\boldsymbol{r} + \bar{D}_r]^4} \tag{6.61}$$

we may transfer the ρ's at the $\boldsymbol{\ell}$'s to the parameters multiplying them:

$$\begin{aligned} \Xi\ :\qquad & \beta \to \rho^2\beta \\ & \gamma \to \rho\gamma \\ & \mu \to \rho\mu \\ & \text{in } Nu : \boldsymbol{\ell} \to \rho\boldsymbol{\ell} \end{aligned}$$

This leads that especially $\det\Omega \to \rho^2 \det\Omega$ and in the substitution:

$$\begin{aligned} \boldsymbol{k} &\to \boldsymbol{k}' - \frac{\gamma}{\alpha}\rho\,\boldsymbol{\ell}' - \frac{1}{\det\Omega}(\beta\eta - \gamma\mu)\boldsymbol{r} \\ \rho\,\boldsymbol{\ell} &\to \rho\,\boldsymbol{\ell}' - \frac{1}{\det\Omega}(\alpha\mu - \gamma\eta)\boldsymbol{r} \end{aligned} \tag{6.62}$$

This means, the weights on $\boldsymbol{\ell}$ we put in Nu translate exactly into weights on $\boldsymbol{\ell}'$. (6.61) after the substitution of $\boldsymbol{k}$ and $\boldsymbol{\ell}$ is given by the integrand of (6.56) where we call $\boldsymbol{k}', \boldsymbol{\ell}'$ now $\boldsymbol{k}, \boldsymbol{\ell}$ again. We transfer the ρ's on the $\boldsymbol{\ell}$'s in the numerator Nu' to the parameters in front. From (6.55) finally it follow the transformation rules for ω and R and we end up with that version of Ξ that has to be applied to the integrand of (6.56) to get $\tilde{I}_1$

$$\begin{aligned} \Xi_0\ :\qquad \omega &\to \rho^2\omega \\ B &\to \rho^4 B \\ C, P &\to \rho^2 C, P \\ E, I &\to \rho^2 E, I \end{aligned}$$

Since Ξ_0 does not depend on $\boldsymbol{\ell}$ anymore it is not affected by the $\boldsymbol{\ell}$ integration leading to the formula (6.58) for I_1. Applying Ξ_0 to (6.58) we see that all

ρ's in the curly brackets cancel. The only effect of Ξ_0 is an overall factor of $\rho^{2\epsilon-2}$, which does not affect the approach of the limit.

$$\tilde{I}_1 = I_1|_{\Xi_0} = \rho^{2\epsilon-2} I_1 \tag{6.63}$$

Putting this into (6.59) we arrive at

$$I_1|_x = \int d^D\boldsymbol{k} d^D\boldsymbol{\ell}\, f_x(\boldsymbol{\ell}, \beta_i) = \Big(I_1|_{\beta_i \,\to\, \rho^{p_i}\beta_i} \Big)_{\rho \,\to\, 0}$$

This is an important result. Any limit in the $\{\alpha_\ell, \boldsymbol{\ell}, \beta_i\}$ space very easily translates into the $\{\alpha_\ell, \beta_i\}$ space: If the $\boldsymbol{\ell}$ integration in unbounded one just drops the $\boldsymbol{\ell}$ part of the limit.

6.3.2 $\int^\Lambda \mathcal{AB}_{\text{coll}}$

We now come to the integration of the collinear approximations in (6.2, 6.3)

$$I_2 = \int d^D\boldsymbol{k} \int d^D\boldsymbol{\ell}\, \frac{Nu}{De^{\,4}}\, \theta(\alpha_\ell\Lambda - |\boldsymbol{\ell}_c|)\,, \qquad \boldsymbol{\ell}_c = \boldsymbol{\ell}', \boldsymbol{\ell}'' \tag{6.64}$$

First, we express $\boldsymbol{\ell}$ through $\boldsymbol{\ell}_c$; the θ-function then translates into an upper bound in the $|\boldsymbol{\ell}_c|$ integration. Thus, in both collinear cases we are led to

$$I_2 = \int d^D\boldsymbol{k} \int_{|\boldsymbol{\ell}_c|<\alpha_\ell\Lambda} d^D\boldsymbol{\ell}_c\, \frac{Nu}{De^{\,4}} \tag{6.65}$$

Remember our discussion of the collinear limits in the mixed representation; in the limit $g||\bar{q}$ we get $\bar{D}_4 = \alpha_2^2 \boldsymbol{\ell}_c^2$, while all other $\bar{D}_i$ no longer depend on $\boldsymbol{\ell}_c$. In the other collinear limit it is $\bar{D}_3$ that plays the rôle of $\bar{D}_4$. That means, the denominator of (6.65) depends on $\boldsymbol{\ell}_c$ only via $\boldsymbol{\ell}_c^2$

$$De = \sum_i \beta_i\, \bar{D}_i = \alpha\, \boldsymbol{k}^2 + \beta\, \boldsymbol{\ell}_c^2 + 2\eta\, \boldsymbol{k}\boldsymbol{r} + \bar{D}_r. \tag{6.66}$$

and the parameter β is proportional to β_4 and β_3, respectively. This is important for the substitution of $\boldsymbol{\ell}, \boldsymbol{k}$: Since we only have to get rid of $\boldsymbol{k}\boldsymbol{r}$ and especially need not substitute $\boldsymbol{\ell}_c$, the integration bound remains simple. We use the substitution (6.53) with $\gamma = \mu = 0$. Note that this leads in particular to $\omega = \beta$. For longitudinal photon polarisation there are three terms possible in the numerator. We will only need the case of $D = 2$ dimensions and arrive at

$$\begin{aligned} I_2 &= \int d^2\boldsymbol{k}\, d^2\boldsymbol{\ell}\, \theta(\alpha_\ell\Lambda - |\boldsymbol{\ell}|)\, \frac{D\,\boldsymbol{k}^2 + E\,\boldsymbol{\ell}^2 + F}{[\alpha\boldsymbol{k}^2 + \omega\boldsymbol{\ell}^2 + R]^4} \\ &= \frac{\pi^2\bar{\Lambda}^2}{6\,\alpha\omega R(R+\bar{\Lambda}^2)} \left[D\frac{1}{\alpha} + E\frac{1}{\omega}\, \frac{\bar{\Lambda}^2}{R+\bar{\Lambda}^2} + F\frac{1}{R}\, \frac{2R+\bar{\Lambda}^2}{R+\bar{\Lambda}^2} \right] \\ &\quad \text{with}: \bar{\Lambda}^2 = \omega(\alpha_\ell\Lambda)^2 \end{aligned} \tag{6.67}$$

It is not difficult to include the transverse polarisation as well; due to the integration bound the integrals exist for $D = 2$. However, we don't need this, because we will treat the transverse polarisation in a different way to the longitudinal one.

In our initial expression for the real corrections (6.2, 6.3) there is the combination $\int d\boldsymbol{k}d\boldsymbol{\ell}[\mathcal{AB} - \mathcal{AB}_{\text{coll}}\,\theta(\alpha_\ell\Lambda - \boldsymbol{\ell}_c)]$ which should be finite in the collinear limit. Lets see how this works. The first part of the combination is given by (6.58), the latter by (6.67), the difference of both is defined in the whole $\{\beta_i\}$ space. For $\epsilon = 0$ and longitudinal polarisation the full integral (6.58) reads

$$I_1^L = \int d^2\boldsymbol{k}\; d^2\boldsymbol{\ell} \frac{D\,\boldsymbol{k}^2 + E\,\boldsymbol{\ell}^2 + F}{[\alpha\boldsymbol{k}^2 + \omega\boldsymbol{\ell}^2 + R]^4} = \frac{\pi^2}{6\,(\alpha\omega)R}\left\{\frac{D}{\alpha} + \frac{E}{\omega} + \frac{F}{R}\right\} \tag{6.68}$$

This is certainly what one gets from (6.67) in the limit $\Lambda \to \infty$. But let us look at this in view of the collinear limit. As discussed in sec. 6.3.1 the limit $g||\bar{q}$ corresponds to $\beta_{i\neq 4} \ll \beta_4$. The only place where β_4 enters I_2 is via β in the denominator (6.66). Since $\omega = \beta$, it follows from (6.67) :

$$\bar{\Lambda}^2 \propto \beta_4 \qquad (\beta_3 \text{ in case of } g||q)$$

The parameter R is a sum of terms each weighted with some β_i. In the collinear corner of the $\{b\}$ space we therefore have

$$\text{coll}: \quad R \ll \bar{\Lambda}^2.$$

In this limit (6.67) reduces to (6.68). Thus, the full expression and the collinear one gets is indeed equal in the collinear limit, as it should be.

Now, let us investigate how the soft limit of the collinear approximation can be approached in the $\{\beta\}$ space. In the same spirit as in sec. 6.3.1 we calculate the soft limit of I_2 :

$$\begin{aligned} I_2|_{\text{soft}} &= \left(\tilde{I}_2\Big|_{\beta_i \,\to\, \rho^{p_i}\beta_i}\right)_{\rho\,\to\,0} \\ \text{where } \tilde{I}_2 &= \int d^D\boldsymbol{k}d^D\boldsymbol{\ell}\;\theta(\alpha_\ell\Lambda - |\boldsymbol{\ell}|)\left[\frac{\tilde{N}u}{\tilde{D}e^4}\right]_{\substack{\boldsymbol{\ell}\,\to\,\rho\boldsymbol{\ell} \\ \alpha_\ell\,\to\,\rho\alpha_\ell}} \end{aligned} \tag{6.69}$$

The p_i are numbers specifying the propagator structure of the actual diagram. The ˜ shall denote that we use the collinear approximation. Note, that the α_ℓ of the integration bound does not get a ρ; the coll/soft approximation is to be integrated over the same region as the collinear approximation. Since the substitution of variables is independent of the integration bounds, all arguments from sec. 6.3.1 that led to an $\boldsymbol{\ell}$-independent substitution rule also apply here. Thus, we need to apply

$$\begin{aligned}\Xi_0 \,:\, \omega &\to \rho^2\omega \\ E &\to \rho^2 E \\ \alpha_\ell &\to \rho\alpha_\ell\end{aligned}$$

to the substituted integrand in (6.67) in order to get $\tilde{I}_2$. The integration will then introduce an $(\alpha_\ell\Lambda)$ (without a ρ !) from the integration bound into the result. (6.67) shows that after integration we have an overall $1/\rho^2$ from $1/\omega$; in the combination E/ω the ρ's cancel. Apart from this the formula only depends on ρ via the ω in $\bar{\Lambda}^2$. Now, we just push the ρ^2 from the ω to the α_ℓ^2

$$\bar{\Lambda}^2 \to \rho^2\omega(\alpha_\ell\Lambda)^2 = \omega(\rho\alpha_\ell\Lambda)^2$$

Thus, instead of giving 'weights' to ω and some α_ℓ we can also put 'weights' to all α_ℓ and no ω. Thanks to this possibility which exists due to the α_ℓ in the integration bound we have

$$\tilde{I}_2 = \frac{1}{\rho^2}\; I_2\big|_{\alpha_\ell\,\to\,\rho\alpha_\ell}$$

and hence:

$$I_2\big|_{\text{soft}} = \left(I_2\big|_{\substack{\alpha_\ell\,\to\,\rho\alpha_\ell \\ \beta_i\,\to\,\rho^{p_i}\beta_i}} \right)_{\rho\to 0} \tag{6.70}$$

Thus, also in case of an (special) $\boldsymbol{\ell}$-integration bound we find that the soft limit (of the collinear approximation) in the $\{\alpha_\ell, \beta_i\}$ space is just the projection of the limit in $\{\alpha_\ell, \boldsymbol{\ell}, \beta_i\}$ space into the $\{\alpha_\ell, \beta_i\}$ space.

6.3.3 $\int_{s_0} \mathcal{AB}_{\text{cen}}$

The third integral appearing in the real corrections reads

$$I_3 = \int d^D\boldsymbol{k} \int d^D\boldsymbol{\ell}\, \frac{Nu}{De^{\,4}}\; \theta(|\boldsymbol{\ell}| - \alpha_\ell\sqrt{s_0}) \tag{6.71}$$

The denominator is not restricted

$$De = \sum_i \beta_i\, \bar{D}_i = \alpha\, \boldsymbol{k}^2 + \beta\, \boldsymbol{\ell}^2 + 2\,\gamma\, \boldsymbol{k}\boldsymbol{\ell} + 2\eta\, \boldsymbol{k}\boldsymbol{r} + 2\mu\, \boldsymbol{\ell}\boldsymbol{r} + \bar{D}_r;$$

We will get rid of the $\boldsymbol{k}\boldsymbol{\ell}$ and the $\boldsymbol{k}\boldsymbol{r}$ term in De by substituting $\boldsymbol{k}$. However, in order to be free of $\boldsymbol{\ell}\boldsymbol{r}$ we need to shift $\boldsymbol{\ell}$ by some term proportional to $\boldsymbol{r}$. The integration bound would appear then as a combined bound on the absolute value of the new $\boldsymbol{\ell}$ and on the angular integration. To avoid this we do not substitute $\boldsymbol{\ell}$ and are confronted with a no more trivial angular integration. Using the general substitution (6.53) but expressing $\boldsymbol{\ell}'$ through $\boldsymbol{\ell}$ and $\boldsymbol{r}$ we arrive at:

$$De = \alpha \boldsymbol{k}' + \omega(\boldsymbol{\ell} + \boldsymbol{\lambda})^2 + R\,, \qquad \boldsymbol{\lambda} = \frac{1}{det\Omega}(\alpha\mu - \gamma\eta)\boldsymbol{r} \tag{6.72}$$

We could certainly include $\boldsymbol{\lambda}^2$ into R, but our aim is to express the results for all integrals in the real corrections through as few functions of $\alpha, \beta, \gamma, \ldots$ as possible.

As for the numerator Nu we note that some terms lead to UV divergent integrals. Looking back to our table of divergences (6.1, 6.2) we see that these terms stem from the diagrams (14,24,44) which contribute to both UV and central limit. However, since in the sum of these diagrams the central divergence drops out, we will treat them in a special way, namely just stretch the $\boldsymbol{\ell}$ integration over the whole space. The other diagrams diverging in the central limit are UV finite. In the numerator of (6.71) we will therefore consider all terms from both photon polarisation except for those leading to an UV divergence. It is easy to show that these are:

$$\begin{aligned} Nu' = {} & D\,\boldsymbol{k}^2 + E\,\boldsymbol{\ell}^2 + F\, + M\boldsymbol{\ell r} \\ & + G\boldsymbol{k}^2\boldsymbol{\ell r}\, + H\boldsymbol{\ell}^2\boldsymbol{\ell r} + J(\boldsymbol{\ell r})^2\; + \; + P\,(\boldsymbol{k\ell})^2 + N\,(\boldsymbol{kr})^2\; + S(\boldsymbol{kr})(\boldsymbol{k\ell}) \end{aligned}$$

We give here only the result in case of longitudinal photon polarisation; for the full formula, see the appendix.

$$I_3 = \int d^2\boldsymbol{k} \int d^2\boldsymbol{\ell}\,\theta(|\boldsymbol{\ell}| - \alpha_\ell s_0)\,\frac{Nu'}{[\alpha\boldsymbol{k} + \omega(\boldsymbol{\ell}+\boldsymbol{\lambda})^2 + R]^4} \tag{6.73}$$

$$I_3^L = \frac{\pi^2}{6\alpha\omega R}\,\left(\frac{D}{\alpha}\,\mathcal{C}_D + \frac{E}{\omega}\,\mathcal{C}_E + \frac{F}{R}\,\mathcal{C}_F + \frac{M}{R}|\boldsymbol{\lambda}|\,\mathcal{C}_M\right) \tag{6.74}$$

$$\begin{aligned} \mathcal{C}_D &= \frac{1}{2}\left\{1 - \frac{1}{\kappa}\Big[\bar{s}_0 - (R + \bar{\boldsymbol{\lambda}}^2)\Big]\right\} \\ \mathcal{C}_E &= \frac{1}{2}\left\{\frac{\bar{\boldsymbol{\lambda}}^2 + R}{R} - \frac{1}{R\kappa}\left[\bar{s}_0\,(R + \bar{\boldsymbol{\lambda}}^2) - 3R^2 - \bar{\boldsymbol{\lambda}}^4\right]\right. \\ &\qquad \left. - \frac{2}{\kappa^3}\left[(R - \bar{\boldsymbol{\lambda}}^2)(R + \bar{\boldsymbol{\lambda}}^2)^2 + \bar{s}_0\,(R^2 + \bar{\boldsymbol{\lambda}}^4 - 6R\bar{\boldsymbol{\lambda}}^2)\right]\right\} \\ \mathcal{C}_F &= \frac{1}{2}\left\{1 - \frac{1}{\kappa}\Big[\bar{s}_0 + (R - \bar{\boldsymbol{\lambda}}^2)\Big] + \frac{2R}{\kappa^3}\Big[\bar{s}_0\,(R - \bar{\boldsymbol{\lambda}}^2) + (R + \bar{\boldsymbol{\lambda}}^2)^2\Big]\right\} \\ \mathcal{C}_M &= -\frac{1}{2}\left\{1 - \frac{1}{\kappa}\Big[\bar{s}_0 + (R - \bar{\boldsymbol{\lambda}}^2)\Big] + \frac{2R}{\kappa^3}\Big[\bar{s}_0\,(3R - \bar{\boldsymbol{\lambda}}^2) + (R + \bar{\boldsymbol{\lambda}}^2)^2\Big]\right\} \end{aligned}$$

here, we defined:

$$\bar{s}_0 \equiv \omega(\alpha_\ell\sqrt{s_0})^2\,, \qquad \bar{\boldsymbol{\lambda}}^2 \equiv \omega\boldsymbol{\lambda}^2$$
$$\text{and}: \quad \kappa \equiv \sqrt{\left(\bar{s}_0 + R + \bar{\boldsymbol{\lambda}}^2\right)^2 - 4\bar{s}_0\,\bar{\boldsymbol{\lambda}}^2} \tag{6.75}$$

The square root in κ stems from the angular integration. Note, that $\bar{s}_0$ is just the square of the lower bound times ω, this is in exact analogy to the definition of $\bar{\Lambda}$ in the last section. It is easy to show that pushing the lower integration bound to zero ($\alpha_\ell = 0$) and setting $\boldsymbol{\lambda} = 0$ leads $\mathcal{C}_D = \mathcal{C}_E = \mathcal{C}_F = 1$. The terms involving M vanishes and we find the result of the integration over the whole space I_1^L (6.68). The same can be shown for the other terms.

Also in this integral we quickly demonstrate how the soft limit looks like in the $\{\alpha_\ell, \beta_i\}$ space. We want to calculate from I_3 the integral of the central approximation taken in the soft limit, $I_3^L|_{\text{soft}}$. As we did not substitute $\boldsymbol{\ell}$, we parametrise ($\boldsymbol{\ell} \to \rho\boldsymbol{\ell}$) in the integrand of (6.73). We may set instead:

$$\begin{aligned} \omega &\to \rho^2\omega \\ \boldsymbol{\lambda} &\to \frac{1}{\rho}\boldsymbol{\lambda} \\ E, G, M, S &\to \rho\, E, G, M, S \\ H, J, P, S &\to \rho^2\, H, J, P, S \end{aligned}$$

This substitution has the following effect on the integrated expression (6.74): The coefficients of the functions $\mathcal{C}_x$ are free of ρ's; there is an overall factor of $1/\rho$. The $\mathcal{C}_x$ depend on ρ only via the ω in $\bar{s}_0$ and $\bar{\boldsymbol{\lambda}}$. However, the ρ dependence in $\bar{\boldsymbol{\lambda}}^2$ cancel. In $\bar{s}_0$ we can shift the ρ to α_ℓ (stemming from the integration bound). Thus, the limit $\boldsymbol{\ell} \to 0$ before integration appears as the limit $\alpha_\ell \to 0$ in the integration bound after integration. In order to reach the soft limit of I_3 we therefore have to set $\alpha_\ell \to \rho\alpha_\ell$ in all α_ℓ in (6.74).The $(\alpha_\ell, \boldsymbol{\ell})$ part of the soft limit reduces after integration to the α_ℓ part.

$$I_3|_{\text{soft}} = \left(I_3|_{\substack{\alpha_\ell \to \rho\alpha_\ell \\ \beta_i \to \rho^{p_i}\beta_i}} \right)_{\rho\to 0} \tag{6.76}$$

6.4 Finite combinations

Now, we are prepared to rewrite the real corrections (6.2, 6.3) being an integral of a sum over diagrams as a sum of integrals. We stick to the case of longitudinal polarisation with $D = 4-2\epsilon$ and scale all transverse momenta with $|Q|$:

$$\boldsymbol{k}, \boldsymbol{\ell}, \boldsymbol{r}, \Lambda, \sqrt{s_0} \to \frac{1}{|Q|}\,\boldsymbol{k}, \boldsymbol{\ell}, \boldsymbol{r}, \Lambda, \sqrt{s_0}.$$

This leads to an $1/(Q^2)^3$ from $\mathcal{AB}$ and $(Q^2)^D$ from $d^D\boldsymbol{k}\, d^D\boldsymbol{\ell}$. We further include the $\alpha\bar{\alpha}_1$ from the phase space into $\mathcal{AB}$.

$$\mathcal{AB}' \equiv \frac{\mathcal{AB}}{\alpha\bar{\alpha}_1} \quad\rightarrow\quad \mathcal{AB}'_{\mathrm{soft}} = \frac{\mathcal{AB}_{\mathrm{soft}}}{\alpha\alpha_2}\ , \ \ldots$$

Let us start with:

6.4.1 The C_F part

$$\begin{aligned}\Phi^{(1,real)}_{\gamma^*}\Big|^{finite}_{C_F} &= \frac{\lambda_{\mathrm{L}}}{4(2\pi)^{6-4\epsilon}\,(Q^2)^{1-2\epsilon}}\int d^{2-2\epsilon}\boldsymbol{k}\, d^{2-2\epsilon}\boldsymbol{\ell}\int_0^1 d\alpha\int_0^{1-\alpha}\frac{d\alpha_\ell}{\alpha_\ell}\\ &\times\sum_{C_F}\Big\{\mathcal{AB}' - \mathcal{AB}'_{\mathrm{soft}} - \big(\mathcal{AB}'_{\bar{\mathrm{q}}} - \mathcal{AB}'_{\bar{\mathrm{q}},\,soft}\big)\,\Theta(\alpha_\ell\Lambda - |\boldsymbol{\ell}'|)\\ &\qquad - \big(\mathcal{AB}'_{\mathrm{q}} - \mathcal{AB}'_{\mathrm{q},\,soft}\big)\,\Theta(\alpha_\ell\Lambda - |\boldsymbol{\ell}''|)\Big\}\end{aligned} \tag{6.77}$$

The sum stretches over the C_F parts of all diagrams. Note, that the factor $\alpha_1\bar{\alpha}_1$ from the phase space gets $\alpha_1\alpha_2$ in the soft limit. Table (6.1,6.2) shows that we only have to care about the $\boldsymbol{\ell}-$uv divergence when we pull the sum apart. For each diagram we introduce Feynman parameters $\{b_i\}$ and perform the $\boldsymbol{k}, \boldsymbol{\ell}$ integration (actually, we have given only the integral of $\mathcal{AB}$ for $\epsilon \neq 0$). Thus, each $\mathcal{AB}$ in momentum space is transformed into β_i space. Let us denote this transform of $\mathcal{AB}$ by X; According to the limits of the $\boldsymbol{\ell}$ integration (see sec 6.3.1 pp) we have three different transformations

$$\int d^{2-2\epsilon}\boldsymbol{k}\, d^{2-2\epsilon}\boldsymbol{\ell}\,\frac{\mathcal{AB}}{\alpha_1\bar{\alpha}_1} = \int \prod d\beta_i\ X \tag{6.78}$$

$$\int d^{2-2\epsilon}\boldsymbol{k}\, d^{2-2\epsilon}\boldsymbol{\ell}\,\frac{\mathcal{AB}_{\mathrm{q,soft}}}{\alpha_1\alpha_2}\,\Theta(\alpha_\ell\Lambda - |\boldsymbol{\ell}''|) = \int \prod d\beta_i\ X_{q,soft} \tag{6.79}$$

$$\int d^{2-2\epsilon}\boldsymbol{k}\, d^{2-2\epsilon}\boldsymbol{\ell}\,\frac{\mathcal{AB}_{\mathrm{cen}}}{\alpha_1\alpha_2}\,\Theta(|\boldsymbol{\ell}| - \alpha_\ell\sqrt{s_0}) = \int \prod d\beta_i\ X_{cen} \tag{6.80}$$

The last one is not needed in the moment. According to the second and third transformation also X_q, $X_{\bar{q}}$ and $X_{cen,soft}$, respectively are determined. Note, that these X are defined such that the δ function is already cancelled.

The $\boldsymbol{\ell}-$uv limit in $\{\beta\}$ space corresponds to $\beta_{i\neq 2} \ll 1$. In case of $\boldsymbol{\ell}-$uv divergent diagrams we always use the β_2 integration to cancel the δ-function; we subtract the $\boldsymbol{\ell}-$uv approximation of each diagram and re-add it.

$$X|_{\boldsymbol{\ell}\text{-uv}} = X|_{\beta_{i\neq 2}\to 0}\ , \quad \text{after performing } \textstyle\int d\beta_2\ \delta(\sum\beta_i - 1)$$

We denote the sum of these re-added pieces by $R^{C_F}_{\boldsymbol{\ell}\text{–uv}}$.

$$
\begin{aligned}
\Phi^{(1,real)}_{\gamma^*}\Big|^{finite}_{C_F} &= \frac{\lambda_{\mathrm{L}}}{4(2\pi)^{6-2\epsilon}\,(Q^2)^{1-2\epsilon}} \sum_{C_F} \int_0^1 d\alpha \int_0^{1-\alpha} \frac{d\alpha_\ell}{\alpha_\ell} \int \prod d\beta_i \\
&\quad \Big(X - X_{\mathrm{soft}} - X|_{\boldsymbol{\ell}\text{–uv}} - (X_q - X_{q,\mathrm{soft}}) - (X_{\bar q} - X_{\bar q,\mathrm{soft}}) \Big) \\
&\quad + \frac{\lambda_{\mathrm{L}}}{4(2\pi)^{6-2\epsilon}\,(Q^2)^{1-2\epsilon}}\, R^{C_F}_{\boldsymbol{\ell}\text{–uv}}
\end{aligned} \tag{6.81}
$$

As discussed in sec.6.2.2 and sec.6.3.1 we would have to approximate X *before* cancellation of the δ function in order to exactly subtract the integral over $\mathcal{AB}_{\boldsymbol{\ell}\text{–uv}}$; then the re-added sum of subtractions would be zero. However, as already discussed in momentum space (sec. 6.1.1) the $\boldsymbol{\ell}-$uv approximation of an $\boldsymbol{\ell}-$uv divergent diagram is also divergent as $\boldsymbol{\ell} \to 0$. Our slightly different definition of the $\boldsymbol{\ell}-$uv subtraction still cancels the $\boldsymbol{\ell}-$uv divergence but does not introduce a new IR-divergence. Let us demonstrate the mechanism at a simplified denominator structure $(c+\boldsymbol{\ell}^2)\bar{D}_2$. We assume another term that cancels any divergences and integrate over $\boldsymbol{\ell}$.

$$
\begin{aligned}
\int_0^\infty d\boldsymbol{\ell}^2\, A &= \int_0^\infty d\boldsymbol{\ell}^2 \frac{1}{(c+\boldsymbol{\ell}^2)\bar{D}_2} = \int d\beta_1 d\beta_2 \int_0^\infty d\boldsymbol{\ell}^2 \frac{\delta(1-\beta_1-\beta_2)}{[\beta_1(\boldsymbol{\ell}^2+c)+\beta_2\bar{D}_2]} \\
&= \int d\beta_1 d\beta_2\; \delta(1-\beta_1-\beta_2)\, \frac{1}{\beta_1(\beta_1 c+\beta_2\bar{D}_2)} = \int_0^1 \frac{d\beta_1}{\beta_1(\beta_1(c-\bar{D}_2)+\bar{D}_2)}
\end{aligned} \tag{6.82}
$$

According to our discussion above we get the integral over $A_{\boldsymbol{\ell}\text{–uv}}$ as the approximation $\beta_{i\neq 2} \ll 1$ in (6.82) before cancellation of the δ function

$$
\int_0^\infty d\boldsymbol{\ell}^2\, A_{\boldsymbol{\ell}\text{–uv}} = \int d\beta_1 d\beta_2\; \delta(1-\beta_1-\beta_2) \frac{1}{\beta_1(\beta_2\bar{D}_2)} = \int_0^1 d\beta_1 \frac{1}{\beta_1(1-\beta_1)\bar{D}_2}
$$

In addition to the limit $\beta_1 \to 0$ corresponding to the $\boldsymbol{\ell}-$uv divergence we meet another divergence at $\beta_1 \to 1$ that corresponds to the limit $\boldsymbol{\ell} \to 0$. However, if we just take the $\boldsymbol{\ell}-$uv limit of (6.82) after cancellation of the δ function we arrive at $1/(\beta_1\bar{D}_2)$ which still provides the $\boldsymbol{\ell}-$uv divergence, but is free of the IR divergence.

After $\boldsymbol{k}, \boldsymbol{\ell}$ integration of the re-added $X|_{\boldsymbol{\ell}\text{–uv}}$ the $\boldsymbol{\ell}$–uv divergence appears as $1/\epsilon$ pole after expansion around $\epsilon = 0$. In the sum these poles cancel and we are left with finite pieces. The $\mathcal{AA}$ and $\mathcal{BB}$ diagrams give the same contribution:

$$
\begin{aligned}
R^{C_F}_{\boldsymbol{\ell}\text{–uv}} &= \int_0^1 d\alpha \int_0^{1-\alpha} \frac{d\alpha_\ell}{\alpha_\ell} \sum_{\mathcal{AA},\mathcal{BB}} \int \prod d\beta_i \;\; [X_{11} + 2X_{12} + X_{22}]_{\boldsymbol{\ell}\text{–uv}} \\
&= 2\, C_F\, \pi^{2-2\epsilon}\, \Gamma(1-2\epsilon)(1-\epsilon)\, \frac{1}{\epsilon} \int_0^1 d\alpha \int_0^{1-\alpha} d\alpha_\ell\, \alpha_\ell \Bigg\{ \\
&\Bigg(\frac{\alpha^{1-\epsilon}}{\alpha_2} \left[\frac{1}{\alpha_2 - \alpha} \left(\alpha^{-\epsilon} - \alpha_2^{-\epsilon}\right) - \epsilon \left(\alpha^{-\epsilon} + \alpha_2^{-\epsilon}\right) \right] \Bigg) + \Big(\alpha \to 1 - \alpha - \alpha_\ell \Big) \Bigg\} \\
&= \frac{\pi^2\, C_F}{24}\, (3\pi^2 - 28) + \mathcal{O}(\epsilon) \qquad (6.83)
\end{aligned}
$$

As the integral of the bracket in (6.81) is finite now for each diagram the leading term of the ϵ expansion is obtained by setting $\epsilon = 0$ in each part of the bracket. Thus, we indeed only needed to compute the integral over the collinear approximations in $D = 2$ dimensions.

The sum of finite integrals reads:

$$
\begin{aligned}
\Phi^{(1,real)}_{\gamma^*}\Big|^{finite}_{C_F} &= \frac{e^2 e_f^2 \sqrt{N_c^2 - 1}}{(2\pi)^6} \Bigg\{ \sum_{C_F} \int_0^1 d\alpha \int_0^{1-\alpha} \frac{d\alpha_\ell}{\alpha_\ell} \int \prod d\beta_i \\
&\quad \Big(X - X_{\text{soft}} - X|_{\boldsymbol{\ell}\text{–uv}} - (X_q - X_{q,\text{soft}}) - (X_{\bar{q}} - X_{\bar{q},\text{soft}}) \Big)_{\epsilon=0} \\
&\quad + \frac{\pi^2\, C_F}{24}\, (3\pi^2 - 28) \Bigg\} \qquad (6.84)
\end{aligned}
$$

6.4.2 The C_A part

We explicitly split the α_ℓ-integration

$$
\begin{aligned}
\Phi^{(1,\text{real})}_{\gamma^*}\Big|^{finite}_{C_A} &= \frac{\lambda_{\text{L}}}{4(2\pi)^{6-4\epsilon}\,(Q^2)^{1-2\epsilon}} \int d^{2-2\epsilon}\boldsymbol{k}\, d^{2-2\epsilon}\boldsymbol{\ell} \int_0^1 d\alpha \Bigg\{ \int_0^{1-\alpha} \frac{d\alpha_\ell}{\alpha_\ell} \\
&\quad \times \sum_{C_A} \Big[\mathcal{AB}' - \mathcal{AB}'_{\text{soft}} - \left(\mathcal{AB}'_{\text{cen}} - \mathcal{AB}'_{\text{cen, soft}}\right) \Theta(|\boldsymbol{\ell}| - \alpha_\ell \sqrt{s_0}) \Big] \\
&\quad - \int_{1-\alpha}^{\infty} \frac{d\alpha_\ell}{\alpha_\ell} \sum_{C_A} \mathcal{AB}'_{\text{cen}}\, \Theta(|\boldsymbol{\ell}| - \alpha_\ell \sqrt{s_0}) \Bigg\} \qquad (6.85)
\end{aligned}
$$

First, we note that according to table (6.1,6.2) there are diagrams whose C_A part is collinear divergent. As the collinear approximations of all C_A parts sum up to zero, we can just subtract this limit for each diagram.

Let us consider the group of diagrams $\{14, 24, 44\}$ (including also $41, 42$). We have mentioned that the central approximations of these diagrams cancel in the sum; we are therefore free to subtract the central limit without the Θ function including s_0.

$$\sum_{12,14,24,44} \mathcal{AB}'_{\text{cen}} = 0$$

In addition, no diagram of this group has either central/soft or is- or lr-divergence.

As for the rest of diagrams we subtract (from 15 and 25) the intersoft limit; by this we subtract zero because, as we have shown:

$$\sum (\mathcal{AB}' - \mathcal{AB}'_{\text{soft}})_{is} = 0$$

Thus, we write

$$\begin{aligned}
\Phi^{(1,real)}_{\gamma^*}\Big|^{finite}_{C_A} &= \frac{\lambda_{\text{L}}}{4(2\pi)^{6-4\epsilon}\,(Q^2)^{1-2\epsilon}} \int d^{2-2\epsilon}\boldsymbol{k}\, d^{2-2\epsilon}\boldsymbol{\ell} \int_0^1 d\alpha \Bigg\{ \int_0^{1-\alpha} \frac{d\alpha_\ell}{\alpha_\ell} \\
\times \Bigg(&\sum_{12,14,24,44} \Big[\mathcal{AB}' - \mathcal{AB}'_{\text{soft}} - \mathcal{AB}'_{\text{cen}} - \big(\mathcal{AB}'_{\text{coll}} - \mathcal{AB}'_{\text{coll,soft}}\big)\,\Theta(\alpha_\ell\Lambda - |\boldsymbol{\ell}_c|)\Big] \\
&+ \sum_{rest} \Big[\mathcal{AB}' - \mathcal{AB}'_{\text{soft}} - \big(\mathcal{AB}'_{\text{cen}} - \mathcal{AB}'_{\text{cen,soft}}\big)\,\Theta(|\boldsymbol{\ell}| - \alpha_\ell\sqrt{s_0}) \\
&\qquad - \big(\mathcal{AB}' - \mathcal{AB}'_{\text{soft}}\big)_{is} - \big(\mathcal{AB}'_{\text{coll}} - \mathcal{AB}'_{\text{coll,soft}}\big)\,\Theta(\alpha_\ell\Lambda - |\boldsymbol{\ell}_c|)\Big]\Bigg) \\
- \int_{1-\alpha}^{\infty} &\frac{d\alpha_\ell}{\alpha_\ell} \sum_{C_A} \mathcal{AB}'_{\text{cen}}\,\Theta(|\boldsymbol{\ell}| - \alpha_\ell\sqrt{s_0})\Bigg\}
\end{aligned} \tag{6.86}$$

The subtraction of $\mathcal{AB}_{\text{coll}}$ stands for that collinear limit which is appropriate for the actual diagram, in some cases we have to subtract both limits. Note, that we subtracted this limit with an upper bound on the $\boldsymbol{\ell}_c$ integration ; this prevents us from an UV divergent $\boldsymbol{\ell}_c$ integration.

The formula (6.86) looks complicated because it contains the information on how to proceed for any diagram. However, for each diagram the formula reduces depending on the limits this diagram contributes to.

Looking back to table (6.1,6.2) we see that the $\boldsymbol{\ell}-$uv divergent diagrams (C_A parts) are (12,14,24,44). As some of these diagrams contribute to the central limit, they don't vanish as $\alpha_\ell \to 0$. This means the α_ℓ integral over the $\boldsymbol{\ell}-$uv approximation of such a diagram will be divergent as well. Therefore, we also have to subtract the $\boldsymbol{\ell}-$uv limit of $\mathcal{AB}_{\text{cen}}$. Since we subtracted $\mathcal{AB}_{\text{cen}}$ without integration bound, the integration of the re-added

$\boldsymbol{\ell}-$uv limit will be simple. In exact analogy to the C_F case we introduce Feynman parameters, integrate over $\boldsymbol{k}, \boldsymbol{\ell}$ in D dimensions and subtract and re-add the $\boldsymbol{\ell}-$uv approximations.

$$
\begin{aligned}
\Phi^{(1,real)}_{\gamma^*}\Big|^{finite}_{C_A} &= \frac{\lambda_{\mathrm{L}}}{4(2\pi)^{6-4\epsilon}\,(Q^2)^{1-2\epsilon}}\Bigg\{ \\
&\sum^{*}_{12,14,24,44}\int_0^1 d\alpha\int_0^{1-\alpha}\frac{d\alpha_\ell}{\alpha_\ell}\int\prod d\beta_i \\
&\Big(X - X^0 - (X-X^0)_{\boldsymbol{\ell}\text{–uv}} - X_{\mathrm{soft}} - (X_{\mathrm{coll}} - X_{\mathrm{coll,soft}})\Big) \\
&+\sum^{*}_{rest}\int_0^1 d\alpha\int_0^{1-\alpha}\frac{d\alpha_\ell}{\alpha_\ell}\int\prod d\beta_i \\
&\Big(X - X_{\mathrm{soft}} - (X_{\mathrm{cen}} - X_{\mathrm{cen,soft}}) - (X - X_{\mathrm{soft}})_{is} - (X_{\mathrm{coll}} - X_{\mathrm{coll,soft}})\Big) \\
&-\sum^{*}_{C_A}\int_0^1 d\alpha\int_{1-\alpha}^{\infty}\frac{d\alpha_\ell}{\alpha_\ell}\int\prod d\beta_i\, X_{\mathrm{cen}} \\
&+R^{C_A}_{\boldsymbol{\ell}\text{–uv}}\Bigg\}
\end{aligned}
\tag{6.87}
$$

While X_{cen} stems from $\mathcal{AB}_{\mathrm{cen}}\Theta(|\boldsymbol{\ell}| - \alpha_\ell\sqrt{s_0})$ we defined

$$
X^0 = X|_{\alpha_\ell=0}\,,
$$

which originates from the unbounded $\boldsymbol{\ell}$ integration of $\mathcal{AB}_{\mathrm{cen}}$.

As discussed in sec. 6.2.2 we deal with the lr divergence by choosing the same Feynman parameters for an $\mathcal{AA}_{ij}$ and $\mathcal{AB}_{ij}$ diagram. This ensures the cancellation of this divergence when the β_i integration is carried out for the sum of the two diagrams. The * on the sum in (6.87) indicates that in case of an lr divergent diagram we must not pull the sum of $\mathcal{AA}$ and $\mathcal{AB}$ diagram apart.

Finally we compute the sum of the re-added $\boldsymbol{\ell}-$uv subtractions

$$
\begin{aligned}
R^{C_A}_{\boldsymbol{\ell}\text{–uv}} &= \int_0^1 d\alpha \int_0^{1-\alpha} \frac{d\alpha_\ell}{\alpha_\ell} \sum_{\mathcal{AA},\mathcal{BB}} \int \prod d\beta_i \Big([2X_{12} + 2X_{14} + 2X_{24} + X_{44}]_{\boldsymbol{\ell}\text{–uv}} \\
&\qquad - [2X^0_{12} + 2X^0_{14} + 2X^0_{24} + X^0_{44}]_{\boldsymbol{\ell}\text{–uv}} \Big) \\
&= -C_A\, \pi^{2-2\epsilon}\, \Gamma(1-2\epsilon)\, \frac{1}{\epsilon} \int_0^1 d\alpha \int_0^{1-\alpha} d\alpha_\ell \Big\{ \\
&\Big(\alpha^{1-\epsilon} \Big[\frac{\alpha}{\alpha_2 - \alpha} \left(\alpha^{-\epsilon} - \alpha_2^{-\epsilon} \right) - \epsilon\, \alpha_2^{-\epsilon} \Big] \Big) + \Big(\alpha \to 1 - \alpha - \alpha_\ell \Big) \Big\} \\
&= -\frac{\pi^2\, C_A}{48}\, (3\pi^2 - 28) + \mathcal{O}(\epsilon)
\end{aligned}
\tag{6.88}
$$

The final result for the C_A part is obtained by inserting $R^{C_A}_{\boldsymbol{\ell}\text{–uv}}$ into (6.87) and setting $\epsilon = 0$ in all expressions :

$$
\begin{aligned}
\Phi^{(1,real)}_{\gamma^*}\Big|^{finite}_{C_A} &= \frac{e^2 e_f^2 \sqrt{N_c^2 - 1}}{(2\pi)^6} \Big\{ \\
&\sum^{*}_{12,14,24,44} \int_0^1 d\alpha \int_0^{1-\alpha} \frac{d\alpha_\ell}{\alpha_\ell} \int \prod d\beta_i \\
&\Big(X - X^0 - (X - X^0)_{\boldsymbol{\ell}\text{–uv}} - X_{\text{soft}} - (X_{\text{coll}} - X_{\text{coll,soft}}) \Big)_{\epsilon=0} \\
&+ \sum^{*}_{rest} \int_0^1 d\alpha \int_0^{1-\alpha} \frac{d\alpha_\ell}{\alpha_\ell} \int \prod d\beta_i \\
&\Big(X - X_{\text{soft}} - (X_{\text{cen}} - X_{\text{cen,soft}}) - (X - X_{\text{soft}})_{is} - (X_{\text{coll}} - X_{\text{coll,soft}}) \Big)_{\epsilon=0} \\
&- \sum^{*}_{C_A} \int_0^1 d\alpha \int_{1-\alpha}^{\infty} \frac{d\alpha_\ell}{\alpha_\ell} \int \prod d\beta_i \;\; X_{\text{cen}}\big|_{\epsilon=0} \\
&- \frac{\pi^2\, C_A}{48}\, (3\pi^2 - 28) \Big\}
\end{aligned}
\tag{6.89}
$$

We will see in chapter 8 that the subtraction procedure for longitudinal photon polarisation summarised in the formulae (6.84,6.89) indeed provides convergent integrals for each diagram and therefore enables the computation of the real corrections to the photon impact factor.

Chapter 7

The Integration for transverse polarisation

Since no numerical studies for transverse polarisation have yet been made we only outline in this chapter our strategy on how to integrate the real corrections in that case. The main reason for the different procedure compared to the longitudinal case is the UV divergence (see table 6.1,6.2). It is in particular the overlap of collinear and UV divergence what changes the situation. Consider a diagram that is divergent in the collinear limit, that is, when a certain linear combination of $\boldsymbol{\ell}$ and $\boldsymbol{k}$ tends to zero. As in the UV limit ($\boldsymbol{\ell} \sim \boldsymbol{k} \to \infty$) linear combinations of $\boldsymbol{k}$ and $\boldsymbol{\ell}$ are unaffected the UV approximation may still be collinear divergent. After $\boldsymbol{k}, \boldsymbol{\ell}$ integration over full space UV divergent terms appear as $1/\epsilon$ poles (see eq.6.58)

$$\int d^{2-2\epsilon}\boldsymbol{k} \int d^{2-2\epsilon}\boldsymbol{\ell}\ \frac{\boldsymbol{k}^4}{[\alpha \boldsymbol{k}^2 + \omega \boldsymbol{\ell}^2 + R]^4} = \frac{1}{\epsilon}\ \frac{\pi^2}{6\,\alpha^3\,\omega} + \mathcal{O}(1)$$

However, the collinear subtraction as demanded by the definition of the real corrections (6.2,6.2) is a finite integral:

$$\begin{aligned}\int d\boldsymbol{k}^2 \int d\boldsymbol{\ell}^2\ &\frac{\boldsymbol{k}^4}{[\alpha \boldsymbol{k}^2 + \omega \boldsymbol{\ell}^2 + R]^4}\ \Theta(|\boldsymbol{\ell}| - \alpha_\ell \Lambda) \\ &= \frac{\pi}{3\omega} \int d^2\boldsymbol{k} \left(\frac{\boldsymbol{k}^4}{[\alpha \boldsymbol{k}^2 + R]^3} - \frac{\boldsymbol{k}^4}{[\alpha \boldsymbol{k}^2 + R + \omega(\alpha_\ell \Lambda)^2]^3} \right)\end{aligned}$$

Thus, the subtraction procedure for the (UV-finite) sum of diagrams does not work for single diagrams, since the collinear divergences of UV divergent diagrams are not cancelled.

The sum of the collinear approximations of all diagrams is quite simple, it is basically the LO impact factor times a splitting function. As the solution of the problem, we therefore subtract for each diagram the integral over full space of its collinear approximation . What we additionally subtract by this we add again, however, not for each diagram, but for the sum.

7.1 The C_F part

For transverse polarisation we rewrite the analogue to the expression for the longitudinal case (6.77) as

$$\Phi_{\gamma^*}^{(1,real)}\Big|_{C_F}^{finite} = \frac{\lambda_{\mathrm{T}}}{4(2\pi)^{6-4\epsilon}(Q^2)^{2\epsilon}}\Bigg\{W_\Lambda + \int_0^1 d\alpha \int_0^{1-\alpha} \frac{d\alpha_\ell}{\alpha_\ell} \int d^{2-2\epsilon}\boldsymbol{k}\, d^{2-2\epsilon}\boldsymbol{\ell}$$
$$\times \sum_{C_F} \Big(\mathcal{AB}' - \mathcal{AB}'_{\text{soft}} - \big(\mathcal{AB}'_{\text{coll}} - \mathcal{AB}'_{\text{coll,soft}}\big)\Big)\Bigg\}, \tag{7.1}$$

$$W_\Lambda = \int_0^1 d\alpha \int_0^{1-\alpha} \frac{d\alpha_\ell}{\alpha_\ell} \int d^{2-2\epsilon}\boldsymbol{k}\, d^{2-2\epsilon}\boldsymbol{\ell}$$
$$\times \sum_{C_F} \Big(\big(\mathcal{AB}'_{\text{coll}} - \mathcal{AB}'_{\text{coll,soft}}\big)\ \Theta(|\boldsymbol{\ell}_c| - \alpha_\ell \Lambda)\Big) \tag{7.2}$$

We again symbolically denote by the subscript 'coll' the appropriate collinear limit or limits of the actual diagram.

Obviously we have achieved that the collinear divergences of $\mathcal{AB}$ are properly cancelled. However, this was not for free. Since $\mathcal{AB}_{\text{coll}} \sim 1/\boldsymbol{\ell}_c^2$, we are confronted with a new UV divergence, since $\boldsymbol{\ell}_c$ has no upper bound anymore now. We could subtract this divergence and integrate the sum of re-added terms in $D \neq 2$ dimensions. However, as too many diagrams provide collinear divergences we choose another way. Let us think of a diagram with one $\bar{q}$-collinear divergence. In this collinear limit $\bar{D}_4$ basically gets $\boldsymbol{\ell}_c^2$ while all other $\bar{D}_i$ get independent of $\boldsymbol{\ell}_c$. After introduction of Feynman parameters and integration over $\boldsymbol{k}, \boldsymbol{\ell}$ the $\boldsymbol{\ell}_c \to \infty$ limit of $\mathcal{AB}_{\bar{q}}$ corresponds to $\beta_4 \ll \beta_{i\neq 4}$. We will therefore introduce a cutoff parameter λ in the β_4 integration and approach the divergent integral from 0 to λ in $D \neq 2$ dimensions analytically. Denoting by β_c that β which corresponds to the actual collinear limit we write:

$$\Phi_{\gamma^*}^{(1,real)}\Big|_{C_F}^{finite} = \frac{\lambda_{\mathrm{T}}}{4(2\pi)^{6-2\epsilon}(Q^2)^{2\epsilon}}\Bigg\{W_\Lambda + R^{C_F}_{\boldsymbol{\ell}\text{–uv}} + \sum_{C_F} \int_0^1 d\alpha \int_0^{1-\alpha} \frac{d\alpha_\ell}{\alpha_\ell}\Bigg[$$
$$\int_\lambda^1 d\beta_c \int \prod d\beta_i \Big(X - X_{\text{soft}} - X|_{\boldsymbol{\ell}\text{–uv}} - (\hat{X}_{\text{coll}} - \hat{X}_{\text{coll,soft}})\Big) +$$
$$\int_0^\lambda d\beta_c \int \prod d\beta_i \Big(X - X_{\text{soft}} - X|_{\boldsymbol{\ell}\text{–uv}}\Big) - R_{coll}\Bigg]\Bigg\} \tag{7.3}$$

$$R_{coll} = \int_0^\lambda d\beta_c \int \prod d\beta_i \Big(\hat{X}_{\text{coll}} - \hat{X}_{\text{coll,soft}}\Big) \tag{7.4}$$

Here, we used the definition

$$\int d^{2-2\epsilon}\boldsymbol{k}\, d^{2-2\epsilon}\boldsymbol{\ell}\ \mathcal{AB}_{\text{cen}} = \int \prod d\beta_i\ \hat{X}_{\text{coll}}$$

and $\hat{X}_{\text{coll,soft}}$ accordingly. Note, that we can indeed calculate the second integral in (7.3) and R_{coll} separately, because the collinear limit corresponds to $\beta_c \to 1$ and is therefore excluded in these integrals.

How to deal with diagrams that provide both collinear divergences ? The divergences we introduce overlap at $\beta_3 \sim \beta_4 \to 0$. Therefore, we cannot separate them by cuts in the β_i integration. As the solution, we split such a diagram into two

$$\frac{Nu}{DDD_3D_4} = \frac{Nu}{DDD_3(D_3+D_4)} + \frac{Nu}{DDD_4(D_3+D_4)}$$

Now, each of the two has only one collinear divergence and can be treated as described above.

The $\boldsymbol{\ell}-$uv limit of X in (7.3) is obtained exactly as in the longitudinal case. We re-add all subtracted $\boldsymbol{\ell}$–uv approximations ($R^{C_F}_{\boldsymbol{\ell}\text{–uv}}$) and perform the β integrals analytically. As UV divergent terms can also be $\boldsymbol{\ell}-$uv divergent we obtain double poles in ϵ that cancel.

$$\begin{aligned}
R^{C_F}_{\boldsymbol{\ell}\text{–uv}} &= \int_0^1 d\alpha \int_0^{1-\alpha} \frac{d\alpha_\ell}{\alpha_\ell} \sum_{\mathcal{AA},\mathcal{BB}} \int d\beta_c \prod d\beta_i\ [X_{11} + 2X_{12} + X_{22}]_{\boldsymbol{\ell}\text{–uv}} \\
&= 4\, C_F\, \pi^{2-2\epsilon}\, \frac{\Gamma(2\epsilon)}{\epsilon}(1-\epsilon)^2 \int_0^1 d\alpha \int_0^{1-\alpha} d\alpha_\ell\, \alpha_\ell \Bigg\{ \\
&\Bigg(\frac{\alpha_2^2+\alpha^2}{\alpha_2^2\,\alpha^\epsilon} \left[\frac{1}{\alpha_2-\alpha}\left(\alpha^{-\epsilon} - \alpha_2^{-\epsilon}\right) - \epsilon\left(\alpha^{-\epsilon} + \alpha_2^{-\epsilon}\right) \right] \Bigg) + \Big(\alpha \to 1-\alpha-\alpha_\ell \Big) \Bigg\} \\
&= \frac{1}{\epsilon}\,\frac{\pi^2}{12}(3\pi^2-20) - \frac{\pi^2}{6}(3\pi^2-20)(\gamma_E + \operatorname{Log}\pi) \\
&\quad + \frac{\pi^2}{2}\left(\pi^2 \operatorname{Log} 2 + \frac{7}{2}\zeta(3)\right) + \pi^2\left(\frac{5}{9} - \frac{\pi^2}{2}\right)
\end{aligned} \tag{7.5}$$

The remaining pole is a pure UV pole, because the $\Gamma(2\epsilon)$ in (7.5) indicates that all $\boldsymbol{\ell}-$uv divergent terms are also UV divergent; we therefore write:

$$R^{C_F}_{\boldsymbol{\ell}\text{–uv}} = \frac{1}{\epsilon_{\text{UV}}} a_1 + a_2 + \mathcal{O}(\epsilon)$$

X and all approximation in (7.3) may provide UV divergences in shape of ϵ poles. After expansion in ϵ they have the general form

$$X, X_{\text{soft}}, X|_{\boldsymbol{\ell}\text{–uv}}, \hat{X}_{\text{coll}}, \hat{X}_{\text{coll,soft}} \sim \frac{1}{\epsilon_{\text{UV}}} c_1 + c_2 + \mathcal{O}(\epsilon)$$

Let us now have a closer look at W_Λ defined in (7.2). For the $\bar{q}$ collinear case it reads (see sec. 5.1)

$$\begin{aligned} W_\Lambda = & 4\, C_F \int_0^1 d\alpha \int_0^{1-\alpha} d\alpha_\ell \, \frac{\alpha^2+\alpha_2^2}{\alpha_2} \left[P_{gq}\left(\frac{\alpha_\ell}{\alpha_2}, \epsilon\right) - 2\frac{\alpha_2}{\alpha_\ell}\right] \\ & \times \int d^{2-2\epsilon} \frac{\boldsymbol{\ell}'}{\boldsymbol{\ell}'^2} \, \Theta(\alpha_\ell \Lambda - |\boldsymbol{\ell}'|) \int d^{2-2\epsilon}\boldsymbol{k} \, \left(\frac{\boldsymbol{k}+\boldsymbol{r}}{D(\boldsymbol{k}+\boldsymbol{r})} - \frac{\boldsymbol{k}}{D(\boldsymbol{k})}\right)^2 \end{aligned} \tag{7.6}$$

with the splitting function $P_{gq}(z, \epsilon)$. The $\boldsymbol{\ell}'$ integration gives an ϵ pole. While ϵ_{UV} corresponds to the limit of infinite distance from the origin in the $\boldsymbol{k}, \boldsymbol{\ell}$ space, this ϵ arises as we go in a certain direction in this space to infinity, namely $\boldsymbol{\ell}' \to \infty$; let us therefore represent it by 'C'. This pole appears because of our extension of the integration of $\mathcal{AB}_{\text{coll}}$ to infinity. The remaining $\boldsymbol{k}$ integral is UV finite, therefore:

$$W_\Lambda = \frac{1}{\epsilon_{\text{C}}} d_1 + d_2 + \mathcal{O}(\epsilon).$$

Let us finally analyse R_{coll} , (7.4). As collinear and UV divergences may overlap the integrand may have terms $\sim \Gamma(2\epsilon)$ that would lead to an ϵ_{UV} pole. The divergence as $\beta_c \to 0$ appears as the factor $1/\beta_c^{1-\epsilon}$. Introducing a function $F(\beta_c, \epsilon)$ being regular at $\beta_c \to 0$ we write

$$R_{coll} = \int \prod d\beta_i \int_0^\lambda d\beta_c \, \frac{1}{\beta_c^{1-\epsilon}} \, F(\beta_c, \epsilon) \tag{7.7}$$

We suppressed the dependence of F on the other β_i. With the expansion of F,

$$F(\beta, \epsilon) = \frac{1}{\epsilon} F^{-1}(\beta) + F^0(\beta) + \epsilon \, F^1(\beta)$$

and using partial integration we extract the pole corresponding to $\beta_c \to 0$

$$\begin{aligned} \int_0^\lambda d\beta \, \frac{1}{\beta^{1-\epsilon}} \, F(\beta, \epsilon) &= \frac{1}{\epsilon} \left[\lambda^\epsilon \, F(\lambda, \epsilon) - \int_0^\lambda d\beta \; \beta^\epsilon \; \partial_\beta F(\beta, \epsilon) \right] \\ &= \frac{1}{\epsilon^2} \, F^{-1}(0) \\ &+ \frac{1}{\epsilon} \left[F^0(0) + F^{-1}(\lambda) \, \text{Log}\, \lambda \; - \int_0^\lambda d\beta \; \text{Log}\, \beta \; \partial_\beta \, F^{-1}(\beta) \right] \\ &+ \Bigg[F^1(0) + F^0(\lambda) \; \text{Log}\, \lambda + \frac{1}{2} \, \text{Log}^2(\lambda) \, F^{-1}(\lambda) \\ &\quad - \int_0^\lambda d\beta \; \left(\text{Log}\, \beta \; \partial_\beta \, F^0(\beta) + \frac{1}{2} \, \text{Log}^2(\beta) \; \partial_\beta \, F^{-1}(\beta) \right) \Bigg] \end{aligned} \tag{7.8}$$

In the second step we exchanged the derivation with respect to ϵ and β. Thus, R_{coll} has the pole structure :

$$R_{coll} = \frac{1}{\epsilon^2}\, g_1 + \frac{1}{\epsilon}\, g_2 + g_3 + \mathcal{O}(\epsilon)$$

The poles are of mixed nature, either UV of C or both in case of ϵ^2.

Now, let us summarise what we have done so far. We have rewritten the definition of the real correction in D dimensions (7.3) to ensure finite β and α, α_ℓ integrals for each diagram. Expanding the formula in ϵ we got poles from different sources. Nearly each diagram will provide us with ϵ poles. Together with those from W_Λ they all have to cancel in the sum. The residues of the poles from each diagram are integrals over $\beta_i, \alpha, \alpha_\ell$. The achievement of the whole procedure is that these integrals are finite and can be computed numerically.

What has to be done in the future in order to calculate the residues of the poles and the finite terms ? $R^{C_F}_{\boldsymbol{\ell}\text{–uv}}$ is explicitly given in (7.5). As for W_Λ, the integral (7.6) has to be calculated analytically to get the finite term and the coefficient of the pole. Apart from $R^{C_F}_{\boldsymbol{\ell}\text{–uv}}$ and W_Λ that have to be calculated only once, there are poles and finite terms that have to be extracted for each diagram. According to (7.3), we need for each diagram the expression X and approximations of X. These expressions are obtained from the matrix element in this thesis by the introduction of Feynman parameters and via the integration formula (6.58). This formula has to be expanded analytically in ϵ and can be then incorporated in a MATHEMATICA routine. Then, this program can provide analytical expressions for the finite term an the residues for each diagram. Once the program has determined the various approximations of X, the integrand of R_{coll} (7.4) is known. The function $F(\beta_c, \epsilon)$ in (7.7) can be determined and the expansion of F in ϵ can be calculated. The finite terms and residues of R_{coll} are then obtained via (7.8). All the last steps including the derivations in (7.8) can be done by the computer program. In the end this program will provide for each diagram the residues and the finite terms as functions of α, α_ℓ and of the Feynman parameters which can easily be integrated numerically.

Since all ϵ poles have to cancel, one can restrict the computation just described to the finite terms. One could also compute the coefficients and check the cancellation numerically. As for the double poles it even seems realistic to perform their cancellation analytically starting from the expressions in momentum space.

7.2 The C_A part

All arguments that have led to (6.86) in the longitudinal case also hold here. However, due to the problem of the overlap of UV and collinear divergences we again subtract the collinear approximation without upper bound on $\boldsymbol{\ell}_c$. Since $\sum \mathcal{AB}'^{C_A}_{\text{coll}} = 0$ we can do this without re-adding anything.

$$\begin{aligned}
\Phi^{(1,real)}_{\gamma^*}\Big|^{finite}_{C_A} &= \frac{\lambda_{\mathrm{T}}}{4(2\pi)^{6-4\epsilon}(Q^2)^{2\epsilon}} \int d^{2-2\epsilon}\boldsymbol{k}\, d^{2-2\epsilon}\boldsymbol{\ell} \int_0^1 d\alpha \Bigg\{ \int_0^{1-\alpha} \frac{d\alpha_\ell}{\alpha_\ell} \\
&\times \Bigg(\sum_{12,14,24,44} \Big[\mathcal{AB}' - \mathcal{AB}'_{\text{soft}} - \mathcal{AB}'_{\text{cen}} - \big(\mathcal{AB}'_{\text{coll}} - \mathcal{AB}'_{\text{coll,soft}}\big) \Big] \\
&\quad + \sum_{rest} \Big[\mathcal{AB}' - \mathcal{AB}'_{\text{soft}} - \big(\mathcal{AB}'_{\text{cen}} - \mathcal{AB}'_{\text{cen,soft}}\big)\, \Theta(|\boldsymbol{\ell}| - \alpha_\ell\sqrt{s_0}) \\
&\qquad - \big(\mathcal{AB}' - \mathcal{AB}'_{\text{soft}}\big)_{is} - \big(\mathcal{AB}'_{\text{coll}} - \mathcal{AB}'_{\text{coll,soft}}\big) \Big] \Bigg) \\
&- \int_{1-\alpha}^{\infty} \frac{d\alpha_\ell}{\alpha_\ell} \sum_{C_A} \mathcal{AB}'_{\text{cen}}\, \Theta(|\boldsymbol{\ell}| - \alpha_\ell\sqrt{s_0}) \Bigg\}
\end{aligned} \tag{7.9}$$

We proceed exactly as in the transverse C_F case

$$\begin{aligned}
\Phi^{(1,real)}_{\gamma^*}\Big|^{finite}_{C_A} &= \frac{\lambda_{\mathrm{T}}}{4(2\pi)^{6-4\epsilon}(Q^2)^{2\epsilon}} \Bigg\{ \sideset{}{^*}\sum_{12,14,24,44} \int_0^1 d\alpha \int_0^{1-\alpha} \frac{d\alpha_\ell}{\alpha_\ell} \Bigg[\int_\lambda^1 d\beta_c \int \prod d\beta_i \\
&\times \Big(X - X^0 - (X - X^0)_{\boldsymbol{\ell}\text{–uv}} - X_{\text{soft}} - \big(\hat{X}_{\text{coll}} - \hat{X}_{\text{coll,soft}}\big) \Big) \\
&+ \int_0^\lambda d\beta_c \int \prod d\beta_i \Big(X - X^0 - (X - X^0)_{\boldsymbol{\ell}\text{–uv}} - X_{\text{soft}} \Big) - R_{coll} \Bigg] \\
&\quad + \sideset{}{^*}\sum_{\text{rest}} \int_0^1 d\alpha \int_0^{1-\alpha} \frac{d\alpha_\ell}{\alpha_\ell} \Bigg[\int_\lambda^1 d\beta_c \int \prod d\beta_i \\
&\times \Big(X - X_{\text{soft}} - (X - X_{\text{soft}})_{\text{is}} - (X_{\text{cen}} - X_{\text{cen,soft}}) - \big(\hat{X}_{\text{coll}} - \hat{X}_{\text{coll,soft}}\big) \Big) \\
&+ \int_0^\lambda d\beta_c \int \prod d\beta_i \Big(X - X_{\text{soft}} - (X_{\text{cen}} - X_{\text{cen,soft}}) - (X - X_{\text{soft}})_{\text{is}} \Big) - R_{coll} \Bigg] \\
&\quad + R^{C_A}_{\boldsymbol{\ell}\text{–uv}} - \sideset{}{^*}\sum_{C_A} \int_0^1 d\alpha \int_{1-\alpha}^{\infty} \frac{d\alpha_\ell}{\alpha_\ell} \int \prod d\beta_i\, X_{\text{cen}} \Bigg\}
\end{aligned} \tag{7.10}$$

We have subtracted and re-added the $\boldsymbol{\ell}-$uv approximation and split the β_c integration. R_{coll} has been defined in the last section

$$R_{coll} = \int_0^\lambda d\beta_c \int \prod d\beta_i \Big(\hat{X}_{\text{coll}} - \hat{X}_{\text{coll,soft}} \Big) \tag{7.11}$$

The ' ˆ ' on X indicates that the $\boldsymbol{\ell}$ integration of $\mathcal{AB}_{\rm coll}$ was unbounded. Remember also the $*$ on the $\sum$ indicating that in case of lr divergent diagrams we use the same Feynman parameters for the $\mathcal{AB}_{ij}$ and $\mathcal{AB}_{ij}$ diagram and perform the integration of the sum of both.

The sum of the re-added $\boldsymbol{\ell}-$uv subtractions reads:

$$\begin{aligned}
R^{C_A}_{\boldsymbol{\ell}\text{–uv}} &= \int_0^1 d\alpha \int_0^{1-\alpha} \frac{d\alpha_\ell}{\alpha_\ell}\Bigg([2X_{12}+2X_{14}+2X_{24}+X_{44}]_{\boldsymbol{\ell}\text{–uv}} \\
&\qquad - [2X^0_{12}+2X^0_{14}+2X^0_{24}+X^0_{44}]_{\boldsymbol{\ell}\text{–uv}}\Bigg) \\
&= -2\,C_A\,\pi^{2-2\epsilon}\,\frac{\Gamma(2\epsilon)}{\epsilon}(1-\epsilon)\int_0^1 d\alpha \int_0^{1-\alpha} d\alpha_\ell \Bigg\{ \\
&\left(\frac{\alpha_2^2+\alpha^2}{\alpha_2\,\alpha^\epsilon}\left[\frac{\alpha}{\alpha_2-\alpha}\left(\alpha^{-\epsilon}-\alpha_2^{-\epsilon}\right)-\epsilon\,\alpha_2^{-\epsilon}\right]\right)+\Big(\alpha\to 1-\alpha-\alpha_\ell\Big)\Bigg\} \\
&= -\frac{1}{\epsilon}\,\frac{\pi^2}{24}(3\pi^2-20)+\frac{\pi^2}{12}(3\pi^2-20)(\gamma_E+\operatorname{Log}\pi) \\
&\quad -\frac{\pi^2}{4}\left(\pi^2\operatorname{Log}2+\frac{7}{2}\zeta(3)\right)+\pi^2\left(\frac{8}{9}+\frac{17}{72}\pi^2\right) \qquad (7.12)
\end{aligned}$$

After expansion of (7.10) in ϵ we get again for each diagram ϵ poles from $X, X_{soft}, \ldots$ and from R_{coll} (the latter will also provide us with double poles). The coefficients should be finite $\alpha_\ell, \alpha, \beta_i$ integrals. Together with the ϵ pole from $R^{C_A}_{\boldsymbol{\ell}\text{–uv}}$ we expect full cancellation of all poles in the sum of all diagrams.

For diagrams of group 'rest' in (7.9) the integral of the central approximation has a lower bound, but we have not calculated this integral in $D \neq 4$ dimensions. However, as one can see from our table of divergences (6.1,6.2) the diagrams in question (15, 25) are UV finite and it is not necessary to know the integral in $D \neq 4$ dimensions.

The basic features for the further procedure in the computation of the residues and finite terms are the same as outlined above for the C_F part.

Chapter 8

Numerical results

The numerical evaluation of the real corrections to the photon impact factor will give us not only first numbers but also represents a stringent test of the subtraction procedure we have developed. In this chapter we consider the case of longitudinal photon polarisation.

We have evaluated the formulae (6.84, 6.89) for the C_F and C_A part of the real corrections. The procedure is split into two parts as follows: We have written a MATHEMATICA program that is first called for each diagram and introduces Feynman parameters. In that mixed representation it then checks in which limits the diagram diverges and determines the approximations. According to the three integrals (6.58, 6.67, 6.74) the $\boldsymbol{k}, \boldsymbol{\ell}$ integration for $\epsilon = 0$ is then performed. We obtain an expression that depends on α, α_ℓ and the Feynman parameters β_i, on $\boldsymbol{r}^2$ and on the cutoff parameters Λ, s_0. In the second part specific values for $\boldsymbol{r}^2, \Lambda$ and s_0 are chosen and the $\alpha, \alpha_\ell, \beta_i$ integrals for each diagram are carried out numerically with the Monte Carlo routine VEGAS. The numbers from all diagrams are then added; we get:

$$\Phi_{\gamma^*}^{(1,real)}\Big|_{C_F}^{finite} \quad \text{and} \quad \Phi_{\gamma^*}^{(1,real)}\Big|_{C_A}^{finite} \qquad \text{as functions of } \boldsymbol{r}^2\,, \Lambda\,, s_0$$

Throughout this chapter we continue to use the dimensionless variables; $\boldsymbol{r}^2$, Λ^2 and s_0 are scaled with Q^2 and dimensionless.

As the first result we saw that for some set of $\boldsymbol{r}^2, \Lambda, s_0$ the integration of each diagram is indeed convergent. We have therefore succeeded to deal with all divergences that emerge by treating Feynman diagrams separately.

The formula (5.33) for the complete next-to-leading corrections to the impact factor contains besides the finite parts of the real and virtual corrections also some further terms that stem from the re-added subtractions. In particular, there are terms depending on Λ and the energy scale s_0. Let us include these term in our analysis. Note, that $\Phi_{\gamma^*}^{(1,virtual)}\Big|^{finite}$ is independent of s_0; only the divergent terms of the virtual corrections contained s_0.

We rewrite (5.33) as

$$\Phi^{(1)}_{\gamma^*} = \Phi^{(1,virtual)}_{\gamma^*}\Big|^{finite} - \frac{2\Phi^{(0)}_{\gamma^*}}{(4\pi)^2}\left\{\beta_0 \ln\frac{\boldsymbol{r}^2}{\mu^2} + C_F \ln(\boldsymbol{r}^2)\right\}$$
$$+ \int_0^1 d\alpha \int \frac{d\boldsymbol{k}}{(4\pi)^2}\,\mathcal{I}_2(\alpha,\boldsymbol{k})\Bigg\{ - C_A \ln^2 M^2$$
$$+ 2C_F\left[8 - 3\ln\alpha(1-\alpha) + \ln^2 M^2 + \ln^2\frac{\alpha}{1-\alpha}\right]\Bigg\}$$
$$+ \Phi^{(1,real,p)}_{\gamma^*} \tag{8.1}$$

with

$$\Phi^{(1,real,p)}_{\gamma^*} = C_A\,\Phi^{(1,\mathrm{real})}_{\gamma^*}\Big|^{finite}_{C_A} + C_F\,\Phi^{(1,\mathrm{real})}_{\gamma^*}\Big|^{finite}_{C_F} - 3\,C_F\,\frac{\Phi^{(0)}_{\gamma^*}}{(2\pi)^2}\,\ln\Lambda$$
$$+ C_A \int_0^1 d\alpha \int \frac{d\boldsymbol{k}}{(4\pi)^2}\,\mathcal{I}_2(\alpha,\boldsymbol{k})\,\ln^2\alpha(1-\alpha)s_0$$
$$= e^2 e_f^2\,(\Phi_A + \Phi_F + \Phi_\Lambda + \Phi_{s_0}) \tag{8.2}$$

In the last line of (8.2) we have defined labels for the three parts of $\Phi^{(1,\mathrm{real,p})}_{\gamma^*}$. The dependence of $\Phi^{(1)}_{\gamma^*}$ on Λ and s_0 is now entirely contained in $\Phi^{(1,real,p)}_{\gamma^*}$.

We have introduced Λ as upper bound for the integral of the collinear approximation. The NLO correction to the impact factor must be independent from the choice of Λ. This is an important test of the whole calculation. If our subtraction procedure was correct the C_A and C_F term of (8.2) should be independent of Λ separately. Φ_A and Φ_F are obtained as described. Φ_{s_0} is independent of Λ; the Φ_Λ term stems from the re-added collinear subtractions. The LO photon impact factor $\Phi^{(0)}$ was given in (3.27); carrying out the $\boldsymbol{k}$ integration after introduction of Feynman parameters it reads

$$\Phi^{(0)}_{\gamma^*} = \frac{2e^2e_f^2\sqrt{N_c^2-1}}{(2\pi)^2}\int_0^1 d\alpha \int_0^1 dx\,\frac{\alpha(1-\alpha)\,x(1-x)\,\boldsymbol{r}^2}{x(1-x)\boldsymbol{r}^2 + \alpha(1-a)}$$

The remaining integration can easily be performed numerically.

Fig.8.1 shows the Λ dependence of $\Phi^{(1,real,p)}_{\gamma^*}$ for fixed $\boldsymbol{r}^2 = s_0 = 1$ ($N_c = 3$). We see that Φ_F is of the type $a_1 + a_2\ln\Lambda$. Both coefficients come from a sum of many Feynman diagrams; and a_2 turns out to be such that $\Phi_F + \Phi_\Lambda$ is indeed nearly independent of Λ. Note that also the C_A parts of some diagrams were collinear divergent; we introduced Λ by the collinear subtractions since we knew that the sum of these subtractions is zero. Thus, some terms in Φ_A depend on Λ. Fig. 8.1 shows that we treated the collinear subtractions correctly since the Λ dependence nearly completely drops out.

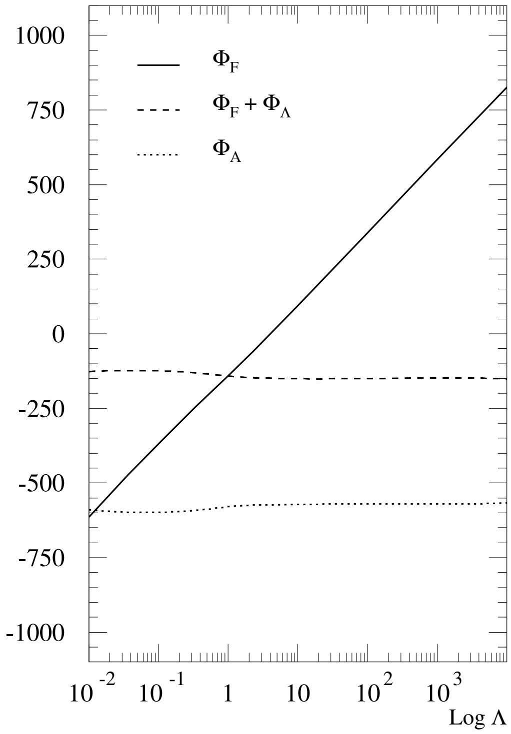

Figure 8.1: The dependence of the real corrections on Λ (with $\boldsymbol{r}^2 = s_0 = 1$)

The deviations from the straight line are most probably due to numerical instabilities.

Let us finally compare the real corrections with the LO impact factor and have a look at the dependence on the energy scale s_0. Remember that s_0 came in as the lower bound in the $\boldsymbol{\ell}$ integration of the central approximation; it is the intrinsic energy scale of the NLO impact factor. According to sec.3.2 the γ^* impact factor at NLO reads $\Phi_{\gamma^*} = g^2\Phi^{(0)}_{\gamma^*} + g^4\Phi^{(1)}_{\gamma^*}$. We only know part of $\Phi^{(1)}_{\gamma^*}$ in the moment, namely $\Phi^{(1,real,p)}_{\gamma^*}$. Let us therefore define

$$\Phi'_{\gamma^*} = g^2\widetilde{\Phi}^{(0)}_{\gamma^*} + g^4\frac{\Phi^{(1,real,p)}_{\gamma^*}}{e^2e_f^2}\,, \qquad \widetilde{\Phi}^{(0)}_{\gamma^*} = \frac{\Phi^{(0)}_{\gamma^*}}{e^2e_f^2}$$

As demonstrated above Φ'_{γ^*} is independent of Λ. It already has the same s_0 dependence as the complete NLO photon impact factor Φ_{γ^*} since

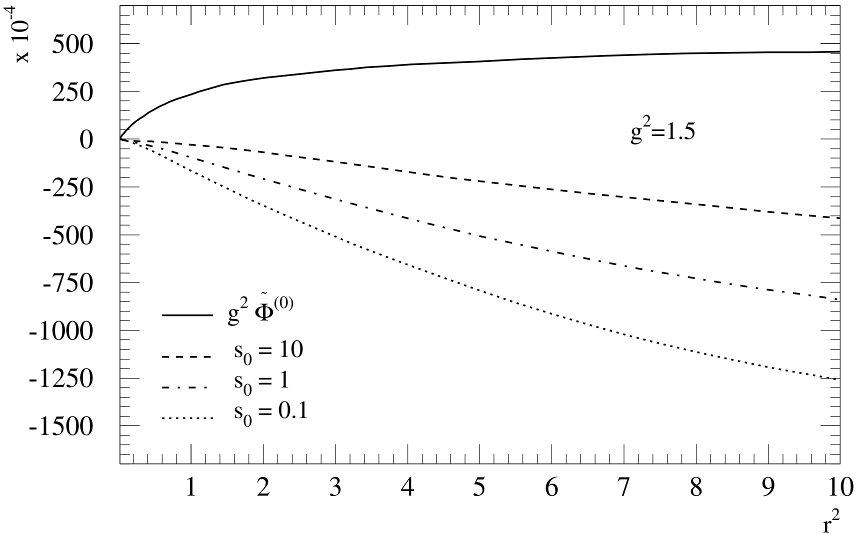

Figure 8.2: Φ'_{γ^*} at different s_0 compared to $g^2\widetilde{\Phi}^{(0)}_{\gamma^*}$

we included all s_0 depending terms in it. As photon virtuality we choose $Q^2 = 15$ GeV^2 as a typical value in $\gamma^*\gamma^*$ scattering. This choice only effects the strong coupling: $\alpha_s(Q^2) = 0.18$ or $g^2 = 1.5$.

Fig.8.2 compares Φ'_{γ^*} to the LO impact factor $g^2\widetilde{\Phi}^{(0)}$ as function of $\boldsymbol{r}^2$ at different values of s_0. The ratio of Φ'_{γ^*} and $g^2\widetilde{\Phi}^{(0)}$ is shown in fig.8.3. The corrections are negative and quite large; they are up to 2.5 times larger (in absolute value) than the LO impact factor. However, this is not of so much significance because we considered here only part of the corrections. The absolute value of the complete NLO corrections is unclear and may well turn out to be very small and positive.

As for the s_0 dependence of the real corrections, note that the difference between the values of Φ'_{γ^*} taken at different s_0 and fixed $\boldsymbol{r}^2$ (fig.8.2) will be the same as in case of the complete NLO impact factor Φ_{γ^*}. The smaller s_0 the smaller Φ'_{γ^*} gets. So, the NLO photon impact factor descreases towards smaller values of s_0.

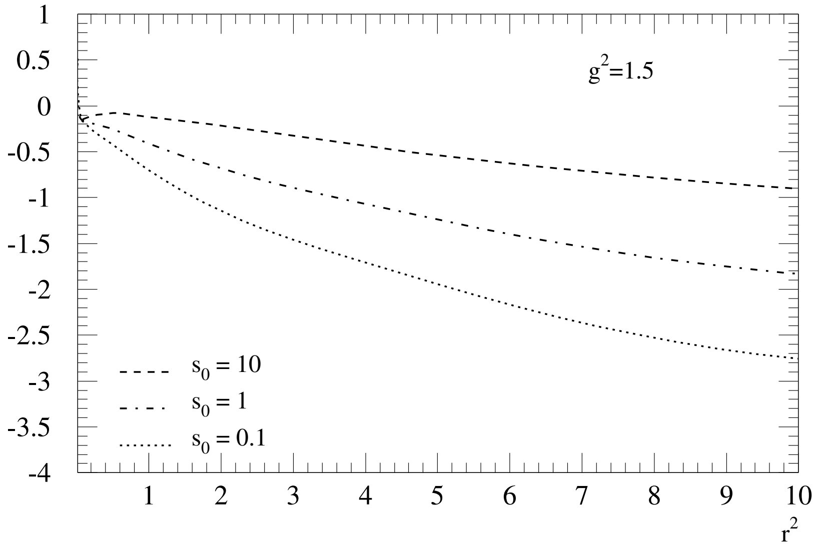

Figure 8.3: The ratio $\Phi'_{\gamma^*}/(g^2\widetilde{\Phi}^{(0)}_{\gamma^*})$ at different s_0

Chapter 9

Summary and outlook

We have considered the scattering of virtual photons in the high energy limit of QCD. In a perturbative approach, high energy scattering processes can be investigated using the BFKL formalism: the large logarithms of the energy generated in this limit are resummed to all orders in α_s. The total $\gamma^*\gamma^*$ cross section is written in terms of the universal BFKL Green function and the photon impact factors.

From the process $e^+ + e^- \to e^+ + e^- + X$ the $\gamma^*\gamma^*$ total cross section has been measured at LEP [34, 35]. Although there are theoretical uncertainties, the growth with energy given by LO BFKL turned out to be too strong. Next-to-leading corrections seemed to be definitely needed.

The results for the NLO corrections to the BFKL resummation are promising, first studies lower the intercept ω_{BFKL}. However, for the calculation of the $\gamma^*\gamma^*$ total cross section the photon impact factor at NLO is needed. The computation of this impact factor will enable the first complete test of NLO BFKL.

This impact factor is important also from another point of view. The colour dipole picture was the basis of a very successful description of HERA data in inclusive DIS and diffractive processes. The modification of this picture at NLO should come out of the calculation of the NLO γ^* impact factor. In particular, the $q\bar{q}g$ Fock-component of the photon wave function is expected to arise in our calculation.

The main subject of this thesis is the calculation of the NLO real corrections to the γ^* impact factor. To this end, we have calculated the squared amplitude for the process $\gamma^* + q \to q\bar{q}g + q$ for longitudinal and transverse photon polarisation. In configuration space the result was found to factorise in a way that supports the photon wave function interpretation. This is considered as a first step in the calculation of the $q\bar{q}g$-component of this wave function. From the squared amplitude we extracted the square of the vertex $\Gamma_{\gamma^* \to q\bar{q}g}$. In order to obtain the real corrections we had to subtract the limit where the gluon is separated in rapidity from the $q\bar{q}$ pair since this configuration belongs to the LLA. This subtraction introduced an energy scale (we called it s_0) into the photon impact factor. The dependence of both the BFKL Green function and the impact factors at NLO on the energy scale is a consequence of the NLLA, at LL s_0 was arbitrary.

Making use of the subtraction method we extracted the divergences stemming from the collinear and/or soft gluon. Thereby, we introduced a parameter Λ as an upper integration bound in the collinear subtraction; the real corrections must be independent of Λ. We have shown explicitly the cancellation of the infrared divergences from virtual and real corrections. The NLO γ^* impact factor was written in a form which includes the real corrections as a finite combination of various limits of $\Gamma^2_{\gamma^*\to q\bar{q}g}$ under the phase space integral.

In order to allow further investigations of the NLO impact factor the phase space integration in the real corrections was approached analytically. To this end, Feynman parameters were introduced, which enforced the independent treatment of each Feynman diagram. As a consequence, various divergences that cancel in the sum of all diagrams had to be dealt with. For both longitudinal and transverse photon polarisations a procedure was worked out that provides convergent integrals for each diagram; the integration over the transverse momenta of the outgoing quarks and gluon ($\boldsymbol{k}$ and $\boldsymbol{\ell}$) was carried out analytically. The procedure states how to derive from each matrix element given in this thesis a finite contribution to the real corrections.

In the case of longitudinal photon polarisation this procedure was incorporated in a MATHEMATICA routine. This program provides for each diagram an analytical expression depending on $\boldsymbol{r}^2/Q^2$, the Feynman parameters, the Sudakov variables α, α_ℓ, and the parameters Λ and s_0. $\boldsymbol{r}$ and Q^2 are the Reggeon momentum and the photon virtuality, respectively. The remaining integrals were carried out numerically and the value of the real corrections to the (longitudinal) photon impact factor for given values of $\boldsymbol{r}^2/Q^2, \Lambda$ and s_0 were computed. Since the virtual corrections are not yet known numerically it is not possible at present to estimate the size of the next-to-leading corrections compared to the LO impact factor. However, the finite result for the real corrections shows that in the case of the longitudinal polarisation our procedure to deal with the divergences indeed works. We have also proven that the dependence on the cutoff Λ drops out for this photon polarisation - our calculation successfully passed this important test. Since the dependence of the NLO γ^* impact factor $\Phi_{\gamma^*}(s_0)$ on the energy scale s_0 only stems from the real corrections, it was also possible to numerically compute the difference $\Phi_{\gamma^*}(s_0) - \Phi_{\gamma^*}(s_1)$ for two scales s_0 and s'. In order to judge the strength of the scale dependence the complete NLO corrections are needed.

As for the rôle of the energy scale s_0, some remarks have to be made. Starting from the n-gluon production amplitude in the LLA, the emission of an additional gluon leads to different contributions to the NLLA. Emitted in the fragmentation region of one initial particle it contributes to the NLO corrections to the respective impact factor. Produced in MRK or near the 'first' gluon of the BFKL ladder one obtains NLO corrections to the kernel. Since there is no natural border, the parameter s_0 was introduced to separate the MRK from the QMRK. It can be understood as a cutoff in the gluon rapidity (or in α_ℓ) that separates the NLO contributions to the impact factor from those belonging to the kernel due to the emission of a gluon. Obviously, the cross section is independent of s_0. Our result for the s_0 dependence of the impact factor therefore has a simple interpretation. We found the impact factor to decrease as s_0 gets smaller. On the other hand, the contribution from the BFKL Green function to the cross section is proportional to $(s/s_0)^\omega$ and therefore increases towards smaller values of s_0 providing a s_0-independent cross section.

What are the future steps and opportunities?

First of all, the numerical analysis has to be extended to the case of transverse photon polarisation. The procedure of how to deal with this polarisation has been formulated in this thesis. In order to get numerical results, one first has to calculate W_Λ which is defined in (7.6) analytically and expand (6.58) in the space time dimension parameter ϵ. A MATHEMATICA routine has to be written that provides the expressions for the finite terms and the residues of the poles as discussed in chapter 7. Then, the numerical integration can be carried out exactly as in the longitudinal case.

As for the extensions of the colour dipole picture we have investigated the factorisation of the squared amplitude for $\gamma^* + q \to q\bar{q}g + q$. For the calculation of the $q\bar{q}g$ Fock component of the photon wave function one has to include in the analysis also the subtraction of the central region and especially the infrared divergences. Only the combined investigation of real and virtual corrections will allow to separate the NLO corrections to the $q\bar{q}$ component and the LO $q\bar{q}g$ component of the γ^* wave function. The infrared finite formulation of the virtual and real corrections in this thesis is also a good starting point to address further important questions, as, for example, colour transparency at NLO.

As already mentioned, the matrix elements we obtained for the process $\gamma^* + q \to q\bar{q}g + q$ enable the calculation of 3-jet production in DIS using the k_T factorisation scheme. Together with the known NLO corrections to the process $\gamma^* + g \to q\bar{q}$ also the complete NLO calculation of 2-jet production in this scheme is possible. All matrix elements have been calculated and, together with a suitable jet-definition, they can be incorporated in an event generator.

Let us now outline the further steps in the calculation of the γ^* impact factor at NLO and in particular towards one of the main goals, the $\gamma^*\gamma^*$ total cross section. The solution of the BFKL equation is often formulated in the Mellin space. In this case, the computation of a total cross section requires a Mellin transform of the impact factor w.r.t. the t-channel momentum. Also the collinear limit is usually studied by considering the corresponding poles in Mellin space. The introduction of Feynman parameters in the real corrections enables the analytical integration over the Reggeon momentum $\boldsymbol{r}$ and in particular the calculation of the Mellin transform. The expressions provided by our MATHEMATICA routine can directly be used to analytically perform a Mellin transform for longitudinal photon polarisation. A similar routine can be written for transverse polarisation. As for the virtual corrections, they have been calculated except for the integration over the $q\bar{q}$ phase space. Due to the complexity of the expressions the calculation of the Mellin transform here is a quite extensive task.

However, avoiding the Mellin transform the $\gamma^*\gamma^*$ total cross section can also be calculated in momentum space. In [40] a procedure is presented how to solve the forward NLO BFKL equation; the BFKL Green function is obtained as a function of the Reggeon momenta and the energy. It has to be convoluted with the γ^* impact factor to obtain $\sigma^{tot}_{\gamma^*\gamma^*}$. Thus, the numerical value of the photon impact factor as a function of $\boldsymbol{r}$ is needed. In this thesis the real corrections have been fully calculated for longitudinal photon polarisation. The numerical analysis has to be extended also to the transverse photon polarisation as outlined above. What remains to be done for the virtual corrections is the (numerical) evaluation of the $q\bar{q}$ phase space integration.

Five years after the beginning of the work on the NLO photon impact factor a stage has been reached, where the last technical problem can be expected from the numerical integration over the $q\bar{q}$ phase space. The computation of the NLO BFKL Green function in momentum space is promising. So, one can hope to obtain first results for the $\gamma^*\gamma^*$ total cross section in the near future.

The comparison with data will show if the BFKL approach is suitable to describe the scattering of small sized objects in the high energy limit. This is a crucial step towards the understanding of the interplay between perturbative and non-perturbative physics in the transition to the case of large, hadronic scattering objects.

Appendix

The formulae for the Feynman parametrisation used in sec. 6.2 are special cases of:

$$\prod_{i=1} \frac{1}{D_i^{p_i}} = \frac{\Gamma(\sum_i p_i)}{\prod_i \Gamma(p_i)} \int_0^1 \prod_i \left(d\beta_i \, \beta_i^{p_i-1} \right) \frac{\delta(1-\sum_i \beta_i)}{[\sum_i \beta_i D_i]^{\sum_i p_i}}$$

As an overview we state here also the three basic integrals needed to perform the $\boldsymbol{k}$ and $\boldsymbol{\ell}$ integration (see 6.58, 6.67 and 6.74).

$$\begin{aligned} Nu' &= A\,\boldsymbol{k}^4 + B\,\boldsymbol{\ell}^4 + C\,\boldsymbol{k}^2\boldsymbol{\ell}^2 + D\,\boldsymbol{k}^2 + E\,\boldsymbol{\ell}^2 + F \\ &\quad + P\,(\boldsymbol{k}\boldsymbol{\ell})^2 + I\,(\boldsymbol{\ell}\boldsymbol{r})^2 + N\,(\boldsymbol{k}\boldsymbol{r})^2 \end{aligned}$$

$$\begin{aligned} I_1 &= \int d^{2-2\epsilon}\boldsymbol{k}\; d^{2-2\epsilon}\boldsymbol{\ell}\; \frac{Nu'}{[\alpha\boldsymbol{k}^2 + \omega\boldsymbol{\ell}^2 + R]^4} \\ &= \frac{\pi^{2-2\epsilon}}{6\,(\alpha\omega)^{1-\epsilon} R^{2\epsilon}} \Bigg\{ \Gamma(2\epsilon) \Bigg[(2-\epsilon)(1-\epsilon) \left(\frac{A}{\alpha^2} + \frac{B}{\omega^2} \right) \\ &\qquad\qquad + (1-\epsilon)^2 \, \frac{C + \frac{1}{2}P}{\alpha\omega} \Bigg] + \\ &\quad + (1-\epsilon)\Gamma(1-2\epsilon)\,\frac{1}{R} \left(\frac{D + \frac{\boldsymbol{r}^2}{2}N}{\alpha} + \frac{E + \frac{\boldsymbol{r}^2}{2}I}{\omega} \right) + \Gamma(2+2\epsilon)\frac{F}{R^2} \Bigg\} \end{aligned}$$

$$\begin{aligned} I_2 &= \int d^2\boldsymbol{k}\; d^2\boldsymbol{\ell}\; \theta(\alpha_\ell\Lambda - |\boldsymbol{\ell}|)\, \frac{D\,\boldsymbol{k}^2 + E\,\boldsymbol{\ell}^2 + F}{[\alpha\boldsymbol{k}^2 + \omega\boldsymbol{\ell}^2 + R]^4} \\ &= \frac{\pi^2 \bar{\Lambda}^2}{6\,\alpha\omega R(R+\bar{\Lambda}^2)} \left[D\frac{1}{\alpha} + E\frac{1}{\omega}\,\frac{\bar{\Lambda}^2}{R+\bar{\Lambda}^2} + F\frac{1}{R}\,\frac{2R+\bar{\Lambda}^2}{R+\bar{\Lambda}^2} \right] \\ &\quad \text{with} : \bar{\Lambda}^2 = \omega(\alpha_\ell\Lambda)^2 \end{aligned}$$

$$
\begin{aligned}
Nu'' = \; & D\,\boldsymbol{k}^2 + E\,\boldsymbol{\ell}^2 + F \; + M\boldsymbol{\ell}\boldsymbol{r} \\
& + G\boldsymbol{k}^2\boldsymbol{\ell}\boldsymbol{r} \; + H\boldsymbol{\ell}^2\boldsymbol{\ell}\boldsymbol{r} + J(\boldsymbol{\ell}\boldsymbol{r})^2 \; + \; +P\,(\boldsymbol{k}\boldsymbol{\ell})^2 + N\,(\boldsymbol{k}\boldsymbol{r})^2 \; + S(\boldsymbol{k}\boldsymbol{r})(\boldsymbol{k}\boldsymbol{\ell})
\end{aligned}
$$

$$
\begin{aligned}
I_3 = & \int d^2\boldsymbol{k} \int d^2\boldsymbol{\ell}\; \theta(|\boldsymbol{\ell}| - \alpha_\ell s_0)\, \frac{Nu''}{[\alpha\boldsymbol{k} + \omega(\boldsymbol{\ell}+\boldsymbol{\lambda})^2 + R]^4} \\
= & \frac{\pi^2}{6\alpha\omega R} \left(\frac{D + \frac{\boldsymbol{r}^2}{2}N}{\alpha}\,\mathcal{C}_D + \frac{E}{\omega}\,\mathcal{C}_E + \frac{F}{R}\,\mathcal{C}_F + \frac{M}{R}|\boldsymbol{\lambda}|\,\mathcal{C}_M \right. \\
& \left. + \frac{G + \frac{1}{2}S}{\alpha}|\boldsymbol{\lambda}|\,\mathcal{C}_G + \frac{H}{\omega}|\boldsymbol{\lambda}|\,\mathcal{C}_H + \frac{J}{\omega}|\boldsymbol{r}|^2\,\mathcal{C}_J \right)
\end{aligned}
$$

$$
\begin{aligned}
\mathcal{C}_D = & \frac{1}{2}\left\{ 1 - \frac{1}{\kappa}\Big[\bar{s}_0 - (R + \bar{\boldsymbol{\lambda}}^2)\Big] \right\} \\
\mathcal{C}_E = & \frac{1}{2}\left\{ \frac{\bar{\boldsymbol{\lambda}}^2 + R}{R} - \frac{1}{R\kappa}\Big[\bar{s}_0\,(R + \bar{\boldsymbol{\lambda}}^2) - 3R^2 - \bar{\boldsymbol{\lambda}}^4\Big] \right. \\
& \left. - \frac{2}{\kappa^3}\Big[(R - \bar{\boldsymbol{\lambda}}^2)(R + \bar{\boldsymbol{\lambda}}^2)^2 + \bar{s}_0\,(R^2 + \bar{\boldsymbol{\lambda}}^4 - 6R\bar{\boldsymbol{\lambda}}^2)\Big] \right\} \\
\mathcal{C}_F = & \frac{1}{2}\left\{ 1 - \frac{1}{\kappa}\Big[\bar{s}_0 + (R - \bar{\boldsymbol{\lambda}}^2)\Big] + \frac{2R}{\kappa^3}\Big[\bar{s}_0\,(R - \bar{\boldsymbol{\lambda}}^2) + (R + \bar{\boldsymbol{\lambda}}^2)^2\Big] \right\} \\
\mathcal{C}_M = & -\frac{1}{2}\left\{ 1 - \frac{1}{\kappa}\Big[\bar{s}_0 + (R - \bar{\boldsymbol{\lambda}}^2)\Big] + \frac{2R}{\kappa^3}\Big[\bar{s}_0\,(3R - \bar{\boldsymbol{\lambda}}^2) + (R + \bar{\boldsymbol{\lambda}}^2)^2\Big] \right\} \\
\mathcal{C}_G = & \frac{1}{2}\left\{ \frac{R - \bar{\boldsymbol{\lambda}}^2}{\bar{\boldsymbol{\lambda}}^2} - \frac{1}{\kappa\bar{\boldsymbol{\lambda}}^2}\Big[(R + \bar{\boldsymbol{\lambda}}^2)^2 + \bar{s}_0\,(R - \bar{\boldsymbol{\lambda}}^2)\Big] \right\} \\
\mathcal{C}_H = & \left\{ \frac{R^2 - \bar{\boldsymbol{\lambda}}^4 - 2\bar{\boldsymbol{\lambda}}^2 R}{2R\bar{\boldsymbol{\lambda}}^2} \right. \\
& - \frac{1}{2\kappa R\bar{\boldsymbol{\lambda}}^2}\Big[\bar{\boldsymbol{\lambda}}^6 + \bar{\boldsymbol{\lambda}}^4 R + 9\bar{\boldsymbol{\lambda}}^2 R^2 + R^3 - \bar{s}_0\,(\bar{\boldsymbol{\lambda}}^4 + 2\bar{\boldsymbol{\lambda}}^2 R - R^2)\Big] \\
& \left. + \frac{1}{\kappa^3}\Big[-\bar{\boldsymbol{\lambda}}^6 + \bar{\boldsymbol{\lambda}}^4 R + 5\bar{\boldsymbol{\lambda}}^2 R^2 + 3R^3 + \bar{s}_0\,(\bar{\boldsymbol{\lambda}}^4 - 10\bar{\boldsymbol{\lambda}}^2 R + 5R^2)\Big] \right\} \\
\mathcal{C}_J = & \left\{ \frac{R^2 + 2\bar{\boldsymbol{\lambda}}^4 + \bar{\boldsymbol{\lambda}}^2 R}{4R\bar{\boldsymbol{\lambda}}^2} \right. \\
& - \frac{1}{4\kappa R\bar{\boldsymbol{\lambda}}^2}\Big[-2\bar{\boldsymbol{\lambda}}^6 + \bar{\boldsymbol{\lambda}}^4 R - 4\bar{\boldsymbol{\lambda}}^2 R^2 + R^3 + \bar{s}_0\,(2\bar{\boldsymbol{\lambda}}^4 + \bar{\boldsymbol{\lambda}}^2 R + R^2)\Big] \\
& \left. - \frac{1}{\kappa^3}\Big[-\bar{\boldsymbol{\lambda}}^6 - \bar{\boldsymbol{\lambda}}^4 R + \bar{\boldsymbol{\lambda}}^2 R^2 + R^3 + \bar{s}_0\,(\bar{\boldsymbol{\lambda}}^4 - 6\bar{\boldsymbol{\lambda}}^2 R + R^2)\Big] \right\}
\end{aligned}
$$

here, we defined:

$$
\bar{s}_0 \equiv \omega(\alpha_\ell\sqrt{s_0})^2\,, \qquad \bar{\boldsymbol{\lambda}}^2 \equiv \omega\boldsymbol{\lambda}^2
$$

Bibliography

[1] J. R. Forshaw and D. A. Ross, *Quantum chromodynamics and the pomeron*, Cambridge 1997 (Cambridge lecture notes in physics 9)

[2] E. A. Kuraev, L. N. Lipatov and V. S. Fadin, Sov. Phys. JETP **45** (1977) 199 [Zh. Eksp. Teor. Fiz. **72** (1977) 377]; I. I. Balitsky and L. N. Lipatov, Sov. J. Nucl. Phys. **28** (1978) 822 [Yad. Fiz. **28** (1978) 1597].

[3] V. S. Fadin and L. N. Lipatov, Phys. Lett. B **429** (1998) 127

[4] M. Ciafaloni and G. Camici, Phys. Lett. B **430** (1998) 349

[5] V. S. Fadin and L. N. Lipatov, Phys. Lett. B **429** (1998) 127

[6] A. H. Mueller, Nucl. Phys. Proc. Suppl. **18C** (1991) 125

[7] J. Bartels, A. de Roeck and M. Loewe, Z. Phys. C **54** (1992) 635

[8] J. Kwiecinski, A. D. Martin and P. J. Sutton, Phys. Rev. D **46** (1992) 921

[9] A. H. Mueller and H. Navelet, Nucl. Phys. B **282** (1987) 727.

[10] J. Bartels, S. Gieseke and C. F. Qiao, Phys. Rev. D **63** (2001) 056014 [Erratum-ibid. D **65** (2002) 079902]

[11] V. S. Fadin, R. Fiore and A. Quartarolo, Phys. Rev. D **50** (1994) 2265

[12] J. Bartels, S. Gieseke and A. Kyrieleis, Phys. Rev. D **65** (2002) 014006

[13] S. Catani and M. H. Seymour, Nucl. Phys. B **485** (1997) 291 [Erratum-ibid. B **510** (1997) 503]

[14] V. S. Fadin and A. D. Martin, Phys. Rev. D **60** (1999) 114008

[15] J. Bartels, D. Colferai, S. Gieseke and A. Kyrieleis, Phys. Rev. D **66** (2002) 094017

[16] M. Ciafaloni, Phys. Lett. **B 429** (1998) 363; M. Ciafaloni and D. Colferai, Nucl. Phys. **B 538** (1999) 187

[17] N. N. Nikolaev and B. G. Zakharov, Z. Phys. C **49** (1991) 607.

[18] N. Nikolaev and B. G. Zakharov, Z. Phys. C **53** (1992) 331.

[19] A. H. Mueller, Nucl. Phys. B **335** (1990) 115.

[20] D. Y. Ivanov and M. Wusthoff, Eur. Phys. J. C **8** (1999) 107.

[21] S. Gieseke and C. F. Qiao, Phys. Rev. D **61** (2000) 074028

[22] K. Golec-Biernat and M. Wusthoff, Phys. Rev. D **59** (1999) 014017

[23] K. Golec-Biernat and M. Wusthoff, Phys. Rev. D **60** (1999) 114023

[24] K. Golec-Biernat and M. Wusthoff, Eur. Phys. J. C **20** (2001) 313

[25] V. S. Fadin, R. Fiore, M. I. Kotsky and A. Papa, Phys. Rev. D **61** (2000) 094006

[26] V. S. Fadin, R. Fiore, M. I. Kotsky and A. Papa, Phys. Rev. D **61** (2000) 094005

[27] V. S. Fadin, Zh. Eksp. Teor. Fiz. Pis'ma **61** (1995) 342; V. S. Fadin, R. Fiore and A. Quartarolo, Phys. Rev. D **53** (1996) 2729; V. S. Fadin, M. I. Kotsky, Yad. Fiz. **59**(6) (1996) 1; V. S. Fadin, M. I. Kotsky and R. Fiore, Phys. Lett. B **359** (1995) 181.

[28] V. S. Fadin and L. N. Lipatov, Nucl. Phys. B **406** (1993) 259; V. S. Fadin, R. Fiore and A. Quartarolo, Phys. Rev. D **50** (1994) 5893

[29] V. S. Fadin, M. I. Kotsky and L. N. Lipatov, Phys. Lett. B **415** (1997) 97.

[30] S. Catani, M. Ciafaloni and F. Hautmann, Phys. Lett. B **242** (1990) 97; Nucl. Phys. B **366** (1991) 135; G. Camici and M. Ciafaloni, Phys. Lett. B **386** (1996) 341; V. S. Fadin, R. Fiore, A. Flachi and M. I. Kotsky, Phys. Lett. B **422** (1998) 287

[31] J. Bartels, A. De Roeck and H. Lotter, Phys. Lett. B **389** (1996) 742

[32] S. J. Brodsky, F. Hautmann and D. E. Soper, Phys. Rev. D **56** (1997) 6957

[33] J. Bartels, C. Ewerz and R. Staritzbichler, Phys. Lett. B **492** (2000) 56

[34] M. Acciarri *et al.* [L3 Collaboration], Phys. Lett. B **453** (1999) 333; M.Przybycien, A.DeRoeck,R.Nisius, [OPAL Collaboration] OPAL Physics Note PN456 (2000)

[35] A. Heister *et al.* [ALEPH Collaboration], arXiv:hep-ex/0305107

[36] C. R. Schmidt, Phys. Rev. D **60** (1999) 074003; J. R. Forshaw, D. A. Ross and A. Sabio Vera, Phys. Lett. B **455** (1999) 273

[37] M. Ciafaloni, D. Colferai and G. P. Salam, Phys. Rev. D **60** (1999) 114036

[38] G. P. Salam, Acta Phys. Polon. B **30** (1999) 3679

[39] M. Ciafaloni, D. Colferai, G. P. Salam and A. M. Stasto, arXiv:hep-ph/0307188

[40] J. R. Andersen and A. Sabio Vera, Phys. Lett. B **567** (2003) 116

I would like to thank Prof.J.Bartels for his permanent and extensive support. He draw my attention to the essential issues and always tried to help in the conceptual as well as in the calculational problems. I benefit from his optimism.

I also wish to thank Stefan Gieseke who contributed a great deal to my understanding of the topic. I am very grateful for the fruitful and pleasant collaboration with him and Dimitri Colferai.

For the help and discussions of various kinds I would like to thank Victor Fadin, Gian-Paolo Vacca, Krzysztof Golec-Biernat, Krisztian Peters, Cong-Feng Qiao, Matthias Steinhauser, Luminita Mihaila and Anna Stasto.

I am grateful to the members of the II.Institut für Theoretical Physics and the DESY theory group for creating a stimulating and friendly atmosphere.

This work was supported by the Graduiertenkolleg 'Zukünftige Entwicklungen der Teilchenphysik'.

For the accurate proof-reading of this thesis and his useful suggestions I would like to thank Agustin Sabio-Vera.

I am very grateful to my parents for their unending support.

I wish to thank Ulrike Renken for her patience, the flowers and all her love.